Universitat Autònoma de Barcelona

CARBON SEQUESTRATION
RATES IN COASTAL BLUE CARBON ECOSYSTEMS:
a perspective on climate change mitigation

ARIANE ARIAS ORTIZ

CARBON SEQUESTRATION RATES IN COASTAL BLUE CARBON ECOSYSTEMS:

a perspective on climate change mitigation

ARIANE ARIAS ORTIZ
TESI DOCTORAL 2019

Tutor and thesis director:
DR. PERE MASQUÉ BARRI
Co-directors:
DR. JORDI GARCIA-ORELLANA
DR. CARLOS M. DUARTE

UNIVERSITAT AUTÒNOMA DE BARCELONA
INSTITUT DE CIÈNCIA I TECNOLOGIA AMBIENTALS

UNIVERSITAT AUTÒNOMA DE BARCELONA

INSTITUT DE CIÈNCIA I TECNOLOGIA AMBIENTALS

TESI DOCTORAL

Doctorat en Ciència i Tecnologia Ambientals

Març 2019

Carbon sequestration rates in coastal Blue Carbon ecosystems: a perspective on climate change mitigation

Ariane Arias Ortiz

Tutor and thesis director:

Dr. Pere Masqué Barri

Co-directors:

Dr. Jordi Garcia-Orellana

Dr. Carlos M. Duarte

La veritat vol ser buscada,

però també demana que se l'esperi,

que es vagi per davant seu però mai més enllà

Marina Garcés

Agraïments – Acknowledgements

Amb aquesta tesi acabo una etapa de quatre anys i mig plena de canvis, de reptes, de creixement professional i de maduració personal. Tot i que és la meva tesi és també la tesi de moltes persones que han tingut una funció clau en el plantejament, nus i desenllaç d'aquesta etapa.

Pere, Jordi i Carlos moltes gràcies per ser els meus referents. Vull agrair-vos de manera molt sincera el temps i la confiança que heu dipositat en la meva feina. M'he sentit des de l'inici en una zona de confort que m'ha permès gaudir del que feia. Pere i Jordi, gràcies per obrir-me les portes del LRA (i de l'ECU) i per transferir-me els valors d'una vida professional sana. El que compta és ser una persona que pensa de manera crítica i això és el més valuós que em podíeu transmetre. Carlos, gracias por acogerme en KAUST y por proporcionarme las herramientas y recursos que tenías al alcance. Que hayas formado parte de mi proceso formativo ha sido un enorme placer, tu sabiduría es una gran fuente de inspiración. A tots tres, gràcies pel suport en tot moment, per ajudar-me a superar llindars i per donar-me la seguretat per obrir-me a reptes desconeguts.

Els meus companys de grup, gràcies per ser els meus acompanyants. Moltes gràcies per les dosis de positivisme i bon humor del dia a dia, els somriures ho fan tot més fàcil. Sou irreemplaçables i us trobaré molt a faltar on sigui que vagi. Joan Manuel, gràcies pels infinits cops de mà amb les depos i les muntanyes de cores que arribaven per datar, gràcies pels Gordi-Fridays! sóc impossible d'engreixar, però les dosis de mantega i sucre m'han engreixat, si més no, la felicitat. Sarah, la fábrica de papers, la exprimidora de todas las gangas habidas y por haber, la maquetadora oficial de los videos del LRA, eres cómo la eficiencia del Quantulus para el ^{226}Ra, up to 300%. ¡Si necesitas ponerte las pilas, pon una Sarah en tu vida! Admiro tu capacidad para trabajar sin decaer. Eres súper fuerte (¡y no porque vayas al SAF!). Contigo de compi de despacho ha sido muy fácil mantener el ritmo de trabajo, gracias por transmitirme tu motivación *to get things done*. Marc, et vaig conèixer com a *"tamizator"* (com deia el Maxi) no saps la de feina que em vas treure de sobre tamisant tots aquells testimonis. Si no ho haguessis fet potser jo no tindria 4 capítols a la tesi, o probablement no l'hauria acabat, o encara pitjor, l'hauria deixat de tant tamisar! No sé com

no vas sortir corrents del LRA, en tot cas, me n'alegro molt que t'hi hagis quedat. Aaron, totes les línies que escrigui aquí es queden curtes per poder-te agrair tota l'ajuda que m'has donat aquest últim any de tesi. Espero poder-te ajudar jo també de la mateixa manera quan ho necessitis. Gràcies pel cop de mà amb les figures de l'article de Nature Climate Change, gràcies per encarregar-te de la llista de figures i taules d'aquesta tesi, per l'aprovisionament de galetes príncipe a l'hora de berenar i per sempre preguntar-nos a tots com estem i com ens va. Ets un enorme exemple de superació. No tinc cap mena de dubte que te'n sortiràs amb la tesi estupendament i tota l'ajuda que reparteixes et retornarà, t'ho mereixes. Carolina, moltes gràcies pel feedback amb la beca de la NOAA i per tots els detalls que tens quan vens al LRA, sóc molt fan que hagis substituït les estovalles de la sala del microones, la sala ja no és (del tot) un niu de depressió. M'he sentit sempre molt acompanyada per tothom que ha passat pel grup, Esther gràcies pel cop de mà amb l'entrevista de la Caixa que em va garantir poder fer aquest doctorat. Valentí, merci pel teu sentit de l'humor (des de la teva tesi que tenim pendent un partit). Giada, gracias por tu disposición para apuntarte a todos los planes (excepto a cenar con Jordi en Roma) y por la Puglia *experience* (en lo primero que pienso es en el croissant asesino). Muntsa, ets positivisme elevat a infinit, super profe de pràctiques, de problemes i de projectes, i ara super scientist de Woods Hole! i amb quina tranquil·litat i bon humor ho portes, t'admiro. Viena, m'ha encantat creuar-me amb tu, la teva manera d'improvisar i viure la vida em fascina, i si alguna cosa no va massa bé, no passa res, tu rius. Jo necessito una mica d'això. Gràcies per obrir-me les portes de casa teva a Perth, per les laundry sessions i els wedges amb sweet chili a Joondalup. Poques persones tenen la paciència i perseverança per no desconnectar del que és lluny, tu saps un munt de cuidar les teves amistats d'arreu, així que gràcies per no ser una amistat passatgera sinó de les que es queden. Maxi con tu POWER, tu ENERGY y tu FUNDAMENTO he tirado para adelante para acabar esto, eskerrik asko! Almu, me hubiese venido genial tu alegría, tu calidez y tus abrazos estos últimos días. Núria, gràcies per acollir-nos a Zurich i per ajudar-me amb les presentacions de les ASLOs i OSM que sempre portava per acabar (un clàssic).

Colleagues at ECU, FIU, SU and co-authors, thanks for being my additional sources of inspiration. Paul, Oscar thank you very much for including me in your research, much of what I learnt and produced in this thesis is indeed inspired in your work. Oscar, gràcies

addicionals per no perdre els nervis durant els meus inicis, quan m'arribaven caixes de 50 kg amb mostres que havia de seleccionar i m'enfadava com una mala cosa. Anna, and all the students and staff at CMER, thanks for making me feel part of the group since day one. Glòria, el turbo que portes és la canya. Gràcies per endinsar-me en el món de la foto i de la creativitat, gràcies per les màster-classes i per venir a Madagascar! Quins dies més intensos, sense la teva energia i positivisme no ho haguéssim aconseguit. Gràcies a tu i el Pere per obrir-me les portes de casa vostra, incloure'm en els vostres plans i fins i tot alimentar-me de tant en tant! Thanks to the Swedish team (Mats, Martin G., Maria, Martin D.) thanks for including me in Madagascar's project, that field trip was a real expedition. Also thank you for having me at Stockholm University, those were a really nice 3 weeks (snowy indeed!). And from the cold-temperate to the subtropics. Jim F. thanks for hosting me during summer 2017 at the Seagrass Ecosystems Research Lab and letting me use facilities and resources there. Thanks for the amazing paella too. Sampling across Florida Bay was such an experience, lots of diving, lots of cores lots of work still to get done… Sara, Jason, Christian, Kaya and Kai thanks for welcoming me as you did and for making me feel I was part of the team, my gratitude to you is giant since coring one of the world's largest seagrass ecosystems wouldn't have been possible without your help and involvement. I loved spending time in the field (and out of the field) with you exploring ideas and having lively conversations about science. Special thanks to the co-authors of the articles I present in this thesis, your constructive feedback has made me grow as a researcher and have showed me what research quality is. Hope we can continue working together in the future.

La meva família m'ha donat la llar, gràcies per cuidar-me i per recordar-me d'on vinc i qui sóc. Gixane Alfredo i Marc, us volia dedicar la tesi, però se la dedicaré a la Tere (la Teresa de Aragón!) perquè ha estat i serà un gran exemple de fortalesa. M'agradaria que aquesta tesi també fos seva i així ens acompanyi al final d'aquesta etapa. A vosaltres us puc dedicar temps de qualitat, que us el mereixeu per aguantar l'altre cara de la tesi, l'estrès, el mal humor i la frustració de no tenir mai temps...vosaltres l'heu patit més que la resta perquè malauradament la confiança fa fastig. Tot i així, gràcies per no tenir-m'ho en compte, per deixar-me fer i no posar mai barreres, gràcies per no condicionar-me en res i estimar-me per qui sóc i no pel que aconsegueixo. Marta, tu també ets part de la meva llar, has patit el meu

final de tesi com si també fos el teu, ho hem aconseguit :). Gràcies per haver-te sabut posar en el meu lloc, per encarregar-te de la casa i per no tenir en compte la meva inutilitat absoluta durant les últimes setmanes. Gràcies per no deixar que em rendís.

Els meus amics han estat tant importants com la meva família, la Nadine, els de teresianes, patinatge, guinardbronx vosaltres heu sigut la meva via d'escapament aquests anys i la meva oportunitat de fugir de la tesi, de la ciència i de la recerca i satisfer altres interessos que res tenen a veure amb la meva carrera professional. La meva salut mental us ho està eternament agraïda.

I el Roc que ho és tot, guia i referent, acompanyant, inspiració. És llar i és via d'escapament. Infinites gràcies.

TABLE OF CONTENTS

8

List of Figures

List of Tables

List of abbreviations and acronyms

BCE: blue carbon ecosystem
C: carbon
CaCO$_3$: calcium carbonate
CAR: carbon accumulation rate
CF-CS: Constant Flux: Constant Sedimentation
CIC: Constant Initial Concentration
CH$_4$: methane.
C:N: ratio between organic carbon and nitrogen
CO$_2$: carbon dioxide
CO$_2$e: carbon dioxide equivalent
CRS: Constant Rate of Supply
DBD: dry bulk density
δ^{13}C: carbon isotopic signature
δ^{15}N: nitrogen isotopic signature
DIC: dissolved inorganic carbon
DOC: dissolved organic carbon DW (%): percentage of dry weight. EA: elemental analyzer
GHG: greenhouse gas
GPP: gross primary production
IC: inorganic carbon
IPCC: Intergovernmental Panel on Climate Change.
λ: decay rate
^{210}Pb: radionuclide lead-210
^{210}Pb$_{xs}$: excess ^{210}Pb
^{210}Pb$_{sup}$: supported ^{210}Pb
LOI: Loss of Ignition technique NCP: net community production
MAR: mass accumulation rate
NCP: net community production
NEP: net ecosystem production
N: nitrogen
OC or **C$_{org}$**: organic carbon
OM: organic matter
POC: particulate organic carbon
R: respiration
SAR: sediment accumulation rate
TAlk: total alkalinity

List of manuscripts

Published:

I. **Arias-Ortiz, A.**, Masqué, P., Garcia-Orellana, J., Serrano, O., Mazarrasa, I., Marbà, N., Lovelock, C.E., Lavery, P.S., Duarte, C.M. (2018) Reviews and syntheses: ^{210}Pb-derived sediment and carbon accumulation rates in vegetated coastal ecosystems – setting the record straight. *Biogeosciences*, 15, 6791-6818. *Chapter 3*

II. **Arias-Ortiz, A.**, Serrano O., Masqué, P., Lavery, P.S., Mueller, U., Kendrick, G.A., Rozaimi, M. et al. (2018) A marine heatwave drives massive losses from the world's largest seagrass carbon stocks. *Nature Climate Change* 8, no. 4: 338. *Chapter 5*

Submitted:

I. **Arias-Ortiz, A.**, Masque, P., Glass, L., Benson, L., Kennedy, H., Duarte, C.M., Garcia-Orellana, J., Benitez-Nelson, C.R., Humphries, M.S., Ratefinjanahary, I., Ravelonjatovo, J., Lovelock, C.E. (*subm. to Ecosystems*) "Losses of soil organic carbon with deforestation in mangroves of Madagascar". *Chapter 6*

In preparation:

I. **Arias-Ortiz, A**., Masqué, P., Garcia-Orellana, J., Duarte, C.M., Colarusso, P., Lavery, P., Marbà, M., Mateo, M.A., Mazarrasa, I., Serrano, S., Samper-Villareal, J., Wesselmann, M. (*in preparation*) "Contemporary organic carbon burial rates in seagrass sediments worldwide". *Chapter 4*

Related papers not included in this thesis:

I. Cusack, M., Saderne, V., **Arias-Ortiz, A.**, Masque, P., Krishnakumar, P. K., Rabaoui, L., ... & Elyas, A. A. (2018). Organic carbon sequestration and storage in vegetated coastal habitats along the western coast of the Arabian Gulf. *Environmental Research Letters*, 13(7), 074007.

II. Saderne, V., Cusack, M., Almahasheer, H., Serrano, O., Masqué, P., **Arias-Ortiz, A**., ... & Duarte, C. M. (2018). Accumulation of Carbonates Contributes to Coastal Vegetated Ecosystems Keeping Pace With Sea Level Rise in an Arid Region (Arabian Peninsula). Journal of Geophysical Research: Biogeosciences, 123 (5),1498-1510.

III. Almahasheer, H., Serrano, O., Duarte, C. M., **Arias-Ortiz, A.**, Masque, P., & Irigoien, X. (2017). Low Carbon sink capacity of Red Sea mangroves. *Scientific reports*, 7(1), 9700.

IV. Mazarrasa, I., Marbà, N., Garcia-Orellana, J., Masqué, P., **Arias-Ortiz, A.**, & Duarte, C. M. (2017). Dynamics of carbon sources supporting burial in seagrass sediments under increasing anthropogenic pressure. *Limnology and Oceanography*, 62(4), 1451-1465.

V. Mazarrasa, I., Marbà, N., Garcia-Orellana, J., Masqué, P., **Arias-Ortiz, A.**, & Duarte, C. M. (2017). Effect of environmental factors (wave exposure and depth) and anthropogenic pressure in the C sink capacity of Posidonia oceanica meadows. *Limnology and Oceanography*, 62(4), 1436-1450.

VI. Serrano, O., Ruhon, R., Lavery, P.S., Kendrick, G.A., Hickey, S., Masqué, P., **Arias-Ortiz, A.**, Steven, A., Duarte, C.M. (2016) Impact of mooring activities on carbon stocks in seagrass meadows. *Scientific reports* 6: 23193.

VII. Serrano, O., Ricart, A. M., Lavery, P. S., Mateo, M. A., **Arias-Ortiz, A.**, Rozaimi, M., ... & Duarte, C. (2016). Key biogeochemical factors affecting soil carbon storage in Posidonia meadows. *Biogeosciences*, 13, 4581-4594.

VIII. Marbà, N., **Arias-Ortiz, A.**, Masqué, P., Kendrick, G. A., Mazarrasa, I., Bastyan, G. R., ... & Duarte, C. M. (2015). Impact of seagrass loss and subsequent revegetation on carbon sequestration and stocks. *Journal of Ecology*, 103(2), 296-302.

Chapter 1

Introduction

This chapter briefly introduces the motivation and background for the field of this thesis, which is the role of vegetated coastal habitats in sequestering CO_2 from the atmosphere and the water column. Over the last two centuries, concentrations of greenhouse gases (GHG) in the atmosphere have increased markedly, contributing to global warming and climate breakdown. This has led to a worldwide interest in strategies to sequester carbon (C) to offset anthropogenic CO_2 emissions. Some are based on actions to enhance natural C sinks like the conservation of terrestrial sinks, primarily tropical forests. One potential, but relatively unexplored option is to restore or create wetlands and seagrass areas, with the intent of sequestering C and building up the soils. Indeed, tidal marshes, mangroves and seagrasses (also termed coastal Blue Carbon Ecosystems (BCE)) could offer an opportunity for C sequestration and GHG offsets due to the potential for habitat creation, restoration, C capture enhancement and avoided losses. But understanding the role that these habitats play in global C budgets, as well as for their inclusion as a component in schemes for climate change mitigation and adaptation requires determining precisely how much carbon these ecosystems hold, and how it accumulates over time. Yet to-date, uncertainties in C sequestration rates of coastal BCE are large as well as the fate of the sedimentary C after habitat degradation. This thesis contributes to refine estimates of C accumulation rates in sediments of coastal BCE generally, and to expand estimates of C accumulation rates in seagrass meadows globally. In addition, the magnitude of sedimentary C losses resulting from habitat degradation is also addressed in two specific Chapters, illustrating the relevance of the conservation of these ecosystems.

Over the last two centuries, atmospheric greenhouse gas (GHG) concentrations have increased markedly. The projected warming of 2–5 ºC by 2100 is expected to be driven by continued rises in GHG concentrations leading to increased frequency and intensity of extreme events (droughts, floods, heatwaves or hurricanes), ice-free Arctic, sea-level rise and increased damage to and erosion of coastal areas. In addition, simultaneous ocean acidification and the vulnerability of ecosystems under stress will be magnified (Gattuso et al., 2015; Hoegh-Guldberg et al., 2014) and may bring irreversible impacts to important marine ecosystems (e.g. coral reefs) and their associated services. Although the climate breakdown is global, impacts to society will be dependent on levels of development, vulnerability to climate change, and the options available to different societies, with its effects falling more heavily on those who are already most vulnerable (poorer countries, island nations, indigenous peoples, and communities reliant on healthy ecosystems). Reducing emissions towards carbon (C) neutrality to avoid temperatures rising to 1.5- 2ºC above preindustrial levels (COP 21) is of major concern to reduce the risks and costs of damage and adaptation to climate change, which increase sharply with rises in global temperatures (IPCC, 2018). Reduction in emissions would be possible through directly reducing greenhouse gas (GHG) emissions together with mitigation strategies (Peters et al., 2013). Reducing GHG emissions can be achieved through a shift from fossil fuels to renewable energies or by improving energy efficiency. Mitigation strategies may include C capture and storage (CCS) where CO_2 is generated and the protection and enhancement of natural C sinks (Griscom et al., 2017; Rockström et al., 2017), the latter defined as any process, activity or mechanism that removes CO_2 from the atmosphere (UNFCCC, 1992).

Approximately one-half of total anthropogenic CO_2 emissions (49 Gt CO2e; this is CO_2 equivalents) is at present taken up by the combined C reservoirs of land and ocean (Ballantyne et al., 2012). On land, C is removed by photosynthesis and stored as organic C (OC) in plants and soils of natural ecosystems. Forest biomass can accumulate large amounts of CO_2 during relatively short periods, typically several decades. For this reason, afforestation and reforestation are measures that can be taken to enhance the C sink on land. However, out of all the biological C sequestered in the planet, more than half (55%) is captured by living organisms in the ocean (Bowler et al., 2009). In the open ocean, this

oceanic C cycle is dominated by micro-, nano-, and picoplankton, including bacteria and archaea through the biological C pump (Volk and Hoffert, 2013), but in the coastal domain, biological C sequestration is mainly driven by vegetated coastal ecosystems, and particularly sediments from mangroves, tidal marshes and seagrass meadows (Duarte et al., 2005; Smith 1981). In addition, macroalgae may also have a potential large contribution to C sequestration as has been recently proposed (Krause-Jensen et al., 2018). This important role of vegetated coastal ecosystems in the global oceanic C budget was first highlighted by Smith (1981), but it was not until two decades later when the first estimates of their large C sink capacity were reported (Chmura et al., 2003; Duarte et al., 2005). At the time, vegetated coastal habitats were estimated to contribute up to 10% of the oceanic net primary production and to 50% of the OC burial in the coastal ocean (including estuaries and continental platforms). The total burial of OC in vegetated coastal sediments was estimated at 110 Tg C yr^{-1}, which is comparable to the flux of OC reaching the deep ocean from the biological pump (50 – 390 Tg C yr^{-1}) (1-3% of the biological pump strength 5-13 Gt C yr^{-1}; Henson et al., 2010; Laws et al., 2011), despite occupying only about 0.2% of the ocean surface. The role of tidal marshes, mangroves and seagrass meadows to sequester C was therefore apparent given the efficiency in a per area basis and the important role that their sediments played as C sinks, where OC could be maintained over timescales of decades, centuries or even millennia, hence meeting the requirements of permanence for GHG reduction actions.

The realization of the important role of vegetated coastal ecosystems as C sinks led to the development of a new strategy for climate change mitigation, (Nature Editorial, 2016) termed "Blue Carbon", based on the conservation and restoration of mangroves, tidal marshes and seagrasses, also known as coastal Blue Carbon Ecosystems (BCE) (Duarte et al., 2013a; McLeod et al., 2011; Nellemann et al., 2009). In a similar manner as for terrestrial forests, vegetated costal habitats were identified as an opportunity for C sequestration and GHG offsets because of the potential for habitat creation, restoration, enhancement, and avoided losses. In addition, they presented a safe and cost-effective measure, with strong co-benefits for societies and natural systems due to the various multiple ecosystem services they provide (e.g., coastal protection, food production, habitat for wildlife or buffers of ocean acidification) (Canadell and Raupach, 2008). However, coastal BCE have not yet been

included in existing C mitigation strategies (e.g., the United Nation's program Reducing Emissions from Deforestation and Forest Degradation (REDD+; http://www.un-redd.org/)) or in assessments of global C budgets (e.g. Ciais et al., 2013). Uncertainties in the global extent of seagrasses and tidal marshes, in the fluxes of OC into their sediments (i.e., OC burial rates) and out from the ecosystems (export and remineralization), and in the magnitude of CO_2 emissions after ecosystem disturbance are some of the aspects that require research to improve the current estimates for their inclusion in C-offset programs and global C budget assessments. Additionally, the underrepresentation of coastal BCE, in particular tidal marshes and seagrass meadows, outside North America, Europe or Australia precludes the extrapolation of the available estimates to the entire coastal BCE extent. This thesis contributes to refine estimates of OC accumulation rates in sediments of coastal BCE generally and to expand the estimates of OC accumulation rates in seagrass meadows worldwide. In addition, the magnitude of sedimentary OC losses resulting from habitat degradation is also addressed in two specific studies included in this thesis, illustrating the relevance of conservation of these ecosystems.

1.1 Coastal blue carbon ecosystems

"Coastal BCE, mangrove forests, tidal marshes and seagrass meadows, have much in common with rain forests: they are hot spots for biodiversity, they provide important and valuable ecosystem functions, including carbon storage, and are under thread do to human and climate change impacts" (Nellemann et al., 2009).

Coastal BCE occur along the coast of all continents (except Antarctica), but their nature varies depending on latitude and substrate characteristics. Mangrove and tidal marshes typically grow on soft substrates, muddy or sandy, and occupy the intertidal zone. Mangrove distribution dominates in the tropics and subtropics, while tidal marshes are common features of temperate coastlines (Pennings and Bertness, 2001; Spalding, 2010). Seagrasses are mostly confined to sandy–muddy sediments, although a few species can grow over rock, and occupy the subtidal and occasionally the lower intertidal zone down to a variable depth (up to 90 m), where they are limited by light availability (Duarte, 1991).

Seagrasses are the most widespread among the coastal BCE, occupying between 177,000 to 600,000 km^2 (Green and Short, 2003) (Fig. 1.1; Table 1.1).

Coastal BCE act as sinks for atmospheric CO_2 as tidal marshes, mangroves and seagrasses take up CO_2 through photosynthesis and convert it to OC in plant biomass (i.e., primary production) (short-term storage of OC). Part of this biomass is cycled and released back into the atmosphere by autotrophic (plant) and heterotrophic (consumer) respiration. Mangrove forests, and to a minor extent, seagrass meadows and tidal marshes produce photosynthetic OC well in excess (20-40%) of the ecosystem requirements (Duarte and Cebrián, 1996), hence generally are net autotrophic. Excess OC is buried in their sediments along with organic particles trapped from the water column (Bouillon et al., 2003; Kennedy et al., 2010) or exported to adjacent systems (Duarte and Cebrián, 1996; Mateo et al., 2006). Burial of excess net community production (gross primary production minus autotrophic and heterotrophic respiration) represents an estimate of the size of the C sink associated with coastal BCE (Fig. 1.2). Unlike in terrestrial forests, the sediments of coastal BCE are the main compartment where OC is stored. From 50 to 98% of the OC stocks are found in sediments rather than in living biomass (Chmura et al., 2003; Donato et al., 2011; Fourqurean et al., 2012b). While the OC bound to biomass has a rapid turnover rate (prevailing less than 50 years), the OC accumulated in sediments is locked up as reduced C and can be preserved for decades, centuries and even millennia (Mateo et al., 1997).
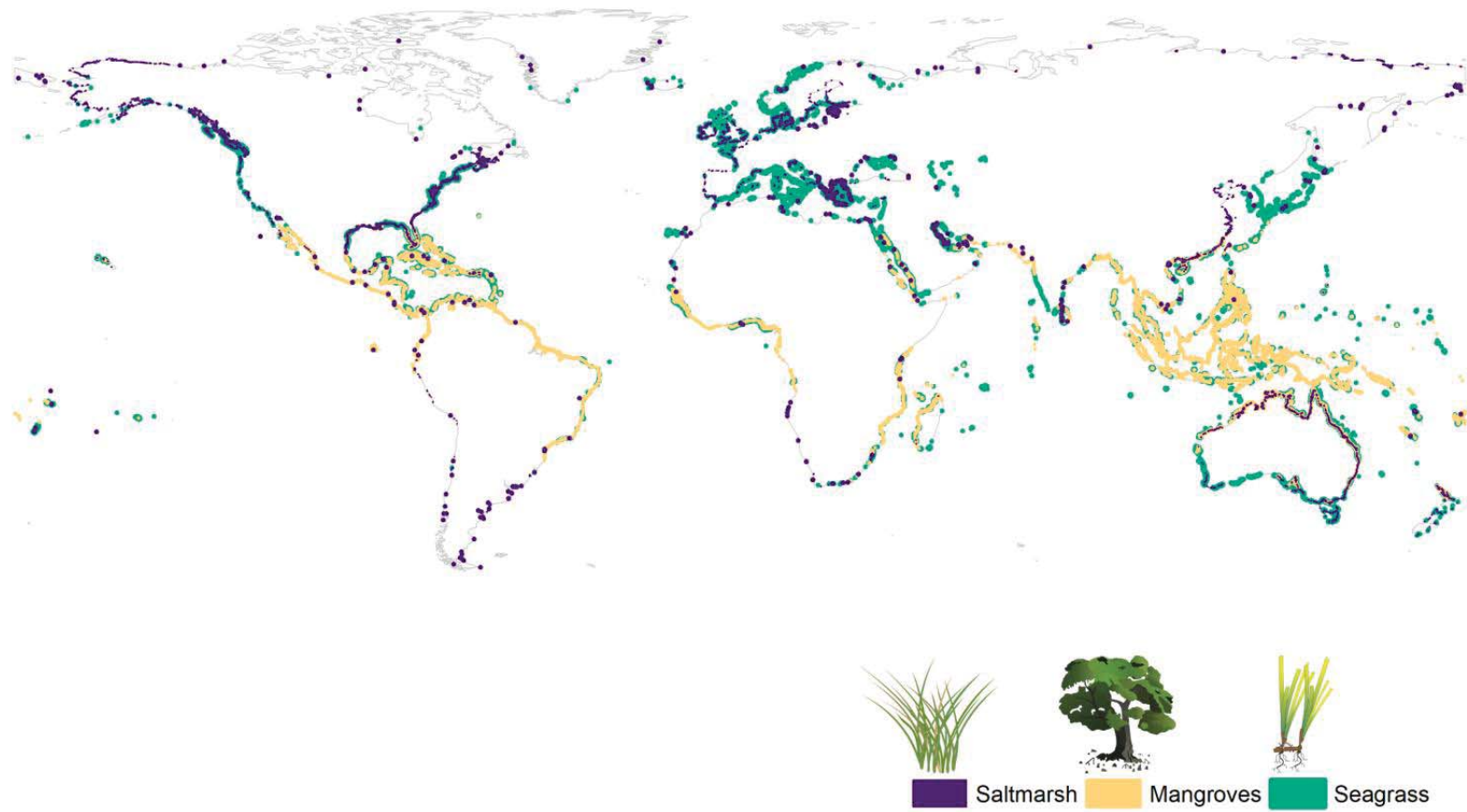
Figure 1.1: Coastal BCE distribution worldwide. Source: UNEP-WCMC (2018).

The OC accumulated in sediments, however, is not static and a fraction of it is constantly cycling between the different global C pools in various molecular forms. Sedimentary C can be emitted back into the atmosphere as CO_2 when soil organic matter is remineralized by microorganisms. Carbon loss can also be caused by root exudates, which liberate organic compounds from protective mineral associations (Keiluweit et al., 2015) or by enhanced oxygen transport into sediments through the roots and rhizomes (Smith et al., 1984). Degradation of refractory OC could be enhanced by repeated sediment resuspension/redeposition cycles (Burdige, 2007), while OC may also be partly exported from sediments to coastal or adjacent waterways as dissolved organic C (DOC) or as part of eroded material (Alongi, 2014) (Fig. 1.2).

Several properties of coastal BCE enhance their ability to store large quantities of OC in their sediments. Together with their high net primary production, they support relatively high sediment accumulation rates (seagrass, mangrove and tidal marsh: ~1.5, 4.5 and 5.5 mm yr^{-1}, respectively) (Duarte et al., 2013b). The submerged canopies in seagrass meadows and the partially submerged vegetation in mangrove and tidal marshes affect flow speed (Peralta et al., 2008) and reduce wave action (Anderson et al., 2011), enhancing particle deposition (Furukawa et al., 1997; Gacia et al., 2002) and trapping a large inflow of particulate OC from surrounding habitats (i.e., allochthonous POC). The growth of their below ground-biomass (i.e. roots and rhizomes) promotes vertical accretion of sediments, contributing to the development of extensive OC deposits that can reach > 3 m thick (e.g., Lo Iocano et al., 2008; Scott and Greenberg, 1983; Woodroffe et al., 1993). Finally, BCE are periodically or permanently flooded with seawater, which reduces the CO_2 and CH_4 emissions from sediment respiration, limiting also sediment exposure to oxygen and resulting in enhanced preservation of OC (Burdige, 2007; Chmura et al., 2003).

The magnitude of OC deposits within the top meter of sediment in tidal marshes (162 Mg C ha^{-1}) and seagrass meadows (140 Mg C ha^{-1}) is similar, on average, to that in the upper 1-m soil in terrestrial forests (180 ± 100 Mg C ha^{-1}), while the top meter of mangrove sediments (280 Mg C ha^{-1}) store 50% more OC than forests soils on land (Atwood et al., 2017; Duarte et al., 2013b; Lal, 2005; Prentice et al., 2001).
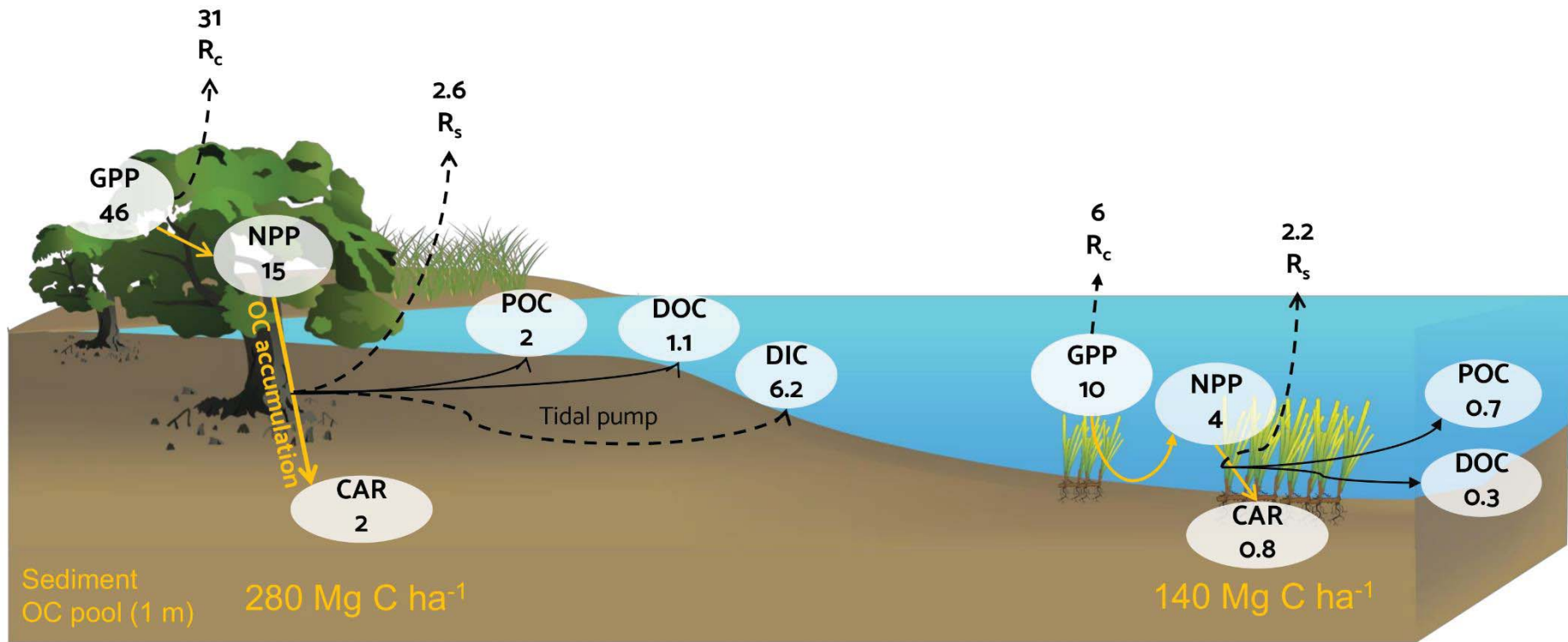
Figure 1.2: Major pathways of carbon flow through mangroves and seagrass ecosystems. Solid golden arrows represent mean values of organic carbon uptake and sequestration, black arrows represent carbon losses through export and tidal exchange. Dashed arrows represent losses of carbon through respiration, hence a net flux to the atmosphere or ocean DIC pool. All values are in Mg C ha^{-1} yr^{-1}. Abbreviations: DIC, dissolved inorganic carbon; DOC, dissolved organic carbon; GPP, gross primary production; NPP, net primary production; POC, particulate organic carbon; Rc, canopy respiration; Rs, sediment respiration. Sources: Alongi et al. (2014); Duarte et al. (2010); Duarte et al. (2017). Images of vegetated coastal habitats: Tracey Saxby, IAN (http://ian.umces.edu/imagelibrary/).
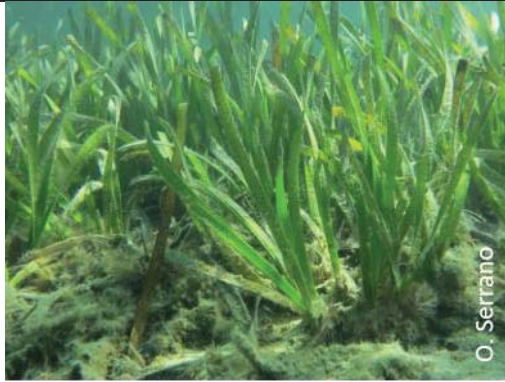
Most importantly, because of the capacity of BCE for trapping particles, the OC accumulation in sediments is ~40 times faster than that in terrestrial forests (5 g C m^{-2} yr^{-1}) (McLeod et al., 2011) (Table 1). Therefore, vegetated coastal ecosystems could be more valuable as C sinks per unit area than terrestrial forests, making them extremely valuable for nature-based approaches to climate change mitigation (Kroeger et al., 2017; Laffoley and Grimsditch, 2009; Nellemann et al., 2009).

Land use and land cover change of terrestrial ecosystems contribute about 12% of anthropogenic C emissions annually (Houghton et al., 2012). Like terrestrial forests, coastal BCE could contribute to CO_2 emissions if lost or degraded (Lovelock et al., 2017b). Indeed, coastal BCE have been shrinking worldwide (0.2 – 2.6 % yr^{-1}; Table 1.1). Losses of seagrass have been caused mostly by increased nutrient inputs and coastal transformation (Waycott et al., 2009), and tidal marshes and mangroves have been lost due to changes in land use, disturbance of hydrologic regimes and land reclamation (FAO, 2007; Templet and Meyer-Arendt, 1988; Valiela et al., 2001). The effects of climate change, such as ocean warming and extreme events are exacerbating this trend. For instance, the thermal regime of the Mediterranean Sea already exceeds the upper thermal limit of the endemic *Posidonia oceanica* in the Eastern basin and as a consequence of heatwaves and strong water stratification during the summer in the Western basin (Chefaoui et al., 2018; Jordà et al., 2012; Marbà and Duarte, 2009). Additionally, marine heatwaves have also led to losses of the temperate seagrasses *Amphibolis antarctica* and *Posidonia australis* in Western Australia (Fraser et al., 2014a; Nowicki et al., 2017). While warming is not projected to have significant direct effects on mangroves and tidal marshes, these ecosystems are highly sensitive to sea-level rise (Kirwan and Megonigal, 2013; Lovelock et al., 2015), particularly where landward migration is limited due to coastal development and steep topography or where insufficient sediment is delivered to support accretion. The loss of coastal BCE goes hand in hand with the reduction of a natural pathway to sequester CO_2 and a means to manage climate change risks such as increased coastal vulnerability. Recent models suggest that average loss rates of coastal BCE during the last 20 yr have caused global CO_2 emissions ranging between 0.15 and 1.10 Pg CO_2e yr^{-1}, representing 3 to 20% of the annual rates

attributed to deforestation and forest degradation (Pendleton et al., 2012; van der Werf et al., 2009).

To date, policy responses to climate change and its impacts have largely focused on land-based actions (Field and Mach, 2017), such as the restoration of terrestrial forests or the enhancement of C reserves in agricultural farmland (Pan et al., 2011; Agrawal et al., 2011; Smith et al., 2008), for which C stocks, sequestration rates and the emissions factors of their conversion and degradation are relatively well described (FAO, 2010). Currently our ability to confidently develop policies that focus land management efforts towards conservation and restoration of net blue C sinks is hampered by an insufficient quantitative understanding of the natural processes that determine C sequestration efficiency in BCE and a lack of integrated measurements of C sequestration and emissions across different land uses and with predicted climate change. Despite this lack, several local, state and international organizations and programs (e.g. CSIRO - Australia and the International Blue Carbon Initiative), are focused on maximizing coastal BCE as C sinks and developing guidance for needed research, project implementation and policy priorities (Kelleway et al., 2017).

Table 1.1: Main characteristics of coastal blue carbon ecosystems. OC stocks normalized to the upper 1 meter of sediments.

	Seagrass meadows Marine flowering plants that are found in meadows along the shore of every continent except Antarctica. **Extension:** 177,000 – 600,000 km^2 [a] **NPP:** 4 Mg C ha^{-1} yr^{-1} [b] **Biomass OC stock:** 2.5 Mg C ha^{-1} [c] **Sediment OC stock:** 140 Mg C ha^{-1} [c] **CAR:** 138 ± 38 g C m^{-2} yr^{-1} [d] **Area loss rate:** 0.4 – 2.6% yr^{-1} [e]
	Mangrove forests Tropical/subtropical forests found in coastal areas that are regularly flooded by tidal water. **Extension:** 132,000 – 150,000 km^2 [f] **NPP:** 11.1 Mg C ha^{-1} yr^{-1} [g] **Biomass OC stock:** 160 Mg C ha^{-1} [h] **Sediment OC stock:** 280 Mg C ha^{-1} [h] **CAR:** 163 ± 40 g C m^{-2} yr^{-1} [i] **Area loss rate:** 0.2 – 0.4% yr^{-1} [f]
	Tidal marshes Coastal wetland ecosystems dominated by grass and shrub species that are regularly tidally flooded. **Extension:** 40,000 – 400,000 km^2 [j,k] **NPP:** 8.34 Mg C ha^{-1} yr^{-1} [l] **Biomass OC stock:** ∼25 Mg C ha^{-1} [m] **Sediment OC stock:** 162 Mg C ha^{-1} [n] **CAR:** 240 ± 30 g C m^{-2} yr^{-1} [k] **Area loss rate:** 1 -2 % yr^{-1} [n]

(a) Green and Short, (2003); (b) Duarte et al. (2010); (c) Fourqurean et al. (2012); (d) Mcleod et al. (2011); (e) Waycott et al. (2009); (f) Hamilton and Casey (2016); (g) Alongi, (2014); (h) Donato et al. (2011); (i) Breithaupt et al. (2012); (j) Duarte et al. (2005); (k) Ouyang and Lee, (2014); (l) Duarte and Cebrián, (1996); (m) Chmura et al. (2003a); Tripathee and Schäfer, (2015); (n) Duarte et al. (2013b).

1.2 Defining sediment organic carbon sequestration

Sediment OC sequestration is the process by which C from the atmosphere is fixed via plants or organic residues and stored in soils or sediments (FAO, 2017). Sediment OC sequestration involves three necessary stages: the removal of CO_2 from the atmosphere via plant photosynthesis; 2) the transfer of C from CO_2 to plant biomass; and 3) the transfer of

OC from plant biomass to the sediment where it is stored as sedimentary OC. This pool is characterized by a labile and a refractory OC fractions. The labile fraction encompasses recently incorporated plant residues with high turnover rates (days - few years), which are decomposed by benthic fauna, generally causing CO_2 emissions back into the atmosphere. Therefore, sediment OC sequestration goes beyond capturing atmospheric CO_2 in the short-term but retaining OC in sediment deposits permanently. The issue of C permanence is complex in biological systems, as some releases and reversals may occur due to natural (e.g. a change in temperature, evaporation and precipitation, or varying sediment supply) or anthropogenic processes.

One hundred years is a common time period equated with permanence, with reference often made to the Intergovernmental Panel on Climate Change (IPCC 2007) use of 100 year residency of CO_2 in the atmosphere for computing its Global Warming Potential (GWP) factors (Murray and Kasibhatla, 2013). However, the CO_2 residence time in the atmosphere has a large range because of the different uptake rates by different removal processes (5 to 200 yr^{-1}; IPCC, 2001).

Throughout this thesis, we use the term OC accumulation or burial rates as a synonym for OC sequestration rates.

1.3 Knowledge gaps on carbon sequestration by blue carbon ecosystems

1.3.1 Benchmark methodology to estimate organic carbon accumulation rates

Since the report by Nelleman in 2009, the research efforts on blue carbon have expanded rapidly. However, there is a paucity of studies that have effectively estimated the accumulation rates of OC in sediments, beyond the mere quantification of OC stocks (Fig. 1.3). Although this is true for all BCE, the scarcity of data is especially severe for seagrass meadows, as highlighted in several studies (Johannessen and Macdonald, 2016; Kuwae and Hori, 2019; Macreadie et al., 2018; Mazarrasa et al., 2017). Measurements of the OC stocks currently sequestered in sediments of coastal BCE have been addressed at a fixed depth of 1 m (Fourqurean et al., 2012b; Howard et al., 2014a) and have sometimes been used as a proxy for OC sequestration rates or sequestration efficiency. However, this approach might be

misleading for several reasons. First, there is the fact that many OC deposits, particularly of seagrass meadows, may not reach that potency, thus standardizing stocks to 1 m would lead to an overestimation of these estimates. Second, there is the variability in the period of accumulation of the upper meter OC stocks, which could differ in an order of magnitude and/or could have been discontinuous over time. Comparing 1 m stocks at two sites with differing sedimentation rates may give a misleading impression of the OC sequestration efficiency at each site, while giving an incorrect view of the spatial distribution of the rate of OC accumulation (see Fig. 1.4 for a case example). Knowing the rate at which sediments accumulate in coastal BCE, the proportion of OC that is buried, and the processes that affect this rate are among the critical aspects to be answered for assessing the role of vegetated coastal ecosystems in global C budgets (Duarte, 2017), as well as for proper environmental management (Syvitski et al., 2009) and C-offset valuation (Needelman et al., 2018).
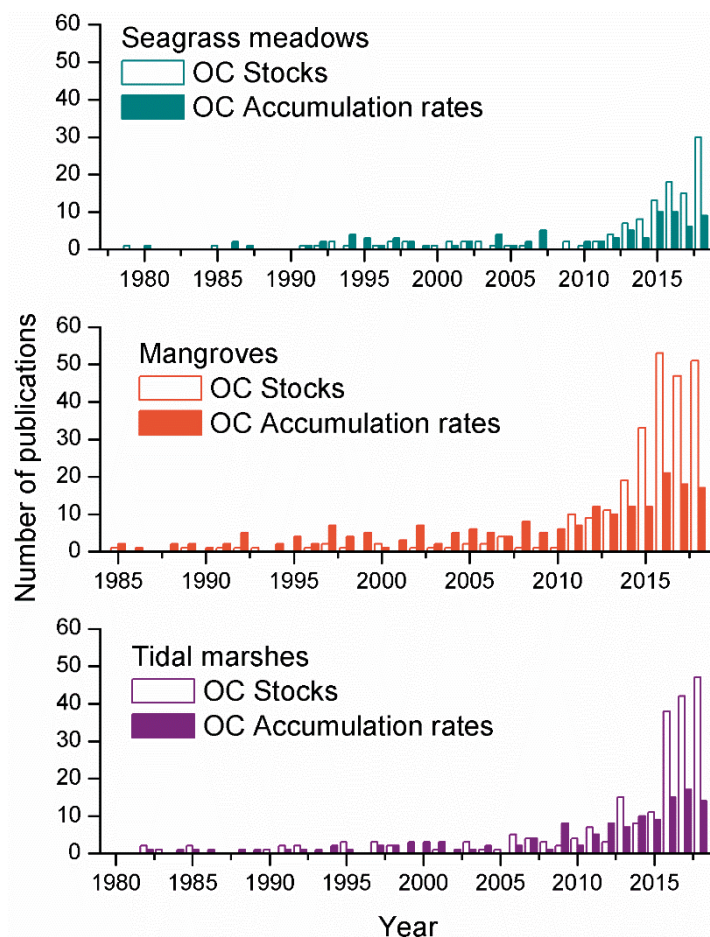
Figure 1.3: Number of publications reporting organic carbon stocks and accumulation rates in coastal BCE, Source: Web of Knowledge, accessed 09 October 2018.

Common methods for determining sediment and OC accumulation rates in BCE include the use of marker horizons or Surface Elevation Tables (SETs) or the dating of sediments using radioactive isotopes such as ^{210}Pb and ^{137}Cs, and/or [14]C. Each of these methods work on different timescales, ranging from months/years to decades/century to millennia. One of the focus of this thesis is the determination of accumulation rates derived from dating methods working at the centennial scale, such as ^{210}Pb or ^{137}Cs, providing a time frame compatible with management actions (Marland et al., 2001; Murray and Kasibhatla, 2013) and enabling the determination of OC accumulation rates and its changes with time due to both natural and human impacts. In *Chapter 3,* a critical review of the current status of ^{210}Pb dating methods of coastal BCE sediments is provided, together with an assessment of the limitations that apply to the determination of last century OC accumulation rates in such ecosystems driven by processes such as bioturbation, physical mixing, changes in accumulation rates, sediment erosion or organic matter remineralization.

	A $(0.052 \ \text{g·cm}^{-2}·\text{yr}^{-1})$*	B $(0.200 \ \text{g·cm}^{-2}·\text{yr}^{-1})$*
Top 1 meter stock (kg OC m^{-2})	20	12
Last 100 yr stock (kg OC m^{-2})	3	5
OC accumulation rate (kg OC m^{-2} yr^{-1})	30	50

Site B is 65% more efficient than A in sequestering OC, although having lower OC stocks in the upper 1 m (Data: Arias-Ortiz et al. 2018)
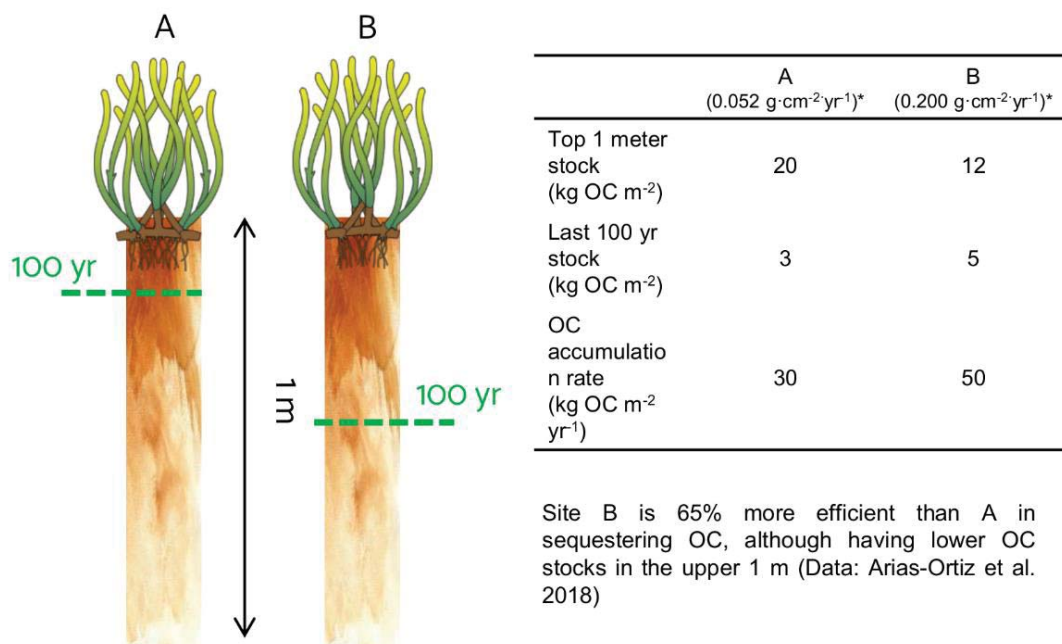
Figure 1.4: The effect of sedimentation rate on the inventory of organic carbon in the upper meter of sediments and on its accumulation rate. * mass accumulation rate estimated by means of ^{210}Pb dating.

1.3.2 Organic carbon accumulation rates in seagrass meadows

At the time this thesis was posed (2014), data on sediment OC stocks from a variety of regions and seagrass species were available and have continued to grow since then (Campbell et al., 2014; Fourqurean et al., 2012b; Röhr et al., 2018) (Fig. 1.3). In contrast, data on OC accumulation rates were remarkably scarce in seagrass ecosystems due to the difficulty in obtaining reliable accretion rates in these environments and the lack of available studies where sediment dating was carried out on seagrass beds compared to other blue carbon ecosystems (i.e., mangroves and tidal marshes). There were only 23 direct measurements of C accumulation rates in seagrass meadows, but these were estimated using different approaches and were restricted to few large species and locations. For example, OC accumulation rates existed for the Mediterranean *Podidonia oceanica* (n = 8; Mateo et al., 1997; Romero et al., 1994; Serrano et al., 2012), for the Australian *P. sinuosa* (n = 4; Serrano et al., 2014) and for the temperate *Zostera marina* (n = 3; Tokoro et al., 2014) estimated on a millennial timescale by means of ^{14}C. In contrast, centennial OC accumulation rates based on ^{210}Pb were available for Australian *P. australis* meadows (n= 4; Lavery et al. 2013b) and for *Thalassia testudinum* beds in Florida Bay (n = 4; Orem et al., 1999).

Due to the lack of estimates of OC accumulation rates in seagrass sediments, previous studies aiming to estimate the global C sink capacity of seagrass meadows combined direct and indirect estimates calculated over different time-scales, which not necessarily represented *in situ* OC accumulation in the seagrass bed (e.g., Duarte et al., 2010; Kennedy et al., 2010; McLeod et al., 2011) (Table 1.2). Most of the estimates of OC sequestration rates compiled in McLeod et al. (2011), the most cited paper reporting global OC sequestration rates in seagrasses, correspond to indirect estimates based on the sum of net community production (NCP) of seagrasses and allochthonous OC trapped in their sediments (references within McLeod et al., 2011: Duarte et al., 2010; Kennedy et al., 2010) which were combined with direct estimates of OC sequestration rates compiled by Duarte et al. (2005). The average of these estimates together provided a OC burial rate per unit area in seagrass meadows of 138 ± 38 g C m^{-2} yr^{-1} (or 48 - 112 Tg C yr^{-1}, globally), which is as much as 18% of the OC sequestered in ocean sediments globally (Kennedy et al., 2010).

Table 1.2: Published values of global OC sequestration rates in seagrass ecosystems. NCP is net community production.

Reference	OC burial rate per unit area			Method	Seagrass areal extent considered	Global OC burial rate
	$g\ C\ m^{-2}\ yr^{-1}$				$x10^3\ km^2$	$Tg\ C\ yr^{-1}$
Duarte et al. (2005)	83			^{14}C, sediment traps, biomass accretion	300	27.4
Duarte et al. (2010)	119	±	26	NCP	300 - 600	21-51 ; 41-101
Kennedy et al. (2010)	160	-	186	NCP + allochthonous OC burial	300 - 600	48 - 56 ; 96-112
McLeod et al. (2011)	138	±	38	Mean of direct and indirect estimates: Duarte et al. (2005, 2010) and Kennedy et al. (2010)	300 - 600	48 - 112

In contrast, a substantial number of direct estimates of OC accumulation rates in mangrove and tidal marsh ecosystems were already available at the time of McLeod's first global assessment of OC sequestration rates in coastal BCE. McLeod et al. (2011) included OC sequestration estimates by Chmura et al. (2003), which provided a thorough compilation of directly measured decadal to century-scale OC accumulation rates in mangrove and tidal marsh systems based on ^{210}Pb, ^{137}Cs and clay marker horizons together with others, also estimated either by ^{210}Pb or ^{14}C (Sanders et al., 2010 and Bird et al., 2004). As a result, tidal marsh and mangrove OC burial rates were estimated at 218 ± 24 and 226 ± 39 g C m^{-2} yr^{-1}, respectively.

Since McLeod et al. (2011), global OC sequestration rates in mangrove and tidal marshes have been reassessed using data on OC content in sediments combined with accumulation rates derived, in its majority, from a single approach, ^{210}Pb and ^{137}Cs dating (Breithaupt et al., 2012; Ouyang and Lee, 2014) (Fig. 1.5). However, a global reassessment of seagrass OC sequestration rates over modern timescales (last ~100 yr) has not yet been carried out. This thesis addresses the current gap in global estimates of sedimentary OC accumulation rates in seagrass ecosystems. In *Chapter 4*, we rely on a compilation and

analysis of 167 records from 62 sites on sediment chronologies based on ^{210}Pb dating and sediment OC concentrations from around the world.
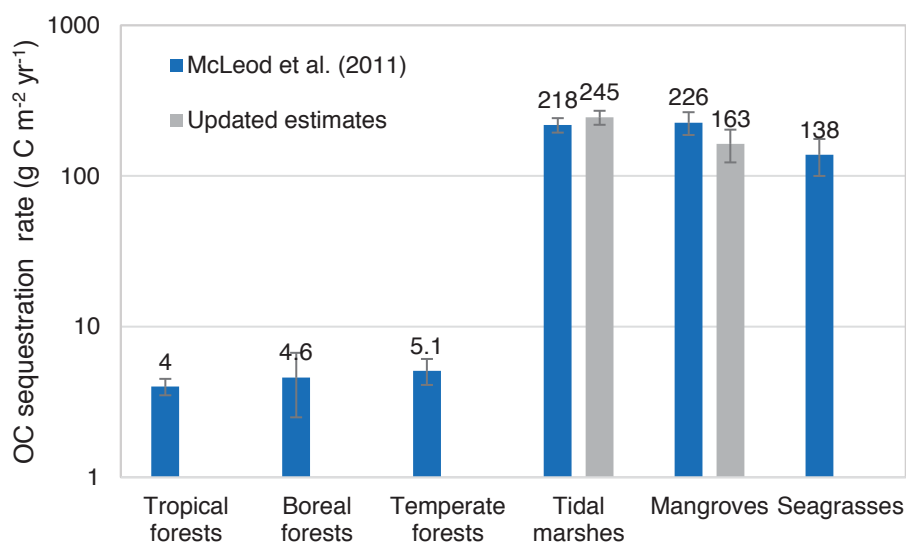
Figure 1.5: Estimates of carbon sequestration rates (g C m^{-2} yr^{-1}) in soils of terrestrial forests and in sediments of coastal vegetated ecosystems. Error bars indicate SE of the mean. Updated estimates by Breithaupt et al. (2012) and Ouyang and Lee (2014) in mangrove and tidal marsh ecosystems, respectively. Notice the logarithmic scale.

1.3.3 Vulnerability of sedimentary organic carbon to losses after disturbance

Although knowledge of sedimentary OC stocks in coastal BCE and rates of sequestration is increasing, there is little understanding of the fate of the OC deposits once vegetated coastal habitats are destroyed or disturbed. Yet, the vulnerability of sedimentary OC to losses following disturbance events is key to estimating the value of the stored OC in coastal BCE. Coastal BCE are being lost and degraded at a high rate (0.2% yr^{-1} to 2% yr^{-1}) (Duarte et al., 2008; Hamilton and Friess, 2018; Waycott et al., 2009) likely giving rise to substantial CO_2 emissions (Lovelock et al., 2017b; Pendleton et al., 2012) that could be avoided and mitigated with improved management (Rogers et al., 2014). Studies valuing C in intact coastal BCE assume that between 25 and 100% of the OC contained in the top meter of sediment is emitted to the atmosphere as CO_2 after habitat disturbance, allowing them to estimate the cost of coastal BCE based on current C pricing (Pendleton et al., 2012; Siikamaki et al., 2012). However, this critical assumption had not yet been proven at the start of this research. Recent studies suggest that sedimentary C losses may change depending

upon the fraction of OC exposed to oxic conditions and the type of BCE (Lovelock et al., 2017b), but also the nature of the OC stored and its recalcitrance (Enríquez et al., 1993; Trevathan-tackett et al., 2018), the time since disturbance (e.g. Lovelock et al., 2011), the type of disturbance (e.g. mangrove conversion to shrimp ponds or to pasture land; Kauffman et al., 2014, 2016), the hydrodynamic energy of the environment (i.e., sediment erosion; Marbà et al., 2015; Serrano et al., 2016) and the importance of lateral fluxes of C via groundwater (or pore-water) exchange (Maher et al., 2013, 2018).

If the vulnerability of sedimentary OC stocks after ecosystem disturbance could be well constrained as well as the uncertainties about the fate of sediment OC, the development of conservation and protection strategies of coastal BCE would be more robustly justified (Cullen-Unsworth and Unsworth, 2018; UNEP, 2014), while C-offset projects that already exist for terrestrial ecosystems could be expanded to coastal BCE (Herr and Landis, 2016). *Chapters 5 and 6* of this work contribute to improving the delimitation of sedimentary OC losses in seagrass and mangrove ecosystems in the event of disturbance by heat waves and clearcutting, respectively.

1.4 Aims and structure of the thesis

The aim of this thesis is to quantify OC sequestration rates and their controls over recent (~100 yr) time scales in natural and degraded coastal blue carbon ecosystems, with emphasis on seagrass meadows and mangrove forests. This is crucial to understand the capacity of coastal BCE to mitigate anthropogenic CO_2 emissions and the potentials for C financing projects, but also to understand the consequences of the widespread destruction of these habitats from an emissions perspective. To accomplish this aim:

i. In *Chapter 2*, we briefly explain the methodology and analysis required to determine organic C accumulation rates in coastal BCE sediments.

ii. In *Chapter 3*, we test the effects of sedimentary processes on ^{210}Pb dating estimates of sediment and OC accumulation rates. We discuss the implications of sedimentary processes such as mixing, changes in the sedimentation rate, erosion, grain size heterogeneity and organic matter (OM) decay in ^{210}Pb-derived chronologies and evaluate the discrepancies associated to OC accumulation rates between ideal and

anomalous ^{210}Pb records in each BCE. This work was published in *Biogeosciences* in November 2018.

iii. In *Chapter 4*, we reassess the OC sequestration rates in seagrass sediments globally, using published and unpublished data (produced by us) of sediment OC content and sedimentation rates derived by ^{210}Pb dating. This approach is similar and readily comparable to those used in global reassessments of OC sequestration rates in mangrove and tidal marshes allowing us to establish direct comparisons between ecosystems as well as to determine their relative contribution in the ocean C budget. This work is in preparation.

iv. In *Chapter 5*, we quantify seagrass area and OC stock losses due to a marine heatwave in Shark Bay, Western Australia, using data from sediment cores, satellite imagery and a published model based on varying proportions of seagrass OC being exposed to oxic conditions following disturbance. This work was published in *Nature Climate Change* in March 2018.

v. In *Chapter 6*, we assess whether and to what extent mangrove deforestation leads to losses of soil OC. This includes the study of the pathways of soil OC loss when forests are degraded, but soils remain in place. We estimate the fate and total change of soil OC since mangrove clearance by comparing biomass C pools, soil properties and OC content between intact and deforested plots as well as by measuring concentrations of DOC in waters nearshore of the intact and deforested mangrove areas. This work has been recently submitted to *Ecosystems*.

Finally, *Chapter 7* consists on a synthesis of the main results and conclusions arising from this thesis, and a brief discussion on the prospects for future research on Blue Carbon in vegetated coastal ecosystems is presented.

Chapter 2

General Methods

This chapter describes the basics of the ^{210}Pb methodology and the main dating models. The analytical procedures for the measurement of ^{210}Pb and sedimentary C are also included. Details on sampling methods, analyses of $\delta^{13}C$ and $\delta^{15}N$ and granulometry as well as DOC in surface waters are included in each chapter where pertinent.

2.1 Basics of the ^{210}Pb method

^{210}Pb is a naturally occurring radionuclide part of the ^{238}U decay chain with a half-life of 22.3 years. Particles that sink and accumulate in the bottom of aquatic systems scavenge ^{210}Pb that is present in the water column due to the decay of ^{222}Rn in 1) the atmosphere and ulterior dry and wet deposition and 2) in the water. This is known as "Excess ^{210}Pb" (^{210}Pb$_{xs}$) and is added to the "Supported ^{210}Pb" (^{210}Pb$_{sup}$), which is continuously produced by in situ decay of ^{226}Ra in bottom sediments. In situ decay of ^{226}Ra present in seawater can also produce ^{210}Pb$_{xs}$, although this fraction is negligible in shallow coastal environments. The accumulation of sediments over time ideally generates a decreasing distribution of ^{210}Pb specific activity as a function of depth (or cumulative mass in g cm^{-2}) governed by the decay of ^{210}Pb$_{xs}$, as illustrated in Figure 2.1.
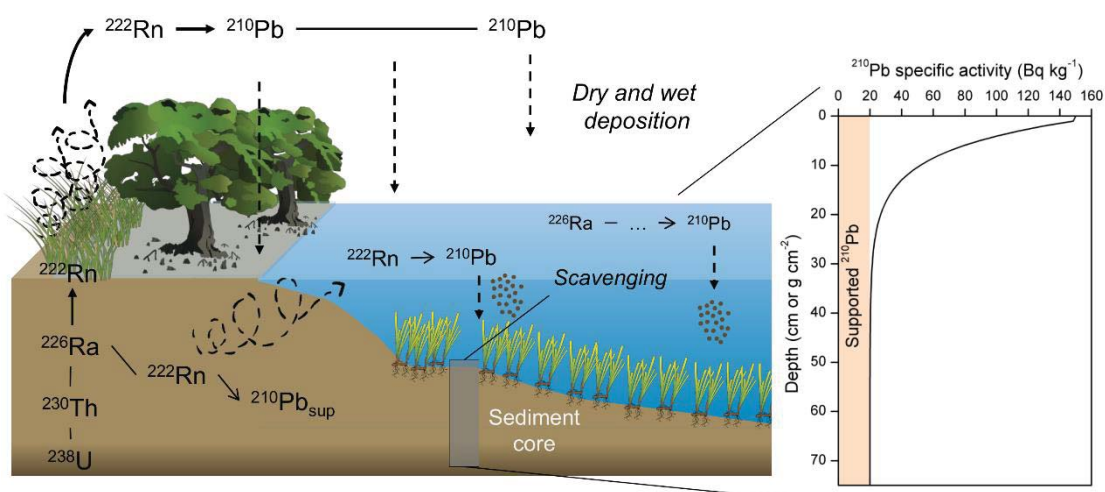
Figure 2.1: ^{210}Pb cycle and idealized ^{210}Pb profile in sediments. Images of vegetated coastal habitats: Tracey Saxby, Integration and Application Network, University of Maryland Center for Environmental Science (http://ian.umces.edu/imagelibrary/).

The ^{210}Pb dating models are based on the interpretation of the ^{210}Pb$_{xs}$ rate of decline in a sediment profile. Under ideal circumstances, ^{210}Pb can accurately date sediments back to about seven half-lives, i.e., about 150 years (the "dating horizon"), whereby the measurement uncertainty becomes too large to detect any ^{210}Pb$_{xs}$. However, chronologies reaching back that far might be rarely achievable in vegetated coastal sediments because these often contain relatively low concentrations of ^{210}Pb (< 100 Bq kg^{-1}). In these cases, the

dating will be restricted to 3–4 ^{210}Pb half-lives, i.e., 65–90 years. The distribution of ^{210}Pb$_{xs}$ in sediments can be described as (Koide et al., 1972):

$$\frac{\partial \rho C}{\partial t} = \frac{\partial}{\partial z} \cdot \left(D_b \rho \frac{\partial C}{\partial Z} \right) - \frac{r\, \partial \rho C}{\partial z} - \lambda \rho C \qquad \text{(Eq. 2.1)}$$

where ρ is sediment bulk density (g cm^{-3}), C is the concentration (or specific activity) of ^{210}Pb$_{xs}$ (Bq g^{-1}), z is depth below the sediment–water interface (cm), D_b is the sediment mixing rate (cm^2 yr^{-1}), r is the sedimentation rate (cm yr^{-1}), λ is the ^{210}Pb decay constant (0.0311 yr^{-1}) and t is time (yr). Commonly, depth (z) is represented as mass depth (m) to correct for compaction. Mass depth (g cm^{-2}) results from the multiplication of z and ρ, and sedimentation rates are expressed as mass accumulation rates (MAR) in g cm^{-2} yr^{-1}, which can be described as $MAR = \rho(v + q)$ where v and q are the accretion and compaction velocities, respectively (Abril, 2003) (Eq. 2.2).

$$\frac{\partial C}{\partial t} = \frac{\partial}{\partial m} \left(k_m \frac{\partial C}{\partial m} \right) - MAR \frac{\partial C}{\partial m} - \lambda C \qquad \text{(Eq. 2.2)}$$

where k_m is the effective mixing coefficient (g^2 cm^{-4} yr^{-1}). Under ideal conditions, where mixing is negligible, the ^{210}Pb$_{xs}$ specific activity satisfies the simple exponential relation:

$$C_m = C_0 \cdot e^{-\lambda t} \qquad \text{(Eq. 2.3)}$$

If the initial ^{210}Pb$_{xs}$ activity (C_0) of the sediment (i.e., that at surface) can be estimated, this equation can be used to calculate the time (t) since burial.

2.1.1 ^{210}Pb dating models

The first dating models were developed in the 1970's based on the above. In marine sediments, the ^{210}Pb technique was first applied by Koide et al. (1972). Since then, a family of dating models has been used to interpret the ^{210}Pb$_{xs}$ depth distribution in marine and freshwater sediment cores, increasing in variety and complexity and involving a large diversity of post-depositional redistribution processes (Table 4). However, there are three models that are most widely used and described here: the Constant Flux : Constant Sedimentation (CF:CS) model (Krishnaswamy et al., 1971), the Constant Rate of Supply (CRS) model (Appleby and Oldfield, 1978) and the Constant Initial Concentration (CIC) model (Robbins, 1978). Although these three models each have specific assumptions, they

share the following: (1) the deposition of $^{210}Pb_{xs}$ is at steady state, (2) there is no post depositional mobility of ^{210}Pb and (3) the deposition of $^{210}Pb_{xs}$ is ideal, i.e., new $^{210}Pb_{xs}$ inputs are deposited above the previously existing material. In the simplest of the cases, the CF:CS model assumes constant $^{210}Pb_{xs}$ depositional flux (Φ) and MAR. In this case, the ^{210}Pb specific activity at the surface (C_0: Bq kg^{-1}) is constant and decreases exponentially with cumulative mass. The depth of burial m is related to the elapsed time since burial through the rate of sedimentation (MAR) (Eq. 2.4). If there is mixing at the surface of the core, the mean MAR can be calculated from the $^{210}Pb_{xs}$ specific activity profile below the surface mixed layer (SML). If the specific activity of $^{210}Pb_{xs}$ decline in sections, showing two or more exponentially decaying segments, then, a mean MAR can be derived for each segment (Goldberg et al., 1977). In this way the model is, to some degree, able to cope with temporal variations in mass accumulation rates.

$$C_m = C_0 \cdot e^{-\lambda m/MAR}; \; t = \frac{m}{MAR} \qquad \text{(Eq. 2.4)}$$

Variations in the accumulation rate may occur in response to natural processes or anthropogenic influences. Under some such circumstances, the CRS or CIC models could be suitable. The CRS model assumes a constant flux of ^{210}Pb (Φ) to the sediments over time. The initial specific activity is variable and inversely related to MAR (higher MAR leads to lower $^{210}Pb_{xs}$ specific activity and *vice versa*). The dating is based on the comparison of $^{210}Pb_{xs}$ inventories (I_m; Bq m^{-2}) below a given depth (integration of $^{210}Pb_{xs}$ specific activity as a function of the cumulative mass) with the total $^{210}Pb_{xs}$ inventory in the sediment core (I) (Eq. 2.5). The accurate determination of the $^{210}Pb_{xs}$ inventories is critical and required for the application of the CRS model (Appleby, 2001).

$$I_m = I \cdot e^{-\lambda t}; \; MAR = \frac{\lambda I_m}{C_m} \qquad \text{(Eq. 2.5)}$$

The CIC model could be a better choice at locations where sediment focusing is a major factor, where event-deposit layers are present, or if significant hydrologic changes have occurred or there are hiatuses in the sediment record caused by erosion events (Appleby, 2008). The CIC model assumes that the initial $^{210}Pb_{xs}$ specific activity at the sediment-water interface is constant over time, regardless of the sedimentation rate, so that the $^{210}Pb_{xs}$ flux co-varies with MAR. This model permits estimation of the age (t) at any

depth where ^{210}Pb has been measured if the initial specific activity is known (Eq. 2.6). However, the CIC model requires a monotonic decrease of ^{210}Pb$_{xs}$ specific activity down-core to avoid age reversals, which is rare in most vegetated coastal sediments. In that event, the calculation of mean accumulation rates alone using the CF:CS model would be a more reasonable approach, as it might be too ambitious to calculate a detailed stepwise chronology based on often limited number of data points decreasing monotonically.

$$C_m = C_0 \cdot e^{-\lambda t} \qquad \text{(Eq. 2.6)}$$

While the CIC or CF:CS models have been typically used in the marine environment, the CRS model is the most preferred in lake sediments and is becoming widespread applied in estuarine environments and vegetated coastal ecosystems (Andersen, 2017; Breithaupt et al., 2014). Some of the reasons could be that it suffers less from problems associated with non-monotonic features in the ^{210}Pb record and is relatively insensitive to mixing (Appleby et al., 1983; Appleby and Oldfield, 1992; Oldfield et al., 1978). The selection and use of a particular model should be based on the nature of the ^{210}Pb$_{xs}$ specific activity and MAR. For further details on the main aspects relevant to the application of ^{210}Pb dating models in lacustrine or estuarine environments, two detailed and comprehensive book chapters by Appleby (2001) and Andersen (2017) are recommended. This thesis focuses specifically on analysis of ^{210}Pb dating of sediments in vegetated coastal ecosystems.

Table 2.1: Summary of the main ^{210}Pb-based models for sediment dating (adapted from Mabit et al., 2014).

Model	Assumptions	Analytical Solutions	References
CIC: Constant Initial Concentration	[1], $\Phi(t)/MAR(t) = Cte$	$C_m = C_0 \cdot e^{-\lambda t}$	(Robbins, 1978; Robbins and Edgington, 1975)
CF:CS: Constant Flux: Constant Sedimentation	[1], [2], [3]	$C_m = C_0 \cdot e^{-\lambda m/MAR}; \quad t = \dfrac{m}{MAR}$	(Krishnaswamy et al., 1971)
CRS: Constant Rate of Supply	[1], [2]	$I_m = I \cdot e^{-\lambda t}; \quad MAR = \dfrac{\lambda I_m}{C_m}$	(Appleby, 2001; Appleby and Oldfield, 1978)
CMZ:CS Complete Mixing Zone with constant SAR	[2], [3], $k_m = \infty, m \geq m_a$ $k_m = 0, m < m_a$	$C_m = C = \dfrac{\Phi}{MAR + \lambda m_a}, m \geq m_a$ $C_m = C \cdot e^{-\lambda (m-m_a)/MAR}, m < m_a$	(Robbins and Edgington, 1975)
CF:CS-Constant Diffusion	[2], [3], $k_m = Cte$	$C_m = \dfrac{\Phi}{MAR - k_m \beta} e^{-\beta m};$ $\beta = \dfrac{MAR - \sqrt{MAR^2 + 4\lambda k_m}}{2 k_m}$	(Laissaoui et al., 2008; Robbins, 1978)
CF:CS-depth dependent diffusion and/or translocational mixing	[2], [3], $k_m = f_m$; may include local sources and sinks	General numerical solution	(Abril, 2003; Abril and Gharbi, 2012; Robbins, 1986; Smith et al., 1986)
IMZ: Incomplete Mixing Zone	[2], [3]	A linear combination of solutions for CF-CS and CMZ-CS with coefficients g and $(1 - g)$, being $g \in [0, 1]$	(Abril et al., 1992)
SIT: Sediment Isotope Tomography	[1]	$C_m = C_0 \cdot e^{-B \cdot m} \cdot$ $\cdot e^{\sum_{n=1}^{N} a_n sin\left(\frac{n\pi m}{m_{max}}\right) + \sum_{n=1}^{N} b_n\left(1 - cos\frac{n\pi m}{m_{max}}\right)}$	(Carroll and Lerche, 2003)
NID-CSR: Non-Ideal-Deposition, Constant Sedimentation Rate	[1], [2], [3], fractioning of fluxes, depth distribution	$C_m = C_1 \cdot e^{-\lambda m/MAR} + C_2 \cdot e^{-\alpha m};$ $C_2 = \dfrac{-\alpha g \Phi}{\alpha MAR - \lambda};$ $C_1 = \dfrac{(1-g)\Phi}{MAR} - C_2$	(Abril and Gharbi, 2012)
CICCS: constant initial concentration and constant sedimentation rate	[1], [2]	$MAR = \lambda \dfrac{I - I_{ref}}{C_r};$ I_{ref} = local fallout ^{210}Pb inventory; C_r = Initial [210]Pb$_{xs}$ in catchment-derived sediment.	(He and Walling, 1996b)
IP-CRS: Initial Penetration-Constant Rate of Supply	[2], initial mobility of [210]Pb$_{xs}$ downward; two compartments 0 to z_k and z_k to ∞	$C_{i\,(z)} = A_i e^{\theta + (i)z} + B_i e^{\theta - (i)z};$ $from\ 0\ to\ z_k$ $C_{i\,(z)} = A_i e^{\sigma + (i)z} + B_i e^{\sigma - (i)z} + \dfrac{F_i}{\lambda};$ $from\ z_k\ to\ \infty$ $F_i = \dfrac{f_i}{(z_i - z_{i-1})} \sum_{m=1}^{k} \int_{z_{m-1}}^{z_m} r_m C_m\, dz;$ $\sum f_i = 1$ $See\ reference\ for\ constants$	(Olid et al., 2016)
TERESA: Time estimates from random entries of sediments and activities	[1], [210]Pb$_{xs}$ fluxes are governed by horizontal inputs, correlation with MAR	$C_1 = C_0 \cdot e^{-\lambda \Delta T_0} \cdot \dfrac{1 - e^{-\lambda \Delta T_1}}{\lambda \Delta T_1}$ $C_m = C_0 \cdot e^{-\lambda\left(T_0 + \frac{\Delta_{m-1}}{MAR_{m-1}}\right)} \cdot \dfrac{1 - e^{-\lambda \Delta T_m}}{\lambda \Delta T_m}$	(Abril, 2016; Botwe et al., 2017)

[1] Non post-depositional redistribution; [2] constant [210]Pb$_{xs}$ fluxes at the SWI; [3] constant MAR. Constants: C_m: [210]Pb$_{xs}$ activity concentration in sediments at mass depth m; I: total inventory of [210]Pb$_{xs}$; I_m: excess inventory accumulated below depth m; k_m: effective mixing coefficient (Db^2); m_a: mass thickness of top sediment zone; Φ: Flux of [210]Pb$_{xs}$ onto the sediment; g: fraction of [210]Pb$_{xs}$ flux distributed within a certain mass depth; F_i: additional supply of [210]Pb$_{xs}$ to layer i.

2.2 ^{210}Pb and ^{226}Ra analyses

The specific activities of ^{210}Pb were determined by α-spectrometry through the analysis of its granddaughter ^{210}Po assuming secular equilibrium between the two radionuclides at the time of analyses. ^{210}Po analyses were carried out following the method described in Sanchez-Cabeza et al. (1998) that involves total digestion of sediment samples, preconditioning and auto-plating of ^{210}Po isotopes into silver disks for measurement.

Before total digestion, plant material and shells were removed from sediment samples when pertinent and samples were homogenized using a pestle and mortar. Then, between 150 and 300 mg of dry sediment aliquots were transferred into 100 mL Teflon liners and digested in a concentrated acid media (HNO_3:HF, 9:3 mL) using an analytical microwave in the presence of a known amount of ^{209}Po added as an internal tracer (A = 0.395 ± 0.014 Bq g^{-1} at 30 Oct 2011). After digestion, 15 mL of H_3BO_3 (v/v 4%) were added to complex fluorides by microwaving at 180ºC for 45 min. After allowing the samples to cool down to ambient temperature, they were transferred into Teflon beakers, rinsing the liners with 1M HCl, and evaporated until incipient dryness. When dry, 1 to 2 mL of concentrated HCl (37%) were added and evaporated, and repeated 2 more times.

Preconditioning was done by adding 100 mL of 1M HCl to dry digestates and heating under reflux at 80-90 ºC on a stirring plate for about 15 to 30 min. Then, solutions were transferred into glass beakers, rinsing the Teflon beakers with 1M HCl, and were heated under the previous conditions. Ascorbic acid ($C_6H_8O_6$) was added in small quantities to reduce Fe^{3+} to Fe^{2+} until a colorless was obtained.

Silver discs, one side of which was covered by a neutral lacquer, were dipped into the aqueous solutions and Po isotopes were spontaneously plated on the disc in solution at a temperature of approximately 90 ºC for about 8 hours and while stirring. After plating, discs were removed, rinsed with deionized water, air dried and stored in labeled envelopes.

For each set of samples an analytical blank, replicates (usually the upper cm of each sediment core) and a reference material (IAEA 315, Marine Sediment) were run alongside to assess contamination, reproducibility and accuracy of the results.

^{210}Po and ^{209}Po were measured using PIPS (Passivated Implanted Planar Silicon) and silicon surface barrier α-spectrometers (CANBERRA, model PD-45.18 A.M. and EG&G Ortec Mod. SSB, respectively). This measurement method was chosen to the detriment of γ-spectrometry due to:

- Sample size limitations: OC and N, δ^{13}C δ^{15}N and grain size analyses were also conducted using the same sediment slices, hence in most occasions, less than 2 g of dry sample were available for ^{210}Pb analyses.

- Total number of samples was large (~12 samples per core, > 50 cores): α-spectrometry has a higher sample throughput and generally lower counting time. Additionally, a total of 26 α-detectors are available at the Environmental Radioactivity Laboratory, while there only 4 γ-detectors are installed.

- Specific activities of ^{210}Pb were generally low (at surface ~50 Bq kg^{-1};): α-spectrometry has lower background and higher sensitivity compared to γ-spectrometry.

The specific activities of ^{226}Ra in seagrass and mangrove sediments were determined by γ-spectrometry via its daughter nuclide ^{214}Pb emissions at 295 and 352 keV using calibrated geometries in a HPGe detector (CANBERRA, Mod. GCW3523 and Mod. SAGe Well). Sample pre-treatment consisted in placing a known amount of homogenized dry sample into a cylindrical polyethylene counting vial (5.65 cm^3) according to previously calibrated geometries for different sample volumes: V_1 = 5.65 cm^3; V_2 = 4.94 cm^3; V_3 = 4.24 cm^3; V_4 = 3.53 cm^3; V_5 = 2.83 cm^3; V_6 = 2.12 cm^3; V_7 = 1.41 cm^3. To avoid diffusion of ^{222}Rn, counting vials were sealed and stored for 21 days to ensure secular equilibrium between ^{226}Ra and its daughter radionuclides. Samples were counted for as long as necessary to reach uncertainties lower than 5% but with a maximum counting time of 400,000 s. The spectrum analysis to obtain the specific activities of the radionuclides of interest was carried out using the Genie 2000 Gamma Analysis Software. An advantage of γ-spectrometry is that it allows simultaneous determination of ^{226}Ra as well as other radionuclides (e.g., ^{137}Cs, ^{141}Am, ^{228}Th). However, specific activities of ^{137}Cs or ^{141}Am, for instance, were below the

minimum detectable activity in most of the analyzed samples. The specific activities of ^{226}Ra measured in mangrove and seagrass sediments were usually low and ranged between 9 ± 2 and 33 ± 3 Bq kg^{-1} and 2.3 ± 2.0 and 18 ± 2 Bq kg^{-1}, respectively. Indeed, biogenic seagrass sediments returned extremely low counting rates, of similar order of magnitude as background activities (12 ± 2 Bq kg^{-1}). Because background and sample measurements are not carried out simultaneously, little changes in the background activity over time were leading to significantly different ^{226}Ra results for a same sample. For that reason, Liquid Scintillation Counting was used to determine ^{226}Ra specific activities in seagrass sediments by ^{222}Rn emanation to a scintillation cocktail. When counting a ^{226}Ra aqueous solution with an immiscible scintillant, its α emitter-daughter ^{222}Rn (highly soluble and selectively extracted in oil-based scintillators) and α emitter-granddaughters ^{218}Po and ^{214}Po are counted simultaneously. Because the probability of these α decays is in all cases close to one, the maximum counting efficiency that can be reached using this method is up to 300%, as opposed to γ-spectrometry, where final counting efficiencies for ^{226}Ra normally do not usually exceed a few percent.

We applied methods adapted from Masqué et al. (2002). Briefly, the solution from which the Po was auto-plated (about 80 - 100 mL) was recovered and heated under reflux for about 30 min with 5 mL of concentrated HNO$_3$ to destroy ascorbic acid and its degradation compounds, thus obtaining a clear solution. This solution was then evaporated to incipient dryness, and small amounts of 0.5 M HCl were added to dissolve the residue. This operation was carried out two more times to ensure the elimination of HNO$_3$. The total volume was then adjusted to 10 mL using 0.5 M HCl in a 20 mL low-diffusion PE counting vial. Then 10 mL of OptiScint HiSafe cocktail was carefully added by avoiding disturbing the interface formed by the two immiscible liquids in the vial. Vials were kept for 21 days in a dark temperature-controlled area (i.e., the lab fridge), in order to wait for radioactive equilibrium and to minimize chemiluminescence. The samples were counted sequentially using an ultralow background liquid scintillation system, Quantulus 1220TM (Wallac, Turku, Finland) for 1 h each, during a minimum of 15 cycles, PSA was set at 145. Blanks, replicates and the reference material (IAEA 315) were run in parallel. Detection efficiency

for each sample was determined with the standard quenching parameter (SQP(E)) through a calibration curve and averaged $230 \pm 20\%$.

2.3 Carbon and Nitrogen analyses

The OC content of sediments is readily measurable and for samples analyzed in this thesis an elemental analyzer was used to determine sediment OC, after sample acidification with HCl (for details refer to the methods section in each chapter). This method is widely used in the blue carbon literature and provides a direct measurement of the OC content, but also organic nitrogen content, in the analyzed material. Likewise, total C and nitrogen (TC and TN) can also be determined if samples are not acidified prior to combustion in the CN analyzer. Inorganic C (IC) can be estimated by subtracting OC from TC.

The other common method being used is Loss On Ignition (LOI), where dried samples at 60 ºC are combusted between 450 - 550ºC during approximately 4 to 8 hours (Heiri et al. 2001; Fourqurean et al. 2014). Both methods are a combustion processes but LOI gives a measurement of the organic matter content (OM) as a percent of the sample dry weight and is calculated as follows:

$$\%LOI = \frac{DW\ before\ combustion - DW\ after\ combustion}{DW\ before\ combustion} \cdot 100 \quad \text{(Eq. 2.7)}$$

where DW is dry weight of the sample.

Values reported as %OM need to be converted to OC% through the linear fit between %OM and %OC determined for a set of samples from the same study area using both methods. If such empirical relation is not available, researchers have developed general equations to convert OM% to OC% that are specific to each coastal BCE (Table 2.2).

The advantage of using an elemental analyzer is that the nitrogen (N) content of the sediment is also obtained, hence gives a value on nutrient availability and C:N ratio, which is an indication on the quality and decomposition phase of the organic matter (Christensen, 1992). The relationship between OC and N can be used to estimate the stability of the organic matter, and if the C:N ratio does not change over time (i.e., depth, given that there is a no mixing of the sediment) this can be an indication of stable recalcitrance OC (Mateo et al., 2006). Stable isotopes of sedimentary OC and N, $\delta^{13}C$ and $\delta^{15}N$, were analyzed in studies

contained in *Chapter 5 and 6* to determine individual contributions of different OM sources to the sedimentary OM pool. Concentrations of DOC in surface waters were measured in the study in *Chapter 6*. Because these methods are specific, please refer to the *Methods* section within each chapter.

Table 2.2: General relationship between % LOI and % OC for the different coastal BCE. Other location-specific equations are reported in Howard et al. (2014b).

Coastal BCE	Conversion equation	Reference
Seagrass	$\%OC = 0.43 \cdot \%LOI - 0.33$	Fourqurean et al. (2012)
Mangrove	$\%OC = 0.415\ \%LOI + 2.89$	Kauffman and Donato, (2012)
Tidal marsh	$\%OC = 0.40\ \%LOI + 0.0025(\%LOI)^2$	Craft et al. (1991)

2.4 Estimation of organic carbon accumulation rates

The OC accumulation rate (CAR) can be obtained by measuring the content of OC in sediments and ascribing dates to either the entire profile of interest or to specific intervals, or by estimating sediment accumulation rates as described in equation 2.8.

$$CAR = \frac{\sum_{n=i}^{t} (\%OC_i \cdot m_i)}{m_t} \cdot MAR_t \qquad \text{(Eq. 2.8)}$$

where *(%OC$_i$ · m$_i$)* is the mass per unit area of OC at layer *i* (g C m^{-2}), *m$_t$* is the cumulative mass over the period (*t*) (g m^{-2}) and *MAR$_t$* is the mean mass accumulation rate of the period of interest (*n-t*) (g m^{-2} yr^{-1}). When CAR is examined over the last century, *m$_t$* is the cumulative mass down to the ^{210}Pb$_{xs}$ horizon (i.e., the depth at which ^{210}Pb$_{xs}$ specific activity approaches zero) and *MAR$_t$* is the mean, last century, mass accumulation rate.

Chapter 3

²¹⁰Pb-derived sediment and carbon accumulation rates in vegetated coastal ecosystems - setting the record straight[1,2]

In this chapter, we discuss the use of the ^{210}Pb dating technique to determine the rate of OC accumulation in coastal BCE. We review the most widely used ^{210}Pb dating models to assess their limitations in these ecosystems, often composed of heterogeneous sediments with varying inputs of organic material and often affected by sediment mixing and changes in sedimentation rates or erosion. Through a range of simulations, we consider the most relevant processes that impact the ^{210}Pb records in vegetated coastal ecosystems and evaluate how anomalies in ^{210}Pb specific activity profiles affect sediment and OC accumulation rates (CAR). Our results show that the discrepancy in sediment and derived CAR between anomalous and ideal ^{210}Pb profiles is within 20% if the process causing such anomalies is well understood. While these discrepancies might be acceptable for the determination of mean sediment CAR over the last century, they may not always provide a reliable geochronology or historical reconstruction. Reliable estimates of CAR might be difficult at sites with slow sedimentation, intense mixing and/or that are affected by multiple sedimentary processes. Additional tracers or geochemical, ecological or historical data need to be used to validate the ^{210}Pb derived results.

---

[1] Based on: Arias-Ortiz, A., Masqué, P., Garcia-Orellana, J., Serrano, O., Mazarrasa, I., Marbà, N., Lovelock, C. E., Lavery, P. and Duarte, C. M.: Reviews and syntheses: ²¹⁰Pb-derived sediment and carbon accumulation rates in vegetated coastal ecosystems: setting the record straight, Biogeosciences, 15, 6791–6818, doi:10.5194/bg-2018-78, 2018.

[2] Data to replicate the dating models and formulas used to conduct the simulations in this chapter can be found online in the Supplement, Excel Tables S1–S7 https://www.biogeosciences.net/15/6791/2018/

3.1 Introduction

Recognition of the globally significant role of vegetated coastal habitats, including tidal marsh, mangrove and seagrass, as sinks of carbon dioxide (CO_2) (Duarte et al., 2013b) has generated interest in the potential to mitigate CO_2 emissions through the management of these ecosystems, an approach termed "Blue Carbon" strategy (Duarte et al., 2013b; McLeod et al., 2011; Nellemann et al., 2009). However, efforts to include vegetated coastal ecosystems into existing carbon mitigation strategies have met with an important limitation: there is a paucity of estimates of OC sequestration rates, particularly in seagrass habitats (Johannessen and Macdonald, 2016, 2018; Macreadie et al., 2018).

Two interrelated measurements of importance to the rate of OC sequestration are the sediment OC content and the sediment accumulation rate. To date, most of the research has focused in the first term, which informs about the OC stock sequestered in sediments (Howard et al., 2014a; Pendleton et al., 2012). However, OC stocks alone cannot be used to fully assess the OC storage capacity or to establish comparisons among sites. Measurements of OC accumulation rates (CAR) address the question of how much OC is sequestered in a specified time period and quantify the ongoing sink capacity. In general, CAR is obtained by measuring the concentration of OC in sediments and ascribing dates to either the entire profile of interest or to specific intervals, or by estimating sediment accumulation rates. Determination of mean CAR is partially dependent on the time scale of interest and the dating methods used. ^{210}Pb has been shown to be an ideal tracer for dating aquatic sediments deposited during the last ca. 100 yr, providing a time frame compatible with management actions (Marland et al., 2001) and enabling the determination of CAR and its changes with time due to natural or human impacts. Due to the relatively long integration period (decades to a century), mean ^{210}Pb-derived CAR estimates are not affected by interannual variability, hence allowing the assessment of shifts in OC accumulation from the "baseline" condition (i.e., the OC that naturally cycles through an ecosystem; Howard et al., 2017). Although several review papers have elaborated the applications of ^{210}Pb as a tracer in lacustrine and marine environments (Appleby, 2001; Baskaran et al., 2014; Du et al., 2012; Kirchner and Ehlers, 1998; Mabit et al., 2014; Sanchez-Cabeza and Ruiz-Fernández, 2012; Smith, 2001), little attention has been paid to the potential limitations of the ^{210}Pb dating method in

vegetated coastal sediments. Experience shows that vegetated coastal environments often prove to be more challenging than lake or marine sediments (Saderne et al., 2018).

Vegetated coastal ecosystems may act as closed systems, where the sediment accumulation is mainly associated with the build-up of autochthonous organic and inorganic material (McKee, 2011). In this situation, ^{210}Pb is deposited primarily from atmospheric fallout at steady state, with no post depositional mobility except for physical or biological mixing of the sediments (e.g. Alongi et al., 2004; Cochran et al., 1998; Marbà et al., 2015). In some cases, however, the process responsible for incorporating ^{210}Pb into the sediments might be more complex. Vegetated coastal ecosystems may receive both autochthonous and allochthonous sediments from the upstream catchment, coastal erosion or from the offshore zone during storm events (Turner et al., 2007), or in response to land use change (Mabit et al., 2014; Ruiz-Fernández and Hillaire-Marcel, 2009). Their sediments might be reworked through the action of fauna (bioturbation), tides, currents, and waves as well as through boat anchoring, dredging or fishing activities (e.g. Mazarrasa et al., 2017; Sanders et al., 2014; Serrano et al., 2016a; Smoak et al., 2013). Effects associated with climate change, such as sea level rise and extreme climatic events, may also have an impact on rates of production and decomposition of organic matter (OM) and on sediment and OC accumulation (Alongi et al., 2008; Arias-Ortiz et al., 2018a; Mudd et al., 2010). In such instances, sediment redistribution processes and complex accretion dynamics may violate some of the assumptions of the ^{210}Pb dating models, producing anomalous ^{210}Pb specific activity profiles that are difficult to interpret.

Sediments of vegetated coastal ecosystems are known to be heterogeneous, consisting of coarse grained sediments or bedrock covered by deposits of fine grained sediments that settled as vegetation established (McGlathery et al., 2012; Olff et al., 1997). The percentage of living (e.g. roots) and recently formed organic material is greatest in the upper 10 cm and may be affected by varying inputs of detrital sediment within vegetated coastal ecosystems and by its relative rate of decomposition. While tidal marsh and mangrove sediments have relatively high organic matter content (on average 25%) (Breithaupt et al., 2012; Cochran et al., 1998), mineral deposits account for the majority (>85%) of the accumulated substrate in seagrass sediments (Koch, 2001; Mazarrasa et al.,

2015) (Table 3.1). ^{210}Pb has a strong affinity for fine sediments (Chanton et al., 1983; Cundy and Croudace, 1995; He and Walling, 1996a) and organic matter (Wan et al., 2005), thus any changes in these parameters due to sediment redistribution processes or to natural heterogeneity may also result in unique types of ^{210}Pb specific activity profiles in sediment cores of vegetated coastal ecosystems, adding complexity to the determination of sediment model age and sedimentation rates.

Table 3.1: Common values of main parameters of vegetated coastal sediments (seagrass, mangrove and tidal marshes): average dry bulk density (DBD), range of sedimentation rates (mean values are provided in brackets) and organic matter (OM) content, median organic carbon (OC) contents, and decay rate of buried OC (from above ground biomass to refractory sediment OC).

Habitat Type	DBD[a] (g cm^{-3})	Sediment and mass accumulation rate [b]		OM[c] (%)	OC[d] (%)	Decay rate of buried OC[e] (d^{-1})
		SAR (mm yr^{-1})	MAR (g cm^{-2} yr^{-1})			
Seagrass	1.03	0.61 – 6 (2)	0.06 – 0.62 (0.21)	0.5-16.5	2.5	0.01- 0.00005
Mangrove	0.45	1.0 – 36 (7.7)	0.05 – 1.62 (0.33)	7-25	7.0	0.03 – 0.00005
Tidal marsh	0.43	0.7 - 42 (6.2)	0.03 – 1.81 (0.26)	5-80	9.0	0.005 - 0.00005

[a] Seagrass (Fourqurean et al., 2012b); Mangrove (Donato et al., 2011) and Tidal marsh (Craft, 2007; Hatton et al., 1983). [b] Seagrass (Duarte et al., 2013b), mangroves (Breithaupt et al., 2012) and tidal marsh (Ouyang and Lee, 2014). [c] Seagrass (Koch, 2001); Mangrove (Breithaupt et al., 2012); Tidal marsh (Cochran et al., 1998; Ember et al., 1987). [d] Seagrass (Fourqurean et al., 2012b); Mangrove (Breithaupt et al., 2012); Tidal marsh (Chmura et al., 2003). [e] Seagrass, mangrove and tidal marsh (Lovelock et al., 2017b).

Here, we present how the processes of mixing, changes in the sedimentation rate, erosion, grain size heterogeneity and OM decay impact the depth distribution of ^{210}Pb in vegetated coastal sediments. We compare sediment and OC accumulation rates derived from disturbed and ideal ^{210}Pb profiles and assess the discrepancy between them. Through a set of simulations, based on examples from the literature and using various ^{210}Pb dating models, we assess the limitations that apply to the determination of last century OC accumulation rates in such ecosystems. Finally, we provide guidance on complementary analyses to accompany the ^{210}Pb dating technique that can improve sediment and derived OC accumulation rate estimates.

3.2 Methods

We performed a literature review of studies on sediment accumulation in vegetated coastal ecosystems in the Web of Science^{TM} (accessed August 23, 2018) with the keywords mangrove sediment, salt marsh OR saltmarsh OR tidal marsh sediment, seagrass sediment AND ^{210}Pb OR Pb-210 OR lead-210. The search produced 86, 223 and 27 results, respectively, all of them using one or more of the three models described above, probably due to its simplicity, with some exceptions such as Klubi et al. (2017) that additionally uses the TERESA model (Table 2.1). From the literature review, we identified the most common sedimentary processes that result in anomalous types of ^{210}Pb$_{xs}$ specific activity profiles with depth. These could be summarized in five main processes: mixing, increasing sedimentation, erosion, changes in sediment grain size, and decay of organic matter (OM). Then, we simulated the target processes on initial undisturbed seagrass, mangrove and tidal marsh sediments to determine the potential discrepancies in MAR between ideal and anomalous ^{210}Pb$_{xs}$ profiles and analyse the limitations of the ^{210}Pb dating technique to derive CAR in these ecosystems. Throughout this work, we refer to "deviation" in MAR or CAR as the difference between the value which has been computed and the value estimated from the ideal ^{210}Pb$_{xs}$ profile.

3.2.1 Numerical simulations

All simulations started from an ideal ^{210}Pb$_{xs}$ profile, complying with all assumptions, that was then manipulated to reflect the potential effect of each process. The ideal ^{210}Pb$_{xs}$ profile was modelled considering the following: (1) a constant flux of ^{210}Pb$_{xs}$ (Φ) of 120 Bq m^{-2} yr^{-1} i.e., the average global atmospheric flux reported by Preiss et al. (1996); (2) a MAR of 0.2 g cm^{-2} yr^{-1} and dry bulk density (DBD) of 1.03 g cm^{-3} to represent seagrass sediments; and (3) a MAR of 0.3 g cm^{-2} yr^{-1} and DBD of 0.4 g cm^{-3} to represent mangrove/tidal marsh sediments based on typical values representative of these ecosystems (Duarte et al. 2013) (Table 3.1). Simulated surface activity per unit area of ^{210}Pb$_{xs}$ ($I_{0;}$ in Bq m^{-2}) in ideal profiles was estimated through equation 3.1. Then equation 3.2 was applied to estimate ^{210}Pb$_{xs}$ activities per unit area along the ideal profile (Supplementary, Table S1).

$$I_0 = \frac{\Phi}{\lambda}\left(1 - e^{-\lambda\, m_0/MAR}\right) \tag{Eq. 3.1}$$

$$I_m = I_0 \cdot e^{-\lambda\, m/MAR} \tag{Eq. 3.2}$$

Activities of ^{210}Pb$_{xs}$ per unit area *(I$_m$)* were then converted to activities per unit mass, *C$_m$* in Bq kg^{-1}, by dividing *I$_m$* by the cumulative mass *(m)* and converting g to kg at each layer. Ideal profiles were then altered to simulate the following processes/scenarios: mixing (surface and deep mixing), increasing sedimentation (by 20%, 50%, 100% and 200%), erosion (recent and past), changes in sediment grain size (coarse and heterogeneous) and OM decay (under anoxic and oxic conditions, and with labile OM contribution in sediments containing 16.5% and 65% OM) (Table 3.2). Refer to Appendix A for a detailed description of the methodology used to conduct each simulation.

The CF:CS and CRS dating models were applied to the simulated ^{210}Pb$_{xs}$ profiles to determine the average MAR for the last century (Table 2.1). The CIC model was excluded from the simulations presented in this study because in anomalous ^{210}Pb$_{xs}$ profiles: 1) the CRS model would lead to more reasonable approaches when the flux of ^{210}Pb$_{xs}$ is constant; and 2) when that is not the case (e.g., simulations of erosion or heterogeneous grain size), determination of mean accumulation rates alone by the CF:CS model would be a more reasonable approach. The models were applied in accordance with the simulated process. For instance, MAR was determined below the surface mixed layer in mixing simulations using the CF:CS, and piecewise in those with a change in average MAR (Appendix A). However, the models were also applied considering that (1) ^{210}Pb$_{xs}$ profiles of mixing simulations were generated by increasing MAR and *vice versa*, and (2) erosion was not a factor in simulated scenarios H to J. This was done to test the potential disagreement in MAR and CAR relative to the ideal profile if the incorrect process was assumed and dating models were applied. Once the dating model was established, the OC accumulation rate (CAR) was estimated through equation 8 assuming average sediment OC contents of 2.5% in seagrass and 8% in mangrove/tidal marsh, in both ideal and simulated sediment profiles.

Table 3.2: Summary description of the numerical simulations conducted to test for the effects of sedimentary processes on $^{210}Pb_{xs}$ specific activity profiles in seagrass and mangrove/tidal marsh sediments. MAR and CAR results derived from simulated profiles were compared with MAR and CAR estimates derived from the ideal $^{210}Pb_{xs}$ profiles reported here. k_s is the decay rate of the refractory sediment organic matter (OM) under anoxic conditions and k_{ox} is that in oxic conditions. K_{lb} is the decay constant of the labile OM derived from seagrass and mangrove/tidal marsh ecosystems (0.01 yr^{-1} and 0.03 yr^{-1}, respectively).

Influencing Factor	Scenario	Description	MAR Ideal profile (g cm^{-2} yr^{-1})		CAR Ideal profile (g C m^{-2} yr^{-1})	
			Seagrass	Mangrove/ Tidal marsh	Seagrass	Mangrove/ Tidal marsh
Mixing	A	Random upper 5 cm	0.20	0.30	50	240
	B	Random upper 5 cm	0.20	0.30	50	240
	C	Random upper 5-10 cm	0.20	0.30	50	240
Increasing MAR in recent years	D	Increased basal MAR by 20%	0.21	0.31	52	248
	E	Increased basal MAR by 50%	0.22	0.32	54	259
	F	Increased basal MAR by 100%	0.23	0.35	59	278
	G	Increased basal MAR by 200%	0.27	0.40	67	317
Erosion	H	Removal of $^{210}Pb_{xs}$ inventory from 0-5 cm	0.20	0.30	50	240
	I	Removal of $^{210}Pb_{xs}$ inventory from 5-10 cm	0.20	0.30	50	240
	J	Removal of $^{210}Pb_{xs}$ inventory from 10-15 cm	0.20	0.30	50	240
Grain size	K	Coarse sediment (70% coarse, 20% medium sand, 10% silt)	0.20	0.30	50	240
	L	Fine surface sediments (50 - 80% of clays at surface)	0.20	0.30	50	240
	M	Coarse surface sediments (50 - 80% of sands at surface)	0.20	0.30	50	240
	N	Heterogeneous grain size (alternated sand layers with clay layers)	0.20	0.30	50	240
OM decay		16.5% OM				
	O	100% w/ ks = 0.00005 d^{-1}	0.17	0.25	34	150
	P	50% w/ kox = 0.0005 d^{-1}	0.17	0.25	16	116
	Q	50% w/ k_{lb} = 0.01 d^{-1} or 0.03 d^{-1}	0.17	0.25	14	111
		65% OM				
	R	100% w/ ks = 0.00005 d^{-1}	0.07	0.10	62	156
	S	50% w/ kox = 0.0005 d^{-1}	0.07	0.10	33	100
	T	50% w/ k_{lb} = 0.01 d^{-1} or 0.03 d^{-1}	0.07	0.10	30	94

Under ideal conditions, CAR were 50 and 240 g OC m^{-2} yr^{-1} in seagrass and mangrove/tidal marsh sediments, respectively. While this overall model structure was used in all simulated scenarios, MAR and CAR rates under ideal conditions varied from those reported above in increasing MAR and OM decay simulations to represent real increases in accumulation, changes in OM content and associated losses of sediment mass with depth (Table 3.2).

3.3 Results and Discussion

3.3.1 Types of $^{210}Pb_{xs}$ specific activity profiles

Seven distinct types of $^{210}Pb_{xs}$ specific activity profiles can be identified in vegetated coastal sediments based on examples from the literature (Fig. 3.1). Type I is produced by constant sediment accumulation in steady state conditions (i.e. 'ideal' profiles). The other six types of $^{210}Pb_{xs}$ profiles summarize the most common disturbances encountered in vegetated coastal sediments that are related to the presence of mixing (physical or bioturbation), increasing MAR, erosion, or alteration by intrinsic features of sediments such as heterogeneous grain size distribution and decay of OM.

- Type II illustrates a moderate decrease in the slope of $^{210}Pb_{xs}$ specific activities in the upper part of the sediment core, which is often attributed to higher MAR (Cearreta et al., 2002; Haslett et al., 2003; Swales and Bentley, 2015), but can also be related to a mixing process (Gardner et al., 1987).

- Type III, showing constant $^{210}Pb_{xs}$ specific activities along the upper part of the core overlaying an exponential decaying trend, is usually interpreted as the outcome of mixing as a result of bioturbation or sediment resuspension, re-deposition and reworking (Jankowska et al., 2016; Sanders et al., 2010a; Serrano et al., 2016b; Sharma et al., 1987; Smoak and Patchineelam, 1999). This profile type has also been related to rapid accumulation of homogeneous sediment or to recent increases in MAR (Walsh and Nittrouer, 2004).

- Type IV profiles show a reverse $^{210}Pb_{xs}$ pattern at surface and have been attributed to a variety of factors. Similar to type III, this profile type can be caused by mixing processes in vegetated coastal ecosystems (Sanders et al., 2010b; Serrano et al., 2016b;

Yeager et al., 2012) or by the deposition of allochthonous older material (Johannessen and Macdonald, 2018). It could also be produced by an acceleration of the sedimentation rate, as interpreted by Greiner et al. (2013b), Smoak et al. (2013) and Bellucci et al. (2007) in seagrass, mangrove and tidal marsh, respectively, or by the decay of OM, as modelled by Chen and Twilley (1999) and Mudd et al. (2009), and observed by Church et al. (1981) in tidal marsh sediments containing > 30% OM in top layers. Additionally, type IV profiles could also be explained by non-ideal deposition (i.e. a fraction of the new $^{210}Pb_{xs}$ input onto the sediment is not retained at the surface but penetrates to deeper layers), a process reported in peatlands and in sediments with very high porosities (> 90%) at the sediment-water interface (Abril and Gharbi, 2012; Olid et al., 2016).

- Type V profiles show scattered $^{210}Pb_{xs}$ specific activities, which might reflect periodic occurrence of processes that can cause type III or IV profiles and often are interpreted as evidence of repetitive reworking in the overall mixed sediment column (Alongi et al., 2001; Serrano et al., 2016b; Smoak and Patchineelam, 1999). However, this profile form has also been explained by the deposition of $^{210}Pb_{xs}$ outpacing its decay (λ = 0.03111 yr^{-1}) (Alongi et al., 2005) or by a heterogeneous grain-size sediment distribution with depth (Chanton et al., 1983; Kirchner and Ehlers, 1998; Sanders et al., 2010a), which could indicate varying $^{210}Pb_{xs}$ fluxes due to flood events, major land use-changes or changes in vegetation cover (Appleby, 2001; Marbà et al., 2015).

- Types VI and VII represent low $^{210}Pb_{xs}$ activities with depth, apparently showing low, negligible modern net accumulation of sediments. Such profiles are usually related to an abundance of coarse sediments or to erosion processes, as shown in tidal marsh sediments (Ravens et al., 2009) and bare sediments that were previously vegetated with seagrass in Greiner et al. (2013b), Marbà et al. (2015) and Serrano et al. (2016c).

These examples identified from the literature reveal that various sedimentary processes might produce similar types of $^{210}Pb_{xs}$ specific activity profiles. Any particular $^{210}Pb_{xs}$ profile can accommodate a range of mathematical modelling approaches (see below), which lead to development of differing chronologies and MAR estimates. Hence, the identification of the process driving accumulation and causing variation in the $^{210}Pb_{xs}$ record aids in the determination of the OC accumulation rates.

(5) Change/heterogeneous sediment composition

(6) OM decay

(7) Erosion (Past or recent)

(8) Coarse sediment composition

(I) Exponential $^{210}Pb_{xs}$ decline

(II) Shift in the slope of $^{210}Pb_{xs}$ profile

(III) SML overlying exponential $^{210}Pb_{xs}$ profile

(IV) Reverse $^{210}Pb_{xs}$ pattern at surface

(V) Stair-stepped $^{210}Pb_{xs}$ profile

(VI) Low/constant $^{210}Pb_{xs}$ profile

(VII) Low $^{210}Pb_{xs}$ concentrations and inventories

Steady-state accumulation (1)

Mixing (physical or bioturbation) (2)

Change in MAR (acceleration or reduction) (3)

Rapid MAR (4)

(1)
- ✓ Use independent tracers to validate chronology

(2)
- ✓ Check if depth distribution of other elements is homogeneous with depth.
- ✓ Analyze short-lived radionuclides at the SML.
- ✓ Check for burrowing evidence → e.g. X-ray radiographs or visual description of sed. core.
- ✓ CRS or CF:CS model below SML → check residence time of ^{210}Pb in SML.
- ✓ The profile is likely undatable if entirely affected by mixing.

(3)
- ✓ Use independent tracers to validate MAR in regions with different slope.
- ✓ Check for variations in geochemical or physical parameters in the profile.
- ✓ Test sensitivity to acceleration according to DBD and apparent MAR.
- ✓ Check historical records of natural or anthropogenic events.
- ✓ Apply CRS or CF:CS model piecewise.

(4)
- ✓ Analyze short-lived radionuclides.
- ✓ Analyze ^{226}Ra if supported ^{210}Pb is not reached.
- ✓ Check historical records of event sedimentation.
- ✓ The profile is likely undatable by ^{210}Pb if other chronological tools are unavailable.

(5)
- ✓ Check if changes in grain size distribution, DBD and OM content also occur.
- ✓ Normalize radionuclide concentrations to the parameter driving $^{210}Pb_{xs}$ distribution.
- ✓ Analyze ^{226}Ra in all sections.
- ✓ CF:CS model in normalized profiles.
- ✓ The profile is likely undatable if normalization fails and other chronological tools are unavailable.

(6)
- ✓ Only if OM is high (> 30 %) and mostly labile (0.01–0.03 d^{-1})

(7)
- ✓ Compare $^{210}Pb_{xs}$ inventories with those at a reference site.
- ✓ Check for coarser grain size.
- ✓ Presence of short-lived radionuclides at reference site to check entire core recovery.
- ✓ CF:CS or CIC models to estimate mean MAR.

(8)
- ✓ Analyze radionuclides in the fine sediment fraction (sieve to <63 μm or <125 μm) → check new profile
- ✓ ^{226}Ra by gamma spectroscopy
- ✓ Check for records of event sedimentation
- ✓ If sieving increases $^{210}Pb_{xs}$ concentrations but its shape is similar, the profile is undatable and cannot be used for accumulation rate calculations.

Figure 3.1: Diagnostic features for seven distinct types of $^{210}Pb_{xs}$ profiles in vegetated coastal sediments (based on the literature and results from simulations in this study) and recommended actions to interpret each profile type and the sedimentary processes most likely involved. Characteristics of each profile type are explained in section 3.3.1. The solid line in Type VII represents the $^{210}Pb_{xs}$ specific activity profile at a reference undisturbed site.

3.3.2 Simulated sediment and OC accumulation rates (MAR and CAR)

We ran simulations for sedimentary processes (mixing, enhanced sedimentation, erosion) and heterogeneous sediment composition with depth (grain size distribution and OM decay). Results of the modelled $^{210}Pb_{xs}$ profiles are summarized in Figures 3 and 4 and Supplementary Tables S1-S7. We estimated mean 100-yr MAR and CAR for the simulated profiles by applying the CF:CS and CRS models, and results were compared with those from their respective ideal non-disturbed $^{210}Pb_{xs}$ profiles. The estimated deviations in accumulation rates from those expected under ideal conditions are shown in Figure 5 for seagrass and mangrove/tidal marsh ecosystems. These deviations are driven by variations in MAR caused by anomalies in ^{210}Pb profiles as the OC fraction $\left(\frac{\sum_{n=i}^{t} (\%C_{org_i} \cdot m_i)}{m_t}\right)$ was considered to be the same in both ideal and disturbed sediment profiles.

3.3.2.1 Mixing

Simulations of surface mixing (A and B in Fig. 3.2a) yielded $^{210}Pb_{xs}$ profiles similar to types II and III (Fig. 3.1), while deep mixing (scenario C) led to stepwise $^{210}Pb_{xs}$ profile forms similar to type V. Calculated MAR and CAR deviated between 4 and 80% from the ideal value in seagrass sediments, while such deviation was negligible ($\leq$7%) in mangrove/tidal marsh sediments due to the smaller proportion (5 - 10%) of the $^{210}Pb_{xs}$ profile affected by mixing (Fig. 3.4a and 3.4c). In both cases, higher deviations from the expected rates were associated with deep mixing and with the use of the CF:CS model since this model interprets any divergence from the 'ideal' exponential decrease of the $^{210}Pb_{xs}$ activity with depth to reflect random variation. In contrast, the CRS model is based on the $^{210}Pb_{xs}$ inventory (I), that is unaffected by vertical mixing.

Profiles of mixing in sediments could be equally explained by an increase in the sedimentation rate in recent years. If the incorrect process was assumed and dating models were applied accordingly, mean MAR and CAR were largely overestimated in seagrass sediments, by 20, 30 and 95%, using the CF:CS model in surface (scenario A, B) and deep mixing simulations, respectively (Fig. 3.4b). In mangrove/tidal marsh sediments, overestimation in mean MAR and CAR was substantial (30%) when deep mixing was

considered to be caused by an increase in MAR (Fig. 3.4d). A process mismatch between mixing and increased sedimentation in recent years did not cause large deviations (between 2 and 5%) in MAR and CAR derived by the CRS model. The CRS model outputs are similar if mixing or changes in accumulation rates are present, albeit ages within the mixed layer cannot be reported if mixing occurs.

3.3.2.2 Increasing sedimentation rates

Simulated increases in MAR from 20% to 200% (scenarios D to G, Fig. 3.2b) resulted in similar profile forms as those simulated with surface mixing. Increases in MAR were modelled over the last 30 yr, a period over which more than a 100% increase (2-fold) was needed to produce a reversal of $^{210}Pb_{xs}$ specific activities with depth under this simulation (type IV profiles). The influence of change in MAR was better captured with the CRS model. The CF:CS model, in contrast, failed to account for rapid and large increases in MAR. Deviations from the ideal value ranged from 0 to 15% in scenarios D and E (20% to 50% increase in MAR) and were up to 60% for a 100% increase in MAR (scenario F). Calculated MAR in scenario G (200% increase in MAR) was underestimated by a 30%, as piecewise dating is not applicable in profiles with constant or reversed activities of $^{210}Pb_{xs}$ with depth. In such situations, additional tracers or times markers are required to estimate MAR and CAR in the layer of constant $^{210}Pb_{xs}$ activities (see section 3.4.2). Deviations from the expected value ranged from 0 to 4% when using the CRS model (Fig. 3.4a and 3.4c). Results were similar for both ecosystem types. If the recent increase in MAR was interpreted as mixing, the mean MAR and CAR were underestimated between 10 and 30% in both habitat types using the CF:CS model (Fig. 3.4b and 3.4d). In contrast, the deviation from the ideal value was ≤ 5% if the CRS model was applied.

3.3.2.3 Erosion

We ran three simulations (H, I and J) to represent recent (H) and past erosion events (I and J) (Fig. 3.2c). Simulations of erosion yielded lower $^{210}Pb_{xs}$ specific activities than those of the ideal reference profile (type VII, Fig. 3.1), and $^{210}Pb_{xs}$ dating horizons were found at shallower depths in these simulations (Fig. 3.2c). Consequently, $^{210}Pb_{xs}$ inventories

(I) in eroded profiles were lower than expected (reference ideal profile I_{ref}: 3900 Bq m^{-2}). Inventories of simulated seagrass sediments had a deficit of 2,400 Bq m^{-2} (60%), 1,250 Bq m^{-2} (30%) and 600 Bq m^{-2} (15%) in erosion scenarios H, I, and J, respectively, while these deficits were of 900 Bq m^{-2} (22%), 700 Bq m^{-2} (19%) and 600 Bq m^{-2} (15%) in mangrove/tidal marsh sediments. Because seagrass ecosystems have lower sedimentation rates, a greater proportion of the $^{210}Pb_{xs}$ inventory was comprised in the top 10 cm of the sediment column and thus missing because of erosion. Simulations of past erosion events, which can be identified deeper in the profile, produced breaks in the slope of the $^{210}Pb_{xs}$ profiles similar to those of type II (Fig. 3.1). Simulated erosion scenarios did not result in a large impact in the CF:CS-derived MAR and CAR estimates under the conditions of this simulation (Fig. 3.4). Derived MAR and CAR were underestimated by 7% and 2% in seagrass and mangrove habitats, respectively. The CRS model cannot be applied to eroded $^{210}Pb_{xs}$ profiles unless the missing inventory is known and the total (I) and depth-specific (I_m) $^{210}Pb_{xs}$ inventories can be corrected. Assuming erosion was not a factor, the application of the CRS model to our simulated profiles underestimated MAR and CAR by up to 25% in seagrass and by 10% in mangrove/tidal marsh sediments (Fig 3.4b and 3.4d). Therefore, we caution against the use of the CRS model in profiles that show $^{210}Pb_{xs}$ inventories that are lower than those expected via atmospheric $^{210}Pb_{xs}$ deposition or relative to nearby undisturbed sites (Fig. 3.2c). The comparison between sediment records can provide information about the degree of erosion (see section 3.4.3). In our simulations, the OC stocks over the last 100 yr were 20% and 5% lower in seagrass and in mangrove/tidal marsh sediments, respectively, compared to the corresponding ideal non-eroded profile. Part of this is likely related to the fact that the concentration of OC is not changed, which in reality may actually change since fine sediments, where OC is more efficiently adsorbed, are more easily eroded and OM is remineralized when exposed to oxic conditions during resuspension (Burdige, 2007; Lovelock et al., 2017b) (see simulations 3.3.2.4 and 3.3.2.5). Consequently, losses of sediment OC could be significantly larger, as shown in some recent studies (Macreadie et al., 2013, 2015; Marbà et al., 2015; Serrano et al., 2016b).
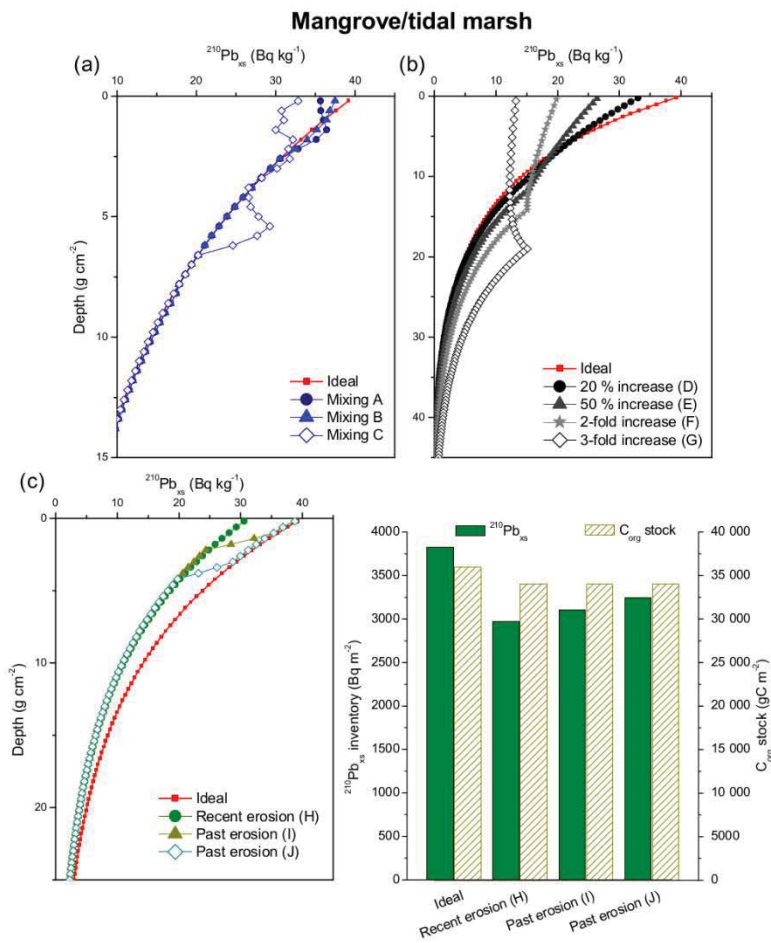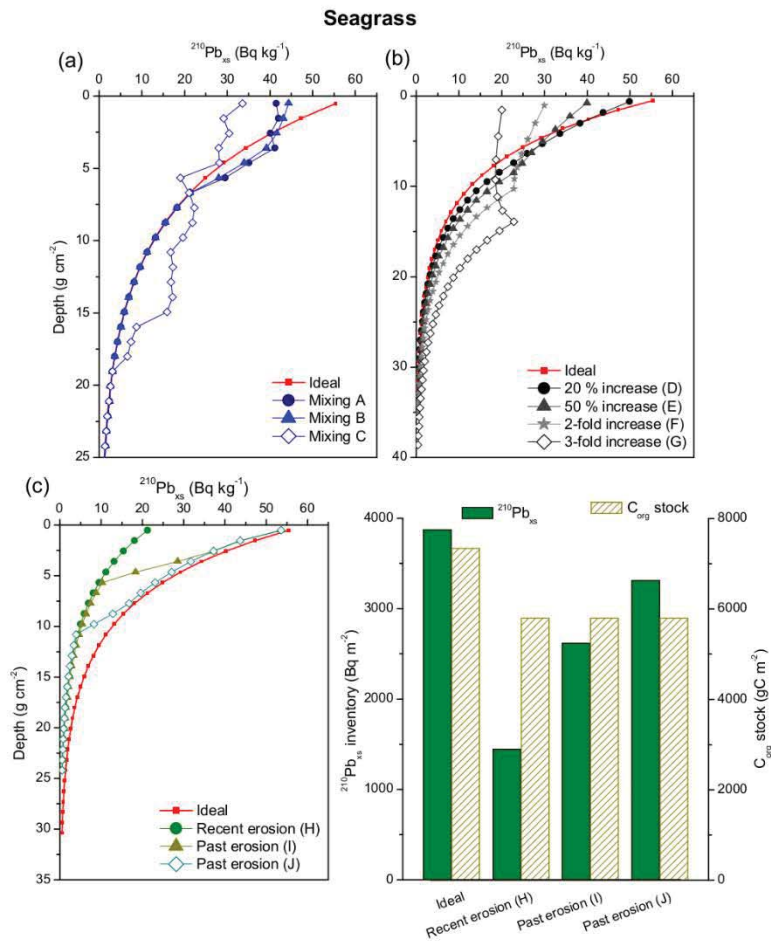
Figure 3.2: Simulated $^{210}Pb_{xs}$ specific activity profiles of mixing (a), increase in sedimentation rates (b) and erosion processes (c) in vegetated coastal sediments. Several dry bulk density (DBD) and mass accumulation rates (*MAR*) are used to represent the effects of these processes in seagrass sediments (Left: DBD 1.03 g cm^{-3}; *MAR* = 0.2 g cm^{-2} yr^{-1}; OC = 2.5%) and in mangroves and tidal marsh sediments (Right: DBD: 0.4 g cm^{-3}; *MAR* = 0.3 g cm^{-2} yr^{-1}; OC = 8%). Bar charts illustrate the deficits in $^{210}Pb_{xs}$ inventories and OC stocks after erosion events. See appendix A for detailed description of each scenario.

3.3.2.4 Sediment grain size distribution

Coarse sediments are often unsuitable for ^{210}Pb dating as they may lead to very low ^{210}Pb$_{xs}$ specific activities. We simulated ^{210}Pb$_{xs}$ profiles in a sediment consisting of 70% coarse sand (scenario K, Fig. 3.3a). This led to diluted ^{210}Pb$_{xs}$ specific activities with depth similar to those produced by erosion processes. In contrast to erosion simulations, coarse but homogeneous grain size distribution with depth did not have any impact in MAR and CAR estimated by the CF:CS model, since the dilution effect did not cause any anomaly in the slope of the ^{210}Pb$_{xs}$ profile. However, the CRS model underestimated the sedimentation rate by 10% in both habitats (Fig. 3.4). The reduction of ^{210}Pb$_{xs}$ specific activities may cause the limits of detection of ^{210}Pb$_{xs}$ (0.35 Bq kg^{-1} in our simulations) to be reached at shallower depths than in the ideal profile. In this simulation, the limits of detection were 4 and 6 cm shallower in seagrass and in mangrove/tidal marsh sediments, respectively (Supplementary, Table S5a and S5b). This conduced to the overestimation of the sediment age at bottom layers by the CRS model, and underestimated mean MAR, due to the omission of a higher fraction of the integrated ^{210}Pb$_{xs}$ activity per unit area from I_m and I at depths greater than those at which the limit of detection was reached (MacKenzie et al., 2011). This effect is known as the "old-date error" of the CRS model and can be corrected as described in Binford (1990) and Appleby (2001). Because we have assumed the same OC content in ideal than in simulated profiles, CAR estimates vary similarly to MAR. However, OC content would likely co-vary with grain size, and we therefore expect lower OC content with coarser sediments (Dahl et al., 2016; Sanders et al., 2012).

Simulations of varying grain size distribution with depth (scenarios L M and N) led to stepwise ^{210}Pb$_{xs}$ profile forms (Fig. 3.3b). A sharp increase in ^{210}Pb$_{xs}$ specific activities in surface layers can be produced by the presence of finer sediments where ^{210}Pb is preferentially associated (scenario L). As a result, sedimentation rates were 2 to 20% lower than those estimated for the ideal profile in both habitat types using the CF:CS and the CRS models, respectively. (Fig. 3.4). The CRS model assumes that ^{210}Pb$_{xs}$ specific activities are inversely related to the sedimentation rate, and thus higher ^{210}Pb$_{xs}$ activities led to lower accumulation rates.

When coarser sediments dominate at the surface layers (scenario M), the simulated profiles obtained were similar to those with mixing and accelerated sediment accumulation in recent years (types II, III and IV). The dilution of ^{210}Pb specific activities caused by the deposition of coarse sediments in surface layers was interpreted by the CRS model as an increase in the sedimentation rate, however, this effect was compensated in part by the "old-date error". With coarser sediments at surface layers, the CF:CS model applied piecewise overestimated average MAR and CAR by only 1% in both habitat types, while the CRS model resulted in a 5% overestimation (Fig. 3.4). If changes in grain size are considered throughout the entire ^{210}Pb$_{xs}$ profile (scenario N), the deviations in accumulation rates were up to 10% using both models in both habitat types. Indeed, the deposition of coarse sediments may indicate exceptional increases in sedimentation in the case of storm surge deposits or pulsed sediment deliveries. In these cases, the CF:CS model could be applied if the event layer can be identified and can be subtracted to produce a corrected depth-profile from which to determine the CF:CS derived ages and mean mass accumulation rate. However, the presence of coarse sediments is often related to a reduction in the deposition of fine particles or to the transport and erosion of these in high energy environments, leading to a variation in the ^{210}Pb$_{xs}$ flux onto the sediment surface, considered constant through time by the two dating models. Where heterogeneous sediment layers are present, some corrections, such as the normalization of ^{210}Pb$_{xs}$ specific activities are required before the application of any of the ^{210}Pb dating models to obtain more accurate estimates of MAR and CAR (see section 3.4.4).

3.3.2.5 Organic matter decay

Two different scenarios with low and high sediment organic matter (OM) content (16.5% and 65%, respectively) were modelled in relation to OM decay. In both scenarios simulated MAR and CAR were overestimated relative to those derived from ideal profiles. Variation in OM decay (from a starting level of 16.5%) only slightly affected ^{210}Pb$_{xs}$ specific activity profiles (Fig. 3.3c) causing a small overestimation of MAR and CAR of between 2 and 5% in both habitats and by both models, under any of the rates of decay considered in this simulation (0.00005 d^{-1}, 0.0005 d^{-1} and 0.01 - 0.03 d^{-1}) (Fig. 3.4a and 3.4c). Organic

matter decay in very rich organic sediments (65% OM) caused increased $^{210}Pb_{xs}$ specific activities at surface (scenarios R and T) and subsurface sediments where decay of OM is greater, leading to reversal of the $^{210}Pb_{xs}$ profile (such as in type IV) in simulated scenario S. Derived CAR were 20 - 30% higher as estimated by the CF:CS model and 10 – 20% using the CRS model, in both habitat types (Fig. 3.4a and 3.4c).

Mass accumulation in vegetated coastal ecosystems is the result of the balance between material accretion (detritus and sediment) from autochthonous and allochthonous sources, decomposition and erosion (e.g. Mateo et al., 1997). Assuming there is no erosion, the estimates of MAR and CAR by means of ^{210}Pb are the net result of mass accumulation with time, and hence integrate both burial and decomposition of organic matter over a centennial time scale. Because mean CAR rates are based on the OC presently available and not the amount originally deposited, their determination will be dependent on the time scale over which they are calculated.
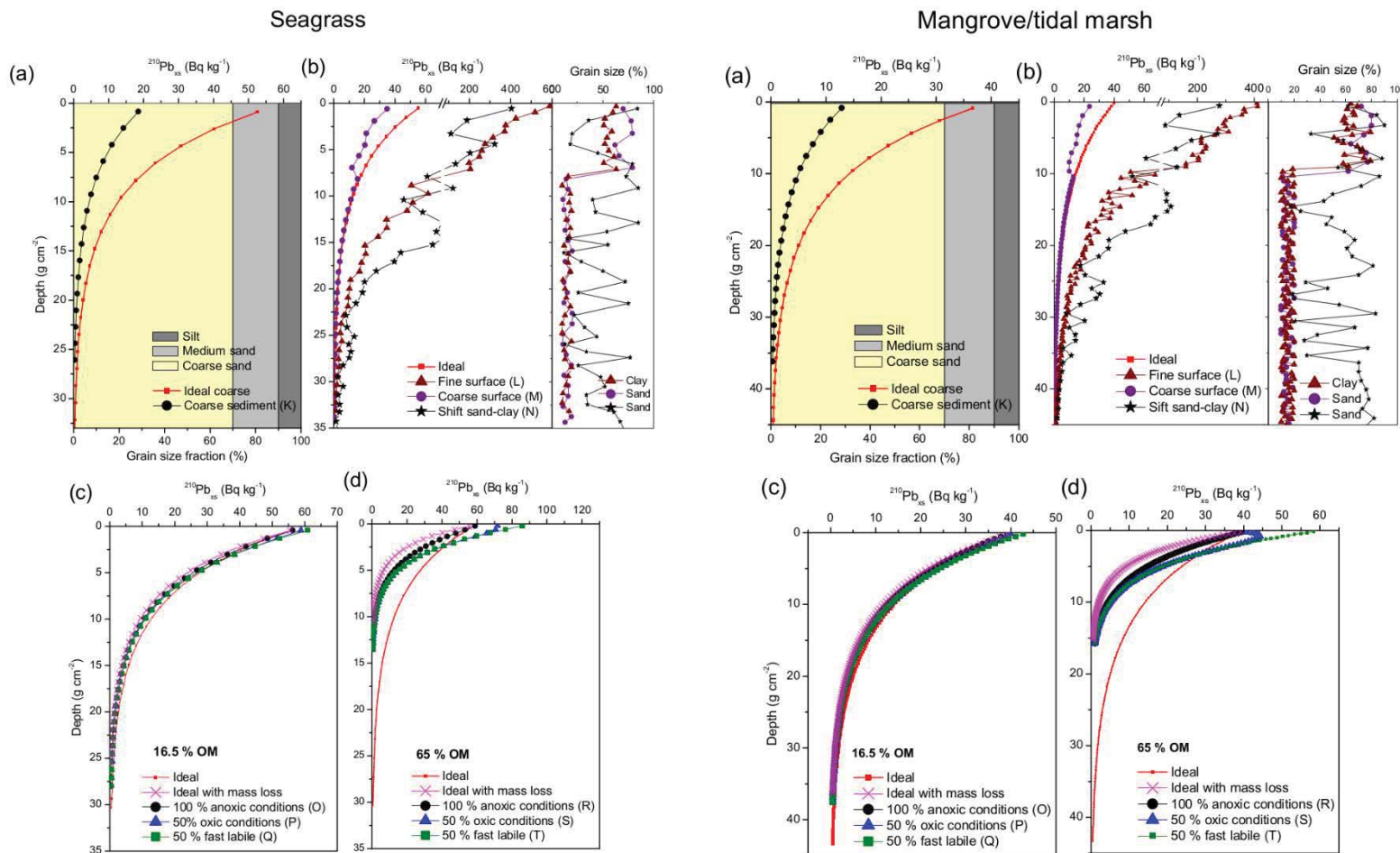
Figure 3.3: Simulated $^{210}Pb_{xs}$ specific activity profiles resulting from changes in sediment composition and organic matter decay. Coarse homogeneous grain size (a); heterogeneous grain size with depth (b), were triangles and dots represent an $^{210}Pb_{xs}$ profile in sediments consisting of fines (< 63 μm) or sands (> 125 μm) at surface layers, respectively; (c and d) organic matter decay from starting level of 16.5% and 65%, respectively (considering different scenarios described in appendix A) in seagrass (Left: DBD 1.03 g cm^{-3}; MAR = 0.2 g cm^{-2} yr^{-1}) and mangrove/tidal marsh sediments (Right: DBD: 0.4 g cm^{-3}; MAR = 0.3 g cm^{-2} yr^{-1}).
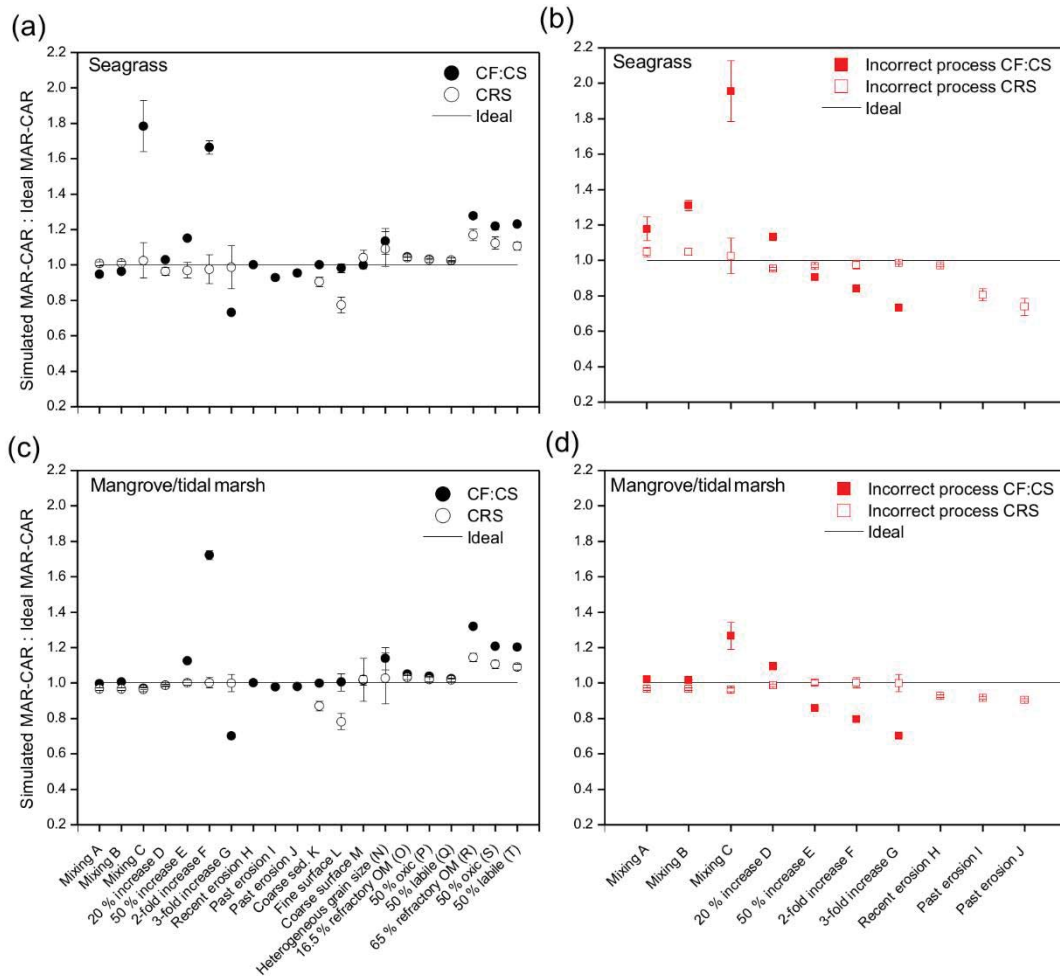
Figure 3.4: Ratio of average 100-yr OC accumulation rates (CAR) between simulated and ideal ^{210}Pb profiles produced by various sedimentary processes in seagrass (a,b) and mangrove/tidal marsh habitats (c,b). Left: the correct process is assumed and models are applied: Right: incorrect process is assumed and models are applied accordingly. Error bars represent the result of error propagation. Uncertainties for mean MAR were derived from SE of the regression and SE of the mean using the CF:CS and CRS models, respectively. Ratios of simulated/ideal sedimentation rates (MAR) are equal to those for CAR, determined from multiplying MAR by the fraction of OC in sediments (Eq. 2.8), which was considered constant between ideal and simulated profiles. In simulations of increasing sedimentation and organic matter decay, new MAR and CAR were estimated for ideal ^{210}Pb profiles to represent real changes in accumulation, organic matter decay and associated changes in sediment mass with depth.

3.3.2.6 General remarks

Among the various ecosystems considered here, average last 100-yr MAR and CAR derived from the CF:CS and the CRS models were less vulnerable to anomalies in mangrove/tidal marsh compared to seagrass sediments. Higher sedimentation rates lead to deeper ^{210}Pb$_{xs}$ dating horizons and thus the fraction of ^{210}Pb profile affected by anomalies was lower in mangrove/tidal marsh than in seagrass sediments. Anomalies caused by deep mixing or 2- to 3-fold acceleration in sedimentation had larger effects on the CF:CS derived

accumulation rates, while alterations caused by heterogeneous grain size composition or underestimation of ^{210}Pb$_{xs}$ inventories primarily affected the CRS model results (Fig. 3.4). Care must be taken in these cases since the discrepancy in mean MAR relative to the ideal value could range between 20% and 80%. Our simulations showed that the decay of OM results in an overestimation of the accumulation rate, which was most severe in very rich organic sediments regardless of the model used (> 50% OM). However, this effect could reasonably be ignored in most cases since vegetated coastal ecosystems rarely contain OM concentrations >25% (Table 3.1), for which the deviation in computed MAR was below 10%. Overall, simulations showed that the variability in MAR and hence CAR due to sedimentary processes and differences in sediment composition was moderately low when appropriate dating models were applied and interpreted. Deviations in the determination of MAR and CAR, generally within 20%, confirmed that the ^{210}Pb dating technique is secure (Fig. 3.4). However, failure to account for the correct process affecting ^{210}Pb specific activity profiles could lead to deviations in mean MAR and CAR exceeding 20% (Fig. 3.4c, d).

MAR and CAR were most overestimated, from 20 to 95% in simulations with low accumulation rates, when acceleration was interpreted in mixed ^{210}Pb$_{xs}$ profiles and the CF:CS model was applied piecewise. Deep mixing confounded with an increase in MAR generated the largest overestimation of mean CAR in both habitat types. In contrast, if mixing was assumed in ^{210}Pb$_{xs}$ profiles showing a recent increase in MAR, mean accumulation rates were underestimated by up to a 30% using the CF:CS model below the "surface mixed layer". Indeed, the CRS model was less sensitive to anomalies in ^{210}Pb$_{xs}$ profiles, however, its application requires accurate determination of the ^{210}Pb$_{xs}$ inventory at each depth (I_m) and in the entire record *(I)*, which can be problematic, for instance when all samples along a sediment core have not been analysed or when sediment erosion has occurred at the core location. When the total ^{210}Pb$_{xs}$ inventory is underestimated, be it through erosion, poor detection limits or insufficient core length, this generates erroneous dates and underestimation of average MAR and CAR. Underestimation of accumulation rates will depend largely on the proportion of the missing fraction of the ^{210}Pb$_{xs}$ inventory from I_m and *I*. In our simulations, MAR and CAR were underestimated by 10 to 25%. While uncertainties within a 20% might be acceptable for the determination of mean MAR and CAR over a centennial time scale, they may not allow the

determination of a detailed geochronology, historical reconstruction, or to ascertain rates of change and fluxes at specific times. In that event additional tracers or geochemical, ecological and historical data need to be used to validate the ^{210}Pb-derived results and reduce uncertainties caused by anomalies in ^{210}Pb$_{xs}$ profiles in vegetated coastal sediments.

3.4 Approaches and Guidelines

Retrieving reliable CAR depends on the correct determination of MAR and the diagnosis of the intervening sedimentary process. However, similarities in simulation outcomes and variations associated with anomalies in ^{210}Pb$_{xs}$ profiles point to the need for additional sources of evidence to discriminate between alternative processes and constrain ^{210}Pb-derived estimates. ^{137}Cs or other independent radioactive tracers can be used to corroborate ^{210}Pb geochronologies. However, in its absence, geochemical information combined with knowledge on events related to land-use and/or environmental changes (e.g. by means of aerial photographic evidence; Swales et al., 2015) can also be used as a tool to validate ^{210}Pb geochronologies and interpret ^{210}Pb$_{xs}$ profiles. In Figure 2 we have summarized the steps to characterize ^{210}Pb profiles and the sedimentary processes most likely involved and suggest several techniques to complement the ^{210}Pb dating method to obtain reliable MAR and CAR.

Prior to analysis, researchers can have control over some factors such as coring, sampling, or sample-handling, that can create artefacts in ^{210}Pb profiles and therefore contribute to dating error. Guidelines for core sampling for the analysis of ^{210}Pb and other radionuclides have been described in detail, for example, in Brenner and Kenney (2013) and in the technical report IAEA-TECDOC-1360 (2003). Some knowledge on the expected sedimentation rate is useful to decide how to section a sediment core for ^{210}Pb measurements, as well as the length that a core must have to reach the depth of the ^{210}Pb$_{xs}$ horizon. Low sedimentation rates ($\sim$1-2 mm yr^{-1}) and/or coarse sediments may imply that the ^{210}Pb datable part of sediment cores is limited to the very top centimetres. In such situation, fine sectioning intervals (0.5 cm) would be required. Longer cores (of about 100 cm) should be collected if high sedimentation rates are expected (several mm yr^{-1}) so that the entire ^{210}Pb$_{xs}$ inventory is captured and the CRS model can be applied. These can be sliced at thicker intervals without compromising the temporal resolution of the ^{210}Pb record. If the order of magnitude of the sedimentation rate is not known

a priori, it is best to choose fine sampling intervals (e.g, at 0.5 cm along the upper 20 cm, at 1 cm from 20 to 50 cm, and at 2 cm below 50 cm) to ensure sufficient resolution.

After collection, a visual description (e.g., colour, sediment texture, presence of roots, organisms or layers) of the sediments and measurement of parameters such as water content, OM and grain size are relatively low-cost actions that provide information to interpret ^{210}Pb distribution and the pattern of accumulation. Indeed, the type of sediment (e.g., fine vs. coarse, rich in carbonates, homogeneous or with organic debris embedded) is a factor that should be considered (IAEA-TECDOC-1360, 2003). Coarse particles or coarse-grained carbonates where ^{210}Pb$_{xs}$ is less preferentially adsorbed (Wan et al., 1993) may hinder the detection of any ^{210}Pb$_{xs}$ in vegetated coastal sediments. In such situations, the analysis of ^{210}Pb in the smaller sediment fraction (i.e. < 63μm or < 125 μm) is recommended to concentrate ^{210}Pb and reduce the dilution effect caused by coarse fractions. However, the application of the CRS model would then be limited to those cases where the ^{210}Pb$_{xs}$ is contained entirely in the sieved sediment fraction. Sieving combined with ^{210}Pb dating has been applied to mangrove sediments from arid regions where ^{210}Pb$_{xs}$ flux is low (Almahasheer et al., 2017) and to carbonate-rich seagrass sediments in Florida Bay (Holmes et al., 2001). Similarly, large organic material such as roots and leaves should be removed from the sediment samples prior to ^{210}Pb analyses as these may contribute to the dilution of the ^{210}Pb$_{xs}$ specific activity.

The analytical methods for ^{210}Pb measurements can also be chosen depending upon the amount of sample available and its expected specific activity. While indirect determination of ^{210}Pb by alpha spectrometry of its granddaughter ^{210}Po requires little amount of sample (150 – 300 mg) and will provide a significant better limit of detection (< 1 Bq kg^{-1}), direct determination of ^{210}Pb by gamma spectrometry can simultaneously provide data for supported ^{210}Pb (^{226}Ra) and relevant radionuclides, such as ^{137}Cs, ^{228}Th, ^{7}Be, ^{40}K, to validate the ^{210}Pb geochronologies. For a detailed description of the analytical methods and their advantages and disadvantages see for instance Corbett and Walsh, (2015) and Goldstein and Stirling, (2003).

3.4.1 General validation of ^{210}Pb models

3.4.1.1 Artificial radionuclides

Independent validation of the chronology is essential to ensure a high level of confidence in the results (Smith, 2001). Varved sediments used to validate chronologies in lakes do not occur in vegetated coastal sedimentary sequences, and thus transient signals such ^{137}Cs or $^{239+240}$Pu become the most commonly used option to validate ^{210}Pb chronologies (Lynch et al., 1989; Sanders et al., 2010a). ^{137}Cs and $^{239+240}$Pu were released to the environment through the testing of high-yield thermonuclear weapons in 1950s to 1960s and can be used as chronometers in sediments either by assuming that the peak in activity corresponds to the fallout peak in 1963 or 1965 in the Northern and Southern hemispheres, respectively, and/or that the depth of its first detection corresponds to the onset of fallout in the mid-1950s (Ribeiro Guevara and Arribére, 2002; Stupar et al., 2014). In addition, ^{137}Cs can also display a peak of elevated activity in sediment cores from Europe, corresponding to the emissions caused by the Chernobyl accident in 1986, which can also help to validate ^{210}Pb chronologies (Callaway et al., 1997).

However, the use of ^{137}Cs might have some limitations in vegetated coastal sediments. Two-thirds of the ^{137}Cs activity released due to the tests in the atmosphere decayed after 5 decades, rendering the identification of peaks and its correspondence to the mid 50's and 60's depths more difficult to determine. In addition, the detection of ^{137}Cs is more difficult in sediment cores from habitats located in the Southern hemisphere and near the Equator. The low ^{137}Cs bomb-test fallout and Chernobyl inputs in these regions (Kelley et al., 1999; Ruiz-Fernández and Hillaire-Marcel, 2009), the greater solubility of ^{137}Cs in seawater ($K_d = 10^2$ to 10^3, Bruland, 1983) and the presence of sands and carbonates, particularly in seagrass sediments (Koch, 2001), are conditions that do not favour the adsorption of ^{137}Cs (He and Walling, 1996a), and may lead to its mobility (Davis et al., 1984). This effect could be intensified in the intertidal zone, which is not permanently submerged due to periodic changes in the water table. High contents of OM can also affect the distribution of ^{137}Cs in sediments as it is preferentially accumulated in leaf litter and may be absorbed by living roots (Olid et al., 2008; Staunton et al., 2002). In addition, decomposition of the organic phase in organic-rich sediments may cause mobility of this radionuclide (Davis et al., 1984). These factors together may compromise the

use of ^{137}Cs to validate ^{210}Pb geochronologies in vegetated coastal ecosystems. In contrast, Pu isotopes ([239]Pu half-life = 24,100 yr and [240]Pu half-life = 6,500 yr), although they are also dependent on the distribution of bomb-test fallout, would appear to offer several advantages over ^{137}Cs in these environments, since [239+240]Pu is relatively immobile under both freshwater and saltwater conditions (Crusius and Anderson, 1995). For instance, Sanders et al. (2016) determined sedimentation rates and [239+240]Pu penetration depths to study nutrient and CAR in intertidal mangrove mudflats of Moreton Bay, Australia. Nevertheless, and because of the limitations to validate older ^{210}Pb dates near the base of the core, and the low inventories of bomb-test fallout in sediments of Southern Hemisphere latitudes, alternative tracers might need to be used.

3.4.1.2 Geochemical information of sediments

Besides the irregular shape of [210]Pb$_{xs}$ profiles, the absence of a secondary radioactive tracer to validate ^{210}Pb results can make interpretation even more complicated. However, geochemical information in sediments can provide the potential for an additional temporal frame and can also help to explain sedimentary processes that could be misinterpreted (e.g., mixing, increasing MAR, higher primary productivity or reduction of sediment supply). Analyses of additional proxies (pollen, diatom, nutrient concentrations, stable isotopes or trace metal records; López-Merino et al., 2017) that are based on well-described historical events at the study sites (e.g. pollution, crops and land-clearance) could be used in the absence of secondary radioactive tracers to corroborate ^{210}Pb derived dates and accumulation rates. For instance, stable Pb isotopes or total Pb concentrations in sediments are related to the history of use of leaded gasoline in the area and can be used to identify age marks corresponding to peaks in its use or changes in lead sourcing. An example can be found in seagrass sediment cores from Florida Bay, USA (Holmes et al., 2001) or in Gehrels et al. (2005) that combines a marsh elevation reconstruction with a precise chronology derived from pollen analysis, stable isotopes ([206]Pb, [207]Pb), ^{210}Pb and artificial radionuclides (^{137}Cs, [241]Am). Additionally, profiles of trace and heavy metals and of carbon $\delta^{13}C$ and nitrogen $\delta^{15}N$ isotopic composition of OM provide information about environmental changes for which historical information may be well known, i.e., human settlement, onset of tourism industry, temporal evolution of cropland areas or

histories of variation in plant communities (Garcia-Orellana et al., 2011; Mazarrasa et al., 2017; Ruiz-Fernández and Hillaire-Marcel, 2009; Serrano et al., 2016f).

3.4.2 Mixing or Rapid sedimentation

The methods described above for the general validation of ^{210}Pb models can also serve to discriminate between mixing or increasing MAR in recent years. ^{137}Cs and $^{239+240}$Pu can also be used as tracers of bioturbation (Crusius et al., 2004) or acceleration of MAR during the past 50 years (Appleby, 1998; Cearreta et al., 2002; Lynch et al., 1989; Sharma et al., 1987). For instance, demonstration of acceleration versus fast mixing could be supported when it is possible to find the distinct ^{137}Cs or $^{239+240}$Pu peaks in the same zone where ^{210}Pb$_{xs}$ activities are constant (Appleby, 2001). Changes along the profiles of geochemical elements consistent with shifts in ^{210}Pb$_{xs}$ specific activities often can be associated with changes in sedimentation or erosion processes. For instance, instantaneous depositional event layers can be identified in the sedimentary record as isolated minima of ^{210}Pb$_{xs}$ specific activities (Jaeger and Nittrouer, 2006; Smoak et al., 2013), but also as variations in grain size composition, OM, water content or dry bulk density (Smoak et al., 2013; Walsh and Nittrouer, 2004) (Appendix B1). Changes in sediment mineralogy can be discerned trough X-ray radiographs, X-ray fluorescence and CAT-scans (described below), but also through other radionuclides, like ^{226}Ra and ^{40}K, the profiles of which can be measured together with those of ^{210}Pb through gamma spectrometry. In particular ^{40}K is also part of the mineral matrix and is often used as a surrogate for the lithogenic sediment fraction (Garcia-Orellana et al., 2006; Peterson, 2009; Xu et al., 2015).

3.4.2.1 Geophysical analyses

Prior to core sectioning and subsampling, non-destructive geophysical analyses such as X-ray radiographs, X-ray fluorescence (XRF), CAT-scans (Computerized Axial Tomography) or magnetic susceptibility can be conducted to identify changes in the composition of sediments with depth and in MAR or provide evidence of mixing. For instance, using X-ray radiographs many features and physical sedimentary structures may be visible (Sun et al., 2017) and if preserved, could support the interpretation of a rapid increase in sedimentation (Walsh and Nittrouer, 2004). Pulsed sediment deliveries or erosion could be identified by discontinuous

physical stratification, and sediment mixing by the presence of active burrows or the absence of sedimentary stratification (Chanton et al., 1983).

3.4.2.2 Short-lived radionuclides (^{234}Th, ^{228}Th, ^{7}Be)

Radionuclides such as ^{234}Th, ^{7}Be and ^{228}Th with properties such as particle-reactivity and relatively short half-lives (24.1 days, 53.3 days and 1.9 years, respectively) are suitable to quantify sedimentation processes at scales from several months (^{234}Th and ^{7}Be) to a decade (^{228}Th). Excess ^{234}Th and ^{7}Be are sensitive indicators of mixing in the zone of constant, scattered or reversed ^{210}Pb$_{xs}$ specific activity profiles and are the most widely used (Types II, III, IV, Fig, 2) (Cochran and Masqué, 2005; Sommerfield and Nittrouer, 1999). Demonstrating the presence of any of these short-lived radionuclides can give confidence that there is little material missing from the top of the sediment record and no recent erosion, which is essential for the application of the CRS model. An example is documented by Smoak and Patchineelam (1999) for a ^{210}Pb$_{xs}$ profile affected by bioturbation in a mangrove ecosystem in Brazil (Appendix B2).

Recent increases in MAR could be estimated in vegetated coastal ecosystems from the slope of the best-fit line of the plot of excess ^{228}Th against cumulative mass, as Alongi et al. (2005) showed in a mangrove ecosystem in Jiulongjiang Estuary, China (Appendix B3). However, the use of ^{228}Th to derive recent increases in sedimentation is restricted to habitats with high accumulation rates (i.e. > 4 mm yr^{-1}) with the last 10 yr comprised in the upper centimetres. Its application is also limited due to the often very low excess activities in coastal waters and the constraint that sediments must contain a significant lithogenic/detrital fraction. In general, the use of short-lived radionuclides might be indicated to assess the magnitude of mixing or recent erosion in vegetated coastal sediments.

Mixing, either due to bioturbation or hydrodynamic energy, is the most common process affecting vegetated coastal sediment records. Although the presence of vegetation and anoxic sediments tends to reduce the depth of sediment mixing (Duarte et al., 2013b), the mixed layer can extend to depths of 10-15 cm in marine sediments (Boudreau, 1994). If surface mixing occurs, valid estimates of sedimentation rates (within 5% variability as shown in section

3.3.2.1) can still be obtained using the dating models described above, however this is only possible in sediments where $^{210}Pb_{xs}$ is buried below the mixed layer prior to decay, i.e., the residence time of sediments in the mixed layer must be shorter than the effective dating time scale (~100 yr) (Crusius et al., 2004). In the example from Smoak and Patchineelam (1999) (Appendix B2), where mixing extends to a depth of 11 cm, the sedimentation rate had to be higher than 1.1 mm yr^{-1} in order for ^{210}Pb to be a useful chronometer (residence time in the mixed layer = 110 mm / 1.1 mm yr^{-1} = 100 yr, which is within the effective dating time scale of ^{210}Pb).

3.4.2.3 Maximum penetration depth of $^{210}Pb_{xs}$

A chronology cannot be estimated if mixing affects the whole or the vast majority of the sediment record such as in the deep mixing simulation in seagrass sediments in this work. However, information such as the total historical inventory of elements, like nutrients accumulated at a site, and the maximum conservative sedimentation rate can still be estimated. The penetration-depth method (Goodbred and Kuehl, 1998; Jaeger et al., 2009) uses the maximum penetration depth of $^{210}Pb_{xs}$ (depth of disappearance) as a marker horizon for sediments that are ~100 yr old. Low surface $^{210}Pb_{xs}$ specific activities can greatly restrict the age of the ^{210}Pb dating horizon, therefore this is an issue that should be considered when establishing the age of the $^{210}Pb_{xs}$ horizon. For surficial specific activities less than ~100 Bq kg^{-1} this could be as little as 3–4 ^{210}Pb half-lives, i.e., 65–90 years. By locating the dating horizon, independently of the alteration of sedimentary processes and of assumptions of the CF:CS or CRS models, an upper estimate of the average MAR can be derived. Note that by using this method, the rates of change or fluxes cannot be estimated and these types of $^{210}Pb_{xs}$ profiles may be of little use in establishing chrono-stratigraphies since are unlikely to have good records of other environmental parameters.

3.4.3 Erosion: $^{210}Pb_{xs}$ inventories (*I*)

Assessing the extent of erosion requires the comparison of the $^{210}Pb_{xs}$ inventories between reference i.e., undisturbed locations (I_{ref}) and eroded sites (I). Because $^{210}Pb_{xs}$ is particle reactive, once deposited in sediments, its subsequent lateral redistribution is primarily

controlled by resuspension and transport processes, and thus a deficit in $^{210}Pb_{xs}$ inventories relative to undisturbed sediments may indicate loss or mobilisation of sediment particles. This approach has been used in terrestrial soils (Martz and Jong, 1991; Walling et al., 2003) and more recently to assess erosion of seagrass sediments (Greiner et al., 2013; Marbà et al., 2015; Serrano et al., 2016b) (Appendix B4). Because the $^{210}Pb_{xs}$ inventories at a reference undisturbed location may be spatially variable, we recommend the use of a reference inventory value based on several cores (i.e., mean ± 2SE). The consistency of the resulting reference inventory value can then be assessed by comparing it with the $^{210}Pb_{xs}$ inventory measured in a nearby undisturbed soil characterized by minimal slope or with that expected from the local atmospheric flux of $^{210}Pb_{xs}$ (Φ). See Preiss et al. (1996) for global and regional ranges of atmospheric fluxes. The expected inventory (I_{ref}) can then be derived as $I_{ref} = \Phi/\lambda$, where λ is the decay constant of ^{210}Pb (0.03111 yr^{-1}).

3.4.4 Heterogeneous sediment composition

3.4.4.1 Normalization of $^{210}Pb_{xs}$ specific activity

Dating models assume rapid and non-discriminatory removal of radionuclides from the water column regardless of major changes in grain size or OM content along a sediment record. Radionuclide adsorption onto sediments is strongly governed by the binding capacity of the settling particles (Cremers et al., 1988; Loring, 1991), thus its scavenging is increased by fine-grained texture (He and Walling, 1996a) and OM particles (Yeager and Santschi, 2003). Variations in the influx of these particles into vegetated coastal sediments may proportionally affect the influx of particle bound $^{210}Pb_{xs}$ (as long as it is still available), thus violating the assumption of constant flux of the CRS and CF:CS models and leading to subsections and irregularities of $^{210}Pb_{xs}$ profiles. Constant or reversed patterns in $^{210}Pb_{xs}$ activity profiles, which could be easily mistaken for reworked deposition, could be caused, for instance, by vertical fluctuations of grain size due to seasonal variations of sediment discharge or reoccurring tidal currents. Sediment studies often attempt to minimize these effects by normalizing radionuclide specific activities to granulometric or geochemical parameters that reduce the influence of preferential adsorption by fine sediments and OM (Álvarez-Iglesias et al., 2007; Loring, 1991; Wan et al., 2005), allowing to obtain $^{210}Pb_{xs}$ profiles showing an exponential decreasing trend

with depth (Kirchner and Ehlers, 1998; Sun et al., 2017). Radiometric applications in coastal sediments have traditionally opted for grain size normalizers such as the < 4 μm, < 63 μm fraction or Al content (Álvarez-Iglesias et al., 2007; Sanders et al., 2010b; Sun et al., 2017; Walsh and Nittrouer, 2004), while in dynamic, sandy-rich coastal systems where the mud fraction is small, normalization by OM content has been shown to be also effective (Van Eaton et al., 2010). Equation 3.3 can be used to normalize $^{210}Pb_{xs}$ specific activities ($^{210}Pb_{xs\text{-}NORM}$ in Bq kg^{-1}) by grain size fractions, OM content or other geochemical parameters that control the variation of the input of $^{210}Pb_{xs}$.

$$^{210}Pb_{xs\text{-}NORM} = {}^{210}Pb_{xs\text{-}MEAS}(NP_{AVG}/NP_m) \qquad\qquad (Eq.\ 3.3)$$

where $^{210}Pb_{xs\text{-}MEAS}$ is the measured specific activity of the bulk sample at depth m, and (NP_{AVG}/NP_m) is the ratio between the core average normalizing parameter to its content at depth m. For instance, multiplication by this ratio corrects measured ^{210}Pb activities for variations in OM with respect to an average core value.

3.4.4.2 ^{226}Ra specific activity profiles

$^{210}Pb_{xs}$ specific activity is determined by subtracting supported ^{210}Pb, assuming it is in equilibrium with ^{226}Ra, to total ^{210}Pb specific activity. This is straightforward when gamma spectrometry is employed since the total ^{210}Pb and $^{210}Pb_{sup}$ (i.e., ^{226}Ra) can be quantified simultaneously. On occasions, particularly when ^{210}Pb is determined by alpha spectrometry, ^{226}Ra is not measured, and supported ^{210}Pb is most often determined from the region of constant and low ^{210}Pb specific activities at depth, or alternatively, from a number of determinations of ^{226}Ra via gamma spectrometry or liquid scintillation counting (LSC) along the core. This method assumes that ^{226}Ra or $^{210}Pb_{sup}$ are constant throughout the sediment core (Binford, 1990). However, this might not be always the case, especially in heterogeneous profiles consisting of a variety of sediment types (Aalto and Nittrouer, 2012; Armentano and Woodwell, 1975; Boyd and Sommerfield, 2016) or in records containing episodes of rapid sedimentation (Chanton et al., 1983). In addition, equilibrium of $^{210}Pb_{sup}$ with ^{226}Ra might be compromised in surface sediments, where ^{222}Rn is deficient (Appleby, 2001). Although variations in ^{226}Ra specific activities with depth are small in most cases, accurate determination of ^{226}Ra might be crucial in sediments with low total ^{210}Pb (e.g., due to the presence of coarse sediments), where

slight variations in the $^{210}Pb_{sup}$ fraction may result in significant errors in the estimation of $^{210}Pb_{xs}$ and derived accumulation rates (Diemer et al., 2011). Therefore, we recommend measuring ^{226}Ra specific activity profiles or to, at least, use depth-specific ^{226}Ra values at several depths along a sediment profile to estimate $^{210}Pb_{xs}$.

3.5 Conclusions

The ^{210}Pb dating technique provides crucial information for the study of carbon sequestration in vegetated coastal sediments and can also provide accurate geochronologies for the reconstruction of environmental processes. However, ^{210}Pb based geochronologies may be difficult to conduct in mangrove, tidal marsh and seagrass ecosystems, where unaltered sedimentary records are rare.

Shallow vegetated coastal sediments are often affected by a number of processes such as mixing and bioturbation, accelerated sedimentation or erosion and might be composed of heterogeneous sediments. These factors may lead to anomalies in the $^{210}Pb_{xs}$ specific activity profiles, and thus produce erroneous geochronologies and biased mean last-century MAR and CAR. Discrepancies in mean MAR and CAR between irregular and ideal ^{210}Pb profiles simulated in this study are within 20% if the intervening sedimentary process is well diagnosed. Otherwise, these deviations may range between 20% and 100%, with higher errors associated with the application of 1) the CF:CS model in records showing intense mixing or large increases in MAR, and 2) the CRS model in incomplete $^{210}Pb_{xs}$ sediment profiles. Additional tracers or geochemical, ecological or historical data can be used to identify the process causing anomalies in $^{210}Pb_{xs}$ profiles and reduce uncertainties in derived accumulation rates. Using the procedures in section 3.4, researchers have been able to obtain reliable chronologies and CAR in vegetated coastal sediments. Special caution, however, should be applied in those sites where sediments might be altered by multiple processes (leading to profile types V or VI shown in this study) and where other chronological tools or time markers are not available (e.g., ^{137}Cs). Sites that have slow accumulation rates and/or intense mixing may unlikely be datable and derived CAR estimates may be largely overestimated. Mistakes would include assigning discrete ages in mixed sediments or extrapolating an age-depth model for a core that should be considered undatable to depths down the core or to nearby sites. While attention should be paid to the

limitations of ^{210}Pb-derived results in vegetated coastal ecosystems, the guidelines provided here should help interpreting complex ^{210}Pb profiles obtained from vegetated coastal sediments and to develop a strategy to strengthen the evaluation of MAR and CAR.

Chapter 4

Contemporary organic carbon burial rates in seagrass sediments worldwide[1]

Seagrass meadows are increasingly credited with burying large quantities of organic carbon (OC) in their sediments. However, this process is relatively under-studied due to the difficulty in determining rates of sediment accretion or burial of plant material over long timescales (> decades) in these environments. Published estimates of OC burial in seagrasses sediments average 138 ± 38 g C m^{-2} yr^{-1} (or 50 - 110 Tg C yr^{-1}, globally). These estimates, based on measurements of seagrass net community production and the few available rates of sediment organic C burial, were strongly influenced by data from organic C-rich Posidonia oceanica meadows sustaining high rates of C accumulation. Here, we review contemporary (i.e. last century; derived from ^{210}Pb dating) seagrass OC burial rates at regional and global scales. We compiled published and unpublished estimates of sediment accumulation and OC burial rates from 167 seagrass records from 62 sites across the globe. This included data from previously less studied temperate regions beyond the Mediterranean and an additional 19 records from adjacent unvegetated areas. Our results show that seagrass ecosystems bury 24 (+6; -4) g C m^{-2} yr^{-1} (95% C.I.), accounting for a global OC burial ranging between 6 and 18 Tg C yr^{-1}. Although our estimate of seagrass OC burial is 7 times lower than previously thought, it accounts for 4 to 8% of the total marine OC burial in the ocean, a disproportionately large contribution given they occupy less than 0.1% of the ocean surface. Seagrass-bare comparisons further supported previous conclusions that seagrasses reduce sediment resuspension and erosion, enhancing the preservation of organic C in sediments.

---

[1] This Chapter is under preparation by A. Arias-Ortiz, P. Masqué, Jordi Garcia-Orellana, C.M. Duarte, P. Colarusso, P. Lavery, N. Marbà, M.A. Mateo, I. Mazarrasa, O. Serrano, J. Samper-Villareal, and M. Wesselmann

4.1 Introduction

The global extent of seagrass sediments is less than 0.1% of the area of the coastal ocean, yet they are estimated to account for 10 to 18% of its total organic carbon (OC) burial (Duarte et al., 2005; Kennedy et al., 2010). Seagrass sediments are estimated to bury OC at an areal rate of 138 ± 38 g C m^{-2} yr^{-1}, which is 30 times higher than in terrestrial forest soils (McLeod et al., 2011). This has led to the formulation of seagrass conservation and restoration plans to contribute to blue carbon strategies to mitigate climate change (Nellemann et al., 2009). However, the rate of OC accumulation in seagrass sediments is relatively under-studied due to the difficulty in determining rates of sediment accretion or burial of plant material over long timescales (> decades) in these environments. Dynamic patterns of sedimentation, sediment mixing, microbial remineralization, hydrodynamic energy and the fact that not all seagrass species form extensive deep root mattes often hinder the use of common methods to estimate long-term OC burial rates. These methods include the dating of sediments by means of ^{210}Pb and ^{137}Cs coupled with measurements of OC content or radiocarbon dating of plant materials. Indeed, past attempts at estimating the global OC burial in seagrass sediments were based on only 5 directly measured OC burial rates for the large Mediterranean species *Posidonia oceanica* (Duarte et al., 2005) that where combined with indirect estimates from seagrass net community production (NCP) (this is gross primary production minus respiration by autotrophs and heterotrophs) (Duarte et al., 2010) and burial of allochthonous OC (Kennedy et al., 2010; McLeod et al., 2011) (Table, C1). While a significant fraction of seagrass NCP might be stored in the sediments as roots and rhizome material for millennia (Mateo et al., 1997), the fate of the excess seagrass production is poorly resolved.

The spare abundance of direct estimates of OC burial rates in seagrass ecosystems contrast with the 10-fold greater number of estimates on carbon stock size available (∽630) (Campbell et al., 2014; Fourqurean et al., 2012b; Kindeberg et al., 2018; Röhr et al., 2018). Sedimentary OC stocks addressed at length advise about the total OC inventory currently sequestered from the atmosphere and contribute to understanding potential CO_2 emissions if meadows are degraded and stocks are lost (Lovelock et al., 2017a; Macreadie et al., 2014; Marbà et al., 2015). However, they do not inform about the carbon sink efficiency of these ecosystems (i.e., the rate at which OC is incorporated in the sediment layer) or their potential

to mitigate CO_2 emissions since the time taken to accumulate the observed stocks may vary in several orders of magnitude (Lavery et al., 2013). The often-established relationship between large OC stocks and a large capacity to sequester C has led to recent criticism (Johannessen and Macdonald, 2016, 2018), highlighting the lack of a firm understanding of OC burial rates in seagrass sediments, with current available estimates representing an insufficient basis to estimate the role of seagrasses as carbon sinks.

With the expansion of the research efforts on blue carbon, several studies in the past decade have included directly measured OC burial rates for individual or groups of seagrass meadows differing in species and geographic regions (e.g., references in Table C2). These new estimates show significantly downward rates of OC accumulation ranging between 0.4 ± 0.2 and 93 ± 7 g C m^{-2} yr^{-1} suggesting that seagrass sediments could be a lower C sink than previously acknowledged. Despite the discrepancy between past and recent estimates, a revision of seagrass C burial rates has not been conducted since Mcleod et al. (2011), as opposed to the other coastal blue carbon ecosystems (i.e., tidal marshes and mangroves) where global burial rates of OC have been reassessed on a centennial scale combining sedimentary OC content with sedimentation rates derived from ^{210}Pb, ^{137}Cs or a combination of the two radionuclides (100% of the estimates in Breithaupt et al., 2012 and 64% of estimates in Ouyang and Lee, 2014). ^{210}Pb derived OC accumulation rates meet different challenges as outlined in Arias-Ortiz et al. (2018). Principally, sediment mixing may overestimate OC burial rates, while negligible net sediment accumulation precludes the determinations of them, leading to a substantial bias of published rates towards depositional environments.

Here, we address the current gap in global estimates of OC burial rates in seagrass sediments by compiling and synthesizing published and unpublished estimates of centennial scale (hereafter: contemporary) OC content, sedimentation and OC burial rates in 167 seagrass meadows across the globe. Additionally, we separately consider unvegetated sites adjacent to seagrass meadows. As a novelty, we include all available sites (vegetated or unvegetated) were negligible accumulation was reported. Understanding of the C sink capacity within seagrass sediments will help to strengthen the global seagrass carbon budget, thereby allowing this component to help quantify and/or validate other aspects of the seagrass C budget such as import, export, and remineralization. Global OC sequestration rates in mangrove and tidal

marsh sediments have also been reassessed on a centennial timescale, hence this work will serve to compare the OC sequestration efficiency between ecosystems as well as to determine their relative contribution to the ocean C budget.

4.2 Methods

We compiled published and unpublished data on OC accumulation rates in seagrass meadows and adjacent un-vegetated sediments. A literature review was conducted with the objective of finding direct estimates of centennial scale C burial rates in seagrass ecosystems. Additionally, we looked for quantitative parameters including ^{210}Pb specific activity profiles and derived centennial scale mass accumulation rates (g cm^{-2} yr^{-1}), C content (%) and sediment dry bulk density (DBD). Study location, seagrass species and type of ^{210}Pb profile (as in Arias-Ortiz et al., 2018) were noted where available. An effort was made to record or estimate core mass depths (g cm^{-2}) apart from depths (cm). Compaction of sediments may occur during coring, however this was not always measured or reported in the literature. Therefore, sedimentation rates were assessed as mass accumulation rates (MAR), which are independent of core compaction. Accordingly, and where not directly reported, OC burial rates were estimated as the product of the fraction of %C accumulated over a period t (C_t) by the MAR of that period (MAR_t):

$$CAR = C_t \cdot MAR_t \qquad \text{(Eq. 4.1)}$$

When available we compiled the OC content and DBD at each segmented interval to estimate C_t, otherwise mean values were recorded and used to estimate OC burial rates. When only organic matter (OM) was reported, it was converted to OC using the general equation (Eq. 4.2) developed by Fourqurean et al., (2012b), with the exception of sites in Florida Bay, where a specific equation was available (Eq. 4.3) (Fourqurean et al., 2012a).

$$C(\%) = 0.43 \cdot OM(\%) - 0.33 \qquad \text{(Eq. 4.2)}$$

$$C(\%) = 0.54 \cdot OM(\%) - 0.99 \qquad \text{(Eq. 4.3)}$$

24 published studies reported sedimentation rates in accretion units (cm yr^{-1}), these were converted to MAR in mass units using DBD values for the same site. When rates were estimated for specific time intervals (Greiner et al., 2013) these were recalculated to represent the mean

MAR of the dated period if ^{210}Pb specific activity profiles were made available. We amended the dataset of published estimates (n = 84) with unpublished values for 102 additional sites sampled by the authors. This yielded a total of 186 sites with data on sediment OC burial (both measurable and negligible) in coastal areas occupied by seagrasses, of which 19 corresponded to unvegetated patches adjacent to seagrass meadows (Tables C2 and C3).

We analyzed the distribution as well as skewness and kurtosis of the data and a Shapiro-Wilk test provided an indication of normality for the untransformed and log-transformed versions of the dataset. These results were used to assess which parameter (the arithmetic mean, median or geometric mean) was best suited to represent the central tendency of our data. The arithmetic mean or average was used if data followed a normal distribution, the geometric mean if a skewed distribution was made symmetrical by a log transformation, and the median if either the untransformed and log-transformed data set did not follow a normal distribution.

Estimates of OC burial rates were grouped in seagrass bioregions described by Short et al. (2007) (i.e., Temperate North Atlantic, Temperate North Pacific, Mediterranean, Tropical Atlantic, Tropical Indo-Pacific and Temperate Southern Oceans). Then, mean OC burial rates per unit area were estimated for each bioregion and globally. Global burial rates per unit area were estimated using two approaches. First, we used the geometric mean to characterize the central tendency of OC burial rates in seagrass sediments. Second, an area-weighted average was used, for which the relative contribution of each bioregion to the total seagrass extent was estimated. This was done by assigning estimates of seagrass coverage of specific areas described in the world Atlas of Seagrasses in their corresponding bioregion. The total extent given from these estimates was then considered the absolute seagrass area from which the relative contribution of each bioregion could be estimated (Table C4). Where recent updated estimates were available, such as for the Mediterranean region (Telesca et al., 2015), these were used instead of those reported in the Atlas.

Differences in OC content, MAR or OC burial rates between bioregions and seagrass species were analyzed using one-way ANOVA after log-transforming each of the data sets. When records that showed negligible sediment accumulation were included in the MAR or OC burial rate datasets, these were added as zeros. This precluded the log-transformation of these

datasets. In these situations, the non-parametric Mann-Whitney test was used to assess significant differences. All statistics were run using a level of significance of 0.05.

Over a 3-fold bracket exists in the global area reported for seagrass meadows (177,000 - 600,000 km^2) (Charpy-Roubaud et al., 1990; Green and Short, 2003). While the lower value is based in the total documented area and is an acknowledged underestimate (Short et al. 2003), most of the previous assessments of C burial rates in seagrass meadows have assumed a lower estimate of 300,000 km^2 (Duarte et al 2005). Therefore, here we use 300,000 and 600,000 km^2 as the lower and upper values to upscale seagrass OC burial rates to the global seagrass extent.

Bare sediments were treated separately, but the same univariate procedures and approaches were used to classify them, and estimate mean global OC burial rates in bare sediments adjacent to seagrass meadows. For those sites from which data for sediments from adjacent vegetated and un-vegetated patches were reported (7 sites; 30 records vegetated+bare), OC burial rates were also compared. We used a paired Sample Sign test to assess the difference between adjacent vegetated and un-vegetated sites since data was not normally distributed.

As opposed to recent reassessments of OC burial rates in tidal marshes and mangroves, here we additionally account for cases where intense mixing or negligible excess ^{210}Pb specific activities precluded the determination of sediment and OC accumulation rates. Sites where intense mixing (> ½ of the total dated depth) occurred, but maxima MAR and C burial rates were reported, were considered in the first computation of mean OC burial rates. Then, these records were excluded to assess potential overestimation of the result. Where negligible recent accumulation was recorded (i.e., where excess ^{210}Pb specific activities remained undetectable along the sediment core) (n = 31), we assumed contemporary OC burial was also negligible i.e., zero. We report, however, global OC burial rates in seagrass sediments with (n = 146) and without (n = 115) considering these cases.

4.3 Results

The dataset compiled on seagrass OC burial rates (Table C2) contained 167 individual estimates, derived from a total of 62 different sites from published and unpublished data. Thirty-five of the records were affected by intense sediment mixing but maxima C burial rates were

reported in 14 of them only. Negligible sediment and OC accumulation were reported in 31 out of the 167 records. Overall, a total of 115 records from our primary dataset reported favorable OC burial rates. Estimates were grouped according to seagrass bioregions (Short et al., 2007) for which we estimated their relative contribution to the total seagrass area according to various sources (Green and Short, 2003; Telesca et al., 2015) (Table C4). Most (70%) of the records were derived from eastern north American, Mediterranean and Australian seagrass meadows (Fig. 4.1). In contrast, we were unable to find any record of OC burial rates for seagrass meadows in the Pacific and Atlantic coasts of South America, South Africa, Atlantic coast of Africa, South and South East Asia, New Zealand and the West Pacific. Overall, estimates covered a latitudinal range between 64ºN and 35ºS, with 55% and 45% of the estimates derived from temperate and tropical and subtropical locations, respectively.
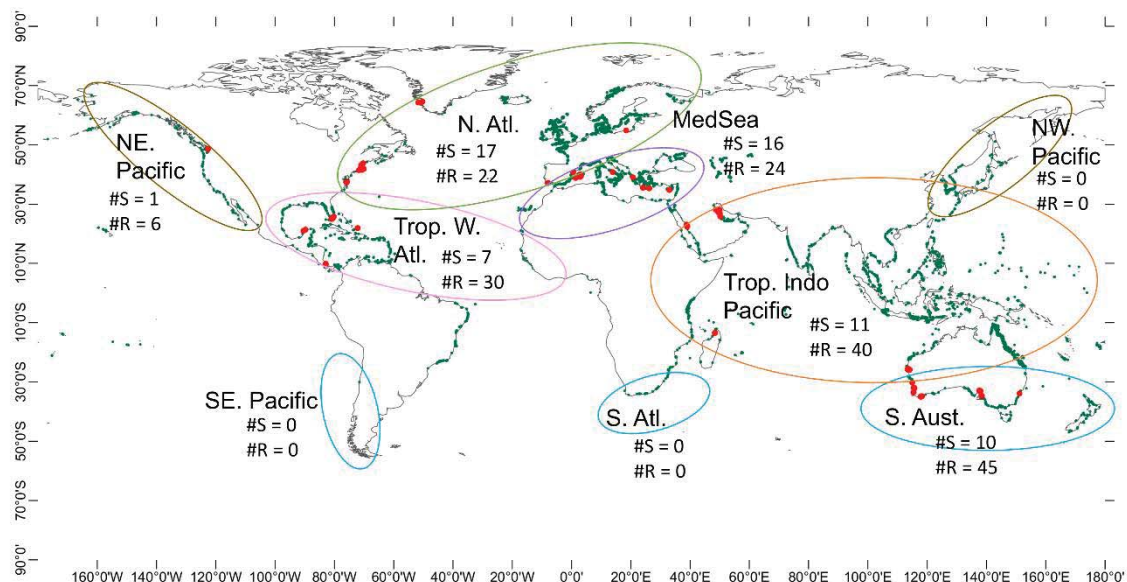
Figure 4.1: Locations of data on organic carbon burial rates in seagrass sediments, showing seagrass bioregions. Number of sites (#S) and records (#R). Global seagrass distribution shown as green dots (data from 2018 UNEP-WCMC) and geographic bioregions as colored circles: Temperate North Atlantic (green), Tropical Atlantic (pink), Mediterranean (purple), Tropical-Indo Pacific (orange), Temperate North Pacific (brown) and Temperate Southern Oceans (light blue).

An additional smaller dataset contained 19 records from barren areas adjacent to seagrass meadows such as bare sand patches or mudflats (Table C3). Eight of these records showed negligible sediment and OC accumulation, while 3 were affected by intense sediment mixing; maxima accumulation rates were reported in 2 of them.

89

Global variability in OC burial rates within vegetated sites was large, rates ranged widely, from 0.4 ± 0.2 (Ameralik, Greenland) to 420 ± 79 g C m^{-2} yr^{-1} (Biscayne Bay, USA) (Fig. 4.2). Regional and local ranges were similarly pronounced within sites and bioregions, but not among them. Within the North and Tropical W. Atlantic, minima and maxima estimates spanned almost two orders of magnitude, while there was an order of magnitude bracket within available estimates in the Mediterranean, the Tropical-Indo Pacific and South Australia regions. Locally, Ria Formosa, Florida Bay and Shark Bay showed some of the greatest variability with over 7-fold difference in OC burial rates between meadows.

The distribution of global OC burial rates in seagrass sediments was positively skewed towards low values (Fig. C1), thus the geometric mean was used to represent the central tendency (Table 4.1). As a result, contemporary OC burial rates in seagrass sediments worldwide were 24 ± 6 g C m^{-2} yr^{-1} (95% C.I. 20 - 30 g C m^{-2} yr^{-1}). This estimate did not vary significantly if the records affected by intense sediment mixing were excluded from computation (26 ± 6 g C m^{-2} yr^{-1}; 95% C.I. 21 - 32 g C m^{-2} yr^{-1}), although it did if records showing negligible sediment accumulation were included, assuming that their contemporary OC burial rate was zero (median: 17 g C m^{-2} yr^{-1}; 95% C.I. 12 - 22 g C m^{-2} yr^{-1}) ($P = 0.003$).

Organic C burial rates measured in seagrass sediments from the Tropical W. Atlantic region were the highest ($P < 0.001$), while no significant differences were observed between rates in the other 5 bioregions ($P > 0.05$) (Fig. 4.2). Considering the differences in regional seagrass area across the globe, we estimated that the area-weighted average of OC burial rates in seagrass sediments was 29 ± 2 g C m^{-2} yr^{-1} and was not significantly different than that estimated through the geometric mean of the entire dataset.
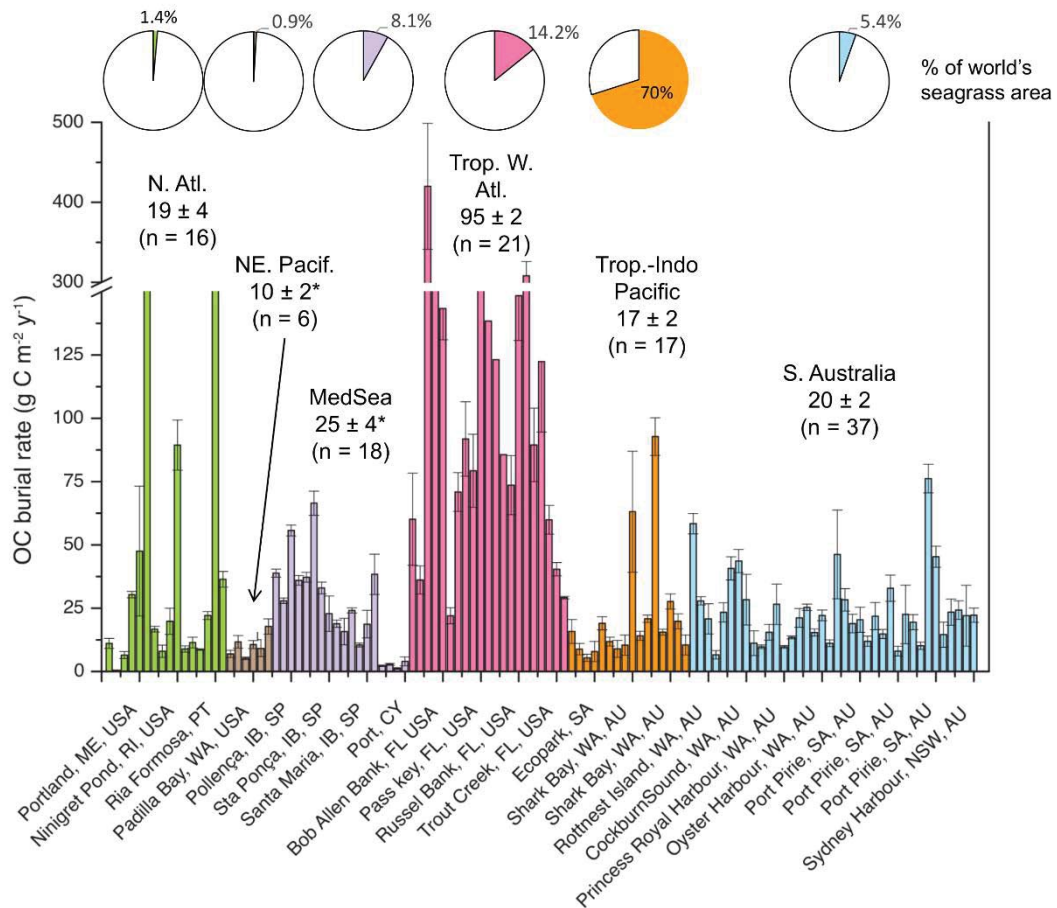
Figure 4.2: Contemporary organic carbon burial rates in seagrass meadows worldwide. The geometric mean ± SD is shown, except for * where the arithmetic mean was used as untransformed data were normally distributed. Pie charts illustrate the percent contribution of seagrass coverage at each bioregion to the global seagrass extent.

A multivariate analysis further confirmed that records were not clustered by bioregions but rather were characterized by having high or low sediment OC content or high MAR (Fig. 4.3). Principal components Pc1 and Pc2 explained 79% of the total variance among sampled seagrass sediments. Pc1 comprised 41% of the variance and was strongly correlated with OC burial rate ($r = 0.92$), MAR ($r = 0.76$) and moderately correlated with latitude ($r = -0.57$). Pc2 explained 38% of the variance and was correlated with sedimentary OC and DBD ($r = -0.77$ and $r = 0.87$, respectively) and moderately correlated with MAR ($r = 0.61$). Overall, MAR was a better predictor of OC burial rates than it was the sediment OC content (Fig. C2).

Table 4.1: Statistical results of distribution analyses for estimates at vegetated sites.

Parameter		Adjustment	Shapiro-Wil pValues	Skewness	Kurtosis	Mean	SD	Low. 95% CI	Up. 95% CI	Use Value
Burial rate ($g \, C \, m^{-2} \, yr^{-1}$)	Global	Unadjusted	< 0.0001	3.38	13.69	45	64	33	56	Geom. Mean: 24 95% C.I.: 20 - 30
		Ln-transformed	0.02659	-0.16	1.45	3.2	1.1	3.0	3.4	
	w/ negligible accumulation	Unadjusted	< 0.0001	3.67	16.54	35	60	25	45	Median: 17 95% C.I.: 12 - 22
		Ln-transformed	< 0.0001	-0.34	-0.72	1.6	1.6	1.3	1.8	
MAR ($g \, cm^{-2} \, yr^{-1}$)	Global	Unadjusted	< 0.0001	3.52	15.04	0.23	0.26	0.19	0.28	Geom. Mean: 0.16 95% C.I.: 0.14 - 0.19
		Ln-transformed	0.27489	0.31	0.62	-1.8	0.8	-2.0	-1.7	
	w/ negligible accumulation	Unadjusted	< 0.0001	3.70	16.56	0.19	0.29	0.15	0.24	Median: 17 95% C.I.: 12 - 22
		Ln-transformed	< 0.0001	2.58	8.59	-0.8	0.2	-0.9	-0.8	
OC (%)	Global	Unadjusted	< 0.0001	1.03	0.15	2.1	1.7	1.8	2.4	Median: 1.7 95% C.I.: 0.98–1.71
		Ln-transformed	< 0.0001	-0.78	0.71	0.37	0.99	0.18	0.55	
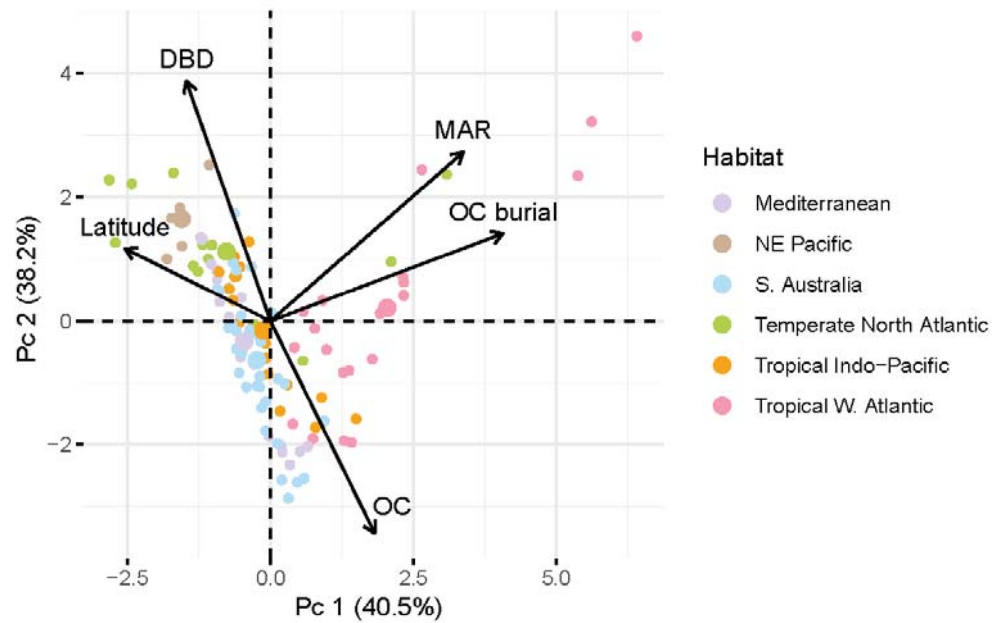
Figure 4.3: Principal component analysis on variables related to organic C burial rates measured in sediment records from vegetated seagrass sites. Biplot of variable vectors onto the component axis showing correlation between the variable and the component and individual factor map

Organic C content and mass accumulation rates (MAR) were obtained for all sites and were subjected to the same univariate procedure (Table 4.1). Organic C content of seagrass sediments varied widely, with a median measured OC of 1.7% of dry weight, and relatively infrequent high values (Fig. C1), resulting in a global average of 2.1%. Median and mean OC% were similar than those found in Fourqurean et al. (2012) for the upper meter of seagrass sediments globally. Global MAR observed in seagrass sediments accounted for 0.16 g cm^{-2} yr^{-1} (95% C.I. 0.14 - 0.19 g cm^{-2} yr^{-1}). This is equivalent to an accretion rate of 1.9 mm yr^{-1} (95% C.I.: 1.6 – 2.2 mm yr^{-1}) assuming a median dry bulk density of seagrass sediments of 0.85 g cm^{-3}, which was estimated from seagrass records where MAR estimates were favorable. However, at least 20% of the records in this study were taken in seagrass non-depositional locations as indicated by negligible specific activities of excess ^{210}Pb. Although colonized by seagrasses, these sediments were characterized by significantly higher DBD (1.18 g cm^{-3}) (P < 0.001) and lower OC content (0.5%) (P < 0.001) than vegetated sites where a net deposition was measured (DBD: 0.85 g cm^{-3}; OC: 1.7%). Considering these records in the computation of MAR within seagrass meadows, we estimated that, globally, median MAR could be lower, at 0.12 g cm^{-2} yr^{-1} (C.I.: 0.10 – 0.16 g cm^{-2} yr^{-1}) or 1.1 – 1.7 mm yr^{-1} (assuming a median DBD of 0.95 g cm^{-3}).

The examination of OC content and MAR across seagrass bioregions and species revealed significant differences in these parameters. Seagrass sediments in the Tropical W. Atlantic, South Australia and the Mediterranean colonized by seagrass species from the genus *Posidonia* and *Thalassia* contained the highest measured sedimentary OC (median: 2.4, 1.8 and 1.7%, respectively). However, MAR did not follow regional or species-specific trends, but was mostly influenced by local depositional settings. The highest MARs were observed in *Thalassia* beds in the tropical W. Atlantic, largely represented by Biscayne Bay and Florida Bay mudbanks (Fig. C3 and C4). Nonetheless, these differences in OC accumulation and storage should be viewed as preliminary owing to the scarcity of data from many locations.

Where OC burial rates were measured concurrently in seagrass meadows and adjacent bare areas (n = 30), no significant differences were observed between them (median bare vs. seagrass: 29 vs. 24 g C m^{-2} yr^{-1}; *P = 0.70*) (Fig. 4.4). Likewise, contemporary MAR

was not significantly different between paired seagrass (0.10 g cm^{-2} yr^{-1}) and bare sediments (0.08 g cm^{-2} yr^{-1}) ($P > 1.00$) as opposed to sedimentary OC content, which was significantly higher in paired vegetated sediments (median bare vs. seagrass: 0.8 vs. 1.6%) ($P < 0.001$). Additionally, a 43% of the records from barren areas showed negligible sediment and OC accumulation in the last century. This percentage was 20% in paired seagrass records.
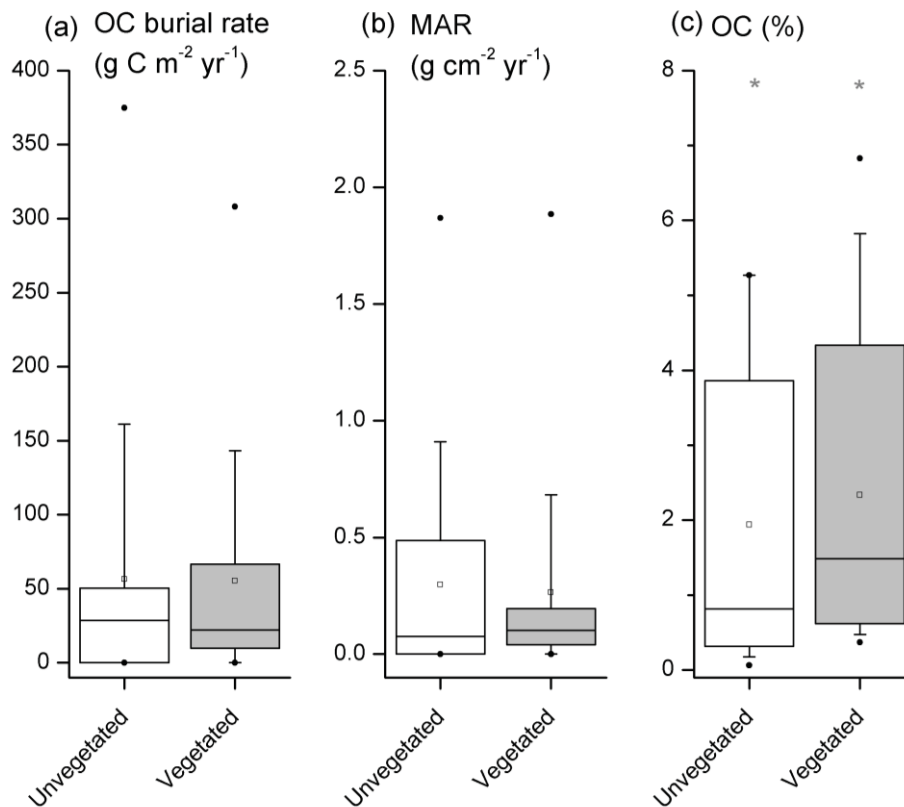
Figure 4.4: Boxplots showing organic carbon burial (a), mass accumulation rates (b) and organic carbon content (c) distribution in seagrass sediments and adjacent unvegetated sites. Boxes encompass the central 50% quantile; the line within the box represents the median and the square the average. The whiskers extend to the 10 and 90% quantiles and the points represent the 1% and 99% quantiles of the distribution. Asterisks show significant differences.

4.4. Discussion

4.4.1 OC burial rates in present and past assessments

The results presented indicate, on the basis of 115 directly measured century-scale OC burial rates, that seagrass meadows accumulate OC in their sediments at a contemporary rate that is between 3 and 7 times lower than previously estimated (Duarte et al., 2005, 2013a; Kennedy et al., 2010; McLeod et al., 2011). The difference between the global rate

estimated in this study and those in past assessments owes to the different methods used and the inclusion of new available estimates from previously less studied regions. Although our data is limited, the dataset compiled here contains about 20 to 30 times more individual estimates of directly measured OC burial rates than those used in past assessments.

The contemporary OC burial rate derived here (24 ± 6 g C m^{-2} yr^{-1}) is well below the geometric mean reported by Duarte et al. (2005) based on a much smaller dataset (n = 5) of directly measured burial rates (83 g C m^{-2} yr^{-1}), suggesting that earlier accounts were biased towards organic-rich *P. oceanica* meadows sustaining high OC accumulation rates. Subsequent assessments utilized the data set from Duarte et al. (2005) but included a synthesis of net community production of seagrass meadows (i.e., net amount of OC produced annually) (Duarte et al., 2010) and the concurrent burial of allochthonous OC (Kennedy et al., 2010) as an estimate of the total OC sink sustained by seagrass meadows. The arithmetic mean of OC burial rates and annual NCP from previous reviews (Duarte et al., 2005, 2010; Kennedy et al., 2010) was 138 ± 38 g C m^{-2} yr^{-1} and was reported by McLeod et al. (2011) as an estimate of the mean sediment OC burial rate in seagrass sediments. Our syntheses, however, has revised this estimate downward by 6 times if the geometric mean is considered and by 3 times when arithmetic means are compared (our arithmetic mean was 44 ± 6 g C m^{-2} yr^{-1}). While our estimate does refer to the total OC accumulation derived from seagrasses and allochthonous sources, it only accounts for the net accumulation in immediate seagrass sediments over the last century, thus excludes OC burial beyond the meadows, OC sequestration in biomass or recent burial of OC that may not have undergone significant diagenesis.

The global OC accumulation rate in seagrass sediments across the globe in recent ($\backsim$ 100 yr) timescales can be calculated by scaling up the estimates derived from this analysis (either the geometric mean or the area-weighted average) to the seagrass global extent. Since the area-weighted average and the geometric mean of OC burial rates were statistically the same, we used the latter for upscaling. The global extent of seagrass meadows, however, is poorly constrained because little or no records on seagrass coverage exists for large areas supporting extensive meadows (e.g., insular Southeast Asia, the east coast of South America and the west coast of Africa). Current estimates of seagrass extent have not improved since

last assessments and range between 300,000 and 600,000 km^2, thus the uncertainty in the upscaling of the C sequestration capacity provided by seagrass sediments remains as large as previously. Using these upper and lower values, we estimate that the global rate of OC accumulation in seagrass sediments ranges (95% C.I. of geom. mean) from 6 to 9 Tg C yr^{-1} (assuming minimal extent) and from 12 – 18 Tg C yr^{-1} (assuming maximal extent), making an annual difference of 42 – 94 Tg C relative to the previous global estimate (48 – 112 Tg C yr^{-1}; McLeod et al., 2011). Indeed, small differences in mean OC burial rates become more pronounced when raised to the global scale.

The OC burial rate in seagrass sediments from this study and past assessments can be compared with that in mangrove and salt marsh sediments and terrestrial forest soils, also considered to act as intense C sinks. On a per area basis, the mean OC accumulation rate in seagrass sediments is between 7 and 9 times lower than both its neighboring coastal mangrove and tidal marshes, but five times larger than that in terrestrial forest soils (Fig. 4.5). This contrasts with previous estimates where seagrasses supported comparable OC burial rates than mangroves and salt marshes and about 30 times higher burial rates than terrestrial forests soils. However, seagrasses are the most widespread among coastal BCE (Green and Short, 2003; Hamilton and Casey, 2016), thus its contribution to the total OC sequestration in vegetated coastal sediments is still large and accounts for 20 - 30%, globally (Table 4.2). Duarte et al. (2005) estimated that the contribution of coastal BCE to the total marine OC burial was 50% by adding the yet unaccounted OC burial by seagrasses, mangroves and tidal marshes to the long-standing estimates of marine OC burial (Berner, 1982; Hedges and Keil, 1995). Correcting for the OC burial rate in seagrass sediments estimated here and for those in mangroves and tidal marsh sediments from recent reassessments, we estimate that the OC burial in sediments of coastal BCE might account for 25 to 30% of the total burial of OC in the ocean, with burial in immediate seagrass sediments contributing between 4 and 8%. On a small scale, seagrass meadows may not be as efficient in burying OC in their sediments as previously thought, however its role as OC sinks on a global scale is remarkable, given they occupy less than 0.1% of the ocean surface.
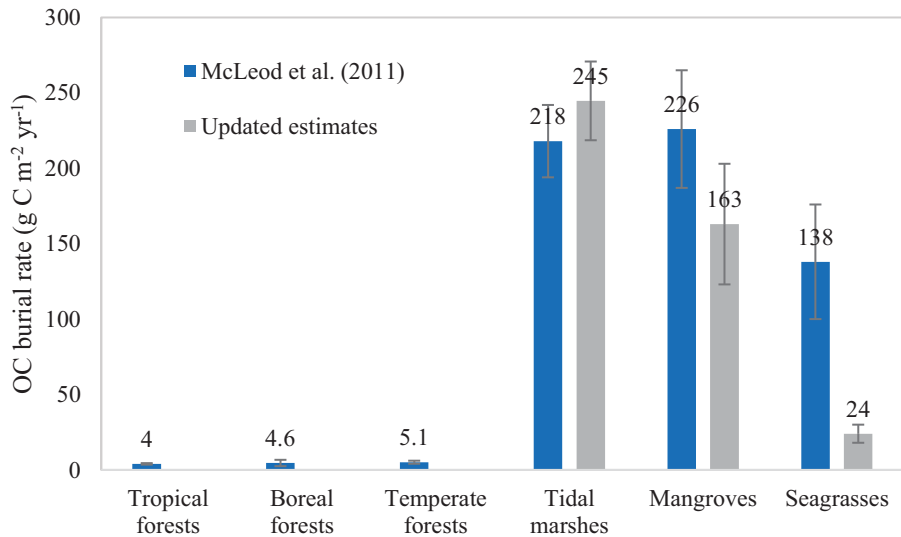
Figure 4.5: Estimates of organic carbon sequestration rates (g C m^{-2} yr^{-1}) in soils of terrestrial forests and in sediments of coastal vegetated ecosystems. Results from pervious and revised assessments are included. Error bars indicate SE of the mean. Updated estimates by Breithaupt et al. (2012), Ouyang and Lee (2014) and this study in mangrove, tidal marsh and seagrass ecosystems, respectively.

Table 4.2: Estimates of organic carbon burial rates in vegetated coastal habitats and their relative contribution to organic carbon burial in the coastal ocean and the global ocean. Modified from Duarte et al. (2005).

Compartment	Area extent 10^3 km^2	Burial g C m^{-2} yr^{-1}		Global burial Tg C yr^{-1}	
Vegetated coastal habitats					
Mangroves[a]	150	163	± 40	26	6
Tidal Marsh[b]	40	245	± 26	10.2	1.1
Seagrass	300-600	24	± 6	7.5 ± 1.5	15 ± 3
Total vegetated habitats		432	± 48	44 ± 6	51 ± 7
% Seagrass				**17 ± 4**	**29 ± 6**
Depositional areas[c]					
Estuaries	1.8	45		81	
Shelf	26.6	17		45	
Total coastal burial				170 ± 6	177 ± 7
% Seagrass				**4.4 ± 0.9**	**8.5 ± 1.7**
Deep Sea burial[c]				6	
Total oceanic burial				176 ± 6	183 ± 7
% Seagrass				**4.3 ± 0.9**	**8.2 ± 1.6**

[a](Breithaupt et al., 2012); [b](Ouyang and Lee, 2014); [c](Duarte et al., 2005 and references within it).

4.4.2 Organic carbon origins and delineation of seagrass OC burial

Carbon sequestration in seagrass sediments is supported by high rates of primary production but also by regular allochthonous sediment inputs (Duarte et al., 2013a). Seagrass meadows tend to be net autotrophic generating a large OC surplus of about 119 ± 26 g C m^{-2} yr^{-1}, which is not used by heterotrophs but is either buried in sediments or exported away (Duarte et al., 2010; Duarte and Chiscano, 1999). Assuming that half of the OC burial rate is supported by allochthonous sources (as was estimated globally; Kennedy et al., 2010), our results suggest that only between 8 and 13% (10 - 15 g C m^{-2} yr^{-1}) of the net seagrass community production is accumulated in situ within seagrass beds as opposed to the previously estimated 30- 50% (Kennedy et al., 2010). The remining 90% of the C fixed by seagrasses might be exported to adjacent shorelines, sediments outside seagrass meadows and in the deep sea (Duarte and Krause-Jensen, 2017; Heck et al., 2008) where it can be returned to the atmosphere as CO_2, buried, or remain in the ocean.

Evidence for export of seagrass-derived organic matter to adjacent bare sediments was provided by Kennedy et al. (2010) through a comparison between OC isotope signatures in seagrass sediments with that in un-vegetated sediments adjacent to the meadows. The authors showed that seagrass OC could be found buried in sediments at least tens of meters beyond the meadows. Here, three study locations provided data both from vegetated and unvegetated sediment $\delta^{13}C$ (Oreska et al., 2018; Serrano et al., 2016c; Arias-Ortiz et al., unpublished), the ratio of which was 1.2, 0.6 and 1.0, respectively, suggesting that a fraction of the accumulated OC was supported by adjacent seagrass meadows. Although the limited evidence presented in this study of seagrass-derived OC being buried in adjacent barren areas, we did not find significant differences in OC burial rates between vegetated and paired unvegetated adjacent sediments where net contemporary accumulation could be measured. On a global scale, the rate of sediment accumulation was the main driver delineating the OC sequestration capacity of both, seagrass beds and adjacent bare areas (Fig. C2), suggesting that local depositional patterns determine where both, seagrass-derived and allochthonous OC are buried.

4.4.3 Importance of seagrass meadows for OC preservation

The long-term sequestration of OC in sediments is not effectuated solely with burial, yet the effective preservation of the buried OC is also required. Seagrasses play a major role in stabilizing sediments thanks to the entangled network of roots (and rhizomes) that prevent sediment resuspension and erosion increasing the retention of sediments and the associated OC (Duarte et al., 2013b). In turn, low oxygen concentrations in seagrass sediments are favored, as opposed to sediments exposed to repeated resuspension/redeposition cycles that act to enhance the degradation of organic matter (Burdige, 2007). If seagrass meadows are lost, the accumulated OC stocks may be subject to oxidizing conditions, thus have more chances to be remineralized faster (Lovelock et al., 2017a). Although limited, our data provided evidence for the enhanced preservation of OC in vegetated sediments. The seagrass–bare comparison illustrated that sediments colonized by seagrasses contained significantly higher OC content ($P < 0.001$), while the proportion of sites showing no net contemporary sediment accumulation was 20% larger in bare than in vegetated sediments.

Lovelock et al. (2017b) modelled potential OC losses under oxic conditions after ecosystem disturbance and compared them with observations of OC stock loss in previous studies. For seagrasses, they found that the loss rate of sediment OC after habitat disturbance represented about 1 to 4%yr^{-1} of the sediment OC stock accumulated in the upper meter. Assuming a median OC stock of 140 Mg C ha^{-1} as in Lovelock et al. (2017b) and as estimated globally; Fourqurean et al., 2012b) we are looking at an annual loss rate that is from 6 to 20 times larger the mean OC accumulation rate in seagrass sediments estimated globally. Conservation of seagrass is crucial to maintain the ecosystem services these habitats provide, including their OC sequestration capacity. However on a local scale, conserving seagrass meadows and avoiding further seagrass loss is a more effective tool in reducing significant GHG emissions substantially reducing mitigation costs.

4.5. Conclusions

The results presented here suggest that the OC burial rate in seagrass sediments should be revised downwards to 24 ± 6 g C m^{-2} yr^{-1} (or 6 – 18 Tg C yr^{-1} globally) to better account for the C sequestration capacity that occurs in immediate seagrass sediments. While

this fraction of the seagrass C budget accounts for 4 to 8% of the total marine OC burial in the ocean, the significance of seagrass ecosystems as C sinks may indeed be larger. We estimated that about 90% (32 – 65 Tg C yr^{-1}) of its net community production is exported to adjacent systems where it can be buried beyond the meadows, preserved in the deep sea or consumed. Because the global OC exported from seagrass meadows might be 4-fold the C sequestered in immediate sediments, evaluating the fate and magnitude of the potential contribution of this fraction to C sequestration is important to improve current estimates of the role of seagrasses as C sinks in the ocean. Although the present dataset of contemporary OC burial rates in seagrass sediments has been expanded beyond the Mediterranean region, Present imbalances in the geographic distribution of the available data could lead to biases of the global estimate. This is especially true if OC burial rates in the tropical Indo-pacific region (which represent 70% of the total seagrass area) were not well constrained. Indeed, small changes in this regional estimate could have a large influence on a global scale. Therefore, beyond the requirement for a more accurate knowledge of global seagrass cover, a more extensive investigation of OC burial rates in major yet unexplored seagrass meadows across the Indo-Pacific such as S. and SE. Asia is needed.

This work is under progress and inclusion of new data from both seagrass and bare areas is planned. In addition, examination of local traits such as water column depth, grain size, hydrological influence or differences in the isotopic composition of OC in sediments will be conducted alongside the exposed results. Because local conditions appear to play a so prominent role in sediment and OC accumulation, this may help to delineate different patterns of deposition across seagrass meadows globally and maybe help to prioritize sites where OC accumulation is enhanced or where risk and impact of OC loss is more severe.

Chapter 5

A marine heatwave drives massive losses from the world's largest seagrass carbon stocks[1,2]

Seagrass ecosystems contain globally significant organic carbon (C) stocks. However, climate change and increasing frequency of extreme events threaten their preservation. Shark Bay, Western Australia, has the largest C stock reported for a seagrass ecosystem, containing up to 1.3% of the total C stored within the top meter of seagrass sediments worldwide. Based on field studies and satellite imagery, we estimate that 36% of Shark Bay's seagrass meadows were damaged following a marine heat wave in 2010/11. Assuming that 10 to 50% of the seagrass sediment C stock was exposed to oxic conditions after disturbance, between 2 and 9 Tg CO_2 could have been released to the atmosphere during the following three years, increasing emissions from land-use change in Australia by 4 - 21% per annum. With heat waves predicted to increase with further climate warming, conservation of seagrass ecosystems is essential to avoid adverse feedbacks on the climate system.

5.1 Introduction

Vegetated coastal ecosystems, including seagrass meadows, mangroves and tidal marshes, are collectively termed "blue carbon" ecosystems storing globally-relevant carbon stocks in their sediments and biomass (McLeod et al., 2011). Their organic carbon (C) sink capacity is estimated to be 0.08-0.22 Pg C yr^{-1} globally (Duarte et al., 2013b), accounting for an offset of 0.6 - 2% of global anthropogenic CO_2 emissions (49 Pg CO_2eq yr^{-1}) (IPCC 2014, 2014). However, blue carbon ecosystems are in decline worldwide (Duarte et al., 2013b), raising concern about a potential re-emission of their C stocks to the atmosphere as CO_2. CO_2 emissions from loss of blue carbon ecosystems are estimated at 0.15 - 1.02 Pg CO_2 yr^{-1}, which is equivalent to 3 – 19% of those from terrestrial land-use change (Pendleton et al., 2012).

Seagrasses are marine flowering plants that consist of 72 species growing across a wide range of habitats (Short et al., 2011). Global estimates of C storage in the top meter of seagrass sediments range from 4.2 to 8.4 Pg C (Fourqurean et al., 2012b), although large spatial variability exists related to differences in biological (e.g., meadow productivity and density), chemical (e.g., recalcitrance of C) and physical (e.g., hydrodynamics and bathymetry) settings in which they occur (Lavery et al., 2013; Serrano et al., 2016d). Since the beginning of the twentieth century, seagrass meadows worldwide have declined at a median rate of 0.9% yr^{-1} mostly due to human impacts such as coastal development or water quality degradation (Waycott et al., 2009). Climate change impacts, such as ocean warming and extreme events (e.g., ENSO), are exacerbating this trend. Marine heat waves have led to losses of foundation seagrass species that form organic-rich sediment deposits beneath their canopies (e.g. *Posidonia oceanica* in the Mediterranean Sea (Marbà and Duarte, 2009) and *Amphibolis antarctica* in Western Australia (Fraser et al., 2014b; Nowicki et al., 2017; Thomson et al., 2014). Seagrass losses and the subsequent erosion and remineralization of their sediment C stocks are likely to continue or intensify under climate change (Waycott et al., 2009), especially in regions where seagrasses live close to their thermal tolerance limits (Walker et al., 2004).

Shark Bay (Western Australia) (Fig. 5.1) contains one of the largest (4,300 km²) and most diverse assemblage of seagrasses worldwide (Walker et al., 1988), occupying between 0.7 and 2.4% of the world seagrass area. Up to 12 seagrass species are found in Shark Bay, storing C in their sediments and shaping its geomorphology. The two most notable seagrass banks, the Wooramel Bank and the Faure Sill, are the result of ~8,000 yr of continuous seagrass growth (Bufarale and Collins, 2015). Despite seagrasses having thrived over millennia in Shark Bay, unprecedented widespread losses occurred in the austral summer of 2010/2011 in both the above- and below-ground biomass of the dominant seagrass *A. antarctica* and to a minor extent *P. australis* (Nowicki et al., 2017; Thomson et al., 2014), the two species forming large continuous beds. For more than 2 months, a marine heat wave elevated water temperatures 2-4°C above long-term averages (Wernberg et al., 2012). The event was associated with unusually strong La Niña conditions during the summer months that caused an increased transfer of tropical warm waters down the coast of Western Australia. With increased rates of seawater-warming in the South-East Indian Ocean and in the continental shelf of Western Australia (Pearce and Feng, 2007), Shark Bay's seagrass meadows are at risk from further ocean warming and acute temperature extremes due to their location at the northern edge of their geographical distribution. This trend could potentially accelerate the loss of one of the largest remaining

Figure 5.1: Shark Bay World Heritage Site with spatial distribution of seagrass. The two most notable seagrass banks are the Faure Sill (FS) and Wooramel (W), to the west is Peron Peninsula (P). The hatched region represents Shark Bay's Marine Park and locations of individual sites within the study region are represented as solid dots. Seagrass spatial distribution (DBCA, 2016).

seagrass ecosystems on Earth and result in large CO_2 emissions. Based on data from 49 sampled sites (Arias-Ortiz et al., 2017), satellite imagery and a published model of soil C loss following disturbance (Lovelock et al., 2017b), we quantify the sediment C stocks and accumulation rates in Shark Bay's seagrasses and estimate the total seagrass area lost after the marine heat wave. We then provide a comprehensive assessment of the potential impact of seagrass losses on sediment C stocks and associated CO_2 emissions in the short- (3 years) and long-term (40 years) related to changes from anoxic to oxic conditions of previously vegetated sediments.

5.2 Methods

Seagrass sediments were sampled using PVC cores (100 - 300 cm long, 6.5 cm internal diameter) that were hammered into the substrate at 0.5 to 4 m water depth. In the laboratory, the PVC corers were cut lengthwise, and the sediments inside the corers were sliced at 1 or 3 cm-thick intervals. Analysis of ^{210}Pb, ^{14}C and grain size were conducted in cores cut at 1 cm resolution (11 cores), while dry bulk density (DBD), %C, δ^{13}C were measured in all cores (28 cores) in alternate slices every 3 cm (upper 50 cm), and every 6 cm (below 50 cm). We combined our data with previously published studies in Shark Bay involving coring in seagrass sediments (Bufarale and Collins, 2015; Fourqurean et al., 2012a; Lavery et al., 2013). From Bufarale and Collins (2015), we took core FDW2 (here W4) dated by ^{14}C and we analyzed grain size, %C and δ^{13}C to include it in the dataset. From Fourqurean et al. (2012a) we included the C data from the 8 long sediment cores (here W5 – W8 and FS15 – FS18) and from Lavery et al. (2013b) we included C and δ^{13}C data of twelve 27 cm-long cores (here P1 and P2) in this study (Arias-Ortiz et al., 2017). Compression of seagrass sediments during coring was corrected by distributing the spatial discordances proportionally between the expected and the observed sediment column layers (Glew et al., 2001) and was accounted for in the calculations of C stocks standardized to 1 m depth and 4,000 cal yr BP. Average compression was 20% and was applied to published data where compression existed but was not measured during sampling (Bufarale and Collins, 2015; Lavery et al., 2013). Published and unpublished cores from this study comprised 49 locations covering a range of 3 seagrass genera forming monospecific and

mixed meadows, 34 contained data deeper than 1 meter with 23 sites extending down to 2-3 meters (Appendix D, Table D3). None of the cores penetrated the entire thickness of seagrass-accumulated sediment estimated to range from 4 to 6 m (Bufarale and Collins, 2015).

The C content of sediments was measured in pre-acidified (with 1 M HCl) samples. One gram of ground sample was acidified to remove inorganic carbon after weighing, centrifuged (3,400 revolutions per minute, for 5 min), and the supernatant with acid residues was carefully removed by pipette, avoiding resuspension. The sample was then washed with Milli-Q water, centrifuged and the supernatant removed. The residual samples were then re-dried at 60ºC and encapsulated in tin capsules for C and δ^{13}C analyses using an Elemental Analyzer - Isotope Ratio Mass Spectrometer (Hilo Analytical Laboratory) at the University of Hawaii. C content (%C) was calculated for the bulk (pre-acidified) samples using the formula $C_{bulk} = C_{acidified} \frac{mass\ acidified}{mass\ pre-acidified}$. The method used to remove inorganic carbon prior to C analyses may lead to the loss of part of the organic C (soluble fraction), thereby potentially leading to an underestimation of sediment C content (Brodie et al., 2011; Phillips et al., 2011). The sediment δ^{13}C signature is expressed as δ values in parts per thousand relative to the Vienna Pee Dee Belemnite. Replicate assays and standards indicated measurement errors of $\pm 0.04\%$ and $\pm 0.1‰$ for C content and δ^{13}C, respectively. The relative contribution of seagrass, macroalgae and seston (that includes living and non-living matter in the water column) and terrestrial matter to seagrass top meter sediment carbon pools was computed applying a three-component isotope-mixing model as described by Phillips and Gregg (2003) and calculated by means of the IsoSource Visual Basic program (Phillips and Gregg, 2003), using a 1% increment and 0.1‰ tolerance. We used literature values for putative C sources and macroalgae and seston were combined as a single C source since their published δ^{13}C endmembers were not significantly different (Appendix D, Table D2).

Sediment grain-size was measured with a Mastersizer 2000 laser diffraction particle analyzer following digestion of bulk samples with 10% hydrogen peroxide at the Centre for Advanced Studies of Blanes. The d_{50} (i.e. the median particle diameter) was used as a proxy for the particle size distribution. Sediments were classified as sand (0.063 - 1 mm), silt (0.004 - 0.063 mm) and clay (< 0.004 mm), and the mud fraction was calculated as the sum of the

fractions of silt and clay (< 0.063 mm) (size scale: Wentworth, 1922). Sand:mud ratio was used as a proxy for depositional conditions and hydrodynamic energy, where higher sand content could be associated with higher energy environments (Flemming, 2000).

Spearman correlation tests were used to assess significant relationships between C concentrations and environmental (i.e. DBD, d50, %sand, %mud and sand:mud ratio) and biological (i.e. %C and δ^{13}C) variables measured in seagrass sediment cores as none of the variables followed a normal distribution (Appendix D, Table D1).

Eleven sediment cores were analyzed for ^{210}Pb concentrations to determine recent (ca. 100 years) sediment accumulation rates. ^{210}Pb was determined through the analysis of ^{210}Po by alpha spectrometry after addition of ^{209}Po as an internal tracer and digestion in acid media using an analytical microwave (Sanchez-Cabeza et al., 1998). The concentrations of ^{210}Pb$_{xs}$ used to obtain the age models were determined as the difference between total ^{210}Pb and ^{226}Ra (^{210}Pb$_{sup}$). Concentrations of ^{226}Ra were determined for selected samples along each core by low-background liquid scintillation counting method (Wallac 1220 Quantulus) adapted from Masqué et al. (2002). Mean sediment accumulation rates over the last 100 years could be estimated for eight out of the eleven sediment cores dated using the CF:CS model below the surface mixed layer when present (Krishnaswamy et al., 1971). Mixing was common from 0 to 4 cm in half of the dated sediment cores, hence average modern accumulation rates should be considered as upper limits. Two to five samples of shells per core from the cores dated by ^{210}Pb were also radiocarbon-dated at the Direct AMS-Radiocarbon Business Unit, Accium Biosciences, USA, following standard procedures (Stuiver and Polach, 1977). The conventional radiocarbon ages reported by the laboratory were converted into calendar dates (cal yr BP) using the Bacon software (Marine13 curve) (Blaauw and Christen, 2011) and applying a marine reservoir correction (i.e. subtracting Delta R value of 85 ± 30 for the East Indian Ocean, Western Australia) (Squire et al., 2013). Average short-term C accumulation rates were estimated by multiplying sediment accumulation rates (g cm^{-2} yr^{-1}) by the fraction of C accumulated to 100 yr depth determined by ^{210}Pb dating. Bacon model output was used to estimate average long-term sediment accumulation rates (g cm^{-2} yr^{-1}) during the last 1,000 yr BP. Long-term C accumulation rates were determined following the same method as for short-term accumulation rates, but the

fraction of C was normalized to 1,000 cal yr BP, as the minimum age of the ^{14}C-dated bottom sediments was 1,117± 61 cal yr BP (Appendix D, Table D4).

C stocks at the 49 locations were estimated for 1 m sediment thickness and for a period of accumulation of 4,000 years, similar to the time of formation of the C deposits (Bufarale and Collins, 2015). We standardized the estimates of sediment C stocks to one meter thick deposits since this allows comparisons with estimates of global stocks. Where necessary (i.e. in 15 cores), we inferred C stocks below the limits of the reported data to 1 m, extrapolating linearly integrated values of C content (cumulative C stock Mg C ha^{-1}) with depth. C content was reported to at least 27 cm in 12 cores out of these 15, while the other 3 cores had C data down to 55 - 83 cm. Correlation between extrapolated C stocks from 27 cm to 1 m and measured C stocks in sediment cores $\geq$ 1 m was r = 0.82 P < 0.001 (Appendix D, Fig. D3a). Sediment C stocks in the $\geq$ 1 meter cores ranged from 23 to 322 Mg C ha^{-1}, with a mean value of 116 $\pm$ 13 Mg C ha^{-1} and median 109 Mg C ha^{-1}. Extrapolating data on cumulative C stocks from cores of at least 27 cm depth at a further 15 sites to 1 m, we estimated C storage at those sites to range between 26 and 313 Mg C ha^{-1}, similar to sites with full inventories. Combining the estimates extrapolated from shallow cores with full core inventories, the resulting mean and median sediment C storage (103 $\pm$ 11 Mg C ha^{-1} and 73 Mg C ha^{-1}, respectively) (Appendix D, Fig. D4) were not significantly different (P > 0.05) from those for full core inventories. We applied ordinary kriging to estimate the top 1 meter C stocks across 2,000 km^2 encompassing the South Wooramel Bank, Faure Sill and Peron Peninsula seagrass banks (Wackernagel, 2003; Webster and Oliver, 2001). We used a maximum of the 16 nearest neighbours within a search circle of radius 25 km. Ordinary kriging inherently declusters the input data and produces smoothed estimates, so that the extremely high or low values found within seagrass meadows of the Bay do not disproportionately influence the global mean.

We estimated seagrass sediment C stocks accumulated over the last 4,000 years in 1 to 3 m long cores where ^{14}C data were available and the length sampled embraced $\geq$ 2,000 yr of sediment and C accumulation (i.e. in 8 cores). The correlation between extrapolated and measured C stocks was r = 0.90 (P < 0.05) (Appendix D, Fig. D3b). Bay-wide estimates of sediment C stocks accumulated over 4,000 cal yr BP were estimated by combining

extrapolated and full 4,000 cal yr BP core inventories and applying collocated cokriging with top meter C stocks as the secondary variable. Correlation between top meter and 4,000 yr BP carbon stocks was 0.6 ($P < 0.01$) and the percentage of noise specific to the background was set to 20%. Spatial variability of C stocks was mapped after applying Ordinary Kriging (OK) to top meter C stocks and collocated co-kriging to millenary C stock (4,000 cal yr BP).

Data on seagrass sediment C stocks accumulated during the last 4,000 yr in *P. oceanica* were extracted or extrapolated from published estimates (Serrano et al., 2016e) of sediment cores with a sampled depth of at least 2,000 yr, as this is the same method we used to estimate long-term C_{org} stocks at Shark Bay.

The extent of seagrass meadows in Shark Bay before and after the extreme climatic event was determined by the Western Australian Department of Biodiversity, Conservation and Attractions as part of a broader long-term seagrass monitoring program. Seagrass extent was derived using a supervised classification of imagery captured by Landsat–5 Thematic Mapper (TM) in 2002 and Landsat–8 Operational Land Imager (OLI) in 2014 (United States Geological Survey (glovis.usgs.gov/)). The spatial resolution of these images is 30 m. The 2002 and 2014 classifications used a combination of historical ground-truthing, long-term monitoring data and expert knowledge for training sites and validation. The imagery was classified into three distinct classes; 'dense seagrass' (> 40% cover); 'sparse seagrass' (< 40% cover) and 'other' which included all remaining habitat types. The Shark Bay Marine Park (SBMP) covers approximately 8,900 km^2 of seafloor. The seagrass mapping presented here covers approximately 78% of SBMP. The entire extent was not mapped due to poor image quality caused by depth and water clarity and the lack of data in some areas.

Net seagrass area losses and shifts in seagrass cover from dense to sparse were considered as damaged areas, where the seagrass sediment organic matter is more exposed oxygen due to erosion and sediment resuspension, hence is more susceptible to being rapidly remineralized. We modelled the potential CO_2 emissions associated with this disturbance and subsequent remineralization of sediment C stocks using equation 5.1 based on varying proportions of sediment C being exposed to oxic conditions following disturbance:

$$C_t = \alpha \cdot C_0 \cdot e^{-k_1 \cdot t} \tag{5.1}$$

where $C_{(0)}$ is the measured C stock in the top meter, a is the fraction of the C stock exposed to oxic conditions and k_1 is the decomposition rate of seagrass sediment C (0.183 yr^{-1}) (Lovelock et al., 2017b) in oxic sediment conditions.

This required a number of assumption which were: (1) the C stock over the top meter (Mg C ha^{-1}) of sampled seagrass meadows was representative of the C stock contained in sediments within the damaged seagrass area prior to the heat-wave; (2) the fraction of the sediment C in disturbed seagrass meadows exposed to oxic environments was in the range of 0.1 to 0.5; (3) the potential contribution of seagrass biomass remineralization to CO_2 emissions was not accounted for due to the lack of knowledge about the export and fate of plant biomass following meadows loss; and (4) there will be no recovery of seagrass in the long-term (i.e., 40 yr). With the exception of the last assumption, these were conservative, in an effort to avoid over-estimation of potential CO_2 emissions. We assessed the loss of C to the atmosphere after 3 years post disturbance (in 2014) and also assessed potential releases over a 40-year time frame consistent of tier 1 and 2 methods of IPCC (2006) for organic soils. The C stock loss per hectare 3 years and 40 years post disturbance was multiplied by the damaged seagrass area (1,125 km^2).

5.3 Results and Discussion

5.3.1 Sediment C content and sources

The C content of seagrass sediments in Shark Bay varied widely (0.01 - 9.00%), with the median (1.5%) and mean ± SE (2.00 ± 0.06%) values for the top meter similar to global estimates (median: 1.8% C; mean ± SE: 2.5 ± 0.1% C) (Fourqurean et al., 2012b), though spatial variability was observed (Fig. 5.2). C content increased eastwards towards Shark Bay's main coastline, inversely to dry bulk density (DBD) (ρ = -0.69; $P \leq 0.001$) (Appendix D, Fig. D1 and Table D1). Seagrass sediments had an average δ^{13}C-value of -13.3 ± 0.1‰ (±SE) throughout the entire Bay and thickness of the sampled sediment deposits. The δ^{13}C signatures of potential C sources (seagrasses: -9.4 ± 1.3‰ (Burkholder et al., 2011); terrestrial-derived C from the Wooramel River: -25.1‰ (Cawley et al., 2012); seston, i.e., suspended organic matter in the water column: -19.3 ± 2.5‰ (Cawley et al., 2012) and macroalgae: -18.1 ± 1.8‰ (Burkholder et al., 2011) indicated that seagrasses were the main

sources of sediment C as allochthonous matter (i.e. terrestrial inputs, seston or macroalgae) could not account for the ^{13}C-enriched C pools stored in seagrass sediments (Appendix D, Table D2). Using a three source mixing model and literature values for putative sources, the average contribution of seagrass to the entire depth of the sediment C stocks was estimated to be ~65% (Appendix D, Fig. D2), higher than the ~50% estimate of seagrass contribution to surface sediments in seagrass ecosystems globally (Kennedy et al., 2010).

The predominantly autochthonous nature of sediment C pools in Shark Bay seagrass meadows and the weak correlation between sediment C and sediment physical properties such as grain size (Appendix D, Table D1) reinforces their significance for carbon sequestration. Seagrass detritus contains relatively high amounts of degradation-resistant compounds (Trevathan-Tackett et al., 2015) compared to seston and algal detritus (Laursen et al., 1996), which are characterized by faster decomposition rates (Enríquez et al., 1993). The relatively high contribution of seagrass matter throughout the 2-3 m thick sediment deposits at Shark Bay is likely related to the low land-derived C inputs and the stability and high productivity of these meadows, which promotes the accumulation of thick organic-rich sediments, comparable to those found in *P. oceanica* meadows in the Mediterranean Sea (Serrano et al., 2016e).

5.3.2 Seagrass C storage hotspot

The C stocks per unit area in the top meter of seagrass sediments in Shark Bay averaged 128 ± 7 Mg C ha^{-1} ($\pm$SE), with 50% of the stocks having values between 92 and 161 Mg C ha^{-1} (Q_1 and Q_3, respectively) (Fig. 5.3a). While this is in agreement with reported median seagrass sediment C stock at a global scale (140 Mg C ha^{-1}) (Fourqurean et al., 2012b), the southeastern half of Shark Bay (i.e., South Wooramel Bank and Faure Sill) constitutes a hotspot of C storage (245 ± 6 Mg C ha^{-1}).

Average sediment C stocks in 1 m-thick deposits in Shark Bay are similar to those in temperate-tropical forests (122 Mg C ha^{-1}) and tidal marshes (160 Mg C ha^{-1}), while the C stocks in Shark Bay's hotspots compare with those of mangroves and boreal forests (255 Mg C ha^{-1} and 296 Mg C ha^{-1}, respectively) (Fourqurean et al., 2012b; Prentice et al., 2001). Assuming that the C stocks in the surveyed area are representative of the entire seagrass

extent (4,300 km^2), we estimated that seagrass sediments at Shark Bay contained a total of 55 ± 3 Tg C in the top 1 meter, which is equivalent to 0.65 - 1.3% of the total C stored in seagrass sediments worldwide (4.2 - 8.4 Pg C) (Fourqurean et al., 2012b).
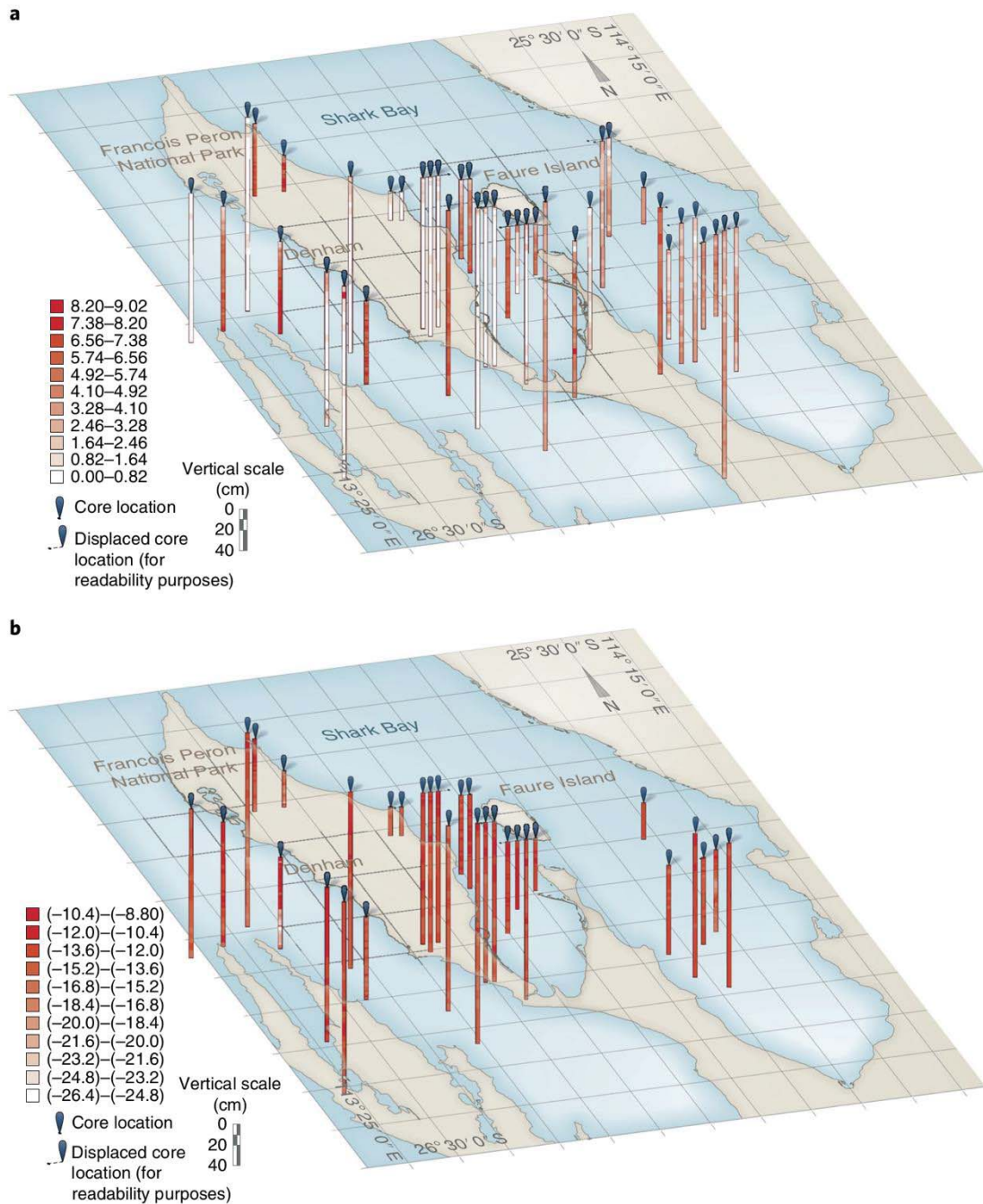
Figure 5.2: Spatial distribution of organic carbon in seagrass sediments of Shark Bay. Measured organic carbon content (percentage of C) (a) and δ13C stable isotopic signature of C (b) along the entire thickness of the sampled sediments. Average δ13C values for the main seagrass banks: Wooramel Bank: − 13.83 ± 0.02%; Faure Sill: − 13.0 ± 0.1% Peron: − 13.4 ± 0.1%.
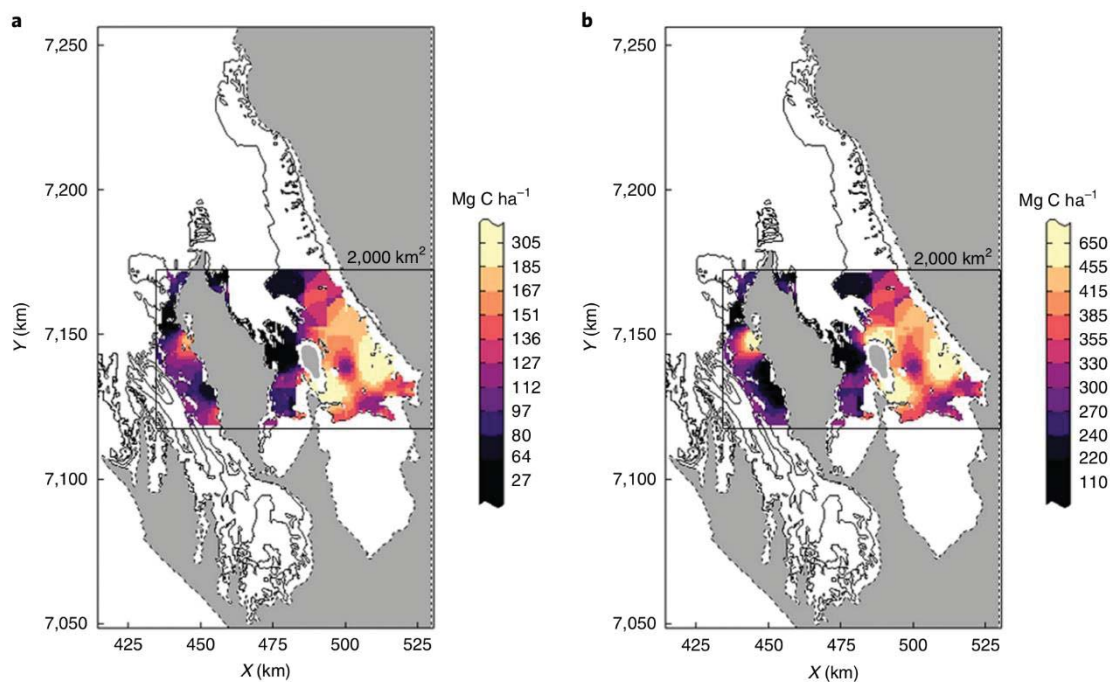
Figure 5.3: Spatial distribution of organic carbon stocks in seagrass sediments of Shark Bay. Top-metre C stocks (a). C stocks accumulated over the last 4,000 cal yr bp (b). The area with C storage estimates covers 2,000 km^2 of seagrass sediments. The integrated sediment C stock within the 2,000 km^2 of surveyed seagrass area was estimated at 24 Tg C in the top metre and 64 Tg C over the last 4,000 cal yr bp.

These estimates are limited to the upper meter of seagrass sediment C stocks (as are the global estimates) and, therefore, are likely underestimates of full C inventories since seagrass C deposits reach several meters in thickness in Shark Bay (Bufarale and Collins, 2015). Seismic profiles combined with ^{14}C dating indicate that the seagrass banks here contain a continuous 4,000 yr record of sediment and C accumulation (Bufarale and Collins, 2015). This corresponds to an average sediment thickness of 3.1 ± 0.4 m, as indicated by long-term sediment accumulation rates estimated in this study (mean ± SE: 0.77 ± 0.11 mm yr^{-1}; Table 5.1), in agreement with vertical accretion rates of ~1 mm yr^{-1} published by others (Bufarale and Collins, 2015; Davis, 1970) and supported by the dominant seagrass δ^{13}C signature of sediment C along the cores. Based on those, the C stocks accumulated over the last 4,000 cal yr BP averaged 334 ± 34 Mg C ha^{-1}. Stocks were as high as 650 Mg C ha^{-1} towards the south of the Wooramel Bank and Faure Sill, and decreased to 110 Mg C ha^{-1} towards the northwest (Fig. 5.3b). Assuming that the average millenary C deposits studied here are representative throughout the entire seagrass extent (4,300 km^2), the seagrass sediments in Shark Bay would have accumulated a total of 144 ± 14 Tg C over the last 4,000 yr. While Mediterranean *P. oceanica* meadows have the highest sediment C stocks per unit

area (372 ± 38 Mg C ha⁻¹) in the top meter (Fourqurean et al., 2012b) and 1027 ± 314 Mg C ha⁻¹ over the last 4,000 yr BP (Serrano et al., 2016e), the vast extent of Shark Bay's meadows makes their sediments the world's largest seagrass C stocks yet reported for a seagrass ecosystem.

Table 5.1: Short- and long-term sedimentation, organic carbon (C) accumulation rates and sediment C stocks accumulated over the last 4,000 yr BP. Sedimentation and C accumulation rates were estimated by ^{210}Pb, ^{14}C dating of sediments and the depth-weighted average of C concentrations (short-term normalized to 100 yr depth, and long-term to 1,000 cal yr BP depth). Uncertainties represent SE of the regression and the result of error propagation for sedimentation rates, and C accumulation rates and stocks, respectively.

Core ID	Sedimentation rates (mm yr⁻¹)		C accumulation (g C m⁻² yr⁻¹)		C stocks 4,000 cal yr BP (Mg C ha⁻¹)
	Short-term (last 100 yr)	Long-term (last 1,000 - 6,000 cal yr BP)	Short-term (last 100 yr)	Long-term (last 1,000 cal yr BP)	
W3	2.3 ± 0.9	0.58 ± 0.08	77 ± 41	14.1 ± 2.6	369 ± 51
W4		1.08 ± 0.33		32.1 ± 13.9	1338 ± 390
FS7	2.3 ± 0.3	1.48 ± 0.06	29 ± 5	12.9 ± 0.7	
FS9	1.7 ± 0.1	0.74 ± 0.03	27 ± 3	8.5 ± 0.4	304 ± 12
FS11	3.1 ± 0.2		123 ± 14		
FS13	2.6 ± 0.2	0.69 ± 0.02	25 ± 3	8.7 ± 0.3	528 ± 14
FS14	4.5 ± 0.5	1.31 ± 0.07	45 ± 7	15.2 ± 1.2	
P5		0.43 ± 0.05		6.7 ± 0.3	242 ± 6
P7		0.66 ± 0.02		11.3 ± 0.3	310 ± 6
P8		0.39 ± 0.02		2.5 ± 0.1	99 ± 2
P10	1.8 ± 0.7	0.39 ± 0.01	15 ± 9	6.4 ± 0.3	167 ± 4
P12	1.6 ± 0.2	0.74 ± 0.03	31 ± 7	16.8 ± 1.1	594 ± 27
Mean ± SE	**2.5 ± 0.3**	**0.77 ± 0.11**	**46 ± 13**	**12 ± 2**	**439 ± 124**

5.3.3 C sequestration in seagrass sediments

Long term (over 1,000 years) C accumulation rates in Shark Bay seagrass meadows ranged from 2.5 to 32.1 g C m⁻² yr⁻¹, with a median of 11.3 g C m⁻² yr⁻¹ (mean ± SE: 12 ± 2 C m⁻² yr⁻¹), while short-term accumulation rates (last 100 years) were estimated at 15 to 123 g C m⁻² yr⁻¹, with a median of 30 g C m⁻² yr⁻¹ (mean ± SE: 46 ± 13 g C m⁻² yr⁻¹) (Table 5.1). These estimates are in the range of modern (i.e. last 100 yr) C accumulation rates of *P. oceanica* in the Mediterranean (Mazarrasa et al., 2017), *P. australis* in Australia (Marbà et al., 2015; Serrano et al., 2016b) and *Thalassia testudinum* in Florida Bay (Orem et al., 1999) (26 – 122 g C m⁻² yr⁻¹). Both the long- and short-term C accumulation rates estimated here exceed those of terrestrial forest soils by 3- to 10- fold (average rates in forest soils: 4.6 ± 1 g C m⁻² yr⁻¹) (McLeod et al., 2011) and equal short-term C accumulation in Australian tidal

marshes (55 ± 2 g C m^{-2} yr^{-1}) (Macreadie et al., 2017).

The 4,300 km^2 of seagrass meadows in Shark Bay contemporarily account for a sequestration of 200 ± 55 Gg C yr^{-1} (range $65 - 527$ Gg C yr^{-1}), which represents 9% of the C sequestered by Australia's vegetated coastal ecosystems (occupying an area of 110,000 km^2) (Atwood et al., 2017; Lavery et al., 2013; Macreadie et al., 2017). This comparison highlights the disproportionate C sequestration capacity of Shark Bay seagrasses, contributing significantly to the C sequestration by seagrasses, mangroves and tidal marshes in Australia.

5.3.4 CO$_2$ emissions after seagrass loss

Seagrass meadows in Shark Bay experienced extensive declines driven by the marine heat wave that impacted the coast of Western Australia in the austral summer 2010/11 (Wernberg et al., 2012). Mapping inside the Marine Park (68% of Shark Bay's area) in 2014 revealed a net reduction of approximately 22% in seagrass habitat from the 2002 baseline (Fig. 5.4). The net loss of seagrass extent was accompanied by a dramatic shift in seagrass cover from dense to sparse across large areas of the Bay, with dense seagrass areas declining from 72% in 2002 to 46% in 2014 (Table 5.2). Most losses occurred across the northern half of the western gulf, and at the northern part of the Wooramel Bank. After the event, water clarity decreased progressively and significantly due to the loss of sediment stabilization. In addition, widespread phytoplankton and bacterial blooms were observed in both gulfs of Shark Bay as a result of increased nutrient inputs to the water column from degraded seagrass biomass and sediment erosion (Nowicki et al., 2017), providing favorable conditions to CO$_2$ emissions (Lovelock et al., 2017a).
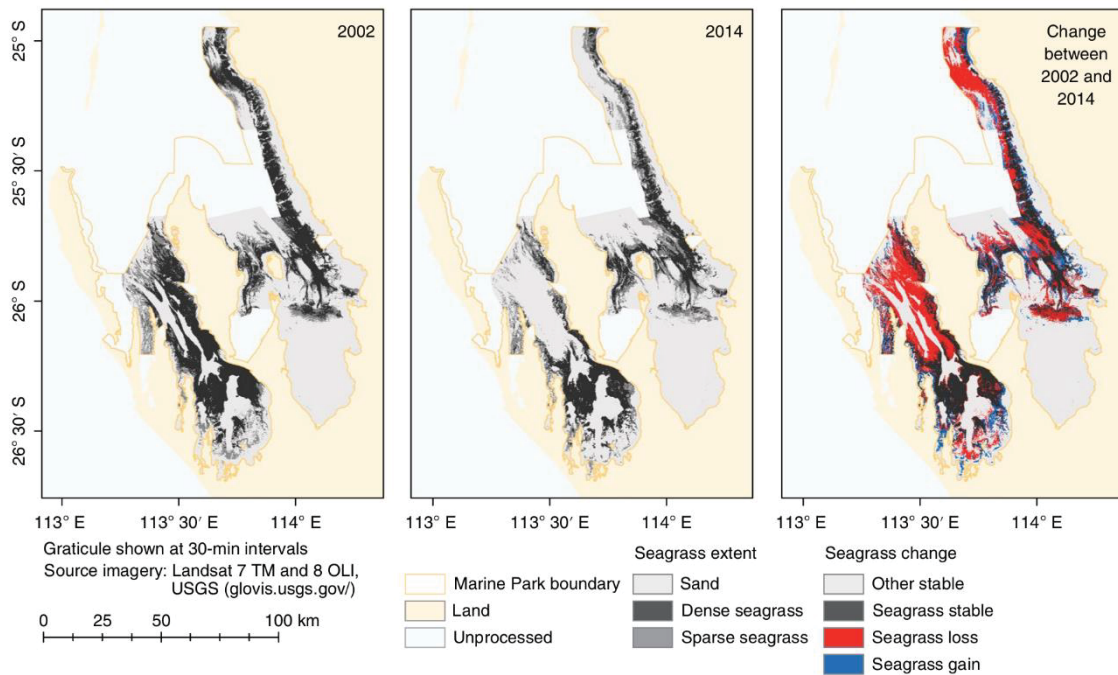
Figure 5.4: Seagrass extent change within Shark Bay's Marine Park before (2002) and after (2014) the marine heatwave in 2010/2011. Black, dense (> 40%) seagrass cover; grey, sparse (< 40%) seagrass cover; red, seagrass loss; dark blue, seagrass gain; light grey, sand; white, no data; gold, Marine Park boundary.

Losses of C and associated CO_2 emissions following degradation of seagrass ecosystems have been documented previously (Lovelock et al., 2017b). Yet, no studies have evaluated the risk of CO_2 emissions associated with seagrass loss due to thermal stress impacts. Carbon remineralization to CO_2 is accelerated after disturbance through the decomposition of dead biomass and from the alteration of the physical and/or biogeochemical environment in which the sediment C was stored (Lovelock et al., 2017a). Vegetation loss also increases the potential for sediment erosion and sediment resuspension in the water column (van der Heide et al., 2011), increasing the oxygen exposure of previously buried sediment organic matter (Burdige, 2007), leading to 2 to 4 times higher remineralization of sediment C under oxic than anoxic conditions (Lovelock et al., 2017b). Carbon in the upper meter of sediments has been considered the most susceptible to remineralization when seagrass meadows are lost (Fourqurean et al., 2012b; Pendleton et al., 2012). However, Lovelock et al. (2017b) recently suggested that the proportions of the C stock that may be exposed to oxic conditions after disturbance in seagrass ecosystems could be lower than previously assumed, likely due to their permanently submerged condition and lower levels of exposure to air. Assuming that between 10 to 50% of the seagrass sediment C stock is exposed to an oxic environment after disturbance (experiencing a decay of 0.183

yr^{-1}; Lovelock et al., 2017b), we estimate that between 4 to 22 Mg C ha^{-1} (4 - 20% of the C stock in the upper meter of sediments) might have been lost in Shark Bay from previously vegetated sediments during the first 3 years after the marine heat wave. This may have resulted in the net emission of 16–80 Mg CO_2-e ha^{-1}, and assuming no seagrass recovery, it could result in cumulative C losses of 10 to 52 Mg C ha^{-1} or 38–190 Mg CO_2-e ha^{-1} (10-50% of the C stock in the upper meter of sediments) 40 years after the event. In addition to accelerated sediment C loss, the reduced seagrass standing stock (i.e. biomass) would in turn lead to a lower capacity of Shark Bay's seagrasses to sequester C. The reduction in the modern C sequestration is estimated at 0.46 ± 0.13 Mg C ha yr^{-1}, and at 52 ± 14 Gg C yr^{-1} over the ~1,100km^2 damaged area.

Excluding potential emissions from remineralization of seagrass biomass and extrapolating estimates per unit area to the total damaged seagrass area, we estimate that the widespread loss of seagrasses in Shark Bay in 2010/11 may have resulted in CO_2 emissions from sediment C stocks ranging from 2 to 9 Tg CO_2 during the following three years after the event. This can be compared to the 14.4 Tg CO_2 estimated to be released annually from land-use change in Australia (Haverd et al., 2013), which did not account for emissions associated with seagrass losses, hence would have increased the national land-use change estimate by 4% to 21% per annum. Cumulative emissions due to seagrass die-off could range between 4 to 21 Tg CO_2 after 40 years assuming no seagrass recovery during this period, a reasonable assumption given that the recovery of *A. antarctica* and *P. australis* has been shown to take decades (>20 yr) (Cambridge et al., 2002; Marbá and Walker, 1999) or not occur over contemporary time scales (Nowicki et al., 2017). If damaged seagrass meadows recover, the estimates of CO_2 emissions after 40 years might be lower than reported here. In addition, CO_2 emissions from organic carbon remineralization may be partially offset by the net dissolution of the underlying carbonate sediments (Burdige et al., 2008). On the other hand, decomposition rates of C may be enhanced in persistent vegetated and degraded areas due to increased seawater temperature that influences respiration (Pedersen et al., 2011). However, the potential and magnitude of such effects is unclear, and therefore, were not considered in this study.

Table 5.2: Effects of the marine heatwave event on seagrass area and organic carbon (C) stocks under degraded seagrass meadows. α is the fraction of sediment C stock within the top meter exposed to oxic conditions. A range of α = 0.10–0.5 was used to estimate CO2 emissions 3 and 40 years after the event. Biomass C loss is not included in the calculations as much of the primary production might be buried or exported, rather than remineralized in situ. *Loss and emission after 40 years of disturbance assuming no seagrass recovery.

	Marine Park area (8,900 km^2)			Extrapolated values for the entire Bay (13,000km^2)		
Baseline seagrass area (km^2)	2689			4300		
Dense	1925			3096		
Sparse	765			1204		
C stock top meter (Tg C)	34	±	14	55	±	22
Seagrass area loss (km^2)	581			929		
Shift to sparse seagrass (km^2)	118			190		
Total damaged seagrass area (km^2)	699			1125		
3 yr net C loss from 1 m sediment stock (Tg C)						
α 0.10	0.30	±	0.05	0.49	±	0.08
α 0.25	0.76	±	0.10	1.23	±	0.15
α 0.50	1.52	±	0.17	2.45	±	0.27
40 yr net C loss from 1 m sediment stock (Tg C)*						
α 0.10	0.72	±	0.27	1.16	±	0.53
α 0.25	1.81	±	0.35	2.91	±	0.62
α 0.50	3.61	±	0.50	5.81	±	0.80
3yr net CO$_2$ emissions (Tg CO$_2$)	1.1	-	5.6	1.8	-	9.0
40 yr potential CO$_2$ emissions (Tg CO$_2$)*	2.6	-	13.2	4.3	-	21.3

5.3.5 Building resilience for climate change mitigation

Conservation of seagrass meadows and their millenary sediment C deposits is an efficient strategy to mitigate climate change, through the preservation of seagrass C sequestration capacity but especially through avoiding CO$_2$ emissions from sediments following habitat degradation, which greatly surpass the annual sequestration capacity by undisturbed seagrass meadows. With increasing frequency of extreme events, there is a necessity to advance our understanding of how seagrass ecosystems, especially those living close to their thermal tolerance limit, will respond to global change threats, both direct and through interactive effects with local pressures. Local threats in Shark Bay include seagrass loss associated with turbidity and nutrient inputs from flooding of poorly-managed pastoral leases, release of gypsum from a salt mine, changes in the trophic dynamics of the system through overfishing or targeted fishing, and more local damage to seagrasses from vessel

propellers and anchors associated with growth in tourism. Current management at Shark Bay includes the declaration of special zones for seagrass protection, promoting public awareness of the significance of seagrass, and providing information on responsible boating (Shark Bay Marine Reserves Management Plan 1996-2006: https://www.sharkbay.org). These practices are well-suited to localized stressors, such as eutrophication (Tomasko et al., 2005), but less-suited to managing global threats such as heat waves, due to the spatial scale and magnitude of these impacts (Björk et al., 2008).

In the face of global threats, management can aim to maintain or enhance the resilience of seagrasses (Kilminster et al., 2015). The heat wave-associated seagrass die-off in 2010/11 mostly affected *A. antarctica* followed by *P. australis*, which are persistent seagrasses with slow growth rates but capable to build large stores of carbohydrates in their rhizomes (Marbà and Walker, 1999). These characteristics provide the species with high levels of resistance to disturbance (Fraser et al., 2014b; Thomson et al., 2014). However, once lost, their capacity to recover is limited and slow, and largely depends on the immigration of seeds or seedlings. Therefore, conservation actions to preserve these seagrass meadows, thereby maintaining their C sequestration capacity and avoiding greenhouse gas emissions (Lovelock et al., 2017a), should primarily aim to avoid the loss of vegetative material and prevent local pressures exacerbating those of global change to enhance their resilience. Actions following acute disturbance could include the removal of seagrass detritus after die-off to reduce detritus loading, lessening the threat of acute eutrophication; and the restoration of impacted areas using seed-based restoration approaches such as the movement of seeds and viviparous seedlings to impacted sites or the provision of anchoring points in close proximity to donor seagrass meadows to enhance recovery (Rivers et al., 2011; Tanner, 2015). Long-term actions should include management to maintain top-down controls so that herbivory is maintained at natural levels (Atwood et al., 2015). More contentious actions could aim to repopulate areas with more resilient seagrass genotypes sourced from outside the impacted sites (Hancock and Hughes, 2014). The wide range of salinity and temperature in the Bay, together with the uneven loss of meadows following the event in 2010/11, may indicate differences in adaptation and resilience among meadows across the Bay. This offers the possibility of identifying heatwave-resistant genotypes and

using these to supplement the genetic diversity and resilience of existing meadows. Genotypic mapping could also allow identifying the meadows at greatest risk of heat waves where management actions may be focused.

5.4 Conclusions

Our results show that seagrass meadows from Shark Bay support the largest seagrass C stocks worldwide, that while making a large contribution to C sequestration by vegetated coastal ecosystems, their loss may disproportionally add to Australian CO_2 emissions. With increasing frequency and intensity of extreme climate events, the permanence of these C stores might be compromised, further stressing the importance of reducing green-house gas emissions and implementing management actions to enhance and preserve natural carbon sinks.

Chapter 6

Losses of soil organic carbon with deforestation in mangroves of Madagascar[1]

Global mangrove deforestation has resulted in substantial carbon dioxide (CO_2) emissions to the atmosphere, but the extent of emissions due to soil organic carbon (C) loss remains difficult to assess due to limited studies. Here, we sampled 5 intact and 5 deforested mangrove soils from Tsimipaika Bay, Madagascar, to examine the fate of soil C after clearing. We analysed sediment grain size, ^{210}Pb specific activity, organic C and nitrogen (N) and their stable isotopes in soils as well as DOC in surface waters and tree biomass. Results showed that no significant soil erosion occurred 10 years after deforestation, however, enhanced soil C remineralization was promoted by soil physical mixing and alteration of physico-chemical properties after disturbance. The magnitude of mixing in deforested soils was 10 times greater, based on ^{210}Pb specific activity profiles. Evidence of soil C loss was observed in the upper 14 g cm^{-2} (or ~ 40 cm), where C stocks in deforested soils were half those in intact soils. This represents a total loss of 180 ± 20 Mg C ha^{-1} or 660 ± 70 Mg CO_2e ha^{-1} from both vegetation (72%) and soil C (28%) a decade after mangrove forest clearance. Although our results suggest that the 20% of the upper meter soil C stock is the most susceptible to remineralization 10 yr after deforestation, its contribution to CO_2 emissions is disproportionally large, given that the annual C loss rate per unit area was 4.5 times higher than the C sequestration rate of intact mangrove soils. Blue carbon interventions and fully implemented actions are currently limited to mangrove reforestation. Our results suggest that conserving mangrove stands and avoiding further deforestation is a key effective tool in reducing significant soil C loss and has the potential to substantially reduce mitigation costs.

6.1 Introduction

Mangroves are an important natural resource in the tropics and sub-tropics and provide a wide range of ecosystem services, including coastal protection, support of fisheries and biodiversity, nutrient cycling and carbon sequestration (Barbier et al., 2011). Their high rates of primary production and the low rates of organic matter decomposition in their flooded soils lead to mangroves having some of the highest soil organic carbon (C) concentrations among forested ecosystems (Donato et al., 2011; McLeod et al., 2011). However, the C stored in their soils is vulnerable, as mangroves have been widely degraded and converted to alternative land-uses, resulting in losses of ecosystem services (Alongi, 2002) and significant carbon dioxide emissions (CO_2) to the atmosphere as previously stored C is remineralized to CO_2 (Lovelock et al., 2017b).

Consequences of mangrove soil disturbance include subsidence; as roots die, soil volume collapses and erosion occurs, resulting in loss of soil C. These effects are generally most severe and longer lasting when caused by anthropogenic versus natural perturbations (Ellison and Farnsworth, 1996; Twilley and Day, 2012). Soil C loss has been observed, for instance, where soils have been excavated for the construction of aquaculture ponds (Kauffman et al., 2014; Ong, 1993). At sites where mangroves have been removed or uprooted due to human activities or where there have been impacts of intense storms, losses of soil C have been inferred from changes in soil elevation (Cahoon et al., 2003; Lang'at et al., 2014) or measured as CO_2 efflux (Lang'at et al., 2014; Lovelock et al., 2011; Sidik and Lovelock, 2013). Although deforestation has been the major cause of forest loss in the past, there are few studies that have directly measured the change in soil C content in mangrove soils when forests are degraded, but soils remain in place (e.g., Adame et al., 2018; Grellier et al., 2017; Kauffman et al., 2016).

A change in soil C content with deforestation of mangroves could occur indirectly as a consequence of biomass loss and/or directly due to a change in factors affecting soil biogeochemical processes, such as a change in temperature, evaporation and precipitation, or varying sediment supply. For example, changes in mangrove biomass may reduce inputs of labile C and nutrients from detritus, and increase soil temperature and water flow through the soil profile due to direct exposure to sunlight and rainfall, which may result in further

122

loss of labile C (Granek and Ruttenberg, 2008). Destructive practices, such as clear cutting, mechanically redistribute C in the soil (Lundquist et al., 2014; Yanai et al., 2003; Zummo and Friedland, 2011), enhancing oxygen diffusion, altering microbial community dynamics and organic carbon remineralization (Kristensen and Alongi, 2006). Physical mixing processes modify the soil structure, transport conditions and soil chemistry, hence potentially changing the availability of C and N for associated microbial and plant communities (Balesdent et al., 2000). For instance, the addition of biodegradable C to deep stable C stores promotes microbial respiration of the added and existing organic pools through a priming mechanism (Bianchi, 2011), and may accelerate C mineralization beyond that directly derived from mechanical mixing, contributing to elevated CO_2 emissions from soils.

Soil OC may also be lost as a consequence of soil erosion or export as dissolved C, a process which may be accelerated through direct exposure of mangrove soils to tidal inundation, rainfall, and waves (Labrière et al., 2015; Thampanya et al., 2006), as well as through changes in the composition and biomass of benthic mats driven by a reduction in mangrove litter loading (Delgado et al., 1991; Duke and Wolanski, 2001; Grellier et al., 2017; McKee, 2011). The natural radionuclide lead-210 (^{210}Pb) ($T_{1/2}$: 22.3 y) can serve as a proxy of sediment erosion and redistribution processes (He and Walling, 1997; Walling et al., 2003). Specifically, comparison of $^{210}Pb_{xs}$ specific activity profiles between soils from intact and cleared forests may allow an assessment of the extent of soil mixing after disturbance, with lower $^{210}Pb_{xs}$ inventories relative to intact soils indicating loss or mobilization of soil material as shown for disturbed seagrass meadows (Marbà et al., 2015).

Overall, soil C storage represents a balance of C inputs and losses, and because soil is the largest reservoir of C in many mangrove ecosystems (Donato et al., 2011), small changes in its pool size may translate into significant CO_2 emissions and changes of C fluxes to coastal waters (Atwood et al., 2017; Gillis et al., 2017). While it is well established that the harvesting of terrestrial forests results in a loss of C in organic and mineral soil horizons (Diochon et al., 2009; Yanai et al., 2003; Zummo and Friedland, 2011), the impact of mangrove deforestation on soil C storage remains limited. Direct assessment of these C losses is important for quantifying CO_2 emissions from mangrove deforestation and in the

valuation of the avoidance of emissions achieved through conservation projects (Herr et al., 2017). Currently, guidance by the International Panel for Climate Change on CO_2 emission from coastal wetlands (IPCC, 2014) has a "*tier 1*" (i.e., default) assumption that soil CO_2 emissions and removals are zero for forest management practices in mangroves. However, the IPCC allows for country-specific "*tier 2*" (i.e., based on direct assessments) to be adopted by using a carbon stock-difference method in order to account for any emissions associated with forest management practices.

In this study we aim to quantify the C loss from deforested mangrove soils in northwest Madagascar. Madagascar contains Africa's fourth largest national extent of mangroves, representing approximately 2% of the global mangrove area. Since 1990, more than 20% of Madagascar's mangrove ecosystems have been heavily deforested because of the increasing demand for charcoal and timber by urban populations (Jones et al., 2016a), which is the primary cause of mangrove deforestation in the broader East African region (FAO, 2007). We sampled soil cores from plots that were either within deforested and intact forest areas to assess the change of soil C after clearing. We described the physical characteristics of soils with depth, quantified the variation in C and N contents, and estimated sediment accumulation rates using ^{210}Pb (Appleby, 2001; Arias-Ortiz et al., 2018c). We further measured dissolved organic C (DOC) in adjacent coastal surface waters to assess possible linkages between mangrove deforestation and increased C export to the coastal ocean. Finally, we use our data to estimate the fate and total change of soil C since mangrove clearance.

6.2 Methods

6.2.1 Study site

This study was conducted in Tsimipaika Bay (previously referred to as Ambanja Bay; Jones et al., 2016a) in northwest Madagascar (48°28'E, 13°30'S), where anthropogenic mangrove loss is particularly prominent due to extensive extraction for charcoal and timber (Jones et al., 2014). Together with Ambaro Bay, the Tsimipaika-Ambaro Bay complex form Madagascar's second most extensive mangrove ecosystem, with over 40,000 ha of mangrove forests (Jones et al., 2016a; Jones et al., 2014). The site is characterized by a sub-humid

tropical climate and is influenced by semi-diurnal tidal ranges varying between maximums of 3.0 – 3.5 m (Rasolofo and Ramilijaona, 2009). Mangrove soils in this region are underlain by alluvial and lake deposits (Jones et al., 2016b) flooded by sea level rise. Contemporary localized mapping supported by field observations indicated that, in 2010, anthropogenic activities had driven substantial deforestation (1,000 ha) mostly on or near the southwest region of the peninsula that separates the two bays (Jones et al., 2014) (Fig. 6.1). Deforestation heavily targets closed canopy mangrove forests followed by the open canopy mangroves (Benson et al., 2017), which represent 30 and 56% of the total mangrove area at the Tsimipaika-Ambaro Bay complex, respectively (Jones et al., 2014). *Rhizophora mucronata is* favoured for the charcoal production process, in which trees are felled by hand and carried to nearby, temporary kilns to be smoked. Non-*Rhizophora* species and unwanted prop roots are burned to heat kilns, although large volumes of downed wood are often discarded at the site.

In November 2016, we sampled soil cores from 5 plots that were cleared between 2006 and 2008 and from 5 plots from an intact forest (Fig. 6.1). The deforested and forested plots were spatially separated by ∼5 km but had relatively similar environmental conditions such as type and proximity of bedrock and nutrient inputs. Within the sampled plots, four species of mangroves were present: *Rhizophora mucronata, Bruguiera gymnorhiza, Ceriops tagal and Sonneratia alba* (Table 6.1). *Intact plots were all well-formed, closed (>60%) canopy mangroves, consisting of* high stature trees (mean height: 9.0 ± 0.5 m) of variable density (800 - 4,700 ha^{-1}). The average diameter at breast height (1.3 m, dbh) was 12 ± 2 cm. Deforested plots used to contain closed canopy mangrove forests (Blue Ventures, personal communication) and this was evident from plots comprised of *Ceriops tagal* or *Bruguiera gymnorhiza* where the boles left in place after tree removal lead to stump densities ranging from 1,000 to 11,400 ha^{-1} (Table 6.1).

Above ground tree biomass at each plot (Appendix E, Table E1) was derived from tree diameter and height measurements using species specific allometric equations along with wood density values previously described in Jones et al. (2016b) for the same area. Tree below-ground-biomass was calculated using the generalized equation presented in Komiyama et al. (2005) and equations from Kauffman and Donato (2012) were used to

estimate the biomass of standing dead wood. From biomass density estimates, the total biomass C stock (Mg C ha^{-1}) was calculated using conversion factors of 0.50 and 0.39 for above and belowground estimates, respectively (Kauffman and Donato, 2012). Plot size for tree measurements was 100 m^2 and estimates of biomass and C stocks were scaled to the hectare-level.
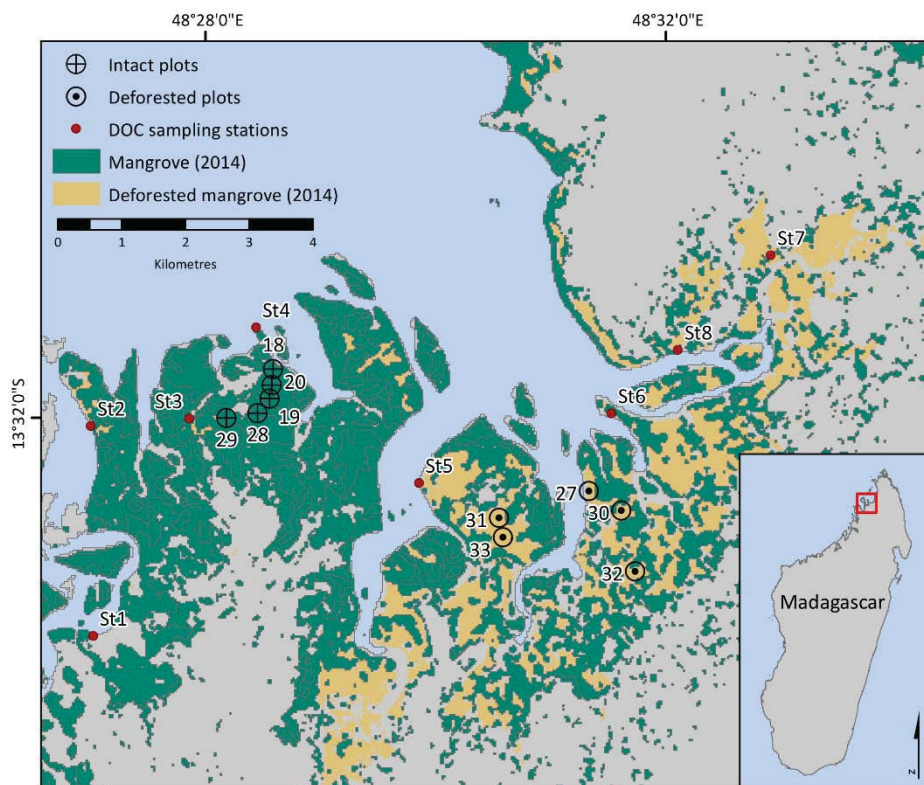
Figure 6.1: Map of Tsimipaika Bay in northwest Madagascar with sampled plot locations in intact and deforested mangrove areas. St labels are surface water sampling locations.

Table 6.1: Site characteristics for sampled mangrove plots of Tsimipaika Bay, Madagascar. Average values for tree height (m), diameter at breast height (dbh) (cm) and trees per hectare (ha^{-1}). Dead tree density in deforested plots equals stump density and regeneration density equals number of seedlings per unit area. Cc stands for Closed canopy, De for Deforested, and n.d. is "no data".

Core ID	Species dominance	Geomorphic position	Tidal inundation	Tree height (m)	dbh (cm)	Live Tree Density (ha^{-1})	Dead Tree Density (ha^{-1})	Regeneration density (ha^{-1})	Canopy cover (%)	Total biomass C (Mg C ha^{-1})
Cc18	*S. alba*	Riverine	freq.	8	18	800	0	0	94	160
Cc19	*B. gymnorhiza*	Riverine	infreq.	10	13	2400	200	5200	95	254
Cc20	*R. mucronata*	Basin	freq.	9	10	4700	200	800	95	238
Cc28	*R. mucronata*	Basin	infreq.	n.d.	10	2900	400	2800	93	128
Cc29	*R. mucronata*	Riverine	freq.	9	9	2900	600	0	98	113
De27	*B. gymnorhiza*	Riverine	freq.	5	7	200	100	0	0.9	3.0
De30	*B. gymnorhiza*	Basin	infreq.			0	1000	2000	0.2	1.8
De31	*R. mucronata*	Basin	freq.			0	100	0	0.2	0.1
De32	*C. tagal*	Riverine	infreq.			0	3000	2400	7	1.4
De33	*C. tagal*	Basin	infreq.			0	11400	4400	0.2	9.5

6.2.2 Sampling and analytical methods

In order to characterize soil biogeochemical properties, PVC tubes (1.5 m long, 6.2 cm inner diameter) were hammered into mangrove soils (one at each plot; Fig 6.1), extracted by hand and transported to the laboratory. Prior to extracting the core, the depth to the sediment surface inside and outside the core was measured in order to calculate compaction during sampling. The PVC corers were cut lengthwise, and the soils inside the corers were sliced at 0.5 cm-thick intervals throughout the first 20 cm, and at 1 cm-thick intervals below this depth. Compaction of mangrove soils during coring was on average $36 \pm 10\%$ and $50 \pm 13\%$ in intact and deforested mangrove soils, respectively, and was corrected by linearly distributing the spatial discordance between the length of the recovered soil and the depth penetrated by the core tube to the sliced soil layers (Glew et al., 2001). Soil slices were weighed wet and then dried at 60ºC until a constant weight was achieved. Soil water content and dry bulk density (DBD) were then calculated. Soil mass per unit area was also estimated at each layer by dividing the dry sample mass by the core tube area sampled. The mass of soil in a given depth layer varies with DBD, while the mass of soil in a specific soil mass layer is equal among sites, hence providing a consistent basis for comparison. Soil collapse due to deforestation (Cahoon et al., 2003; Krauss et al., 2010; Lang'at et al., 2014) and the influence of trampling limits the comparison of soil properties based upon depth or volume. Soil profiles were therefore displayed in terms of soil mass layers (i.e., cumulative mass).

Soil C and N contents were measured at 1 cm resolution throughout the upper 30 cm, and in alternate slices every 5 cm below this depth. The OC and N content of sediments was measured using an elemental analyser (Carlo Erba NA1500). Prior to analysis, soil samples were sieved (1.5 mm) and ground to a fine powder. A sub-sample (~ 20 mg) was weighed into silver cups, acidified with 1 M HCl until there was no visual evidence of effervescence. The sample was then dried at 60ºC and analysed. Inorganic C content was negligible in all samples. Analytical precision (s.d. of n = 26) was $\pm 0.3\%$ for C, $\pm 0.02\%$ for N and ± 4 for molar C:N ratios. Stable isotopes of sediment OC and N (δ^{13}C and δ^{15}N) were analysed at one core per location using an elemental analyser–isotope ratio mass spectrometer (Hilo Analytical Laboratory) at the University of Hawaii. Replicate and control samples (NIST

8704) were also run and the accuracy and precision of $\delta^{13}C$ and $\delta^{15}N$ data were of $\pm$ 0.2‰ and $\pm$ 0.07‰, respectively.

Grain size analyses were conducted down core to evaluate potential erosion, which results in selective and preferential loss of smaller size grain fractions (Arata et al., 2016). Sediment grain-size was measured with a Mastersizer 2000 laser diffraction particle analyzer following digestion of bulk samples with hydrogen peroxide to remove organic matter. Sediments were classified as coarse sand (500 - 1,000 μm), medium sand (250 – 500 μm), fine sand (125 - 250 μm), silt (4 - 63 μm) and clay (< 4 μm) (size scale: Wentworth, 1922).

Specific activities of ^{210}Pb were measured down core in order to assess sediment accumulation rates and $^{210}Pb_{xs}$ inventories. ^{210}Pb was determined through the analysis of its granddaughter ^{210}Po by alpha spectrometry after digestion in acid media using an analytical microwave in the presence of a known amount of ^{209}Po added as an internal tracer (Sanchez-Cabeza et al., 1998). The specific activities of $^{210}Pb_{xs}$ used to obtain the age models were determined as the difference between total ^{210}Pb and ^{226}Ra (supported ^{210}Pb). Specific activities of ^{226}Ra were determined for selected samples along each core by gamma-spectrometry through the emission lines at 295 and 352 keV of its decay product ^{214}Pb using calibrated geometries in a HPGe detector (CANBERRA, Mod. SAGe Well). Mean sediment accumulation rates over the last several decades to century were estimated for intact mangrove soils using the Constant Flux:Constant Sedimentation (CF:CS) model applied below the surface mixed layer (Krishnaswamy et al., 1971) following the recommendations in Arias-Ortiz et al. (2018). Mass accumulation rates (MAR) are expressed in cumulative dry mass units (g cm^{-2} yr^{-1}) and sedimentation or accretion rates (SAR) in mm yr^{-1}. Organic C accumulation rates (CAR) were estimated as the product of the fraction of %C accumulated over a period t (C_t) by the MAR of that period (MAR_t):

$$CAR = C_t \cdot MAR_t \qquad \text{(Eq. 6.1)}$$

The same equation can be applied to estimate organic N accumulation rates.

Carbon stocks were quantified as an equivalent soil mass basis to avoid overestimation of C stocks in soils with greater bulk densities. The soil mass layers used as the basis for comparison were 14 g cm^{-2} (upper), which represented soils accumulated in the

last century (based on the average $^{210}Pb_{xs}$ horizon), 14 - 45 g cm^{-2} (bottom), and 45 g cm^{-2} (total), which was the average mass equivalent depth representing approximately 1 m of soil. Equivalent depths in centimeters for reference mass layers at each core can be found in Table E2. All depths reported in the tables and in the text are decompressed depths. Soil C stocks were also integrated to a fixed depth of 1 m in order to compare to global estimates.

Surface water samples were collected over a tidal cycle at 8 sites along the shore adjacent to the intact (stations 1-4) and deforested (stations 5-8) mangrove areas. The intact sites were sampled during the flood to high slack tide. The deforested sites were sampled during the ebb to low slack tide. Samples for total OC were collected in 20 mL combusted glass vials, acidified to pH of 2 and stored at 4°C until analysis. Samples were analyzed as both filtered (using acid-washed and pre-combusted syringe GF/F filters) and unfiltered samples. Total and dissolved OC were measured using high temperature (720°C) catalytic oxidation (Pt-alumina) on a Shimadzu TOC-V CPN analyzer (Benner and Strom, 1993). Analytical replication (5 injections, 100 μL) of consensus reference material (Florida Straight at 700 m, DOC-CRM program) was run every 10 samples. High concentrations were also measured diluted with distilled and deionized water. Total OC versus DOC concentrations, and high concentration versus diluted samples were found to be the same within error ($\pm$ 50 μM).

6.2.3 Statistics

Water content, DBD, C and N content and molar C:N ratios of the sampled soils were not normally distributed, and thus non-parametric tests were used to assess significant differences between intact and deforested plots (Mann-Whitney test) at a level of significance of < 0.05. We used principal component analysis (PCA) to assess the relationship between soil properties and the two areas studied (intact and deforested mangroves). Sediment grain size, $^{210}Pb_{xs}$ inventories, $\delta^{13}C$ and $\delta^{15}N$, and stocks did follow a normal distribution, hence a two-sample t-test was used to assess significant differences between intact and deforested mangrove soils. Mean $\pm$ SE values are reported throughout the manuscript together with median values where variables were not normally distributed.

6.2.4 Emissions from mangrove forest deforestation

We analyzed C losses and potential emissions from mangrove deforestation based upon the variation in C content in the mangrove soil profiles observed between intact and deforested soils. Likewise, biomass C loss was estimated as the difference between vegetation C stocks in intact and deforested plots. The losses of C were reported as CO_2 equivalents (CO_2e), obtained by multiplying C loss values by 3.67, i.e., the molecular ratio of CO_2 to C. The mean annual rate of C loss from deforested soils was estimated as the total soil C stock loss divided by the time elapsed since disturbance.

6.3 Results

The effect of deforestation was obvious due to differences in mangrove vegetation compared to undisturbed sites. Total biomass C in intact plots ranged from 113 to 254 Mg C ha^{-1}, while in deforested plots this was substantially lower, 0.06 to 9.5 Mg C ha^{-1}, and contained negligible below ground biomass (i.e., roots) (Table 6.1 and Table E1). The effects of deforestation were less clear in soils from deforested mangroves, which contained similar average C and N contents to intact mangroves ($P > 0.05$) (Table 6.2). This was in part because soil properties within the five intact mangrove cores followed a bimodal distribution (Fig. E1). Intact soils Cc19 and Cc20, hereafter referred to as high-DBD intact soils, were depleted in water content and had significantly higher soil DBD and lower C and N contents relative to deforested soils ($P < 0.01$). In contrast, intact plots Cc18, Cc28 and Cc29, hereafter referred to as low-DBD intact soils, had significantly lower DBD and higher water, C and N contents than deforested soils ($P < 0.01$). Consequently, physico-chemical properties of deforested soils fell between those of high-DBD and low-DBD intact soils (Table 6.2).

Multivariate analyses further confirmed that soils from intact mangroves were represented by two clusters of data and that deforested soils were comparable to a mixture of low- and high-DBD intact soils, with characteristics closer to low-DBD intact soils (Fig. 6.2). Principal components Pc1 and Pc2 explained 75% of the total variance among sampled soils. Pc1 comprised 50% of the variance and was strongly correlated with soil DBD ($r = -0.90$), water, and C and N contents ($r = 0.95$, $r = 0.95$ and $r = 0.94$, respectively). Pc2

explained 25% of the variance and was strongly correlated with clay ($r = 0.91$), moderately correlated with C:N ratios ($r = 0.53$), and inversely correlated with sand ($r = -0.77$).

Table 6.2: Main soil characteristics of intact and deforested soils over the upper 45 g cm^{-2} (or ⌣1 m). U and t values of Mann-Witney and Two-sample t- test results are included for the comparison of soil properties between intact and deforested mangrove soils. ***Significance at 0.001 level, ** at 0.01 and * at 0.05. NS is not significant.

Soil Class	Core ID	Statistic	Water content (%)	DBD (g cm^{-3})	C (%DW)	N (%DW)	C:N	Clay (%)
High-DBD Intact	Cc19, 20	Mean ± SE	30.1 ± 0.6	0.881 ± 0.013	2.40 ± 0.08	0.095 ± 0.003	28.6 ± 0.6	11.2 ± 1.0
		Median	29.1	0.877	2.28	0.093	28.0	10.3
Low-DBD Intact	Cc18, 28, 29	Mean ± SE	56.9 ± 0.7	0.347 ± 0.008	7.7 ± 0.2	0.314 ± 0.012	29.6 ± 0.4	15.3 ± 1.10
		Median	58.7	0.36	7.4	0.3	28.9	15
Intact (all)	Cc18, 19, 20, 28, 29	Mean ± SE	47.4 ± 0.9	0.580 ± 0.015	5.7 ± 0.2	0.231 ± 0.011	29.3 ± 0.3	14.0 ± 0.8
		Median	48.7	0.489	5.5	0.199	28.8	13.1
Deforested	De27, 30, 31, 32, 33	Mean ± SE	44.5 ± 0.4	0.415 ± 0.006	5.11 ± 0.15	0.173 ± 0.003	33.5 ± 0.6	28.1 ± 1.3
		Median	44.3	0.414	4.77	0.167	32.6	26.4
Treatment				Prob>|U|				Prob>|t|
Intact (all) vs. Deforested			0.007 **	1.1·10^{-9} ***	1.00 NS	0.11 NS	2.6·10^{-8}***	1.1·10^{-14} ***
High-DBD Intact vs. Deforested			0 ***	5.6·10^{-53}***	4.1·10^{-26}***	1.7·10^{-25}***	7.0·10^{-6}***	9.4·10^{-10} ***
Low-DBD Intact vs. Deforested			0 ***	2.6·10^{-9}***	0***	0***	2.6·10^{-6}***	3.4·10^{-10} ***
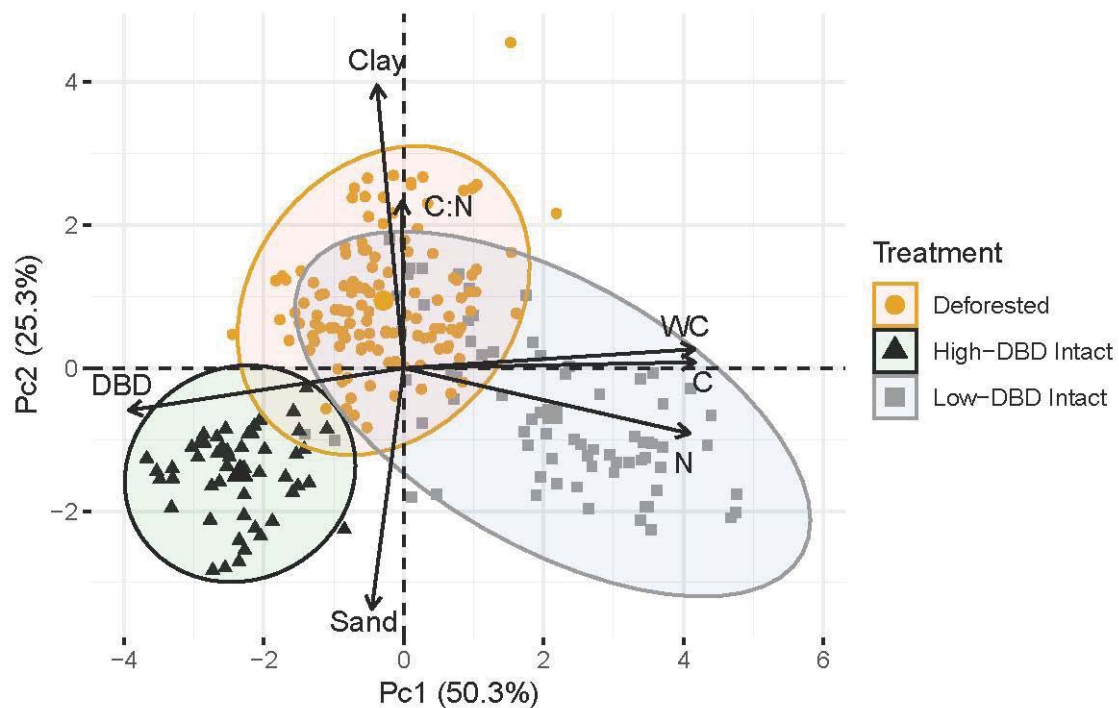
Figure 6.2: Principal component analysis on physico-chemical properties of soils from deforested and intact mangroves. Biplot of variable vectors onto the component axis showing correlation between the variable and the component and individual factor map. Superimposed on the plot are the confidence ellipses for categorical variables: deforested soils (orange circles), low-DBD intact mangrove soils (grey squares) and high-DBD intact mangrove soils (black triangles).

Concentrations of DOC in surface ocean waters varied widely between stations, with higher concentrations occurring during ebb tide (Fig. 6.3). Stations 1 - 3, adjacent to the intact mangrove area and sampled during the flood tide, had the lowest DOC concentrations, averaging 320 ± 30 μmol C L^{-1}. Station 4 also adjacent to the intact area but sampled during the high slack to ebb tide, had an order of magnitude higher surface water DOC of about $3,500 \pm 50$ μmol C L^{-1}. DOC concentrations in surface waters nearshore of the deforested mangroves and sampled during the ebb to low slack tide ranged between 1,000 and 19,400 μmol C L^{-1}, 0.3 to more than 50 times higher than those in waters adjacent to intact sites (min/max, max/min).
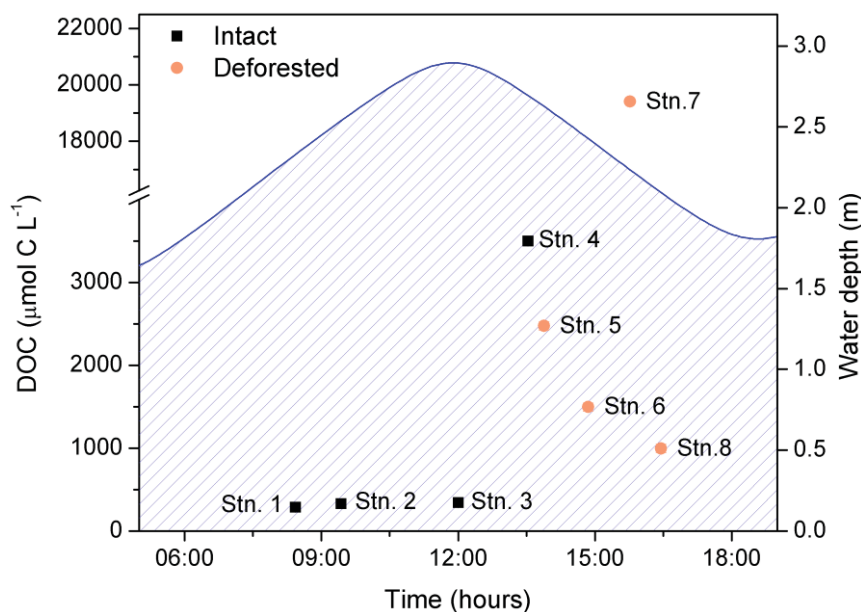
Figure 6.3: Concentrations of DOC in surface water at 8 stations along the shores of the intact and deforested mangrove areas.

6.3.1 Soil physico-chemical properties over the soil profile

Changes in soil physico-chemical properties with depth were observed in low-DBD intact and deforested mangrove soils only. In soils from low-DBD intact mangroves, DBD increased linearly and water content decreased with cumulative mass. Deforested soils, however, displayed a constant and significantly higher DBD, with decreasing water content over the upper 14 g cm^{-2} (or ~ 40 cm) ($P< 0.01$; Table E3) (Fig. 6.4a and b).

Carbon and N content (%DW) in low-DBD intact mangrove soils decreased steadily with depth, opposite the pattern observed in deforested soils, which increased with depth in the upper 14 g cm^{-2} (Fig. 6.4c and d). The mean soil C content of low-DBD intact soils was 8.4 ± 0.2% C in the upper 14 g cm^{-2}, 2-fold higher than in deforested soils (4.7 ± 0.2% C). Below this horizon, however, no significant differences were observed in water, C or N contents between deforested and low-DBD intact soils (Fig.6. 4) (Table E3). Throughout the soil profile, soil properties of high-DBD intact soils remained relatively constant and differed from those in the upper or bottom layers of both low-DBD intact and deforested soils (Table E3).
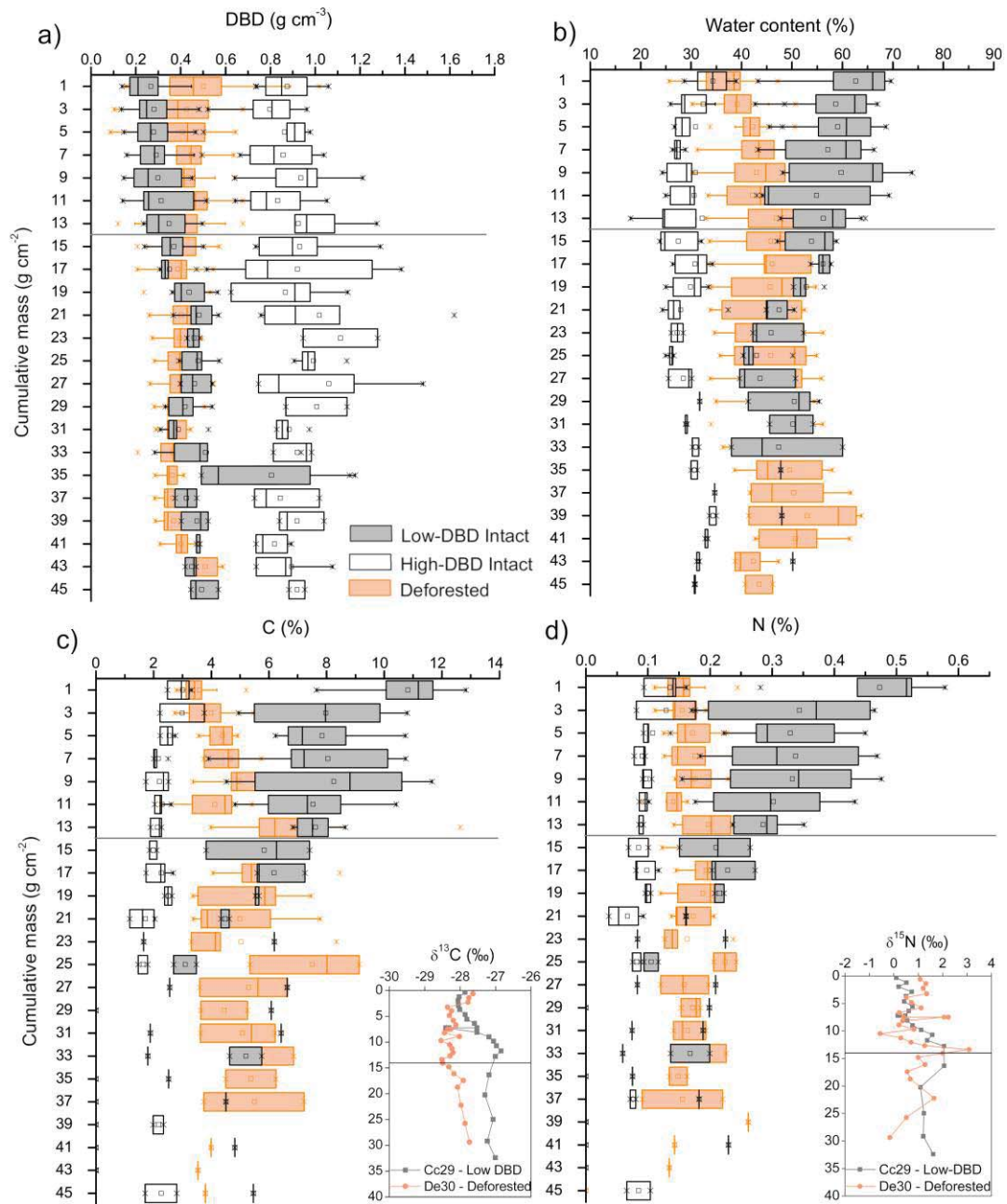
Figure 6.4: Soil properties (bulk density, water, carbon and nitrogen contents) with cumulative mass in intact and deforested mangrove soils. Insets contain soil carbon ($\delta^{13}C$) and nitrogen ($\delta^{15}N$) stable isotopes with cumulative mass in a low-DBD intact and a deforested mangrove soil. The line at 14 g·cm^{-2} indicates the separation between the upper and bottom reference soil mass layers.

C:N molar ratios were high in all sampled soils with averages ranging from 29 to 33, and increasing over the soil profile in low-DBD intact and deforested soils (Fig. E2). Deforested soils were characterized by higher average C:N molar ratios over the total soil profile relative to all intact soils (Table 6.2). However, no significant differences were observed in bottom layers between low-DBD intact and deforested soils (Table E3).

Stable isotopes of C and N were analysed for one low-DBD intact and one deforested soil. Both mangrove soils showed $\delta^{13}C$ values close to -28‰ although C in the deforested soil had lighter average $\delta^{13}C$ values (-28.16 ± 0.05‰) than C in the intact soil (-27.5 ± 0.1‰) (*P < 0.001*). In contrast, the $\delta^{15}N$ signal averaged 0.92 ± 0.10‰ and was not significantly different between the two soil classes (*P = 0.70*). The low-DBD intact soil showed an inverse relationship between C content and the corresponding $\delta^{13}C$ values, which became slightly heavier (+1.2‰) over the upper layer and relatively constant in the bottom layer (Fig. 6.4c). The deforested soil showed an initial change from heavy to lighter $\delta^{13}C$ values at ~ 3 g cm^{-2} before becoming heavier downcore (Fig. 6.4d). $\delta^{15}N$ showed a similar pattern as $\delta^{13}C$ in the intact soil but showed scattered values down core in the deforested soil.

The grain size distribution of all intact and deforested mangrove soils was relatively homogeneous over the soil profile. Silt accounted for 52 ± 5% and 58 ± 6% of dry weight, respectively. However, the average clay content (< 4 μm) was more than twice as high in deforested (28 ± 1%) versus high-DBD (11 ± 1%) and low- DBD intact soils (15 ± 1%) (Fig. E3). No significant differences in clay content were observed with depth in any of the sampled soils (*P > 0.01*; Table E3).

6.3.1.2 ^{210}Pb

In all intact mangrove soils, the $^{210}Pb_{xs}$ specific activity decreased from the surface to below detection at depths between 7 and 17 g cm^{-2} (10 - 50 cm) (Fig. 6.5a). The CF:CS model was subsequently used to estimate the average sedimentation rate over this depth horizon (Krishnaswamy et al., 1971). Mass accumulation rates at intact sites ranged between 0.070 ± 0.014 g cm^{-2} yr^{-1} and 0.223 ± 0.012 g cm^{-2} yr^{-1} (or 0.85 ± 0.11 and 8.4 ± 0.4 mm yr^{-1}; Table 6.3). In deforested mangrove soils, $^{210}Pb_{xs}$ horizons were reached at 10 to 26 g cm^{-2} (17 - 70 cm) but intense soil mixing, indicated by uniform specific activities of $^{210}Pb_{xs}$ throughout deforested soil profiles, precluded the determination of a valid age model and sediment accumulation rates at these sites. Indeed, the cumulative mass of the soil mixed layer was on average 10 times greater in deforested than in intact soils (14 g cm^{-2} versus 1.4 g cm^{-2}) (Table 6.3). The $^{210}Pb_{xs}$ inventories in intact mangrove soils varied widely (600 - 4,800 Bq m^{-2}), although the average (2,210 ± 800 Bq m^{-2}) was not significantly different to

that observed in deforested mangrove soils (mean $1,930 \pm 220$ Bq m^{-2}) ($P = 0.74$), where the ^{210}Pb$_{xs}$ inventory was redistributed over the soil profile via mixing. The ^{210}Pb$_{xs}$ inventories in high-DBD intact mangrove soils averaged 600 ± 100 Bq m^{-2} and were the lowest among all sampled sites. The mean ^{210}Pb$_{xs}$ inventory of low-DBD intact soils was also not significantly different than that of deforested soils ($P = 0.08$).
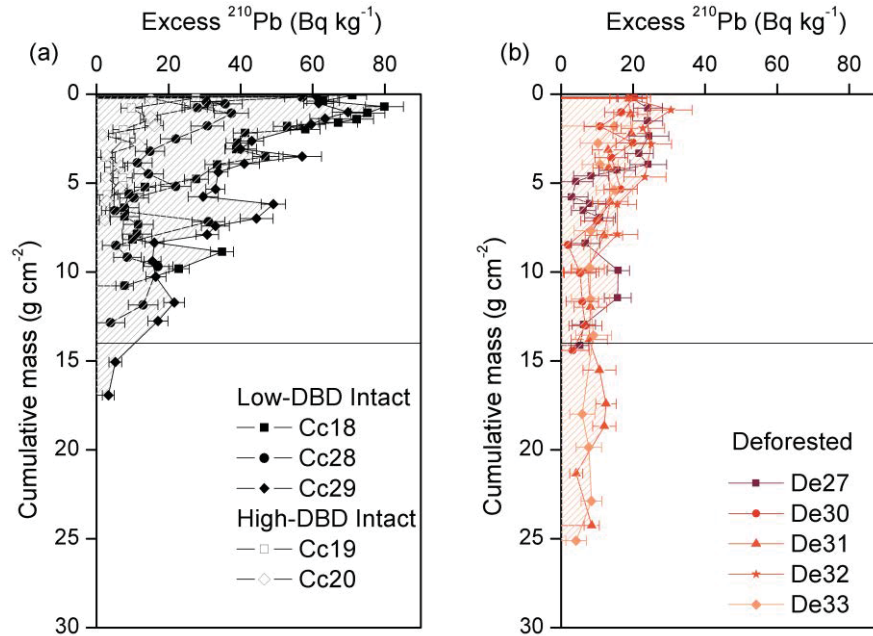
Figure 6.5: ^{210}Pb$_{xs}$ specific activity profiles with cumulative mass in intact (a) and deforested mangrove soils (b). The filled area under the curves illustrates ^{210}Pb$_{xs}$ inventories.

6.3.2 C and N accumulation rates and stocks

The annual burial of C and N within the closed canopy forest ranged from 18 to 176 g C m^{-2} yr^{-1} and from 0.7 to 7.2 g N m^{-2} yr^{-1}, respectively. In low-DBD intact plots, C and N burial rates were the highest and averaged 110 ± 40 g C m^{-2} yr^{-1} and 4 ± 2 g N m^{-2} yr^{-1}, respectively. In high-DBD intact plots these rates were about 5 times lower at 21 ± 3 g C m^{-2} yr^{-1} and 0.9 ± 0.3 g N m^{-2} yr^{-1}, respectively (Table 6.4). In deforested plots, the burial rates of C and N could not be estimated due to the mixing of sediments over the entire ^{210}Pb$_{xs}$ record.

Evidence for soil C and N losses was clear between deforested and low-DBD intact soils in the upper 14 g cm^{-2}, where the stocks of C and N in deforested soils were about 2 times lower than those of low-DBD intact soils (Table 6.4). However, the soil C and N stocks

assessed over i) the total 45 g cm^{-2} or 1 m of soil and ii) the upper, recent sediment record (i.e., ~14 g cm^{-2}), were not significantly different when comparing all intact and deforested soils ($P > 0.05$ in all cases). There were also no significant differences between C and N stocks of low-DBD intact soils and deforested soils integrated over the total 45 g cm^{-2} or 1 m of the soil cores ($P = 0.51$ for C and $P = 0.06$ for N stocks).

Table 6.3: Mass and sediment accumulation rates (MAR and SAR) and $^{210}Pb_{xs}$ inventories in intact and deforested mangrove cores. Mixing and $^{210}Pb_{xs}$ horizon depths in cm can be found in Table E2. The uncertainties represent the SE of the regression for MAR and SAR, and ^{226}Ra specific activities represent the mean and the standard deviation (n = 5 at each core).

Core ID	Type	Mixing depth $g\ cm^{-2}$	$^{210}Pb_{xs}$ horizon $g\ cm^{-2}$	^{226}Ra $Bq\ kg^{-1}$			MAR $g\ cm^{-2}\ yr^{-1}$			SAR $mm\ yr^{-1}$			$^{210}Pb_{xs}$ inventory $Bq\ m^{-2}$		
Cc19	High-DBD	1.7	7	13	±	1	0.07	±	0.014	0.85	±	0.11	500	±	50
Cc20		2.0	9	13	±	1	0.099	±	0.013	1.11	±	0.15	690	±	40
Cc18		0.8	11	19	±	4	0.094	±	0.007	4.1	±	0.2	3170	±	90
Cc28	Low-DBD	1.2	13	13	±	4	0.10	±	0.02	2.3	±	0.4	1920	±	80
Cc29		1.5	17	13	±	2	0.223	±	0.012	8.4	±	0.4	4750	±	80
Mean (SE) high-DBD		**1.9 ± 0.2**	**7.9 ± 0.8**				**0.085**	**±**	**0.015**	**0.98**	**±**	**0.13**	**600**	**±**	**100**
Mean (SE) low-DBD		**1.2 ± 0.2**	**13 ± 2**				**0.14**	**±**	**0.04**	**5**	**±**	**2**	**3280**	**±**	**820**
Mean (SE) Intact		**1.4 ± 0.2**	**11 ± 2**				**0.12**	**±**	**0.03**	**3.35**	**±**	**1.38**	**2210**	**±**	**800**
De27		4	14	25	±	6							1940	±	90
De30		6	14	18	±	4							1200	±	70
De31	Deforested	25	24	13	±	1							2580	±	90
De32		8	10	21	±	6							1870	±	170
De33		26	26	15	±	2							2040	±	100
Mean (SE) Deforested		**14 ± 5**	**18 ± 3**										**1930**	**±**	**220**

Table 6.4: Carbon (C) and nitrogen (N) accumulation rates and stocks in intact and deforested mangrove soils. Stocks at a fixed depth of 1 meter are also included for reporting purposes. Equivalent depths in centimeters for 14 and 45 g cm^{-2} stocks are given in Table E2.

Core ID	Type	C accumulation rate		N accumulation rate		C stock 0-14 g cm^{-2}	C stock 0-45 g cm^{-2}	N stock 0-14 g cm^{-2}	N stock 0-45 g cm^{-2}	C stock 1 m	N stock 1 m
		g C m^{-2} yr^{-1}		g N m^{-2} yr^{-1}		Mg C ha^{-1}		Mg N ha^{-1}		Mg C ha^{-1}	Mg N ha^{-1}
Cc19	High-DBD	18 ± 4		0.68 ± 0.14		32	109	1.3	4	218	8
Cc20		25 ± 3		1.18 ± 0.15		33	91	1.5	4	192	8
Cc18		75 ± 6		3.4 ± 0.3		108	279	4.4	11	190	7
Cc28	Low-DBD	64 ± 11		2.2 ± 0.4		87	248	3.1	9	250	9
Cc29		176 ± 9		7.3 ± 0.4		135	305	5.8	13	229	9
Mean (SE) High-DBD Intact		**21 ± 3**		**0.9 ± 0.3**		**32.4 ± 0.4**	**100 ± 9**	**1.40 ± 0.12**	**3.99 ± 0.06**		
Mean (SE) Low-DBD Intact		**110 ± 40**		**4 ± 2**		**110 ± 14**	**280 ± 20**	**4.4 ± 0.8**	**11.0 ± 1.1**		
Mean (SE) Intact		**70 ± 30**		**3.0 ± 1.2**		**80 ± 20**	**200 ± 40**	**3 ± 1**	**8 ± 2**	**220 ± 10**	**8.3 ± 0.3**
De27						64	268	2.1	8	268	8
De30						69	344	2.2	10	279	8
De31	Deforested					53	194	2.1	7	181	6
De32						57	261	3.1	10	166	6
De33						52	170	2.2	7	135	5
Mean (SE) deforested						**60 ± 3**	**250 ± 30**	**2.3 ± 0.2**	**8.2 ± 0.7**	**210 ± 30**	**7.0 ± 0.5**

6.4 Discussion

Clearing and harvesting of the mangrove forest in Madagascar between 1990 and 2010 has resulted in an estimated net loss of ~ 21% of mangrove cover (Jones et al., 2016a), but the effects of these activities on soil C storage are poorly known. Mangrove soils are heterogeneous, as evidenced from the low- and high-DBD intact mangrove cores in this study and reported elsewhere (Chmura et al., 2003; Ferreira et al., 2010; Kauffman et al., 2014; Otero et al., 2017). Within the relatively small transitional zone between land and sea, physical and chemical conditions of soils can change considerably, even at the scale of meters. High natural variability may be explained by the heterogeneous root distribution of natural mangrove forests (Boto and Wellington, 1984), differences in tidal water flooding and sedimentation rates (Chmura et al., 2003), past storms, coastal evolution and changes in creek configuration (Ferreira et al., 2010; Macnae, 1969; Semeniuk, 1996). Here, we observed a wide range and variability in soil physico-chemical properties and C and N accumulation rates in soils from intact mangroves that were independent of aboveground biomass, mangrove species or distance from shore but showed a 5-fold difference in soil accretion rates between soils in high- and low-DBD intact mangrove plots.

In contrast to the intact mangroves, the deforested mangrove soils had a high level of homogeneity in soil properties including soil C and N content and ^{210}Pb inventories. The fact that cleared mangrove sites appear to have similar soil properties post-clearance is a pattern also noticed by Stoke and Harris (2015) in New Zealand. All our deforested soils showed evidence of disturbance throughout the upper 14 g cm^{-2} (or ~ 40 cm), as indicated by lower water content, higher DBD, more intense mixing and increasing C and N contents with depth. In the bottom 14- 45 g cm^{-2}, soil physical properties and C and N content converged with those of low-DBD intact mangrove soils, suggesting that the latter were representative of deforested soils prior to clearing (Fig. 6.4; Table E3). Isotopic δ^{13}C values of sedimentary OC at low-DBD intact and deforested soils were similar to those of mangrove vegetation (-29.4 to -27‰; Bouillon et al. 2008b) and suggested that the source of organic matter was predominantly of mangrove origin at both sites. Lighter δ^{13}C and δ^{15}N in upper layers of low-DBD intact soils were consistent with the larger mangrove OC and N inputs at the surface. Slightly heavier values in the bottom layers (< ~1.5‰) are likely related to

inputs from other parts of mangrove tissues such as roots, which are usually slightly enriched in $\delta^{13}C$ (Bouillon et al., 2003; Weiss et al., 2016) and due to decomposition (Fourqurean and Schrlau, 2003). This was not observed in the deforested soil because of sediment mixing in the upper layers and mangrove removal.

Comparison between low-DBD intact and deforested soils showed that deforested soils stored 50 ± 14 Mg C ha^{-1} less than low-DBD intact soils in the upper 14 g cm^{-2} ($\sim$40 cm) (Table 6.3). Assuming that this C loss occurred linearly over time, the estimated rate of C loss in the last 10 yr is 5.0 ± 1.4 Mg C ha^{-1} yr^{-1}, which is 4.5 times higher than the annual C sequestration rate in low-DBD intact soils. Soil C loss occurred in addition to the loss from standing biomass, which was on average 130 ± 14 Mg C ha^{-1} (Fig. 6.6). The magnitude of the reduction in soil C stocks 10 yr after deforestation accounted for about 20% of the upper 1-meter C stock in low-DBD intact soils and was 45% the C accumulated in the last century. The difference in C content between low-DBD intact and deforested soils observed here was similar to that measured by Stoke and Harris (2015) in surface soil samples six years after clearing and by Otero et al. (2017) in the upper 20 cm, eight years after mangrove death. In contrast, our C stock loss was lower than the 65% observed by Grellier et al. (2018) in the upper 35 cm two years after mangrove clearing. Our lower values might be related to the lack of erosion observed in the deforested area based on particle size distributions and ^{210}Pb inventories. Unlike the study of Grellier et al. (2018) in Vietnam, our data do not suggest a winnowing of fine particles at deforested sites. In fact, deforested soils contained twice as much clay per soil volume as intact soils throughout the soil profile. Additionally, deforested soils had an average ^{210}Pb$_{xs}$ inventory that was within the range of those measured within intact soils, hence erosion, if any, was not unique to the deforested soils or was compensated by the deposition of eroded mangrove soils from the upper intertidal zone. Nonetheless, differences in C stocks between low-DBD intact and deforested soils could not be explained by net soil erosion.

143
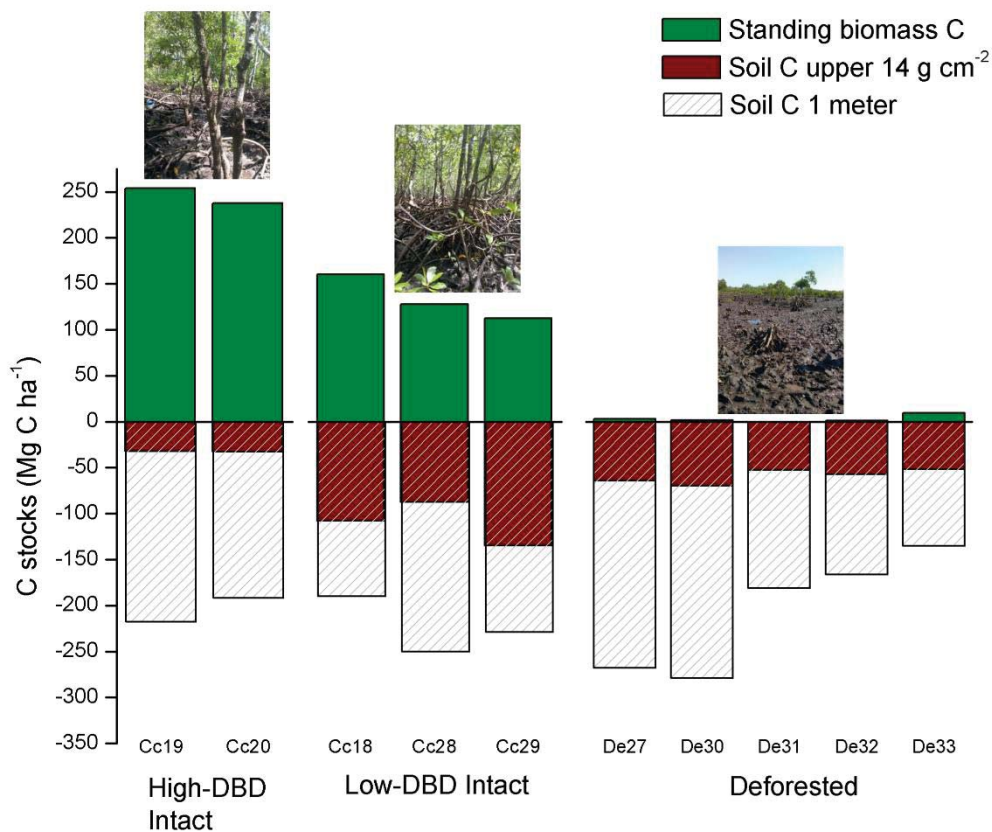
Figure 6.6: Total ecosystem C stocks of intact and deforested mangrove forests of Tsimipaika Bay, Madagascar.

Rather, the observed C losses measured in the upper 14 g cm^{-2} (or ~40 cm) of deforested soils would have occurred largely because of a lack of mangrove-derived C accumulation and enhanced C remineralization promoted by soil physical mixing and alteration of soil conditions since deforestation. As illustrated by the uniform $^{210}Pb_{xs}$ concentrations with depth, all deforested sites in this study showed intense mixing of recent soils throughout the upper 14 g cm^{-2} (or ~40 cm) (Fig. 6.5b), matching the layer where alteration in soil properties and soil C and N losses were observed. Soil mixing may promote the decomposition of C and N by breaking the soil structure and exposing physically protected organic material (Burdige, 2007), as well as increasing aeration, which enhances C mineralization and CO_2 fluxes to the atmosphere (Lovelock et al., 2017a). A greater loss of C and N content from the upper part of deforested soils also suggests that other post-mixing processes may have contributed to increased C and N remineralization, such as the exposure of deforested surface soils to direct solar radiation resulting from the loss of canopy

cover (Bosire et al., 2003; Lovelock et al., 2017a). Further evidence for enhanced C and N remineralization is the negligible below ground biomass (Table E1) and soil compaction, higher dry bulk density and lower water content observed in the upper 14 g cm^{-2} of deforested soils. This is also consistent with the observations of approximately 10 - 20 cm of soil elevation loss from around the tree stumps that remained at the cleared sites (Fig. E4).

The fate of the soil C lost should include emissions to the atmosphere as CO_2 and/or export as dissolved organic or inorganic C (Bouillon et al., 2008a; Maher et al., 2013; Najjar et al., 2018; Pendleton et al., 2012). However, most studies have focused solely on CO_2 emissions (e.g., references in Table 6.5). Converting the C loss rate estimated here to CO_2 equivalents (18 ± 5 Mg CO_2e ha^{-1} yr^{-1}) and assuming no lateral C export, we find that the potential emissions from soils are comparable to soil CO_2 efflux measurements after large- and small-scale mangrove clearing reported by others (e.g. Bulmer et al., 2015; Grellier et al., 2017; Lang'at et al., 2014). Moreover, these potential CO_2 emissions are comparable to those inferred from peat collapse due to hurricane damage (Cahoon et al., 2003) and from stock change methods after conversion to cattle pastures (Kauffman et al., 2016) (Table 6.5). However, estimated emissions were about 4 times lower than those reported when soils were excavated and converted to shrimp ponds (Kauffman et al., 2014, 2018; Sidik and Lovelock, 2013).

The rates of soil CO_2 efflux from cleared tropical and subtropical mangrove forests have been shown to be significantly higher compared to intact mangrove forests (Lang'at et al., 2014; Lovelock et al., 2011). However, whether or not lateral fluxes of dissolved C from cleared mangroves increases, has yet to be studied. Although the data were limited, DOC concentrations of waters nearshore the deforested and intact areas were very high, even during flood tide, far exceeding that typical of seawater (< 100 µM C L^{-1}; Ogawa and Tanoue, 2003). This suggests that mangroves ecosystems, intact or degraded, are an important source of exported DOC. While the increased DOC outwelling observed at deforested stations was likely influenced by expected DOC enrichments at low tide, DOC concentrations of waters nearshore deforested sites were significant (median: 2,000 µmol C L^{-1}) and support the hypothesis that C loss may be still occurring with tidal export 10 yr following deforestation. This is consistent with findings by Maher et al. (2017) that even

century-old sequestered C in mangroves is susceptible to remineralization and export to the coastal ocean. More studies involving sampling along riverine sources and coastal areas over a complete tidal cycle are needed to assess the effect of deforestation on the strength and presence of DOC fluxes.

Table 6.5: C loss rates from degraded mangrove soils reported in the literature compared to this study. To facilitate comparison among most other assessments, C losses are expressed as CO_2 equivalents (CO_2e) obtained by multiplying C loss rate by 3.67. Where rates of C loss were not reported, we estimated a mean annual C loss as the total soil C stock loss divided by the time since disturbance.

References	Disturbance	Years since disturbance	Method for estimating C loss	CO_2 emissions
				Mg CO_2e ha^{-1}yr^{-1}
This study	**Clearing**	**10**	**C stock change**	**18 ± 5**
Grellier et al. (2017)	Clearing	2	C stock change	37
			Gas flux chambers	4 ± 7
Bulmer et al. (2015)	Clearing	0.1-8	Gas flux chambers	21 ± 6
Lang'at et al. (2014)	Clearing	2	C stock change	35 ± 45
			Gas flux chambers	25 ± 7
Lovelock et al. (2011)	Clearing	1	Gas flux chambers	106
		20		30
Kauffman et al. (2016)	Conversion to cattle pastures	7	C stock change	16 ± 6
		30		7 ± 2
Kauffman et al. (2014)	Conversion to aquaculture	29	C stock change	82
Kauffman et al. (2018)	Conversion to aquaculture	10-12	C stock change	107 ± 40
		10-12		184 ± 10
		8		13 ± 5
Sidik and Lovelock, (2013)	Conversion to aquaculture	25	Gas flux chambers in pond floor	16
			Gas flux chambers in pond walls	44
Cahoon et al. (2003)	Hurricane damage	2	Change in soil volume	19

6.5 Conclusions

It is increasingly clear that mangrove deforestation promotes changes in soil properties and functions (soil C storage, nutrient processing, shore level rise) (Grellier et al., 2017; Otero et al., 2017). We show that even in the absence of net soil erosion, mangrove deforestation alters soil physico-chemical properties enhancing the susceptibility of C stocks to remineralization, resulting in potential changes in C fluxes to the coast and large amounts of CO_2 to the atmosphere. Using "*tier 2*" approaches, we estimate that mangrove

deforestation for timber and charcoal in Tsimipaika Bay has resulted in measurable reductions in total ecosystem C stocks, that represents a combined potential loss of 180 ± 20 Mg C ha^{-1} from standing biomass and soil C stocks after a decade since clearing. While C losses from standing biomass are unequivocal and could contribute significantly to CO_2 emissions if harvested timber is used as fuel-wood, emissions from soils may vary because of the large soil heterogeneity of intact mangrove forests and the partial export of C as DOC or DIC to adjacent coastal systems. Taking our estimates as representative of the entire deforested mangrove area in the Tsimipaika-Ambaro Bay complex (1,000 ha), the cumulative C losses from soils and biomass may be as high as 180 ± 20 Gg C, resulting in potential CO_2 emissions of 660 ± 70 Gg CO_2e a decade after deforestation occurred. Although deforested soils occupy a small area (2%) compared to that covered by the closed canopy mangroves (30%), the annual C loss from deforested soils is equivalent to 32% of the C sequestered annually in soils under intact closed canopy mangroves. The disproportionally large contribution of deforested soils to CO_2 emissions is explained given that 1 ha of denuded soil could return to the atmosphere the C equivalent to that sequestered in 4.5 ha of dense mangrove soils, even though our results suggest that only the 20% of the upper meter soil C stock is the most susceptible to remineralization 10 yr after deforestation. Conserving mangrove stands to avoid further deforestation is, therefore, key to avoid significant CO_2 emissions and has a large potential to help reduce mitigation costs. Conservation projects seeking to account for avoided emissions could take into consideration avoided emissions from the soils that are not deforested as well as from loss of biomass.

Chapter 7

Conclusions and Perspectives

The aim of this thesis was to quantify OC sequestration rates and their controls over contemporary time scales (~100 yr) in sediments of natural and degraded coastal BCEs, where sedimentary OC can be preserved for centuries to millennia and constitutes the main component of the OC pool in these ecosystems. This was done in an effort to 1) deliver improved direct estimates of the long-term C sequestration capacity of coastal BCEs, and 2) understand the loss of C sequestration potential associated with the degradation of these habitats, as well as to quantify the loss of the sequestered OC over a period of time after ecosystem disturbance.

The extent to which OC accumulates in coastal BCE's sediments was evaluated using the ^{210}Pb dating technique, which resolves OC burial rates in a timescale compatible with management actions (~100 yr) and provides enough time resolution to evaluate changes in sedimentary OC sequestration associated with habitat disturbance derived from human impacts or recent climate breakdown. The determination of OC accumulation rates in coastal BCE using this technique, however, is often complex, due to the multiple sedimentary processes involved in coastal areas (sediment mixing, erosion, variable sediment inputs, heterogeneous sediment composition and organic matter decay). As per the research in *Chapter 3*, we conclude that, where those processes occur and sedimentation rates are low (< 2 mm yr^{-1}), the estimation of sediment OC sequestration in coastal BCE should be restricted to the average OC accumulation in the last century. This is because the bias in average OC accumulation rates can be as high as 20% even if sedimentary processes have been considered in dating models. Of the three classic ^{210}Pb dating models, the CRS model is less sensitive to anomalies in ^{210}Pb$_{xs}$ profiles and returns most accurate sediment and carbon accumulation estimates regardless of the sedimentary process involved. However, its application is restricted to the accurate

determination of the $^{210}Pb_{xs}$ inventory, which can be problematic when all samples along a sediment core are not analyzed, where sediment erosion has occurred or where the presence of coarse sediments dilutes the $^{210}Pb_{xs}$ specific activities limiting the ^{210}Pb-datable part of a sediment core to the very top centimeters. Studies in coastal BCE ecosystems often require sampling of many sediment cores to account for the large spatial variability in OC storage (e.g., Lavery et al., 2013), and this may limit the number of ^{210}Pb analyses due to budgetary constraints. In addition, the presence of sands and biogenic carbonates, particularly in seagrass sediments (Koch, 2001), are conditions that may lead to the inability to determine full $^{210}Pb_{xs}$ inventories due to dilution of ^{210}Pb specific activities and detection limits. Therefore, the CF-CS model could be the preferred option as it might be too ambitious to produce a detailed chronology based on usually a limited set of data along a sediment core. The disadvantages of using this model include failure to account for rapid changes in accumulation and a large overestimation (up to 90%) of mean accumulation rates where intense mixing occurs. For this reason, it is important to complement the ^{210}Pb derived age models and sedimentation rates with additional tracers or in its absence, with geochemical, ecological or historical data.

Estimates of OC burial rates in seagrass sediments were remarkably few and were based mostly in indirect short-term (annual) estimates of net seagrass community production. In *Chapter 4*, we compiled, reviewed and analyzed 167 published and unpublished OC burial rates in seagrass sediments estimated using ^{210}Pb dating. Considering ^{210}Pb dating models and associated uncertainties and excluding sites where intense mixing was observed, global mean OC accumulation rates in seagrass beds per unit area were estimated to be 24 g C m^{-2} yr^{-1} (95% C.I.: 20 - 30 g C m^{-2} yr^{-1}), accounting for a global OC burial ranging between 6 and 18 Tg C yr^{-1}. This new estimate is 7 times lower than previous estimates (138 $\pm$ 38 g C m^{-2} yr$^{-1;}$ or 48 – 112 Tg C yr^{-1}, globally) and suggests that while 10% of the net seagrass community production is buried and preserved in immediate sediments, the remaining 90% is exported away. Additionally, the rate of sediment accumulation most strongly influenced the OC sequestration efficiency in both seagrass or bare sediments, however the presence of vegetation cover significantly influenced the preservation of the buried OC. On a per area basis, seagrass ecosystems

are 7-10 times less efficient in storing OC per unit area than are mangroves and tidal marshes, however, the extent of the seagrass biome is about 2 times larger, thus its contribution to the total OC sequestration in coastal BCE sediments is large and accounts for between 20 - 30%. On a global scale, annual coastal blue C sequestration in sediments accounts for about 40 – 50 Tg C, representing only about 0.4 to 0.5% of global anthropogenic CO_2 emissions (mainly fossil fuel and deforestation, 10 Pg C yr^{-1}; IPCC, 2013). However, C fluxes to the atmosphere from loss of coastal BCE could increase global emissions by 0.4 to 3% per year.

Physical disturbance of vegetated coastal habitats caused losses of sediment OC over the course of months to years depending on the type of disturbance and the size of the OC stock. Studies in *Chapters 5* and *6* suggested that the proportions of the OC stock susceptible to remineralization after disturbance in seagrass and mangroves could be lower than previously assumed (i.e., the upper meter; Pendleton et al., 2012). While there is no question that the OC in the upper meter of sediments (or deeper) could be lost when ecosystems have been degraded and soils excavated (e.g., mangrove conversion to aquaculture; Kauffman et al., 2014), this general assumption likely oversimplifies the problem. Using satellite imagery and a published model of OC decomposition, we quantified that between 4 and 20% of the C stock in the upper meter of degraded seagrass sediments could have been remineralized during the 3 years following a marine heatwave in Shark Bay, (Western Australia) that took place in 2010-11. In mangroves, direct measurements of sediment OC revealed that 20% of the upper meter OC stock was lost 10 years following deforestation. In both studies, the rates of OC loss in degraded habitats were several times higher than the rates of OC sequestration under intact conditions, suggesting that the real potential of coastal BCEs to mitigate GHG emissions is towards the preservation of existing habitats and restoration of lost habitats, which can result not only in avoided emissions from disturbed sediments after vegetation loss, but also in a recovery of OC sequestration capacity (Marbà et al., 2015). In addition, conserving and restoring coastal BCE is a cost-effective measure providing local adaptation benefits (coastal protection and shore level raise) in addition to other co-benefits such as support

for fisheries, nutrient retention, flood control, water quality improvement, tourism and recreation (Lau, 2013).

7.1 Perspectives

During the past two decades, substantial effort has been devoted to improving our understanding and quantification of the amount of C being sequestered in sediments and biomass of coastal BCEs, as well as of the loss of the sequestered C when ecosystems are degraded. Thanks to such effort, the potential that coastal BCEs have to mitigate climate change by acting as carbon sinks is now evident to scientists and policy makers. Nevertheless, our ability to confidently include C sequestration by coastal BCEs in mitigation schemes is hampered by an insufficient quantitative understanding of net ecosystem carbon budgets (NECB) and lack of integrated measurements of vertical (GHG emissions vs burial) and horizontal (import vs export of POC, DOC and DIC) fluxes across different ecosystem types and conservation statuses. Added to all this is the fact that serious uncertainties in the global area covered by tidal marsh and seagrass habitats still remain and that representations of OC stocks and burial rates outside North America, Europe and Australia are very limited. The most recent compilations of OC stocks and burial rates in coastal BCE (Breithaupt et al., 2012; Chmura et al., 2003; Fourqurean et al., 2012b; Ouyang and Lee, 2014; Röhr et al., 2018) show that spatial variations in OC storage and sequestration can be at least as important as the averaged quantities themselves, and variations at scales as small as a few kilometers can be important for larger scale integrations (IPCC, 2007).

The effectiveness of coastal BCE in mitigating climate change depends on the efficiency in which C is incorporated in the soil/sediment layer, versus that exported as GHG or as dissolved and particulate C to coastal waters. This is the core concept of the NECB, an approach that includes a complete accounting of all C flux pathways and determines the net C accumulation in (or loss from) ecosystems. Quantification of NECBs and their controls is key not only to advice blue carbon offset projects and best restoration practices to maximize C uptake and minimize GHG production, but also to understanding the role of coastal BCE in the Earth's global C budget. While blue carbon management might focus on the in-situ net balance between the C that enters and leaves the ecosystem,

groups involved in assessing the global C budget will inquire about the origin, transformations and fate of the C that cycles through these ecosystems.

7.1.1 An interplay between C burial, GHG emissions and export

While published studies show that ecological restoration is successful in sequestering C and building peat soils (Marbà et al., 2015; Miller et al., 2008), as part of the decomposition process, coastal BCEs also produce greenhouse gas emissions (GHGs: CO_2, water vapor, CH_4, and N_2O) that could offset OC storage in sediments (Hemes et al., 2018; Knox et al., 2015; Rosentreter et al., 2018; Webb et al., 2018). Baseline information on CO_2, water vapor, CH_4, and N_2O fluxes from coastal BCE is very sparse (Maher et al., 2018), but it is required to refine the source/sink interpretation of different types of coastal BCE as well as to advise on how GHG fluxes may change if coastal BCEs are degraded or restored.

Additionally, the extent to which aquatic pathways contribute to the net ecosystem carbon budget (NECB) of different coastal BCE remains poorly understood. Recent studies in mangroves and tidal marshes have shown that the aquatic lateral C export is larger than C sequestration in sediments and comparable to the "missing" fraction of their own net ecosystem production that is not respired nor buried (Maher et al., 2013; Najjar et al., 2018). Lateral exports of POC and DOC from coastal BCEs can sustain coastal and open ocean food webs (Odum, 1980, 2002) and eventually return to the atmosphere as CO_2. However, a fraction of these could escape remineralization and be sequestered in the deep ocean, hence contributing to the long-term sink of atmospheric C (Duarte and Krause-Jensen, 2017). Tidal marshes and mangroves export large amounts of TAlk and DIC to the coastal ocean (Maher et al., 2013; Wang et al., 2016), while clearly a majority of this carbon will return to the atmosphere as CO_2, the concurrent export of TAlk allows for some of this DIC to remain within the coastal ocean (Maher et al., 2018), again suggesting that indeed carbon sequestration could be underestimated by only including carbon burial within coastal BCE sediments.

Significant C export to coastal waters and to the open ocean is likely allowed by the large subsidies of allochthonous C from plankton and terrestrial OC these ecosystems receive through tidal exchange and riverine discharge. For instance, the allochthonous fraction of POC typically comprises 50% of the OC stock in seagrass sediments (Kennedy et al., 2010) and, while it contributes to the large OC burial capacity of coastal BCE, it might lead to double counting difficulties when incorporating coastal BCE into the Earth global C budget, especially where specific sources to the OC burial in sediments have not been assigned. Resolving and incorporating the exchange of C between coastal BCEs, adjacent coastal marine systems, and terrestrial and atmospheric components will help to further constrain their local and global role in carbon budgets, as well as the consequences of losses or gains of these habitats for C flux.

Greenhouse gas emissions, burial, import and export fluxes of dissolved and particulate C may change over time, season, with disturbance and particularly with climate change. Indeed, how climate change impacts may affect NECB is a question becoming increasingly urgent to resolve. Climate change scenarios predict increased warming, changes in precipitation, and water levels (tidal and groundwater), which could affect the C cycle in coastal BCE by affecting plant growth and OC decomposition rates. To predict the long-term C sequestration capacity of coastal BCE, we also need information on how OC burial, GHG exchange and lateral export fluxes may respond to projected future climate conditions. Specifically, this question is paramount to understanding the feedbacks between C dynamics of coastal BCE and climate and to advice how climate change impacts may affect Cap-and-Trade potential for C sequestration.

References

Aalto, R. and Nittrouer, C. a.: 210Pb geochronology of flood events in large tropical river systems, Philos. Trans. R. Soc. A Math. Phys. Eng. Sci., 370, 2040–2074, doi:10.1098/rsta.2011.0607, 2012.

Abril, J. M.: A new theoretical treatment of compaction and the advective-diffusive processes in sediments: a reviewed basis for radiometric dating models, J. Paleolimnol., 30, 363–370, 2003.

Abril, J. M.: A 210Pb-based chronological model for recent sediments with random entries of mass and activities: Model development, J. Environ. Radioact., 151, 64–74, doi:10.1016/j.jenvrad.2015.09.018, 2016.

Abril, J. M. and Gharbi, F.: Radiometric dating of recent sediments: Beyond the boundary conditions, J. Paleolimnol., 48, 449–460, doi:10.1007/s10933-012-9622-5, 2012.

Abril, J. M., García-León, M., García-Tenorio, R., Sánchez, C. I. and El-Daoushy, F.: Dating of marine sediments by an incomplete mixing model, J. Environ. Radioact., 15(2), 135–151, doi:10.1016/0265-931X(91)90048-K, 1992.

Adame, M. F., Zakaria, R. M., Fry, B., Chong, V. C., Then, Y. H. A., Brown, C. J. and Lee, S. Y.: Loss and recovery of carbon and nitrogen after mangrove clearing, Ocean Coast. Manag., 161(April), 117–126, doi:10.1016/j.ocecoaman.2018.04.019, 2018.

Alongi, D. M.: Present state and future of the world's mangrove forests, Environ. Conserv., 29(3), 331–349, doi:10.1017/S0376892902000231, 2002.

Alongi, D. M.: Carbon Cycling and Storage in Mangrove Forests, Ann. Rev. Mar. Sci., 6(1), 195–219, doi:10.1146/annurev-marine-010213-135020, 2014.

Alongi, D. M., Wattayakorn, G., Pfitzner, J., Tirendi, F., Zagorskis, I., Brunskill, G. ., Davidson, A. and Clough, B. .: Organic carbon accumulation and metabolic pathways in sediments of mangrove forests in southern Thailand, Mar. Geol., 179(1–2), 85–103, doi:10.1016/S0025-3227(01)00195-5, 2001.

Alongi, D. M., Sasekumar, A., Chong, V. C., Pfitzner, J., Trott, L. A., Tirendi, F., Dixon, P. and Brunskill, G. J.: Sediment accumulation and organic material flux in a managed mangrove ecosystem: Estimates of land-ocean-atmosphere exchange in peninsular Malaysia, Mar. Geol., 208(2–4), 383–402, doi:10.1016/j.margeo.2004.04.016, 2004.

Alongi, D. M., Pfitzner, J., Trott, L. a., Tirendi, F., Dixon, P. and Klumpp, D. W.: Rapid sediment accumulation and microbial mineralization in forests of the mangrove Kandelia candel in the Jiulongjiang Estuary, China, Estuar. Coast. Shelf Sci., 63, 605–618, doi:10.1016/j.ecss.2005.01.004, 2005.

Alongi, D. M., Trott, L. a., Rachmansyah, Tirendi, F., McKinnon, a. D. and Undu, M. C.: Growth and development of mangrove forests overlying smothered coral reefs, Sulawesi and Sumatra, Indonesia, Mar. Ecol. Prog. Ser., 370, 97–109, doi:10.3354/meps07661, 2008.

Álvarez-Iglesias, P., Quintana, B., Rubio, B. and Pérez-Arlucea, M.: Sedimentation rates and trace metal input history in intertidal sediments from San Simón Bay (Ría de Vigo, NW Spain) derived from 210Pb and 137Cs chronology, J. Environ. Radioact., 98, 229–250, doi:10.1016/j.jenvrad.2007.05.001, 2007.

Andersen, T. J.: Some Practical Considerations Regarding the Application of 210Pb and 137Cs Dating to Estuarine Sediments, in Applications of Paleoenvironmental Techniques in Estuarine Studies, edited by K. Weckström, K. Saunders, P. Gell, and C. Skilbeck, pp. 121–140, Springer, Dordrecht., 2017.

Anderson, M., Smith, J. and McKay, S.: Wave dissipation by vegetation., 2011.

Appleby, P. G.: Dating recent sediments by 210Pb: problems and solutions, in (STUK-A--145), vol. 2, edited by E. Illus, pp. 7–24, Finland., 1998.

Appleby, P. G.: Chronostratigraphic Techniques in Recent Sediments, in Tracking Environmental Change Using Lake Sediments, vol. 1, pp. 171–203, Springer Netherlands., 2001.

Appleby, P. G.: Three decades of dating recent sediments by fallout radionuclides: a review, The Holocene, 18, 83–93, doi:10.1177/0959683607085598, 2008.

Appleby, P. G. and Oldfield, F.: The calculation of lead-210 dates assuming a constant rate of supply of unsupported 210Pb to the sediment, CATENA, 5(1), 1–8, doi:10.1016/S0341-8162(78)80002-2, 1978.

Appleby, P. G. and Oldfield, F.: Applications of lead-210 to sedimentation studies, in Uranium-series disequilibrium: applications to earth, marine, and environmental sciences, edited by M. Ivanovich and R. . Harman, Clarendon Press, Oxford., 1992.

Appleby, P. G., Oldfield, F. and Physics, T.: The assessment of 210Pb data from sites with varying sediment accumulation rates, Hydrobiologia, 103, 29–35, doi:10.1007/BF00028424, 1983.

Arata, L., Meusburger, K., Frenkel, E., A'Campo-Neuen, A., Iurian, A. R., Ketterer, M. E., Mabit, L. and Alewell, C.: Modelling Deposition and Erosion rates with RadioNuclides (MODERN) - Part 1: A new conversion model to derive soil redistribution rates from inventories of fallout radionuclides, J. Environ. Radioact., 162–163, 45–55, doi:10.1016/j.jenvrad.2016.05.008, 2016.

Arias-Ortiz, A., Serrano, O., Masqué, P., Lavery, P., Mueller, U., Kendrick, G., Rozaimi, M., Esteban, A., Fourqurean, J. W., Marbà, N., Mateo, M.-A., Murray, K., Rule, M. and Duarte, C. M.: A marine heat wave drives massive losses from the world's largest seagrass carbon stocks [dataset]., 2017.

Arias-Ortiz, A., Serrano, O., Masqué, P., Lavery, P. S., Mueller, U., Kendrick, G. A., Rozaimi, M., Esteban, A., Fourqurean, J. W., Marbà, N., Mateo, M. A., Murray, K., Rule, M. J. and Duarte, C. M.: A marine heatwave drives massive losses from the world's largest seagrass carbon stocks, Nat. Clim. Chang., 8, 338–344, doi:10.1038/s41558-018-0096-y, 2018a.

Arias-Ortiz, A., Serrano, O., Masqué, P., Lavery, P. S., Mueller, U., Kendrick, G. A., Rozaimi, M., Esteban, A., Fourqurean, J. W., Marbà, N., Mateo, M. A., Murray, K., Rule, M. J. and Duarte, C. M.: A marine heatwave drives massive losses from

the world's largest seagrass carbon stocks, Nat. Clim. Chang., doi:10.1038/s41558-018-0096-y, 2018b.

Arias-Ortiz, A., Masqué, P., Garcia-Orellana, J., Serrano, O., Mazarrasa, I., Marbà, N., Lovelock, C. E., Lavery, P. and Duarte, C. M.: Reviews and syntheses: 210Pb-derived sediment and carbon accumulation rates in vegetated coastal ecosystems: setting the record straight, Biogeosciences, 15, 6791–6818, doi:10.5194/bg-2018-78, 2018c.

Armentano, T. V. and Woodwell, G. M.: Sedimentation rates in a Long Island marsh determined by 210Pb dating, Limnol. Oceanogr., 20(3), 452–456, doi:10.4319/lo.1975.20.3.0452, 1975.

Atwood, T. B., Connolly, R. M., Ritchie, E. G., Lovelock, C. E., Heithaus, M. R., Hays, G. C., Fourqurean, J. W. and Macreadie, P. I.: Predators help protect carbon stocks in blue carbon ecosystems, Nat. Clim. Chang., 5(12), 1038–1045, doi:10.1038/nclimate2763, 2015.

Atwood, T. B., Connolly, R. M., Almahasheer, H., Carnell, P. E., Duarte, C. M., Ewers Lewis, C. J., Irigoien, X., Kelleway, J. J., Lavery, P. S., Macreadie, P. I., Serrano, O., Sanders, C. J., Santos, I., Steven, A. D. L. and Lovelock, C. E.: Global patterns in mangrove soil carbon stocks and losses, Nat. Clim. Chang., 7(7), 523–528, doi:10.1038/nclimate3326, 2017.

Balesdent, J., Chenu, C. and Balabane, M.: Relationship of soil organic matter dynamics to physical protection and tillage, Soil Tillage Res., 53(3–4), 215–230, doi:10.1016/S0167-1987(99)00107-5, 2000.

Ballantyne, A. P., Alden, C. B., Miller, J. B., Tans, P. P. and White, J. W. C.: Increase in observed net carbon dioxide uptake by land and oceans during the past 50 years, Nature, 488(7409), 70–72, doi:10.1038/nature11299, 2012.

Barbier, E. B., Hacker, S. D., Kennedy, C., Koch, E. W., Stier, A. C. and Silliman, B. R.: The value of estuarine and coastal ecosystem services, Ecol. Monogr., 81(2), 169–193, doi:10.1890/10-1510.1, 2011.

Baskaran, M., Nix, J., Kuyper, C. and Karunakara, N.: Problems with the dating of sediment core using excess 210Pb in a freshwater system impacted by large scale watershed changes, J. Environ. Radioact., 138, 355–363, doi:10.1016/j.jenvrad.2014.07.006, 2014.

Bellucci, L. G., Frignani, M., Cochran, J. K., Albertazzi, S., Zaggia, L., Cecconi, G. and Hopkins, H.: 210Pb and 137Cs as chronometers for salt marsh accretion in the Venice Lagoon - links to flooding frequency and climate change, J. Environ. Radioact., 97(2–3), 85–102, doi:10.1016/j.jenvrad.2007.03.005, 2007.

Benner, R. and Strom, M.: A critical evaluation of the analytical blank associated with, Mar.Chem., 41, 153–160, 1993.

Benson, L., Glass, L., Jones, T. G., Ravaoarinorotsihoarana, L. and Rakotomahazo, C.: Mangrove carbon stocks and ecosystem cover dynamics in southwest Madagascar and the implications for local management, Forests, 8(6), 1–21, doi:10.3390/f8060190, 2017.

Bianchi, T. S.: The role of terrestrially derived organic carbon in the coastal ocean: A

changing paradigm and the priming effect, Proc. Natl. Acad. Sci., 108(49), 19473–19481, doi:10.1073/pnas.1017982108, 2011.

Binford, M. W.: Calculatio and uncertainty analysis of 210Pb dates for PIRLA project lake sediment cores, J. Paleolimnol., 3, 253–267, 1990.

Björk, M., Short, F. T., Mcleod, E. and Beer, S.: Managing Seagrasses for Resilience to Climate Change, IUCN, Gland, Gland, Switzerland., 2008.

Blaauw, M. and Christen, J.: Flexible paleoclimate age-depth models using an autoregressive gamma process, Bayesian Anal., 6(3), 457–474, 2011.

Bosire, J. O., Dahdouh-Guebas, F., Kairo, J. G. and Koedam, N.: Colonization of non-planted mangrove species into restored mangrove stands in Gazi Bay, Kenya, Aquat. Bot., 76(4), 267–279, doi:10.1016/S0304-3770(03)00054-8, 2003.

Boto, K. and Wellington, J.: Soil characteristics and nutrient status in a northern Australian mangrove forest, Estuaries, 1984.

Botwe, B. O., Abril, J. M., Schirone, A., Barsanti, M., Delbono, I., Delfanti, R., Nyarko, E. and Lens, P. N. L.: Settling fluxes and sediment accumulation rates by the combined use of sediment traps and sediment cores in Tema Harbour (Ghana), Sci. Total Environ., 609, 1114–1125, doi:10.1016/j.scitotenv.2017.07.139, 2017.

Boudreau, B. P.: Is burial velocity a master parameter for bioturbation?, Geochim. Cosmochim. Acta, 58(4), 1243–1249, doi:10.1016/0016-7037(94)90378-6, 1994.

Bouillon, S., Dahdouh-Guebas, F., Rao, A. V. V. S., Koedam, N. and Dehairs, F.: Sources of organic carbon in mangrove sediments: Variability and possible ecological implications, Hydrobiologia, 495, 33–39, doi:10.1023/A:1025411506526, 2003.

Bouillon, S., Borges, A. V., Castañeda-Moya, E., Diele, K., Dittmar, T., Duke, N. C., Kristensen, E., Lee, S. Y., Marchand, C., Middelburg, J. J., Rivera-Monroy, V. H., Smith, T. J. and Twilley, R. R.: Mangrove production and carbon sinks: A revision of global budget estimates, Global Biogeochem. Cycles, 22(2), 1–12, doi:10.1029/2007GB003052, 2008a.

Bouillon, S., Connolly, R. M. and Lee, S. Y.: Organic matter exchange and cycling in mangrove ecosystems: Recent insights from stable isotope studies, J. Sea Res., 59(1–2), 44–58, doi:10.1016/j.seares.2007.05.001, 2008b.

Bowler, C., Karl, D. M. and Colwell, R. R.: Microbial oceanography in a sea of opportunity, Nature, 459(7244), 180–184, doi:10.1038/nature08056, 2009.

Boyd, B. M. and Sommerfield, C. K.: Marsh accretion and sediment accumulation in a managed tidal wetland complex of Delaware Bay, Ecol. Eng., 92, 37–46, doi:10.1016/j.ecoleng.2016.03.045, 2016.

Breithaupt, J. L., Smoak, J. M., Smith, T. J., Sanders, C. J. and Hoare, A.: Organic carbon burial rates in mangrove sediments: Strengthening the global budget, Global Biogeochem. Cycles, 26(3), doi:10.1029/2012GB004375, 2012.

Breithaupt, J. L., Smoak, J. M., Smith, T. J. and Sanders, C. J.: Temporal variability of carbon and nutrient burial, sediment accretion, and mass accumulation over the past century in a carbonate platform mangrove forest of the Florida Everglades, J. Geophys. Res. Biogeosciences, 119, 2032–2048,

doi:10.1002/2014JG002715.Received, 2014.

Brodie, C. R., Leng, M. J., Casford, J. S. L., Kendrick, C. P., Lloyd, J. M., Yongqiang, Z. and Bird, M. I.: Evidence for bias in C and N concentrations and δ13C composition of terrestrial and aquatic organic materials due to pre-analysis acid preparation methods, Chem. Geol., 282(3–4), 67–83, doi:10.1016/J.CHEMGEO.2011.01.007, 2011.

Bruland, K. .: Trace elements in seawater., in Chemical oceanography, vol. 1, edited by J. P. Riley and G. Skirrow, pp. 415–496, London Academic Press, London., 1983.

Bufarale, G. and Collins, L. B.: Stratigraphic architecture and evolution of a barrier seagrass bank in the mid-late Holocene, Shark Bay, Australia, Mar. Geol., 359, 1–21, doi:10.1016/j.margeo.2014.11.010, 2015.

Bulmer, R. H., Lundquist, C. J. and Schwendenmann, L.: Sediment properties and CO2 efflux from intact and cleared temperate mangrove forests, Biogeosciences, 12(20), 6169–6180, doi:10.5194/bg-12-6169-2015, 2015.

Burdige, D. J.: Preservation of organic matter in marine sediments: Controls, mechanisms, and an imbalance in sediment organic carbon budgets?, Chem. Rev., 107(2), 467–485, doi:10.1021/cr050347q, 2007.

Burdige, D. J., Zimmerman, R. C. and Hu, X.: Rates of carbonate dissolution in permeable sediments estimated from pore-water profiles: The role of sea grasses, Limnol. Oceanogr., 53(2), 549–565, doi:10.4319/lo.2008.53.2.0549, 2008.

Burkholder, D. A., Heithaus, M. R., Thomson, J. A. and Fourqurean, J. W.: Diversity in trophic interactions of green sea turtles Chelonia mydas on a relatively pristine coastal foraging ground, Mar. Ecol. Prog. Ser., 439(Bjorndal 1980), 277–293, doi:10.3354/meps09313, 2011.

Cahoon, D. R., Hensel, P., Rybczyk, J., McKee, K. L., Proffitt, C. E. and Perez, B. C.: Mass tree mortality leads to mangrove peat collapse at Bay Islands, Honduras after Hurricane Mitch, J. Ecol., 91(6), 1093–1105, doi:10.1046/j.1365-2745.2003.00841.x, 2003.

Callaway, J., DeLaune, R. and Jr, W. P.: Sediment accretion rates from four coastal wetlands along the Gulf of Mexico, J. Coast. Res., 13, 181–191, 1997.

Callaway, J. C., DeLaune, R. D. and Patrick, W. H.: Chernobyl ^{137}Cs used to determine sediment accretion rates at selected northern European coastal wetlands, Limnol. Oceanogr., 41(3), 444–450, doi:10.4319/lo.1996.41.3.0444, 1996.

Cambridge, M. L., Bastyan, G. R. and Walker, D. I.: Recovery of Posidonia meadows in Oyster Harbour, southwestern Australia, Bull. Mar. Sci., 71(3), 1279–1289, 2002.

Campbell, J. E., Lacey, E. A., Decker, R. A., Crooks, S. and Fourqurean, J. W.: Carbon Storage in Seagrass Beds of Abu Dhabi, United Arab Emirates, Estuaries and Coasts, 38(1), 242–251, doi:10.1007/s12237-014-9802-9, 2014.

Canadell, J. G. and Raupach, M. R.: Managing Forests for Climate Change Mitigation, Science (80-.)., 320(5882), 1456–1457, doi:10.1126/science.1155458, 2008.

Carroll, J. and Lerche, I.: Sedimentary processes : quantification using radionuclides, Elsevier, Oxford., 2003.

Castañeda-Moya, E., Twilley, R. and Rivera-Monroy, V.: Sediment and nutrient deposition associated with Hurricane Wilma in mangroves of the Florida Coastal Everglades, Estuaries and Coasts, 33, 45–58, doi:10.1007/s12237-009-9242-0, 2010.

Cawley, K. M., Ding, Y., Fourqurean, J. and Jaffé, R.: Characterising the sources and fate of dissolved organic matter in Shark Bay, Australia: A preliminary study using optical properties and stable carbon isotopes, Mar. Freshw. Res., 63(11), 1098–1107, doi:10.1071/MF12028, 2012.

Cearreta, A., Irabien, M. J., Ulibarri, I., Yusta, I., Croudace, I. W. and Cundy, A. B.: Recent Salt Marsh Development and Natural Regeneration of Reclaimed Areas in the Plentzia Estuary , N . Spain, Estuar. Coast. Shelf Sci., 54, 863–886, doi:10.1006/ecss.2001.0862, 2002.

Chanton, J. P., Martens, C. S. and Kipphut, G. W.: Lead-210 sediment geochronology in a changing coastal environment, Geochim Cosmo Acta, 47(15), 1791–1804, doi:10.1016/0016-7037(83)90027-3, 1983.

Charpy-Roubaud, C., Sournia, A. and 1990, undefined: The comparative estimation of phytoplanktonic, microphytobenthic and macrophytobenthic primary production in the oceans, Mar. Microb. Food Webs, 4(1), 31–57, 1990.

Chefaoui, R. M., Duarte, C. M. and Serrão, E. A.: Dramatic loss of seagrass habitat under projected climate change in the Mediterranean Sea, Glob. Chang. Biol., 24(10), 4919–4928, doi:10.1111/gcb.14401, 2018.

Chen, R. and Twilley, R. R.: A simulation model of organic matter and nutrient accumulation in mangrove wetland soils, Biogeochemistry, 44(June 2016), 93–118, doi:10.1007/BF00993000, 1999.

Chmura, G. L., Anisfeld, S. C., Cahoon, D. R. and Lynch, J. C.: Global carbon sequestration in tidal, saline wetland soils, Global Biogeochem. Cycles, 17(4), 1111, doi:1111 10.1029/2002gb001917, 2003.

Christensen, B. T.: Physical Fractionation of Soil and Organic Matter in Primary Particle Size and Density Separates, pp. 1–90, Springer, New York, NY., 1992.

Church, T. M., Lord, C. J. and Somayajulu, B. L. K.: Uranium, thorium and lead nuclides in a Delaware salt marsh sediment, Estuar. Coast. Shelf Sci., 13, 267–275, doi:10.1016/S0302-3524(81)80025-4, 1981.

Cochran, J. and Masqué, P.: Natural radionuclides applied to coastal zone processes, Mar. Radioact., 6, 1–21, doi:https://doi.org/10.1016/S1569-4860(05)80002-6, 2005.

Cochran, J. K., Hirschberg, D. J., Wang, J. and Dere, C.: Atmospheric Deposition of Metals to Coastal Waters (Long Island Sound, New York U.S.A.): Evidence from Saltmarsh Deposits, Estuarine, Coast. Shelf Sci. 46, 503-522, 46, 503–522, doi:10.1006/ecss.1997.0299, 1998.

Copertino, M. S.: Seagrass distribution across Brazilian Coast., 2013.

Craft, C.: Freshwater input structures soil properties, vertical accretion, and nutrient accumulation of Georgia and U.S tidal marshes, Limnol. Oceanogr., 52(3), 1220–1230, doi:10.4319/lo.2007.52.3.1220, 2007.

Craft, C. B., Seneca, E. D. and Broome, S. W.: Loss on Ignition and Kjeldahl Digestion for Estimating Organic Carbon and Total Nitrogen in Estuarine Marsh Soils: Calibration with Dry Combustion, Estuaries, 14(2), 175–179, 1991.

Cremers, A., Elsen, A., Preter, P. De and Maes, A.: Quantitative analysis of radiocaesium retention in soils, Nature, 335(6187), 247–249, doi:10.1038/335247a0, 1988.

Crusius, J. and Anderson, R. F.: Evaluating the mobility of 137Cs, 239+240Pu and 210Pb from their distributions in laminated lake sediments, J. Paleolimnol., 13, 119–141, doi:10.1007/BF00678102, 1995.

Crusius, J., Bothner, M. H. and Sommerfield, C. K.: Bioturbation depths, rates and processes in Massachusetts Bay sediments inferred from modeling of 210Pb and 239 + 240Pu profiles, Estuar. Coast. Shelf Sci., 61(4), 643–655, doi:10.1016/j.ecss.2004.07.005, 2004.

Cullen-Unsworth, L. C. and Unsworth, R.: A call for seagrass protection, Science (80-.)., 361(6401), 446–448, doi:10.1126/science.aat7318, 2018.

Cundy, A. B. and Croudace, I. W.: Physical and chemical associations of radionuclides and trace metals in estuarine sediments: an example from Poole Harbour, Southern England, J. Environ. Radioact., 29(3), 191–211, doi:10.1016/0265-931X(95)00031-5, 1995.

Cusack, M., Saderne, V., Arias-Ortiz, A., Masqué, P., Krishnakumar, P. K., Rabaoui, L., Qurban, M. A., Qasem, A. M., Prihartato, P., Loughland, R. A., Elyas, A. A. and Duarte, C. M.: Organic carbon sequestration and storage in vegetated coastal habitats along the western coast of the Arabian Gulf, Environ. Res. Lett., 13(7), 074007, doi:10.1088/1748-9326/aac899, 2018.

Dahl, M., Deyanova, D., Gütschow, S., Asplund, M. E., Lyimo, L. D., Karamfilov, V., Santos, R., Björk, M. and Gullström, M.: Sediment Properties as Important Predictors of Carbon Storage in Zostera marina Meadows: A Comparison of Four European Areas, edited by X. Wang, PLoS One, 11(12), e0167493, doi:10.1371/journal.pone.0167493, 2016.

Davis, G.: Algal laminate sediments, Gladstone embayment, Shark Bay, Western Australia, in Carbonate Sedimentation and Environments, Shark Bay, Western Australia, vol. 13, edited by B. W. Logan, G. R. Davies, J. F. Read, and D. E. Cebulski, pp. 169–205, American Association of Petroleum Geologists Memoirs, Tulsa., 1970.

Davis, R., Hess, C. and Norton, S.: 137 Cs and 210 Pb dating of sediments from soft-water lakes in New England (USA) and Scandinavia, a failure of 137 Cs dating, Chem. Geol., 44, 151–185, 1984.

DBCA: Marine Habitats of Western Australia, Perth, Western Australia, Australia., 2016.

Delgado, M., de Jonge, V. N. and Peletier, H.: Experiments on resuspension of natural microphytobenthos populations, Mar. Biol., 108(2), 321–328, doi:10.1007/BF01344347, 1991.

Diemer, J., Allan, C., Eckardt, I., Kroening, D. and Vinson, D.: Sedimentation in a piedmont reservoir: Evidence from Brown's Cove, Lake Wylie, North Carolina, Environ. Eng. Geosci., 17(2), 123–142, doi:10.2113/gseegeosci.17.2.123, 2011.

Diochon, A., Kellman, L. and Beltrami, H.: Looking deeper: An investigation of soil carbon losses following harvesting from a managed northeastern red spruce (Picea rubens Sarg.) forest chronosequence, For. Ecol. Manage., 257(2), 413–420, doi:10.1016/j.foreco.2008.09.015, 2009.

Donato, D. C., Kauffman, J. B., Murdiyarso, D., Kurnianto, S. and Stidham, M.: Mangroves among the most carbon-rich forests in the tropics, Nat. Geosci., 4(4), 1–5, doi:10.1038/ngeo1123, 2011.

Du, J. Z., Zhang, J. and Baskaran, M.: Applications of Short-Lived Radionuclides (7Be, 210Pb, 210Po, 137Cs and 234Th) to Trace the Sources, Transport Pathways and Deposition of Particles/Sediments in Rivers, Estuaries and Coasts, in Handbook of Environmental Isotope Geochemistry, pp. 305–329, Springer Berlin Heidelberg, Berlin, Heidelberg., 2012.

Duarte, C. M.: Seagrass depth limits, Aquat. Bot., 40(4), 363–377, doi:10.1016/0304-3770(91)90081-F, 1991.

Duarte, C. M.: Reviews and syntheses: Hidden forests, the role of vegetated coastal habitats in the ocean carbon budget, Biogeosciences, 14(2), 301–310, doi:10.5194/bg-14-301-2017, 2017.

Duarte, C. M. and Cebrián, J.: The fate of marine autotrophic production, Limnol. Oceanogr., 41(8), 1758–1766, doi:10.4319/lo.1996.41.8.1758, 1996.

Duarte, C. M. and Chiscano, C. L.: Seagrass biomass and production: a reassessment, Aquat. Bot., 65(1–4), 159–174, doi:10.1016/S0304-3770(99)00038-8, 1999.

Duarte, C. M. and Krause-Jensen, D.: Export from Seagrass Meadows Contributes to Marine Carbon Sequestration, Front. Mar. Sci., 4(13), 1–7, doi:10.3389/fmars.2017.00013, 2017.

Duarte, C. M., Middelburg, J. J. and Caraco, N.: Major role of marine vegetation on the oceanic carbon cycle, Biogeosciences, 2(1), 1–8, 2005.

Duarte, C. M., Dennison, W. C., Orth, R. J. W. and Carruthers, T. J. B.: The charisma of coastal ecosystems: Addressing the imbalance, Estuaries and Coasts, 31(2), 233–238, doi:10.1007/s12237-008-9038-7, 2008.

Duarte, C. M., Marbà, N., Gacia, E., Fourqurean, J. W., Beggins, J., Barrón, C. and Apostolaki, E. T.: Seagrass community metabolism: Assessing the carbon sink capacity of seagrass meadows, Global Biogeochem. Cycles, 24(4), n/a-n/a, doi:10.1029/2010GB003793, 2010.

Duarte, C. M., Kennedy, H., Marbà, N. and Hendriks, I.: Assessing the capacity of seagrass meadows for carbon burial: Current limitations and future strategies, Ocean Coast. Manag., 83, 32–38, doi:10.1016/j.ocecoaman.2011.09.001, 2013a.

Duarte, C. M., Losada, I. J., Hendriks, I. E., Mazarrasa, I. and Marbà, N.: The role of coastal plant communities for climate change mitigation and adaptation, Nat. Clim. Chang., 3(11), 961–968, doi:10.1038/nclimate1970, 2013b.

Duke, N. and Wolanski, E.: Muddy Coastal Waters and Depleted Mangrove Coastlines — Depleted Seagrass and Coral Reefs, in Oceanographic Processes of Coral Reefs. Physical and Biology Links in the Great Barrier Reef, edited by E. Wolanski, pp. 77–91, CRC Press, Washington, DC., 2001.

Van Eaton, A. R., Zimmerman, A. R., Jaeger, J. M., Brenner, M., Kenney, W. F. and Schmid, J. R.: A novel application of radionuclides for dating sediment cores from sandy, anthropogenically disturbed estuaries, Mar. Freshw. Res., 61(11), 1268–1277, doi:10.1071/MF10028, 2010.

Ellison, A. M. and Farnsworth, E. J.: Anthropogenic Disturbance of Caribbean Mangrove Ecosystems: Past Impacts, Present Trends, and Future Predictions, Biotropica, 28(4), 549, doi:10.2307/2389096, 1996.

Ember, L., Williams, D. and Morris, J.: Processes that influence carbon isotope variations in salt marsh sediments, Mar. Ecol. Prog. se, 36, 33–42, 1987.

Enríquez, S., Duarte, C. M. and Sand-Jensen, K.: Patterns in decomposition rates among photosynthetic organisms: the importance of detritus C:N:P content, Oecologia, 94(4), 457–471, doi:10.1007/BF00566960, 1993.

FAO: The world's mangroves 1980-2005, FAO For. Pap., 153, 89, doi:978-92-5-105856-5, 2007.

FAO: Soil Organic Carbon the Hidden Potential, Food and Agriculture Organization of the United Nations, Rome., 2017.

Ferreira, T. O., Otero, X. L., de Souza Junior, V. S., Vidal-Torrado, P., Macías, F. and Firme, L. P.: Spatial patterns of soil attributes and components in a mangrove system in Southeast Brazil (São Paulo), J. Soils Sediments, 10(6), 995–1006, doi:10.1007/s11368-010-0224-4, 2010.

Flemming, B. W.: A revised textural classification of gravel-free muddy sediments on the basis of ternary diagrams, Cont. Shelf Res., 20(10–11), 1125–1137, doi:10.1016/S0278-4343(00)00015-7, 2000.

Fourqurean, J. W. and Schrlau, J. E.: Changes in nutrient content and stable isotope ratios of C and N during decomposition of seagrasses and mangrove leaves along a nutrient availability gradient in Florida Bay, USA, Chem. Ecol., 19(5), 373–390, doi:10.1080/02757540310001609370, 2003.

Fourqurean, J. W., Kendrick, G. A., Collins, L. S., Chambers, R. M. and Vanderklift, M. A.: Carbon, nitrogen and phosphorus storage in subtropical seagrass meadows: Examples from Florida Bay and Shark Bay, Mar. Freshw. Res., 63(11), 967–983, doi:10.1071/MF12101, 2012a.

Fourqurean, J. W., Duarte, C. M., Kennedy, H., Marbà, N., Holmer, M., Mateo, M. A., Apostolaki, E. T., Kendrick, G. A., Krause-Jensen, D., McGlathery, K. J. and Serrano, O.: Seagrass ecosystems as a globally significant carbon stock, Nat. Geosci., 5(7), 505–509, doi:10.1038/ngeo1477, 2012b.

Fraser, M. W., Kendrick, G. A., Statton, J., Hovey, R. K., Zavala-Perez, A. and Walker, D. I.: Extreme climate events lower resilience of foundation seagrass at edge of biogeographical range, J. Ecol., 102(6), 1528–1536, doi:10.1111/1365-2745.12300, 2014a.

Fraser, M. W., Kendrick, G. A., Statton, J., Hovey, R. K. and Walker, D. I.: Extreme climate events lower resilience of foundation seagrass at edge of biogeographical range, J. Ecol., 102, 1528–1536, doi:10.1111/1365-2745.12300, 2014b.

Furukawa, K., Wolanski, E. and Mueller, H.: Currents and sediment transport in

mangrove forests, Estuar. Coast. Shelf Sci., 44(3), 301–310, doi:10.1006/ecss.1996.0120, 1997.

Gacia, E., Duarte, C. M. and Middelburg, J. J.: Carbon and nutrient deposition in a Mediterranean seagrass (Posidonia oceanica) meadow, Limnol. Oceanogr., 47(1), 23–32, doi:10.4319/lo.2002.47.1.0023, 2002.

Garcia-Orellana, J., Gràcia, E., Vizcaino, A., Masqué, P., Olid, C., Martínez-Ruiz, F., Piñero, E., Sanchez-Cabeza, J. A. and Dañobeitia, J.: Identifying instrumental and historical earthquake records in the SW Iberian margin 210Pb turbidite chronology, Geophys. Res. Lett., 33(24), 1–6, doi:10.1029/2006GL028417, 2006.

Garcia-Orellana, J., Cañas, L., Masqué, P., Obrador, B., Olid, C. and Pretus, J.: Chronological reconstruction of metal contamination in the Port of Maó (Minorca, Spain)., Mar. Pollut. Bull., 62(8), 1632–40, doi:10.1016/j.marpolbul.2011.06.013, 2011.

Gardner, L. R., Sharma, P. and Moore, W. S.: A Regeneration Model for the Effect of Bioturbation by Fiddler Crabs on 2 ' ° Pb Profiles in Salt Marsh Sediments, , 5, 25–36, 1987.

Gattuso, J. P., Magnan, A., Billé, R., Cheung, W. W. L., Howes, E. L., Joos, F., Allemand, D., Bopp, L., Cooley, S. R., Eakin, C. M., Hoegh-Guldberg, O., Kelly, R. P., Pörtner, H. O., Rogers, A. D., Baxter, J. M., Laffoley, D., Osborn, D., Rankovic, A., Rochette, J., Sumaila, U. R., Treyer, S. and Turley, C.: Contrasting futures for ocean and society from different anthropogenic CO2emissions scenarios, Science (80-.)., 349(6243), doi:10.1126/science.aac4722, 2015.

Gehrels, W. R., Kirby, J. R., Prokoph, A., Newnham, R. M., Achterberg, E. P., Evans, H., Black, S. and Scott, D. B.: Onset of recent rapid sea-level rise in the western Atlantic Ocean, Quat. Sci. Rev., 24(18–19), 2083–2100, doi:10.1016/j.quascirev.2004.11.016, 2005.

Gillis, L. G., Belshe, E. F. and Narayan, G. R.: Deforested Mangroves Affect the Potential for Carbon Linkages between Connected Ecosystems, Estuaries and Coasts, 40(4), 1207–1213, doi:10.1007/s12237-017-0210-9, 2017.

Glew, J. R., Smol, J. P. and Last, W. M.: Sediment Core Collection and Extrusion, in Tracking Environmental Change Using Lake Sediments: Basin Analysis, Coring, and Chronological Techniques, edited by W. M. Last and J. P. Smol, pp. 73–105, Springer Netherlands, Dordrecht, Dordrecht., 2001.

Goldberg, E. D., Gamble, E., Griffin, J. J. and Koide, M.: Pollution history of Narragansett Bay as recorded in its sediments, Estuar. Coast. Mar. Sci., 5(4), 549–561, doi:10.1016/0302-3524(77)90101-3, 1977.

Gonneea, M. E., Paytan, A. and Herrera-Silveira, J. A.: Tracing organic matter sources and carbon burial in mangrove sediments over the past 160 years, Estuar. Coast. Shelf Sci., 61(2), 211–227, doi:10.1016/j.ecss.2004.04.015, 2004.

Goodbred, S. L. and Kuehl, S. A.: Floodplain processes in the Bengal Basin and the storage of Ganges–Brahmaputra river sediment: an accretion study using 137Cs and 210Pb geochronology, Sediment. Geol., 121(3–4), 239–258, doi:10.1016/S0037-0738(98)00082-7, 1998.

Granek, E. and Ruttenberg, B. I.: Changes in biotic and abiotic processes following mangrove clearing, Estuar. Coast. Shelf Sci., 80(4), 555–562, doi:10.1016/j.ecss.2008.09.012, 2008.

Green, E. P. and Short, F. T.: World atlas of seagrasses, University of California Press, Berkeley, USA., 2003.

Greiner, J. T., McGlathery, K. J., Gunnell, J. and McKee, B. A.: Seagrass Restoration Enhances "Blue Carbon" Sequestration in Coastal Waters, PLoS One, 8(8), e72469, doi:10.1371/journal.pone.0072469, 2013.

Grellier, S., Janeau, J. L., Dang Hoai, N., Nguyen Thi Kim, C., Le Thi Phuong, Q., Pham Thi Thu, T., Tran-Thi, N. T. and Marchand, C.: Changes in soil characteristics and C dynamics after mangrove clearing (Vietnam), Sci. Total Environ., 593–594, 654–663, doi:10.1016/j.scitotenv.2017.03.204, 2017.

Griscom, B. W., Adams, J., Ellis, P. W., Houghton, R. A., Lomax, G., Miteva, D. A., Schlesinger, W. H., Shoch, D., Siikamäki, J. V., Smith, P., Woodbury, P., Zganjar, C., Blackman, A., Campari, J., Conant, R. T., Delgado, C., Elias, P., Gopalakrishna, T., Hamsik, M. R., Herrero, M., Kiesecker, J., Landis, E., Laestadius, L., Leavitt, S. M., Minnemeyer, S., Polasky, S., Potapov, P., Putz, F. E., Sanderman, J., Silvius, M., Wollenberg, E. and Fargione, J.: Natural climate solutions, Proc. Natl. Acad. Sci., 114(44), 11645–11650, doi:10.1073/pnas.1710465114, 2017.

Hamilton, S. E. and Casey, D.: Creation of a high spatio-temporal resolution global database of continuous mangrove forest cover for the 21st century (CGMFC-21), Glob. Ecol. Biogeogr., 25(6), 729–738, doi:10.1111/geb.12449, 2016.

Hamilton, S. E. and Friess, D. A.: Global carbon stocks and potential emissions due to mangrove deforestation from 2000 to 2012, Nat. Clim. Chang., 8(3), doi:10.1038/s41558-018-0090-4, 2018.

Hancock, N. and Hughes, L.: Turning up the heat on the provenance debate: Testing the "local is best" paradigm under heatwave conditions, Austral Ecol., 39(5), 600–611, doi:10.1111/aec.12122, 2014.

Haslett, S., Cundy, A., Davies, C. and Powell, E.: Salt marsh sedimentation over the past c. 120 years along the west Cotentin coast of Normandy (France): relationship to sea-level rise and sediment supply, J. Coast. Res., 19, 609–620, 2003.

Hatton, R., DeLaune, R. and Jr, W. P.: Sedimentation, accretion, and subsidence in marshes of Barataria Basin, Louisiana, Limnol. Oceanogr., 28(3), 494–502, 1983.

Haverd, V., Raupach, M. R., Briggs, P. R., J. G. Canadell., J. G., Davis, S. J., Law, R. M., Meyer, C. P., Peters, G. P., Pickett-Heaps, C. and Sherman, B.: The Australian terrestrial carbon budget, Biogeosciences, 10(2), 851–869, doi:10.5194/bg-10-851-2013, 2013.

He, Q. and Walling, D. E.: Interpreting Particle Size Effects in the Adsorption of 137Cs and Unsupported 210Pb by Mineral Soils and Sediments, J. Environ. Radioact., 30(2), 117–137, 1996a.

He, Q. and Walling, D. E.: Use of fallout Pb-210 measurements to investigate longer-term rates and patterns of overbank sediment deposition on the floodplains of

lowland rivers, Earth Surf. Process. Landforms, 21(2), 141–154, 1996b.

He, Q. and Walling, D. E.: The distribution of fallout Cs-137 and Pb-210 in undisturbed and cultivated soils, Appl. Radiat. Isot., 48(5), 677–690, 1997.

Heck, K. L., Carruthers, T. J. B., Duarte, C. M., Hughes, A. R., Kendrick, G., Orth, R. J. and Williams, S. W.: Trophic Transfers from Seagrass Meadows Subsidize Diverse Marine and Terrestrial Consumers, Ecosystems, 11(7), 1198–1210, doi:10.1007/s10021-008-9155-y, 2008.

van der Heide, T., van Nes, E. H., van Katwijk, M. M., Olff, H. and Smolders, A. J. P.: Positive feedbacks in seagrass ecosystems - Evidence from large-scale empirical data, PLoS One, 6(1), 1–7, doi:10.1371/journal.pone.0016504, 2011.

Hemes, K. S., Chamberlain, S. D., Eichelmann, E., Knox, S. H. and Baldocchi, D. D.: A Biogeochemical Compromise: The High Methane Cost of Sequestering Carbon in Restored Wetlands, Geophys. Res. Lett., 45(12), 6081–6091, doi:10.1029/2018GL077747, 2018.

Herr, D. and Landis, E.: Coastal blue carbon: Opportunities for nationally determined contributions, Gland, Switzerland and Washington, DC, USA., 2016.

Herr, D., von Unger, M., Laffoley, D. and McGivern, A.: Pathways for implementation of blue carbon initiatives, Aquat. Conserv. Mar. Freshw. Ecosyst., 27(April), 116–129, doi:10.1002/aqc.2793, 2017.

Hoegh-Guldberg, O., Cai, R., Poloczanska, E. S., Brewer, P. G., Sundby, S., Hilmi, K., Fabry, V. J. and Jung, S.: The Ocean, Clim. Chang. 2014 Impacts, Adapt. Vulnerability. Part B Reg. Asp. Contrib. Work. Gr. II to Fifth Assess. Rep. Intergov. Panel Clim. Chang., 1655–1732, doi:10.1017/CBO9781107415386.010, 2014.

Holmes, C. W., Robbins, J., Halley, R., Bothner, M., Brink, M. Ten and Marot, M.: Sediment dynamics of Florida Bay mud banks on decadal time scale, Bull. Am. Paleontol., 361, 31–40, 2001.

Houghton, R. A., House, J. I., Pongratz, J., Van Der Werf, G. R., Defries, R. S., Hansen, M. C., Le Quéré, C. and Ramankutty, N.: Carbon emissions from land use and land-cover change, Biogeosciences, 9(12), 5125–5142, doi:10.5194/bg-9-5125-2012, 2012.

Howard, J., Hoyt, S., Isensee, K., Pidgeon, E. and Telszewski, M.: Coastal Blue Carbon: Methods for Assessing Carbon Stocks and Emissions Factors in Mangroves, Tidal Salt Marshes, and Seagrass Meadows, Conserv. Int. Intergov. Oceanogr. Comm. UNESCO, Int. Union Conserv. Nature. Arlington, Virginia, USA., 1–180, 2014a.

Howard, J., Hoyt, S., Isensee, K., Pidgeon, E. and Telszewski, M.: Coastal Blue Carbon: Methods for Assessing Carbon Stocks and Emissions Factors in Mangroves, Tidal Salt Marshes, and Seagrass Meadows, Conservation, Arlington, Virginia, USA., 2014b.

Howard, J., Sutton-Grier, A., Herr, D., Kleypas, J., Landis, E., Mcleod, E., Pidgeon, E. and Simpson, S.: Clarifying the role of coastal and marine systems in climate mitigation, Front. Ecol. Environ., 15(1), 42–50, doi:10.1002/fee.1451, 2017.

Lo Iocano, C., Mateo, M. A., Gràcia, E., Guasch, L., Carbonell, R., Serrano, L., Serrano,

O. and Dañobeitia, J.: Very high-resolution seismo-acoustic imaging of seagrass meadows (Mediterranean Sea): Implications for carbon sink estimates, Geophys. Res. Lett., doi:10.1029/2008GL034773, 2008.

IPCC: Climate Change 2001: The Scientific Basis. Contribution of Working Group I to the Third Assessment Report of the Intergovernmental Panel on Climate Change, edited by J. Houghton, Y. Ding, G. DJ, N. M, van der L. PJ, D. X, M. K, and J. C, Cambridge University Press, Cambridge, UK and New York, USA., 2001.

IPCC: 2013 Supplement to the 2006 IPCC Guidelines for National Greenhouse Gas Inventories: Wetlands Task Force on National Greenhouse Gas Inventories: Wetlands, edited by T. Hiraishi, T. Krug, T. Kiyoto, N. Srivastava, B. Jamsranjav, M. Fukuda, and T. Troxler, IPCC, Switzerland., 2014.

IPCC: Global Warming of 1.5°C. An IPCC Special Report on the impacts of global warming of 1.5°C above pre-industrial levels and related global greenhouse gas emission pathways, in the context of strengthening the global response to the threat of climate change, edited by A. V. Masson-Delmotte, P. Zhai, H. O. Pörtner, D. Roberts, J. Skea, P.R. Shukla, M. Pirani, W. Moufouma-Okia, C. Péan, R. Pidcock, S. Connors, J. B. R. Matthews, Y. Chen, X. Zhou, M. I. Gomis, E. Lonnoy, T. Maycock, and T. W. (eds. . Tignor., 2018.

IPCC 2014: 2014: Summary for Policymakers, in Climate Change 2014: Mitigation of Climate Change., edited by O. et al. Edenhofer, Cambridge University Press, Cambridge and New York, Cambridge, United Kingdom and New York, NY, USA., 2014.

Jaeger, J., Mehta, A., Faas, R. and Grella, M.: Anthropogenic impacts on sedimentary sources and processes in a small urbanized subtropical estuary, Florida, J. Coast. Res., 25(1), 30–47, 2009.

Jankowska, E., Michel, L. N., Zaborska, A. and Włodarska-Kowalczuk, M.: Sediment carbon sink in low-density temperate eelgrass meadows (Baltic Sea), J. Geophys. Res. Biogeosciences, 121(12), 2918–2934, doi:10.1002/2016JG003424, 2016.

Johannessen, S. C. and Macdonald, R. W.: Geoengineering with seagrasses: is credit due where credit is given?, Environ. Res. Lett., 11(11), 113001, doi:10.1088/1748-9326/11/11/113001, 2016.

Johannessen, S. C. and Macdonald, R. W.: Reply to Macreadie et al Comment on 'Geoengineering with seagrasses : is credit due where credit is given?,' Environ. Res. Lett., 13(2), 028001, doi:10.1088/1748-9326/aaa7b5, 2018.

Jones, T. G., Ratsimba, H. R., Ravaoarinorotsihoarana, L., Cripps, G. and Bey, A.: Ecological Variability and Carbon Stock Estimates of Mangrove Ecosystems in Northwestern Madagascar, Forests, 5(1), 177–205, doi:10.3390/f5010177, 2014.

Jones, T. G., Glass, L., Gandhi, S., Ravaoarinorotsihoarana, L., Carro, A., Benson, L., Ratsimba, H. R., Giri, C., Randriamanatena, D. and Cripps, G.: Madagascar's mangroves: Quantifying nation-wide and ecosystem specific dynamics, and detailed contemporary mapping of distinct ecosystems, Remote Sens., 8(2), doi:10.3390/rs8020106, 2016a.

Jones, T. G., Ratsimba, H. R., Carro, A., Ravaoarinorotsihoarana, L., Glass, L., Teoh, M., Benson, L., Cripps, G., Giri, C., Zafindrasilivonona, B., Raherindray, R.,

Andriamahenina, Z. and Andriamahefazafy, M.: The Mangroves of Ambanja and Ambaro Bays, Northwest Madagascar: Historical Dynamics, Current Status and Deforestation Mitigation Strategy Trevor, in Estuaries: A Lifeline of Ecosystem Services in the Western Indian Ocean, edited by S. et al. Diop, pp. 67–85, Springer International Publishing Switzerland., 2016b.

Jordà, G., Marbà, N. and Duarte, C. M.: Mediterranean seagrass vulnerable to regional climate warming, Nat. Clim. Chang., 2(11), 821–824, doi:10.1038/nclimate1533, 2012.

Kauffman, J. B. and Donato, D. C.: Protocols for the measurement, monitoring and reporting of structure, biomass and carbon stocks in mangrove forests, CIFOR, Bogor, Indonesia., 2012.

Kauffman, J. B., Heider, C., Norfolk, J. and Payton, F.: Carbon stocks of intact mangroves and carbon emissions arising from their conversion in the Dominican Republic, Ecol. Appl., 24(3), 518–527, doi:10.1890/13-0640.1, 2014.

Kauffman, J. B., Hernandez Trejo, H., del Carmen Jesus Garcia, M., Heider, C. and Contreras, W. M.: Carbon stocks of mangroves and losses arising from their conversion to cattle pastures in the Pantanos de Centla, Mexico, Wetl. Ecol. Manag., 24(2), 203–216, doi:10.1007/s11273-015-9453-z, 2016a.

Kauffman, J. B., Hernandez Trejo, H., del Carmen Jesus Garcia, M., Heider, C. and Contreras, W. M.: Carbon stocks of mangroves and losses arising from their conversion to cattle pastures in the Pantanos de Centla, Mexico, Wetl. Ecol. Manag., 24(2), 203–216, doi:10.1007/s11273-015-9453-z, 2016b.

Kauffman, J. B., Bernardino, A. F., Ferreira, T. O., Bolton, N. W., Eduardo, L., Gabriel, D. O. G. and Nobrega, N.: Shrimp ponds lead to massive loss of soil carbon and greenhouse gas emissions in northeastern Brazilian mangroves, Ecol. Evol., 8, 5530–5540, doi:10.1002/ece3.4079, 2018.

Keil, R. G. and Hedges, J. I.: Sorption of organic matter to mineral surfaces and the preservation of organic matter in coastal marine sediments, Chem. Geol., 107(3–4), 385–388, doi:10.1016/0009-2541(93)90215-5, 1993.

Keiluweit, M., Bougoure, J. J., Nico, P. S., Pett-Ridge, J., Weber, P. K. and Kleber, M.: Mineral protection of soil carbon counteracted by root exudates, Nat. Clim. Chang., 5(6), 588–595, doi:10.1038/nclimate2580, 2015.

Kelleway, J., Serrano, O., Baldock, J., Cannard, T., Lavery, P., Lovelock, C. E., Macreadie, P., Masqué, P., Saintilan and N, S. A.: Technical review of opportunities for including blue carbon in the Australian Government's Emissions Reduction Fund, Australia., 2017.

Kelley, J. M., Bond, L. A. and Beasley, T. M.: Global distribution of Pu isotopes and 237Np., Sci. Total Environ., 237, 483–500, 1999.

Kennedy, H., Beggins, J., Duarte, C. M., Fourqurean, J. W., Holmer, M., Marbà, N. and Middelburg, J. J.: Seagrass sediments as a global carbon sink : Isotopic constraints, Global Biogeochem. Cycles, 24(July), 1–9, doi:10.1029/2010GB003848, 2010.

Kilminster, K., McMahon, K., Waycott, M., Kendrick, G. A., Scanes, P., McKenzie, L.,

O'Brien, K. R., Lyons, M., Ferguson, A., Maxwell, P., Glasby, T. and Udy, J.: Unravelling complexity in seagrass systems for management: Australia as a microcosm, Sci. Total Environ., 534, 97–109, doi:10.1016/J.SCITOTENV.2015.04.061, 2015.

Kindeberg, T., Ørberg, S. B., Röhr, M. E., Holmer, M. and Krause-Jensen, D.: Sediment Stocks of Carbon, Nitrogen, and Phosphorus in Danish Eelgrass Meadows, Front. Mar. Sci., 5, 474, doi:10.3389/fmars.2018.00474, 2018.

Kirchner, G. and Ehlers, H.: Sediment geochronology in changing coastal environments: Potentials and limitations of the 137Cs and 210Pb methods, J. Coast. Res., 14(1988), 483–492, 1998.

Kirwan, M. and Megonigal, J.: Tidal wetland stability in the face of human impacts and sea-level rise, Nature, 504, 53–60, 2013.

Klubi, E., Abril, J. M., Nyarko, E., Laissaoui, A. and Benmansour, M.: Radioecological assessment and radiometric dating of sediment cores from dynamic sedimentary systems of Pra and Volta estuaries (Ghana) along the Equatorial Atlantic, J. Environ. Radioact., 178–179, 116–126, doi:10.1016/j.jenvrad.2017.08.001, 2017.

Knox, S. H., Sturtevant, C., Matthes, J. H., Koteen, L., Verfaillie, J. and Baldocchi, D.: Agricultural peatland restoration: effects of land-use change on greenhouse gas (CO_2 and CH_4) fluxes in the Sacramento-San Joaquin Delta, Glob. Chang. Biol., 21(2), 750–765, doi:10.1111/gcb.12745, 2015.

Koch, E.: Beyond light: physical, geological, and geochemical parameters as possible submersed aquatic vegetation habitat requirements, Estuaries, 24(1), 1–17, doi:https://doi.org/10.2307/1352808, 2001.

Koide, M., Soutar, A. and Goldberg, E. D.: Marine geochronology with210Pb, Earth Planet. Sci. Lett., 14(3), 442–446, doi:10.1016/0012-821X(72)90146-X, 1972.

Komiyama, A., Poungparn, S. and Kato, S.: Common allometric equations for estimating the tree weight of mangroves, J. Trop. Ecol., 21(4), 471–477, doi:10.1017/S0266467405002476, 2005.

Krause-Jensen, D., Lavery, P., Serrano, O., Masque, P. and Duarte, C. M.: Sequestration of macroalgal carbon : the elephant in the Blue Carbon room, Biol. Lett., 14, 20180236, 2018.

Krauss, K. W., Cahoon, D. R., Allen, J. A., Ewel, K. C., Lynch, J. C. and Cormier, N.: Surface Elevation Change and Susceptibility of Different Mangrove Zones to Sea-Level Rise on Pacific High Islands of Micronesia, Ecosystems, 13(1), 129–143, doi:10.1007/s10021-009-9307-8, 2010.

Krishnaswamy, S., Lal, D., Martin, J. M. and Meybeck, M.: Geochronology of lake sediments, Earth Planet. Sci. Lett., 11(1–5), 407–414, doi:10.1016/0012-821X(71)90202-0, 1971.

Kristensen, E. and Alongi, D. M.: Control by fiddler crabs (*Uca vocans*) and plant roots (*Avicennia marina*) on carbon, iron, and sulfur biogeochemistry in mangrove sediment, Limnol. Oceanogr., 51(4), 1557–1571, doi:10.4319/lo.2006.51.4.1557, 2006.

Kroeger, K. D., Crooks, S., Moseman-Valtierra, S. and Tang, J.: Restoring tides to reduce

methane emissions in impounded wetlands: A new and potent Blue Carbon climate change intervention, Sci. Rep., 7(1), 11914, doi:10.1038/s41598-017-12138-4, 2017.

Kuwae, T. and Hori, M.: Blue Carbon in Shallow Coastal Ecosystems, Springer Nature, Singapore., 2019.

Labrière, N., Locatelli, B., Laumonier, Y., Freycon, V. and Bernoux, M.: Soil erosion in the humid tropics: A systematic quantitative review, Agric. Ecosyst. Environ., 203, 127–139, doi:10.1016/j.agee.2015.01.027, 2015.

Laffoley, D. and Grimsditch, G. (eds. .: The management of natural coastal carbon sinks, IUCN, Gland, Switzerland., 2009.

Lafratta, A., Serrano, O., Masqué, P., Mateo, M. A., Fernandes, M., Gaylard, S. and Lavery, P. S.: Seagrass soil archives reveal centennial-scale metal smelter contamination while acting as natural filters, Sci. Total Environ., 649, 1381–1392, doi:10.1016/j.scitotenv.2018.08.400, 2019.

Laissaoui, A., Benmansour, M., Ziad, N., Ibn Majah, M., Abril, J. M. and Mulsow, S.: Anthropogenic radionuclides in the water column and a sediment core from the Alboran Sea: Application to radiometric dating and reconstruction of historical water column radionuclide concentrations, J. Paleolimnol., 40(3), 823–833, doi:10.1007/s10933-008-9201-y, 2008.

Lal, R.: Forest soils and carbon sequestration, For. Ecol. Manage., 220(1–3), 242–258, doi:10.1016/j.foreco.2005.08.015, 2005.

Lang'at, J. K. S., Kairo, J. G., Mencuccini, M., Bouillon, S., Skov, M. W., Waldron, S. and Huxham, M.: Rapid losses of surface elevation following tree girdling and cutting in tropical mangroves, PLoS One, 9(9), 1–8, doi:10.1371/journal.pone.0107868, 2014.

Lau, W. W. Y.: Beyond carbon: Conceptualizing payments for ecosystem services in blue forests on carbon and other marine and coastal ecosystem services, Ocean Coast. Manag., 83, 5–14, doi:10.1016/J.OCECOAMAN.2012.03.011, 2013.

Laursen, A. K., Mayer, L. M. and Townsend, D. W.: Lability of proteinaceous material in estuarine seston and subcellular fractions of phytoplankton, Mar. Ecol. Prog. Ser., 136, 227–234, doi:10.2307/24856736, 1996.

Lavery, P. S., Mateo, M. Á., Serrano, O. and Rozaimi, M.: Variability in the Carbon Storage of Seagrass Habitats and Its Implications for Global Estimates of Blue Carbon Ecosystem Service, PLoS One, 8(9), e73748, 2013.

López-Merino, L., Colás-Ruiz, N. R., Adame, M. F., Serrano, O., Martínez Cortizas, A. and Mateo, M. A.: A six thousand-year record of climate and land-use change from Mediterranean seagrass mats, J. Ecol., 105(5), 1267–1278, doi:10.1111/1365-2745.12741, 2017.

Loring, D.: Normalization of heavy-metal data from estuarine and coastal sediments, ICES J. Mar. Sci., 48(1), 101–105, 1991.

Lovelock, C. E., Ruess, R. and Feller, I.: CO2 efflux from cleared mangrove peat, PLoS One, 6(6), e21279, doi:https://doi.org/10.1371/journal.pone.0021279, 2011.

Lovelock, C. E., Friess, D. A. and Krauss, K. W.: The vulnerability of Indo-Paci & c mangrove forests to sea-level rise, Nature, 526, 559–563, 2015.

Lovelock, C. E., Atwood, T., Baldock, J., Duarte, C. M., Hickey, S. and Lavery, P. S.: Assessing the risk of carbon dioxide emissions from blue carbon ecosystems, Front. Ecol. Environ., 15(5), 257–265, doi:10.1002/fee.1491, 2017a.

Lovelock, C. E., Fourqurean, J. W. and Morris, J. T.: Modeled CO2 Emissions from Coastal Wetland Transitions to Other Land Uses: Tidal Marshes, Mangrove Forests, and Seagrass Beds, Front. Mar. Sci., 4(May), 1–11, doi:10.3389/fmars.2017.00143, 2017b.

Lundquist, C. J., Morrisey, D. J., Gladstone-Gallagher, R. V. and Swales, A.: Managing Mangrove Habitat Expansion in New Zealand, in Mangrove Ecosystems of Asia, pp. 415–438, Springer New York, New York, NY., 2014.

Lynch, J. C., Meriwether, J. R., McKee, B. a., Vera-Herrera, F. and Twilley, R. R.: Recent Accretion in Mangrove Ecosystems Based on 137 Cs and 210 Pb, Estuaries, 12(4), 284, doi:10.2307/1351907, 1989.

Mabit, L., Benmansour, M., Abril, J. M., Walling, D. E., Meusburger, K., Iurian, A. R., Bernard, C., Tarján, S., Owens, P. N., Blake, W. H. and Alewell, C.: Fallout 210Pb as a soil and sediment tracer in catchment sediment budget investigations: A review, Earth-Science Rev., 138, 335–351, doi:10.1016/j.earscirev.2014.06.007, 2014.

MacKenzie, A. B., Hardie, S. M. L., Farmer, J. G., Eades, L. J. and Pulford, I. D.: Analytical and sampling constraints in210Pb dating, Sci. Total Environ., 409(7), 1298–1304, doi:10.1016/j.scitotenv.2010.11.040, 2011.

Macnae, W.: A General Account of the Fauna and Flora of Mangrove Swamps and Forests in the Indo-West-Pacific Region, Adv. Mar. Biol., 6(C), 73–270, doi:10.1016/S0065-2881(08)60438-1, 1969.

Macreadie, P. I., Hughes, A. R., Kimbro, D. L., D'Odorico, P. and McGlathery, K.: Loss of 'Blue Carbon' from Coastal Salt Marshes Following Habitat Disturbance, PLoS One, 8(7), e69244, doi:10.1371/journal.pone.0069244, 2013.

Macreadie, P. I., Baird, M. E., Trevathan-Tackett, S. M., Larkum, A. W. D. and Ralph, P. J.: Quantifying and modelling the carbon sequestration capacity of seagrass meadows - A critical assessment, Mar. Pollut. Bull., 83(2), 430–439, doi:10.1016/j.marpolbul.2013.07.038, 2014.

Macreadie, P. I., Trevathan-Tackett, S. M., Skilbeck, C. G., Sanderman, J., Curlevski, N., Jacobsen, G. and Seymour, J. R.: Losses and recovery of organic carbon from a seagrass ecosystem following disturbance., Proceedings. Biol. Sci., 282(1817), 20151537, doi:10.1098/rspb.2015.1537, 2015.

Macreadie, P. I., Ollivier, Q. R., Kelleway, J. J., Serrano, O., Carnell, P. E., Ewers Lewis, C. J., Atwood, T. B., Sanderman, J., Baldock, J., Connolly, R. M., Duarte, C. M., Lavery, P. S., Steven, a. and Lovelock, C. E.: Carbon sequestration by Australian tidal marshes, Sci. Rep., 7, 44071, doi:10.1038/srep44071, 2017.

Macreadie, P. I., Ewers-Lewis, C. J., Whitt, A. A., Ollivier, Q., Trevathan-Tackett, S. M., Carnell, P. and Serrano, O.: Comment on 'Geoengineering with seagrasses: is

credit due where credit is given?,' Environ. Res. Lett., 13(2), 028002, doi:10.1088/1748-9326/aaa7ad, 2018.

Maher, D. T., Santos, I. R., Golsby-Smith, L., Gleeson, J. and Eyre, B. D.: Groundwater-derived dissolved inorganic and organic carbon exports from a mangrove tidal creek: The missing mangrove carbon sink?, Limnol. Oceanogr., 58(2), 475–488, doi:10.4319/lo.2013.58.2.0475, 2013.

Maher, D. T., Santos, I. R., Schulz, K. G., Call, M., Jacobsen, G. E. and Sanders, C. J.: Blue carbon oxidation revealed by radiogenic and stable isotopes in a mangrove system, Geophys. Res. Lett., 44(10), 4889–4896, doi:10.1002/2017GL073753, 2017.

Maher, D. T., Call, M., Santos, I. R. and Sanders, C. J.: Beyond burial: Lateral exchange is a significant atmospheric carbon sink in mangrove forests, Biol. Lett., 14(7), doi:10.1098/rsbl.2018.0200, 2018.

Marbá, N. and Walker, D. I.: Growth, flowering, and population dynamics of temperate Western Australian seagrasses, Mar. Ecol. Prog. Ser., 184(Larkum 1976), 105–118, doi:10.3354/meps184105, 1999.

Marbà, N. and Duarte, C. M.: Mediterranean warming triggers seagrass (Posidonia oceanica) shoot mortality, Glob. Chang. Biol., 16(8), 2366–2375, doi:10.1111/j.1365-2486.2009.02130.x, 2009.

Marbà, N., Arias-Ortiz, A., Masqué, P., Kendrick, G. a., Mazarrasa, I., Bastyan, G. R., Garcia-Orellana, J. and Duarte, C. M.: Impact of seagrass loss and subsequent revegetation on carbon sequestration and stocks, J. Ecol., 103(2), 296–302, doi:10.1111/1365-2745.12370, 2015.

Marbà, N., Krause-Jensen, D., Masqué, P. and Duarte, C. M.: Expanding Greenland seagrass meadows contribute new sediment carbon sinks, Sci. Rep., 8(1), 1–8, doi:10.1038/s41598-018-32249-w, 2018.

Marland, G., Fruit, K. and Sedjo, R.: Accounting for sequestered carbon: the question of permanence, Environ. Sci. Policy, 4(6), 259–268, doi:10.1016/S1462-9011(01)00038-7, 2001.

Martz, L. and Jong, E. de: Using cesium-137 and landform classification to develop a net soil erosion budget for a small Canadian prairie watershed, Catena, 18(3–4), 289–308, 1991.

Masqué, P., Sanchez-Cabeza, J. and Bruach, J.: Balance and residence times of 210Pb and 210Po in surface waters of the northwestern Mediterranean Sea, Cont. Shelf Res., 22(15), 2127–2146, 2002.

Mateo, M. A., Romero, J., Pérez, M., Littler, M. M. and Littler, D. S.: Dynamics of Millenary Organic Deposits Resulting from the Growth of the Mediterranean Seagrass Posidonia oceanica, Estuar. Coast. Shelf Sci., 44, 103–110, doi:10.1006/ecss.1996.0116, 1997.

Mateo, M. A., Cebrián, J., Dunton, K. and Mutchler, T.: Carbon flux in seagrass ecosystems, in Seagrasses: Biology, ecology and conservation, edited by A. Larkum, R. Orth, and C. Duarte, pp. 159–192, Springer Netherlands, Dordrecht, Dordrecht., 2006.

Mazarrasa, I., Marbà, N., Lovelock, C. E., Serrano, O., Lavery, P. S., Fourqurean, J. W., Kennedy, H., Mateo, M. a., Krause-Jensen, D., Steven, a. D. L. and Duarte, C. M.: Seagrass meadows as a globally significant carbonate reservoir, Biogeosciences, 12, 4993–5003, doi:10.5194/bg-12-4993-2015, 2015.

Mazarrasa, I., Marbà, N., Garcia-Orellana, J., Masqué, P., Arias-Ortiz, A. and Duarte, C. M.: Effect of environmental factors (wave exposure and depth) and anthropogenic pressure in the C sink capacity of Posidonia oceanica meadows, Limnol. Oceanogr., 62(4), 1436–1450, doi:10.1002/lno.10510, 2017.

McGlathery, K. J., Reynolds, L. K., Cole, L. W., Orth, R. J., Marion, S. R. and Schwarzschild, A.: Recovery trajectories during state change from bare sediment to eelgrass dominance, Mar. Ecol. Prog. Ser., doi:10.3354/meps09574, 2012.

McKee, K. L.: Biophysical controls on accretion and elevation change in Caribbean mangrove ecosystems, Estuar. Coast. Shelf Sci., 91(4), 475–483, doi:10.1016/j.ecss.2010.05.001, 2011.

McLeod, E., Chmura, G. L., Bouillon, S., Salm, R., Björk, M., Duarte, C. M., Lovelock, C. E., Schlesinger, W. H. and Silliman, B. R.: A blueprint for blue carbon: Toward an improved understanding of the role of vegetated coastal habitats in sequestering CO_2, Front. Ecol. Environ., 9(10), 552–560, doi:10.1890/110004, 2011.

Miller, R. L., Fram, M., Fujii, R. and Wheeler, G.: Subsidence reversal in a re-established wetland in the Sacramento-San Joaquin Delta, California, USA, San Fr. Estuary Watershed Sci., 6(3), 1–20, 2008.

Mudd, S. M., Howell, S. M. and Morris, J. T.: Impact of dynamic feedbacks between sedimentation, sea-level rise, and biomass production on near-surface marsh stratigraphy and carbon accumulation, Estuar. Coast. Shelf Sci., doi:10.1016/j.ecss.2009.01.028, 2009.

Mudd, S. M., D'Alpaos, A. and Morris, J. T.: How does vegetation affect sedimentation on tidal marshes? Investigating particle capture and hydrodynamic controls on biologically mediated sedimentation, J. Geophys. Res. Earth Surf., 115, 1–14, doi:10.1029/2009JF001566, 2010.

Murray, B. C. and Kasibhatla, P.: Equating Permanence of Emission Reductions and Carbon Sequestration: Scientific and Economic Foundations for Policy Options., 2013.

Najjar, R. G., Herrmann, M., Alexander, R., Boyer, E. W., Burdige, D. J., Butman, D., Cai, W.-J., Canuel, E. A., Chen, R. F., Friedrichs, M. A. M., Feagin, R. A., Griffith, P. C., Hinson, A. L., Holmquist, J. R., Hu, X., Kemp, W. M., Kroeger, K. D., Mannino, A., McCallister, S. L., McGillis, W. R., Mulholland, M. R., Pilskaln, C. H., Salisbury, J., Signorini, S. R., St-Laurent, P., Tian, H., Tzortziou, M., Vlahos, P., Wang, Z. A. and Zimmerman, R. C.: Carbon Budget of Tidal Wetlands, Estuaries, and Shelf Waters of Eastern North America, Global Biogeochem. Cycles, 32(3), 389–416, doi:10.1002/2017GB005790, 2018.

Nature Editorial: Blue future, Nature, 529(7586), 255–256, doi:10.1038/529255b, 2016.

Needelman, B. A., Emmer, I. M., Emmett-Mattox, S., Crooks, S., Megonigal, J. P., Myers, D., Oreska, M. P. J. and McGlathery, K.: The Science and Policy of the

Verified Carbon Standard Methodology for Tidal Wetland and Seagrass Restoration, Estuaries and Coasts, 41(8), 2159–2171, doi:10.1007/s12237-018-0429-0, 2018.

Nellemann, C., Corcoran, E., Duarte, C. and (eds), et al.: Blue Carbon: The Role of Healthy Oceans in Binding Carbon: a Rapid Response Assessment, Earthprint., 2009.

Nittrouer, C. A., Sternberg, R. W., Carpenter, R. and Bennett, J. T.: The use of Pb-210 geochronology as a sedimentological tool: Application to the Washington continental shelf, Mar. Geol., 31(3–4), 297–316, doi:10.1016/0025-3227(79)90039-2, 1979.

Nowicki, R. J., Thomson, J. a, Burkholder, D. a, Fourqurean, J. W. and Heithaus, M. R.: Predicting seagrass recovery times and their implications following an extreme climate event, Mar. Ecol. Prog. Ser., 567, 79–93, doi:10.3354/meps12029, 2017.

Odum, E. P.: The status of three ecosystem-level hypotheses regarding salt marsh estuaries: tidal subsidy, outwelling, and detritus-based food chains, Estuar. Perspect., 485–495, doi:10.1016/B978-0-12-404060-1.50045-9, 1980.

Odum, E. P.: Tidal Marshes as Outwelling/Pulsing Systems, in Concepts and Controversies in Tidal Marsh Ecology, pp. 3–7, Kluwer Academic Publishers, Dordrecht., 2002.

Ogawa, H. and Tanoue, E.: Dissolved Organic Matter in Oceanic Waters, J. Oceanogr., 59(2), 129–147, doi:10.1023/A:1025528919771, 2003.

Oldfield, F., Appleby, P. G. and Battarbee, R. W.: Alternative 210Pb dating: results from the New Guinea Highlands and Lough Erne, Nature, 271(5643), 339–342, doi:10.1038/271339a0, 1978.

Olff, H., Leeuw, J. De, Bakker, J. P., Platerink, R. J. and van Wijnen, H. J.: Vegetation Succession and Herbivory in a Salt Marsh: Changes Induced by Sea Level Rise and Silt Deposition Along an Elevational Gradient, J. Ecol., 85(6), 799, doi:10.2307/2960603, 1997.

Olid, C., Garcia-Orellana, J., Martínez-Cortizas, A., Masqué, P., Peiteado, E. and Sanchez-Cabeza, J.-A.: Role of Surface Vegetation in ^{210}Pb-Dating of Peat Cores, Environ. Sci. Technol., 42(23), 8858–8864, doi:10.1021/es801552v, 2008.

Olid, C., Diego, D., Garcia-Orellana, J., Cortizas, A. M. and Klaminder, J.: Modeling the downward transport of 210Pb in Peatlands: Initial Penetration-Constant Rate of Supply (IP-CRS) model, Sci. Total Environ., 541, 1222–1231, doi:10.1016/j.scitotenv.2015.09.131, 2016.

Ong, J. E.: Mangroves - a carbon source and sink, Chemosphere, 27(6), 1097–1107, doi:10.1016/0045-6535(93)90070-L, 1993.

Orem, W. H., Holmes, C. W., Kendall, C., Lerch, H. E., Bates, A. L., Silva, S. R., Boylan, A., Marot, M. and Hedgman, C.: Geochemistry of Florida Bay Sediments: Nutrient History at Five Sites in Eastern and Central Florida Bay, J. Coast. Res., 15(154), 1055–1071, 1999.

Oreska, M. P. J., Wilkinson, G. M., McGlathery, K. J., Bost, M. and McKee, B. A.: Non-seagrass carbon contributions to seagrass sediment blue carbon, Limnol.

174

Oceanogr., 63(S1), S3–S18, doi:10.1002/lno.10718, 2018.

Otero, X. L., Méndez, A., Nóbrega, G. N., Ferreira, T. O., Meléndez, W. and Macías, F.: High heterogeneity in soil composition and quality in different mangrove forests of Venezuela, Environ. Monit. Assess., 189(10), doi:10.1007/s10661-017-6228-4, 2017.

Ouyang, X. and Lee, S. Y.: Updated estimates of carbon accumulation rates in coastal marsh sediments, Biogeosciences, 11(1), 5057–5071, doi:10.5194/bg-11-5057-2014, 2014.

Pearce, A. and Feng, M.: Observations of warming on the Western Australian continental shelf, Mar. Freshw. Res., 58, 914–920, 2007.

Pedersen, M., Serrano, O. and Mateo, M.: Temperature effects on decomposition of a Posidonia oceanica mat, Aquat. Microb. Ecol., 65(2), 169–182, 2011.

Pendleton, L., Donato, D. C., Murray, B. C., Crooks, S., Jenkins, W. A., Sifleet, S., Craft, C., Fourqurean, J. W., Kauffman, J. B., Marbà, N., Megonigal, P., Pidgeon, E., Herr, D., Gordon, D. and Baldera, A.: Estimating Global "Blue Carbon" Emissions from Conversion and Degradation of Vegetated Coastal Ecosystems, PLoS One, 7(9), 2012.

Pennings, S. C. and Bertness, M. D.: Salt Marsh Communities, in Marine Community Ecology, edited by M. Bertness, S. Gaines, and M. Hay, pp. 289–316, Sinauer Associates, Inc, Sunderland., 2001.

Peralta, G., Van Duren, L. A., Morris, E. P. and Bouma, T. J.: Consequences of shoot density and stiffness for ecosystem engineering by benthic macrophytes in flow dominated areas: A hydrodynamic flume study, Mar. Ecol. Prog. Ser., 368(June 2014), 103–115, doi:10.3354/meps07574, 2008.

Peters, G. P., Andrew, R. M., Boden, T., Canadell, J. G., Ciais, P., Le Quéré, C., Marland, G., Raupach, M. R. and Wilson, C.: The challenge to keep global warming below 2 °C, Nat. Clim. Chang. www.nature.com, 3, doi:10.1038/nclimate1783, 2013.

Peterson, R. N.: Natural Radionuclide Applications for Riverine and Coastal Marine Investigations, Florida State University., 2009.

Phillips, D. L. and Gregg, J. W.: Source partitioning using stable isotopes: Coping with too many sources, Oecologia, 136(2), 261–269, doi:10.1007/s00442-003-1218-3, 2003.

Phillips, S. C., Johnson, J. E., Miranda, E. and Disenhof, C.: Improving CHN measurements in carbonate-rich marine sediments, Limnol. Oceanogr. Methods, 9(5), 194–203, doi:10.4319/lom.2011.9.194, 2011.

Poppe, K. L. and Rybczyk, J. M.: Carbon Sequestration in a Pacific Northwest Eelgrass (Zostera marina) Meadow, Northwest Sci., 92(2), 80–91, doi:10.3955/046.092.0202, 2018.

Preiss, N., Mélières, M.-A. and Pourchet, M.: A compilation of data on lead 210 concentration in surface air and fluxes at the air-surface and water-sediment interfaces, J. Geophys. Res., 101(D22), 28847, doi:10.1029/96JD01836, 1996.

Prentice, I., Farquhar, G., Fasham, M., Goulden, M., Heimann, M., Jaramillo, V. J.,

Kheshgi, H. S., LeQuéré, C., Scholes, R. J. and Wallace, D. W. R.: The carbon cycle and atmospheric carbon dioxide, in Climate Change 2001:the Scientific Basis, edited by J. T. et al. Houghton, pp. 185–237, Cambridge University Press, Cambridge, UK, Cambridge, UK., 2001.

Rasolofo, M. and Ramilijaona, O.: Variability in the abundance and recruitment of Fenneropenaeus indicus and Metapenaeus monoceros postlarvae and juveniles in Ambaro Bay mangroves of Madagascar., Nat Faune, 24, 103–109, 2009.

Ravens, T., Thomas, R. and Roberts, K.: Causes of salt marsh erosion in Galveston Bay, Texas, J. Coast. Res., 25(2), 265–272, 2009.

Ribeiro Guevara, S. and Arribére, M.: 137Cs dating of lake cores from the Nahuel Huapi National Park, Patagonia, Argentina: Historical records and profile measurements, J. Radioanal. Nucl. Chem., 252(1), 37–45, doi:10.1023/A:1015275418412, 2002.

Rivers, D. O., Kendrick, G. A. and Walker, D. I.: Microsites play an important role for seedling survival in the seagrass Amphibolis antarctica, J. Exp. Mar. Bio. Ecol., 401(1–2), 29–35, doi:10.1016/J.JEMBE.2011.03.005, 2011.

Robbins, J.: Geochemical and geophysical applications of radioactive lead, in The biogeochemistry of lead in the environment, edited by J. Nriagu, pp. 285–393, Elsevier, Amsterdam., 1978.

Robbins, J. A.: A model for particle-selective transport of tracers in sediments with conveyor belt deposit feeders, J. Geophys. Res., 91(C7), 8542, doi:10.1029/JC091iC07p08542, 1986.

Robbins, J. A. and Edgington, D. N.: Determination of recent sedimentation rates in Lake Michigan using Pb-210 and Cs-137, Geochim. Cosmochim. Acta, 39(3), 285–304, doi:10.1016/0016-7037(75)90198-2, 1975.

Rockström, J., Gaffney, O., Rogelj, J., Meinshausen, M. and Nakicenovic, N. Schellnhuber, H. J.: A Roadmap for Rapid Decarbonization, Science (80-.)., 355(6331), 1269–1271, doi:10.1126/science.aah3443, 2017.

Rogers, K., Saintilan, N. and Copeland, C.: Managed Retreat of Saline Coastal Wetlands: Challenges and Opportunities Identified from the Hunter River Estuary, Australia, Estuaries and Coasts, 37(1), 67–78, doi:10.1007/s12237-013-9664-6, 2014.

Röhr, M. E., Holmer, M., Baum, J. K., Björk, M., Chin, D., Chalifour, L., Cimon, S., Cusson, M., Dahl, M., Deyanova, D., Duffy, J. E., Eklöf, J. S., Geyer, J. K., Griffin, J. N., Gullström, M., Hereu, C. M., Hori, M., Hovel, K. A., Hughes, A. R., Jorgensen, P., Kiriakopolos, S., Moksnes, P.-O., Nakaoka, M., O´Connor, M. I., Peterson, B., Reiss, K., Reynolds, P. L., Rossi, F., Ruesink, J., Santos, R., Stachowicz, J. J., Tomas, F., Lee, K.-S., Unsworth, R. K. F. and Boström, C.: Blue carbon storage capacity of temperate eelgrass (Zostera marina) meadows, Global Biogeochem. Cycles, doi:10.1029/2018GB005941, 2018.

Romero, J., Pérez, M., Mateo, M. A. and Sala, E.: The belowground organs of the Mediterranean seagrass Posidonia oceanica as a biogeochemical sink, Aquat. Bot., 47(1), 13–19, doi:10.1016/0304-3770(94)90044-2, 1994.

Rosentreter, J. A., Maher, D. T., Erler, D. V, Murray, R. H. and Eyre, B. D.: Methane

emissions partially offset " blue carbon " burial in mangroves, Sci. Adv., 4, eaao4985, 2018.

Ruiz-Fernández, A. C. and Hillaire-Marcel, C.: 210Pb-derived ages for the reconstruction of terrestrial contaminant history into the Mexican Pacific coast: Potential and limitations, Mar. Pollut. Bull., 59(4–7), 134–145, doi:10.1016/j.marpolbul.2009.05.006, 2009.

Saderne, V., Cusack, M., Almahasheer, H., Serrano, O., Masqué, P., Arias-Ortiz, A., Krishnakumar, P. K., Rabaoui, L., Qurban, M. A. and Duarte, C. M.: Accumulation of Carbonates Contributes to Coastal Vegetated Ecosystems Keeping Pace With Sea Level Rise in an Arid Region (Arabian Peninsula), J. Geophys. Res. Biogeosciences, 123(5), 1498–1510, doi:10.1029/2017JG004288, 2018.

Sanchez-Cabeza, J. A. and Ruiz-Fernández, A. C.: 210Pb sediment radiochronology: An integrated formulation and classification of dating models, Geochim. Cosmochim. Acta, 82, 183–200, doi:10.1016/j.gca.2010.12.024, 2012.

Sanchez-Cabeza, J. A., Masqué, P. and Ani-Ragolta, I.: 210Pb and210Po analysis in sediments and soils by microwave acid digestion, J. Radioanal. Nucl. Chem., 227(1–2), 19–22, doi:10.1007/BF02386425, 1998.

Sanders, C. J., Smoak, J. M., Sanders, L. M., Waters, M. N., Patchineelam, S. R. and Ketterer, M. E.: Intertidal mangrove mudflat 240+239Pu signatures, confirming a 210Pb geochronology on the southeastern coast of Brazil, J. Radioanal. Nucl. Chem., 283, 593–596, doi:10.1007/s10967-009-0418-7, 2010a.

Sanders, C. J., Smoak, J. M., Naidu, A. S., Sanders, L. M. and Patchineelam, S. R.: Organic carbon burial in a mangrove forest, margin and intertidal mud flat, Estuar. Coast. Shelf Sci., 90(3), 168–172, doi:10.1016/j.ecss.2010.08.013, 2010b.

Sanders, C. J., Smoak, J. M., Waters, M. N., Sanders, L. M., Brandini, N. and Patchineelam, S. R.: Organic matter content and particle size modifications in mangrove sediments as responses to sea level rise, Mar. Environ. Res., 77, 150–155, doi:10.1016/j.marenvres.2012.02.004, 2012.

Sanders, C. J., Eyre, B. D., Santos, I. R., Machado, W., Luiz-silva, W., Smoak, J. M., Breithaupt, J. L., Ketterer, M. E., Sanders, L., Marotta, H. and Silva-filho, E.: Elevated rates of organic carbon, nitrogen, and phosphorus accumulation in a highly impacted mangrove wetland, Geophys. Res. Lett., 41, 2475–2480, doi:10.1002/2014GL059789.Received, 2014.

Sanders, C. J., Santos, I. R., Maher, D. T., Breithaupt, J. L., Smoak, J. M., Ketterer, M., Call, M., Sanders, L. and Eyre, B. D.: Examining 239+240Pu, 210Pb and historical events to determine carbon, nitrogen and phosphorus burial in mangrove sediments of Moreton Bay, Australia, J. Environ. Radioact., 151, 623–629, doi:10.1016/j.jenvrad.2015.04.018, 2016.

Scott, D. B. and Greenberg, D. A.: Relative sea-level rise and tidal development in the Fundy tidal system, Can. J. Earth Sci., 20(10), 1554–1564, doi:10.1139/e83-145, 1983.

Semeniuk, V.: Coastal forms and Quaternary processes along the arid Pilbara coast of northwestern Australia, Palaeogeogr. Palaeoclimatol. Palaeoecol., 123, 49–84,

1996.

Serrano, O., Mateo, M. a., Renom, P. and Julià, R.: Characterization of soils beneath a Posidonia oceanica meadow, Geoderma, 185–186, 26–36, doi:10.1016/j.geoderma.2012.03.020, 2012.

Serrano, O., Lavery, P. S., Rozaimi, M. and Mateo, M. A.: Influence of water depth on the carbon sequestration capacity of seagrass, Global Biogeochem. Cycles, 28(9), 950–961, doi:10.1002/2014GB004872.Received, 2014.

Serrano, O., Lavery, P. S., Duarte, C. M., Kendrick, G. A., Calafat, A., York, P. H., Steven, A. and Macreadie, P. I.: Can mud (silt and clay) concentration be used to predict soil organic carbon content within seagrass ecosystems?, Biogeosciences, 13(17), 4915–4926, doi:10.5194/bg-13-4915-2016, 2016a.

Serrano, O., Ruhon, R., Lavery, P. S., Kendrick, G. A., Hickey, S., Masqué, P., Arias-Ortiz, A., Steven, A. and Duarte, C. M.: Impact of mooring activities on carbon stocks in seagrass meadows, Sci. Rep., 6, 23193, doi:10.1038/srep23193, 2016b.

Serrano, O., Ricart, A. M., Lavery, P. S., Mateo, M. A., Arias-Ortiz, A., Masque, P., Rozaimi, M., Steven, A. and Duarte, C. M.: Key biogeochemical factors affecting soil carbon storage in Posidonia meadows, Biogeosciences, 13(15), doi:10.5194/bg-13-4581-2016, 2016c.

Serrano, O., Ricart, A. M., Lavery, P. S., Mateo, M. A., Arias-Ortiz, A., Masque, P., Rozaimi, M., Steven, A. and Duarte, C. M.: Key biogeochemical factors affecting soil carbon storage in Posidonia meadows, Biogeosciences, 13(15), 4581–4594, doi:10.5194/bg-13-4581-2016, 2016d.

Serrano, O., Lavery, P. S., López-Merino, L., Ballesteros, E. and Mateo, M. A.: Location and Associated Carbon Storage of Erosional Escarpments of Seagrass Posidonia Mats, Front. Mar. Sci., 3, 42, doi:10.3389/fmars.2016.00042, 2016e.

Serrano, O., Davis, G., Lavery, P. S., Duarte, C. M., Martinez-Cortizas, A., Mateo, M. A., Masqué, P., Arias-Ortiz, A., Rozaimi, M. and Kendrick, G. a.: Reconstruction of centennial-scale fluxes of chemical elements in the Australian coastal environment using seagrass archives, Sci. Total Environ., 541, 883–894, doi:10.1016/j.scitotenv.2015.09.017, 2016f.

Serrano, O., Lavery, P., Masque, P., Inostroza, K., Bongiovanni, J. and Duarte, C.: Seagrass sediments reveal the long-term deterioration of an estuarine ecosystem, Glob. Chang. Biol., 22(4), 1523–1531, doi:10.1111/gcb.13195, 2016g.

Sharma, P., Gardner, L. R., Moore, W. S. and Bollinger, M. S.: Sedimentation and bioturbation in a salt marsh as revealed by 210Pb, 137Cs, and 7Be studies, Limnol. Oceanogr., 32(2), 313–326, doi:10.4319/lo.1987.32.2.0313, 1987.

Short, F., Carruthers, T., Dennison, W. and Waycott, M.: Global seagrass distribution and diversity: A bioregional model, J. Exp. Mar. Bio. Ecol., 350(1–2), 3–20, doi:10.1016/j.jembe.2007.06.012, 2007.

Short, F., Polidoro, B. and Livingstone, S.: Extinction risk assessment of the world's seagrass species, Biol. Conserv., 144(7), 1961–1971, 2011.

Short, F. T., Wyllie-Echeverria, S., Ackerman, J. D., Alberte, R. S., Suba, G. K., Procaccini, G., Zimmerman, R. C., Fain, S. R., Backman, T. W. H., Baldwin, J.,

Loworn, J., Bazzaz, F. A., Brix, H., Lyngby, J. E., Schierup, H.-H., Bulthuis, D. A., Burdick, D., Short, F., Wolf, J., Cambridge, M. L., Chiffings, A. W., Brittan, C., Moore, L., McComb, A. J., Cambridge, M. L., McComb, A. J., Churchill, A. C., Nieves, G., Brenowitz, A. H., den Hartog, C., Den Hartog, C., Polderman, P. J. G., Dennison, W. C., Orth, R. J., Moore, K. A., Stevenson, J. C., Carter, V., Kollar, S., Bergstrom, P. W., Batiuk, R. A., Dirnberger, J. M., Kitting, C. L., Dunton, K. H., Fonseca, M., Fisher, J., Fourqurean, J., Zieman, J., Gallegos, M. E., Merino, M., Marbá, N., Duarte, C. M., Giese, G. S., Giesen, W. B. J. T., Van Katwijk, M. M., Den Hartog, C., Güven, K. C., Saygı, N., Öztürk, B., Hanekom, N., Baird, D., Harris, J., Fabris, G., Statham, P., Tawfik, F., Hemminga, M. A., Nieuwenhuize, J., Howard, R. K., Short, F. T., Kirkman, H., Larkum, A. W. D., West, R. J., Muehlstein, L., Muehlstein, L. K., Porter, D., Short, F. T., Muehlstein, L. K., Porter, D., Short, F. T., Nienhuis, P. H., Nienhuis, P. H., van Ierland, E. T., Orth, R. J., Heck, K. L., van Montfrans, J., Philippart, C. J. M., Dijkema, K. S., Pirc, H., Buia, M. C., Mazzella, L., Quammen, M. L., Onuf, C. P., RENN, C. E., Robblee, M., Barber, T., Carlson, P., Durako, M., Fourqurean, J., Muehlstein, L., Porter, D., et al.: Natural and human-induced disturbance of seagrasses, Environ. Conserv., 23(01), 17, doi:10.1017/S0376892900038212, 1996.

Sidik, F. and Lovelock, C. E.: CO2 Efflux from Shrimp Ponds in Indonesia, PLoS One, 8(6), 6–9, doi:10.1371/journal.pone.0066329, 2013.

Siikamaki, J., Sanchirico, J. N. and Jardine, S. L.: Global economic potential for reducing carbon dioxide emissions from mangrove loss, Proc. Natl. Acad. Sci., 109(36), 14369–14374, doi:10.1073/pnas.1200519109, 2012.

Smith, J.: Why should we believe 210Pb sediment geochronologies?, J. Environ. Radioact., 55(2), 121–123, 2001.

Smith, J. ., Boudreau, B. . and Noshkin, V.: Plutonium and210Pb distributions in northeast Atlantic sediments: subsurface anomalies caused by non-local mixing, Earth Planet. Sci. Lett., 81(1), 15–28, doi:10.1016/0012-821X(86)90097-X, 1986.

Smith, R. D., Dennison, W. C. and Alberte, R. S.: Role of Seagrass Photosynthesis in Root Aerobic Processes, Plant Physiol., 74(4), 1055–1058, doi:10.1104/pp.74.4.1055, 1984.

Smoak, J. M. and Patchineelam, S. R.: Sediment mixing and accumulation in a mangrove ecosystem : evidence from 210 Pb , 234 Th and 7 Be, Mangroves Salt Marshes, 3, 17–27, 1999.

Smoak, J. M., Breithaupt, J. L., Smith, T. J. and Sanders, C. J.: Sediment accretion and organic carbon burial relative to sea-level rise and storm events in two mangrove forests in Everglades National Park, Catena, 104, 58–66, doi:10.1016/j.catena.2012.10.009, 2013.

Sommerfield, C. and Nittrouer, C.: Modern accumulation rates and a sediment budget for the Eel shelf: a flood-dominated depositional environment, Mar. Geol., 154(1–4), 227–241, 1999.

Spalding, M.: World Atlas of Mangroves, Routledge, London., 2010.

Squire, P., Joannes-Boyau, R., Scheffers, A. M., Nothdurft, L. D., Hua, Q., Collins, L. B., Scheffers, S. and Zhao, J.: A marine reservoir correction for the Houtman-

Abrolhos archipelago, East Indian Ocean, Western Australia, Radiocarbon, 55(1), 103–114, 2013.

Staunton, S., Dumat, C. and Zsolnay, A.: Possible role of organic matter in radiocaesium adsorption in soils, J. Environ. Radioact., 58(2–3), 163–173, doi:10.1016/S0265-931X(01)00064-9, 2002.

Stuiver, M. and Polach, H. A.: Discussion reporting of 14C data, Radiocarbon, 19(3), 355–363, doi:10.1017/S0033822200003672, 1977.

Stupar, Y. V., Schäfer, J., García, M. G., Schmidt, S., Piovano, E., Blanc, G., Huneau, F. and Le Coustumer, P.: Historical mercury trends recorded in sediments from the Laguna del Plata, Córdoba, Argentina, Chemie der Erde, 74(3), 353–363, doi:10.1016/j.chemer.2013.11.002, 2014.

Sun, X., Fan, D., Tian, Y. and Zheng, S.: Normalization of excess 210 Pb with grain size in the sediment cores from the Yangtze River Estuary and adjacent areas: Implications for sedimentary processes, The Holocene, 1–13, doi:10.1177/0959683617735591, 2017.

Swales, A. and Bentley, S.: Mangrove-forest evolution in a sediment-rich estuarine system: opportunists or agents of geomorphic change?, Earth Surf. Process. Landforms, 40, 1672–1687, 2015.

Swindles, G. T., Galloway, J. M., Macumber, A. L., Croudace, I. W., Emery, A. R., Woulds, C., Bateman, M. D., Parry, L., Jones, J. M., Selby, K., Rushby, G. T., Baird, A. J., Woodroffe, S. A. and Barlow, N. L. M.: Sedimentary records of coastal storm surges: Evidence of the 1953 North Sea event, Mar. Geol., 403(June), 262–270, doi:10.1016/j.margeo.2018.06.013, 2018.

Syvitski, J. P. M., Kettner, A. J., Overeem, I., Hutton, E. W. H., Hannon, M. T., Brakenridge, G. R., Day, J., Vörösmarty, C., Saito, Y., Giosan, L. and Nicholls, R. J.: Sinking deltas due to human activities, Nat. Geosci., 2(10), 681–686, doi:10.1038/ngeo629, 2009.

Tanner, J. E.: Restoration of the Seagrass Amphibolis antarctica—Temporal Variability and Long-Term Success, Estuaries and Coasts, 38(2), 668–678, doi:10.1007/s12237-014-9823-4, 2015.

Tedesco, L. P. and Aller, R. C.: 210 Pb chronology of sequences affected by burrow excavation and infilling; examples from shallow marine carbonate sediment sequences, Holocene South Florida and Caicos Platform, British West Indies, J. Sediment. Res., 67(1), 36–46, doi:10.1306/D42684E6-2B26-11D7-8648000102C1865D, 1997.

Telesca, L., Belluscio, A., Criscoli, A., Ardizzone, G., Apostolaki, E. T., Fraschetti, S., Gristina, M., Knittweis, L., Martin, C. S., Pergent, G., Alagna, A., Badalamenti, F., Garofalo, G., Gerakaris, V., Pace, M. L. and Pergent-martini, C.: Criteria for the evaluation of diploma programs in nursing., Sci. Rep., 5, 12505, doi:10.1038/srep12505, 2015.

Templet, P. and Meyer-Arendt, K.: Louisiana wetland loss: a regional water management approach to the problem, Environ. Manage., 12(2), 181–192, doi:10.1007/BF01873387, 1988.

Thampanya, U., Vermaat, J. E., Sinsakul, S. and Panapitukkul, N.: Coastal erosion and mangrove progradation of Southern Thailand, Estuar. Coast. Shelf Sci., 68(1–2), 75–85, doi:10.1016/J.ECSS.2006.01.011, 2006.

Thomson, J. A., Burkholder, D. A., Heithaus, M. R., Fourqurean, J. W., Fraser, M. W., Statton, J. and Kendrick, G. A.: Extreme temperatures, foundation species, and abrupt ecosystem change: an example from an iconic seagrass ecosystem, Glob. Chang. Biol., 21(4), 1463–1474, doi:10.1111/gcb.12694, 2014.

Tokoro, T., Hosokawa, S., Miyoshi, E., Tada, K., Watanabe, K., Montani, S., Kayanne, H. and Kuwae, T.: Net uptake of atmospheric CO2 by coastal submerged aquatic vegetation, Glob. Chang. Biol., doi:10.1111/gcb.12543, 2014.

Tomasko, D. A., Corbett, C. A., Greening, H. S. and Raulerson, G. E.: Spatial and temporal variation in seagrass coverage in Southwest Florida: assessing the relative effects of anthropogenic nutrient load reductions and rainfall in four contiguous estuaries, Mar. Pollut. Bull., 50, 797–805, doi:10.1016/j.marpolbul.2005.02.010, 2005.

Trevathan-tackett, A. S. M., Kelleway, J., Macreadie, P. I., Trevathan-tackett, S. M., Kelleway, J., Macreadie, P. I., Beardall, J., Ralph, P. and Bellgrove, A.: Comparison of marine macrophytes for their contributions to blue carbon sequestration Beardall , Peter Ralph and Alecia Bellgrove Published by : Wiley on behalf of the Ecological Society of America Stable URL : http://www.jstor.org/stable/24702430 Compari, , 96(11), 3043–3057, 2018.

Trevathan-Tackett, S. M., Kelleway, J., Macreadie, P. I., Beardall, J., Ralph, P. and Bellgrove, A.: Comparison of marine macrophytes for their contributions to blue carbon sequestration, Ecology, 96(11), 3043–3057, doi:10.1890/15-0149.1, 2015.

Tripathee, R. and Schäfer, K. V. R.: Above- and Belowground Biomass Allocation in Four Dominant Salt Marsh Species of the Eastern United States, Wetlands, 35(1), 21–30, doi:10.1007/s13157-014-0589-z, 2015.

Turner, R. E., Swenson, E. M., Milan, C. S. and Lee, J. M.: Hurricane signals in salt marsh sediments: Inorganic sources and soil volume, Limnol. Oceanogr., 52(3), 1231–1238, doi:10.4319/lo.2007.52.3.1231, 2007.

Twilley, R. R. and Day, J. W.: Mangrove Wetlands, in Estuarine Ecology, edited by J. W. Day, B. C. Crump, W. M. Kemp, and A. Yáñez-Arancibia, pp. 165–202, John Wiley & Sons, Inc., Hoboken, NJ, USA., 2012.

UNEP: The importance of mangroves to people: A call to action, edited by J. van Bochove, E. Sullivan, and T. Nakamura, United Nations Environment Programme World Conservation Monitoring Centre, Cambridge., 2014.

UNFCCC: United Nations Framework Convention on Climate Change, Fccc/Informal/84, 1(3), 270–277, doi:10.1111/j.1467-9388.1992.tb00046.x, 1992.

Valiela, I., Bowen, J. L. and York, J. K.: Mangrove Forests: One of the World's Threatened Major Tropical Environments, Bioscience, 51(10), 807, doi:10.1641/0006-3568(2001)051[0807:MFOOTW]2.0.CO;2, 2001.

Volk, T. and Hoffert, M. I.: Ocean Carbon Pumps: Analysis of Relative Strengths and

Efficiencies in Ocean-Driven Atmospheric CO 2 Changes, in The Carbon Cycle and Atmospheric CO2: Natural Variations Archean to Present, edited by E. T. Sundquist and W. S. Broecker, pp. 99–110, American Geophysical Union (AGU)., 2013.

Wackernagel, H.: Multivariate geostatistics: an introduction with applications, Third Edit., Springer, New York, New York., 2003.

Walker, B., Holling, C. and Carpenter, S.: Resilience, adaptability and transformability in social–ecological systems, Ecol. Soc., 9(2), 2004.

Walker, D., Kendrick, G. and McComb, A.: The distribution of seagrass species in Shark Bay, Western Australia, with notes on their ecology, Aquat. Bot., 30, 305–317, 1988.

Walling, D., Collins, A. and Sichingabula, H.: Using unsupported lead-210 measurements to investigate soil erosion and sediment delivery in a small Zambian catchment, Geomorphology, 52(3–4), 193–213, 2003.

Walsh, J. P. and Nittrouer, C. a.: Mangrove-bank sedimentation in a mesotidal environment with large sediment supply, Gulf of Papua, Mar. Geol., 208, 225–248, doi:10.1016/j.margeo.2004.04.010, 2004.

Wan, G. J., Chen, J. a., Wu, F. C., Xu, S. Q., Bai, Z. G., Wan, E. Y., Wang, C. S., Huang, R. G., Yeager, K. M. and Santschi, P. H.: Coupling between 210Pbex and organic matter in sediments of a nutrient-enriched lake: An example from Lake Chenghai, China, Chem. Geol., 224, 223–236, doi:10.1016/j.chemgeo.2005.07.025, 2005.

Wang, Z. A., Kroeger, K. D., Ganju, N. K., Gonneea, M. E. and Chu, S. N.: Intertidal salt marshes as an important source of inorganic carbon to the coastal ocean, Limnol. Oceanogr., 61(5), 1916–1931, doi:10.1002/lno.10347, 2016.

Waycott, M., Duarte, C. M., Carruthers, T. J. B., Orth, R. J., Dennison, W. C., Olyarnik, S., Calladine, A., Fourqurean, J. W., Heck, K. L., Hughes, A. R., Kendrick, G. A., Kenworthy, W. J., Short, F. T. and Williams, S. L.: Accelerating loss of seagrasses across the globe threatens coastal ecosystems., Proc. Natl. Acad. Sci. U. S. A., 106(30), 12377–81, doi:10.1073/pnas.0905620106, 2009.

Webb, J. R., Santos, I. R., Maher, D. T. and Finlay, K.: The Importance of Aquatic Carbon Fluxes in Net Ecosystem Carbon Budgets: A Catchment-Scale Review, Ecosystems, 1–20, doi:10.1007/s10021-018-0284-7, 2018.

Webster, R. and Oliver, M. A.: Geostatistics for environmental scientists (Statistics in Practice), 2nd Editio., edited by S. Senn, M. Scott, and V. Barnett, John Wiley & Sons, Chichester, Chichester., 2001.

Weiss, C., Weiss, J., Boy, J., Iskandar, I., Mikutta, R. and Guggenberger, G.: Soil organic carbon stocks in estuarine and marine mangrove ecosystems are driven by nutrient colimitation of P and N, Ecol. Evol., 6(14), 5043–5056, doi:10.1002/ece3.2258, 2016.

Wentworth, C.: A scale of grade and class terms for clastic sediments, J. Geol., 30(5), 377–392, 1922.

van der Werf, G. R., Morton, D. C., DeFries, R. S., Olivier, J. G. J., Kasibhatla, P. S., Jackson, R. B., Collatz, G. J. and Randerson, J. T.: CO2 emissions from forest

loss, Nat. Geosci., 2(11), 737–738, doi:10.1038/ngeo671, 2009.

Wernberg, T., Smale, D. A., Tuya, F., Thomsen, M. S., Langlois, T. J., Bettignies, T. De, Bennett, S. and Rousseaux, C. S.: An extreme climatic event alters marine ecosystem structure in a global biodiversity hotspot, Nat. Clim. Chang., 3(1), 78–82, doi:10.1038/nclimate1627, 2012.

Wingard, G. L., Hudley, J. W., Holmes, C. W., Willard, D. A. and Marot, M.: Synthesis of age data and chronology for Florida Bay and Biscayne Bay cores collected for ecosystem history of South Florida's estuaries projects, Open File Rep., (1203), 127, 2007.

Woodroffe, C. D., Mulrennan, M. E. and Chappell, J.: Estuarine infill and coastal progradation, southern van diemen gulf, northern Australia, Sediment. Geol., 83(3–4), 257–275, doi:10.1016/0037-0738(93)90016-X, 1993.

Xu, B., Bianchi, T. S., Allison, M. A., Dimova, N. T., Wang, H., Zhang, L., Diao, S., Jiang, X., Zhen, Y., Yao, P., Chen, H., Yao, Q., Dong, W., Sui, J. and Yu, Z.: Using multi-radiotracer techniques to better understand sedimentary dynamics of reworked muds in the Changjiang River estuary and inner shelf of East China Sea, Mar. Geol., 370, 76–86, doi:10.1016/j.margeo.2015.10.006, 2015.

Yanai, R. D., Currie, W. S. and Goodale, C. L.: Soil carbon dynamics after forest harvest: An ecosystem paradigm reconsidered, Ecosystems, 6(3), 197–212, doi:10.1007/s10021-002-0206-5, 2003.

Yeager, K. M. and Santschi, P. H.: Invariance of isotope ratios of lithogenic radionuclides: more evidence for their use as sediment source tracers, J. Environ. Radioact., 69(3), 159–176, 2003.

Yeager, K. M., Brunner, C. a., Kulp, M. a., Fischer, D., Feagin, R. a., Schindler, K. J., Prouhet, J. and Bera, G.: Significance of active growth faulting on marsh accretion processes in the lower Pearl River, Louisiana, Geomorphology, 153–154, 127–143, doi:10.1016/j.geomorph.2012.02.018, 2012.

Zummo, L. M. and Friedland, A. J.: Soil carbon release along a gradient of physical disturbance in a harvested northern hardwood forest, For. Ecol. Manage., 261(6), 1016–1026, doi:10.1016/j.foreco.2010.12.022, 2011.

Appendix

Appendix A: Simulation Methods *Chapter 3*

Mixing

To simulate surface mixing (scenarios A and B), we estimated the accumulated $^{210}Pb_{xs}$ activity per unit area over the top 5 cm of the ideal $^{210}Pb_{xs}$ profile (I_{5cm}: 2126 Bq m^{-2} in seagrass and 723 Bq m^{-2} in mangrove/tidal marsh sediments) (Supplementary, Tables S1a and S1b). We split this inventory within the 5 upper centimetres using a random function, the outputs of which fell within the standard deviation ($\pm SD$) of the mean of the $^{210}Pb_{xs}$ activities in the upper 5 cm (± 107 Bq m^{-2} in seagrass; and ± 9 Bq m^{-2} in mangrove/tidal marsh sediments). To simulate deep mixing (scenario C), we followed the same methodology but we split randomly the $^{210}Pb_{xs}$ inventory within the upper 15 cm, which is a depth reported as deep mixing in seagrass (Serrano et al., 2016b), mangroves and tidal marshes (Nittrouer et al., 1979; Smoak and Patchineelam, 1999) and is characteristic for marine sediments globally (Boudreau, 1994). We ran the simulation several times until we obtained three scenarios (A, B, C) of mixing encompassing a range of surface mixed layers (SML) (Supplementary, Tables S2a and S2b). Mixing A (k_m: ∞ g^2 cm^{-4} yr^{-1}) consisted of constant $^{210}Pb_{xs}$ specific activities with depth in surface layers; mixing B (k_m: 20 - 23 g^2 cm^{-4} yr^{-1}) was characterised by a decrease in the slope of $^{210}Pb_{xs}$ in top layers; and mixing C represented deep mixing from the sediment surface down to 15 cm (k_m: 6 - 25 g^2 cm^{-4} yr^{-1}). $^{210}Pb_{xs}$ activities per unit area (A) were converted to $^{210}Pb_{xs}$ specific activities (C) in Bq kg^{-1}, which we averaged every two layers to represent smooth transitions. Sedimentation and derived CAR were estimated from the modelled profiles using the CF:CS and the CRS models. The CF:CS model was applied below the depth of the visually apparent SML (3 cm) in scenarios A and B to avoid overestimation of MAR. The CF:CS model was applied to the entire profile in deep mixing scenario C in seagrass sediments and below the apparent mixed layer (13 cm) in mangrove sediments. Deep mixing affected 10% of the entire $^{210}Pb_{xs}$ profile of mangrove/tidal marsh sediments and 45% of seagrass sediments. To account for the deviations in mean MAR and CAR

associated with a process mismatch (i.e., as if considering that the actual mixing was caused by an increase in MAR), we applied the CF:CS model piecewise (scenarios B and C) and to the entire profile (scenario A). In the case of the CRS model, ages were determined at each layer and average centennial MAR was estimated dividing the mass of sediment accumulated (g cm^{-2}) down to 100 yr-depth by its age (i.e., 100 yr) in all cases.

Increasing sedimentation

We simulated an enhancement of the MAR that could result, for instance, from increased sediment run-off due to coastal development, by increasing the basal MAR (0.2 g cm^{-2} yr^{-1} and 0.3 g cm^{-2} yr^{-1} in seagrass and mangrove/tidal marsh, respectively) by different magnitudes (20%, 50%, 100% and 200%). Increases in MAR were simulated over the top 6 cm and 23 cm of the idealized ^{210}Pb$_{xs}$ specific activity profiles, which represent the last 30 years of accumulation in seagrass and mangrove/tidal marsh sediments, respectively. Last century mass accumulation rates expected for ideal profiles were estimated by dividing the accumulated mass down to a 100yr-depth (derived from gradual increases in MAR) by its age (Supplementary, Tables S3a and S3b). ^{210}Pb$_{xs}$ specific activities *(C$_m$)* as a result of increased MAR were estimated through equation A1 for each layer. Simulations of increasing MAR generated four profiles per habitat type (scenarios D, E, F and G) (Fig. 3.2b). Average MAR and CAR were estimated from the modelled profiles using the CF:CS and CRS models. The CF:CS model was applied piecewise in scenarios D, E and F, and below the layer of constant ^{210}Pb$_{xs}$ in scenario G.

$$C_m = \frac{\lambda \cdot I_m}{MAR \cdot 10} \tag{A1}$$

where λ is the decay constant of ^{210}Pb (0.0311 yr^{-1}) and I_m is the ^{210}Pb$_{xs}$ inventory accumulated at layer m. 10 allows unit conversion to Bq kg^{-1}.

We also estimated mean MAR and CAR assuming that the process causing scenarios D, E, F and G was mixing. For this, we applied the CF:CS model below the surface mixed layer (6 and 23 cm in seagrass and mangrove/tidal marsh sediments, respectively). The shift in the slope of the ^{210}Pb$_{xs}$ profile in scenario D in seagrass

sediments was minimal, hence we applied the CF:CS model to the entire $^{210}Pb_{xs}$ profile, as this would likely be the method applied by most researchers in a real case. The CRS model was run similarly if mixing or changes in accumulation rates are expected, ages were determined at each layer and average centennial MAR was estimated dividing the mass of sediment accumulated (g cm^{-2}) down to 100 yr-depth by its age (i.e., 100 yr). If mixing is expected, ages within the mixed layer cannot be reported.

Erosion

Erosion in vegetated coastal sediments can occur due to high-energy events (Short et al., 1996), vegetation loss and subsequent destabilization of sediments (Marbà et al., 2015) or mechanical disturbances (e.g. Serrano et al., 2016c). We ran three simulations to represent recent (H) and past erosion events (I and J) (Fig. 3.2c). We started with an ideal $^{210}Pb_{xs}$ profile with a total initial $^{210}Pb_{xs}$ inventory of 3,900 Bq m^{-2}. To simulate erosion, we removed the $^{210}Pb_{xs}$ inventory accumulated in the top 0 - 5 cm (H), middle 5 – 10 cm (I) and 10 – 15 cm sections (J) in sediments from both habitat types (mangrove/tidal marsh and seagrass). Resulting $^{210}Pb_{xs}$ activity per unit area (Bq m^{-2}) were converted to $^{210}Pb_{xs}$ specific activities (Bq kg^{-1}) by dividing by the corresponding mass depth (g cm^{-2}) at each section after correcting the latter for the loss of sediment layers (Supplementary, Tables S4a and S4b). ^{210}Pb specific activities were averaged every two layers to simulate smooth transitions rather than a sharp discontinuity after and erosion event. We estimated the resulting average MAR and CAR using the CF:CS model (applied piecewise in erosion scenarios I and J). The CRS model should not be applied in simulated erosion scenarios since the overall core inventories *(I)* are incomplete. However, we ran the CRS model to test the errors associated with its application in eroded sediments assuming that erosion is not a factor.

Changes in sediment grain size

We simulated various $^{210}Pb_{xs}$ profiles with changes in sediment grain size distribution using the approach described by He & Walling (1996), where the specific surface area of particles exerts a primary control on the $^{210}Pb_{xs}$ adsorbed:

$$C\left(S_{sp}\right) = \mu \cdot S_{sp}^{0.67} \tag{Eq. A2}$$

where C is $^{210}Pb_{xs}$ specific activity (mBq g^{-1}), S_{sp} is the specific surface area of the sediment particles (m^2 g^{-1}), and μ is a constant scaling factor depending upon the initial $^{210}Pb_{xs}$ activity per unit area (mBq m^{-2}). The $^{210}Pb_{xs}$ specific activity in bulk sediments can also be represented by equation A2 replacing S_{sp} by the mean specific surface area S_{mean} (m^2 g^{-1}) of the bulk sample. In this work, we estimated μ at each layer of an ideal $^{210}Pb_{xs}$ profile in seagrass and mangrove/tidal marsh sediments if ideally S_{sp} throughout the core is 0.07 m^2 g^{-1}, corresponding to a mean particle size of 63 μm. The surface area can be estimated as (Jury and Horton, 2004):

$$S_{sp} = \frac{3}{\rho \cdot r} \tag{Eq. A3}$$

where ρ is the density of the sediment particles and r is the mean radius of sediment particles, which are considered spherical.

We estimated the weighted mean specific surface area of a very coarse sediment composed of 70% coarse sand (500 – 1000 μm), 20% medium sand (250 – 500 μm) and 10% silt (4 - 63 μm) (S_{mean} = 0.0153 m^2 g^{-1}), through equation A3 (size scale: Wentworth, 1922). Bulk density (ρ) of sediment fractions were considered: 1.03 g cm^{-3} for silt, 1.6 g cm^{-3} for medium sand and 1.8 g cm^{-3} for coarse sand. Then, we simulated $^{210}Pb_{xs}$ profiles as a function of the specific surface area applying equation A2 to an ideal$^{210}Pb_{xs}$ specific activity profile (scenario K) (Supplementary, Tables S5a and S5b). Second, we simulated a shift to sandy and clayey sediments in surface layers, as could result after the restoration or loss of vegetated coastal ecosystems. The percentages of sands and clay along the core were changed using a random function (from 60 ± 20% in surface to 15 ± 5% in bottom layers; scenarios L and M) (Supplementary, Tables S6a and S6b). The shift was simulated at the same age depth (30 yr before collection) in all scenarios and habitat types. Finally, we simulated a heterogeneous grain size distribution along the entire sediment profile intercalating sand and clay layers randomly with depth (scenario N) (Supplementary, Tables S6a and S6b). The mass depth term was corrected in each case for changes in grain size, which lead to variations in DBD with depth. Bulk density (ρ) of sediment fractions was considered: 0.4 g cm^{-3} for clays and 1.6 g cm^{-3} for medium sands. In addition, the

value of μ was readjusted at each sediment depth of the ideal profile to represent non-monotonic variations in cumulative dry mass. $^{210}Pb_{xs}$ specific activity profiles were estimated as a function of the specific surface area that was estimated at each layer according to the various proportions of clay and sand. The average MAR was estimated using the CF:CS and CRS models. The CF:CS model was applied piecewise in simulated scenarios L and M.

Organic matter decay

$^{210}Pb_{xs}$ in vegetated coastal sediments is deposited in association with mineral particles but also with organic particulates (Krishnaswamy et al., 1971; Yeager and Santschi, 2003). Once buried, sediment organic matter (OM) content usually decays with sediment depth and aging due to remineralization of labile fractions, leading to an enrichment of $^{210}Pb_{xs}$ specific activities. We simulated the resultant $^{210}Pb_{xs}$ profiles derived from this process in two sediments with different OM contents (16.5% and 65%). The first value (16.5% OM) is within the usual range of tidal marsh, mangrove and in the high range for seagrass sediments (Fourqurean et al., 2012b) (Table 6). The second value (65% OM) represents an extreme scenario based in existing studies in seagrass and mangrove ecosystems (Callaway et al., 1997; Serrano et al., 2012). The simulations were run under three OM decay constants assuming: (1) the whole pool of OM is refractory under anoxic conditions, decaying at a rate of 0.00005 d^{-1} in seagrass and in mangrove/tidal marsh sediments (Lovelock et al., 2017b); (2) 50% of the refractory pool is exposed to oxic conditions, decaying at a rate of 0.0005 d^{-1} in mangrove/tidal marsh sediments; and (3) 50% of the OM pool is labile, decaying fast, although exposed to anoxic conditions, at 0.01 d^{-1} and 0.03 d^{-1} in seagrass and mangrove/tidal marsh sediments, respectively (Lovelock et al., 2017b).

The ^{210}Pb enrichment factor (η) can be determined for a given time after deposition as:

$$\eta(t) = \frac{\chi_s + \chi_{org} \cdot e^{-k_{org} \cdot t}}{\chi_s + \chi_{org}} \qquad \text{(Eq. A4)}$$

where χ_s is the mineral fraction of sediments, χ_{org} is the organic fraction of sediments at time 0, k_{org} is the decay constant of the OM in sediments and t is time and can be estimated

as m/MAR. As time (t) increases the exponential term tends to zero, hence the OM stored in the sediment reaches a constant value, where it is no longer decomposed. We assume that the remineralized OM leaves the sediment as CO_2, but in fact a fraction (f) would transform to mineral matter as $\chi_s(t) = \chi_{s(0)} + f \cdot \chi_{org(0)} \cdot \left(1 - e^{-k_{org} \cdot t}\right)$. In our simulations $f = 0$ was assumed.

Then, the $^{210}Pb_{xs}$ specific activity of a sample of age t with initial specific activity C_0 is:

$$C_t = \frac{C_0 \cdot e^{-\lambda t}}{\eta(t)} \tag{Eq. A5}$$

and the total mass accumulated with depth (M) above a layer of age t is:

$$M = MAR \cdot \chi_S \cdot t + MAR \cdot \chi_{org} \cdot e^{-k_{org} \cdot t} \cdot t \tag{Eq. A6}$$

MAR was estimated using the CF:CS and CRS models. The CF:CS model was applied below the $^{210}Pb_{xs}$ reversed profile in scenario S. CAR was estimated through eq. 8. Organic matter (%OM) in mangrove/tidal marsh sediments was transformed to %OC using equations in Table 2.2 by Kauffman and Donato (2012) and Fourqurean et al. (2012) in mangrove/tidal marsh and seagrass sediments, respectively.

For this simulation new MAR and CAR were estimated derived from ideal ^{210}Pb profiles to represent changes in organic matter content due to decay and associated losses of sediment mass with depth. This resulted in lower ideal MAR in seagrass and mangrove/tidal marsh sediments (seagrass: 0.17 g cm^{-2} yr^{-1} and 0.07 g cm^{-2} yr^{-1}; mangrove/tidal marsh: 0.25 g cm^{-2} yr^{-1} and 0.10 g cm^{-2} yr^{-1} in OM decay simulations starting at 16.5% and 65% OM, respectively) (Table 3.2) (Supplementary, Tables S7 a and b).

Appendix B: Case studies *Chapter 3*
B1 Case study of a sedimentation event

Hurricanes and cyclones can lead to the sudden delivery of large amounts of sediments and nutrients to mangroves and tidal marshes, which in turn can result in enhanced production (Castañeda-Moya et al., 2010; Lovelock et al., 2011). Smoak et al. (2013) obtained an $^{210}Pb_{xs}$ specific activity profile consistent with a large pulse of sediment delivered to fringing mangroves in the Everglades, Florida (Fig. B1). The specific activity of $^{210}Pb_{xs}$ was vastly different (several times lower) in sediments accumulated during the event. The sediment accumulation rate estimated by the CRS model for the upper part of the sediment record was six times that of background levels, resulting in a doubled accretion rate, due to the high bulk density of the delivered sediments (Castañeda-Moya et al., 2010). OC concentrations in the abruptly accumulated sediments were lower (5%) than those of the sediments beneath the event layer (20-25%). In fact, event-deposits could consist of coarse sediments (for instance sand and shell sediment layers deposited during storm events characteristic of offshore environments; Swindles et al., 2018), but also of fine sediments that could present lower$^{210}Pb_{xs}$ specific activity compared to surrounding layers (e.g., siltation events due to clearing of the catchment area; Cambridge et al., 2002; Serrano et al., 2016d). Indeed, if the initial $^{210}Pb_{xs}$ specific activity (C_0) is known, the CIC model could be useful to constrain dating when it is difficult to precisely define the thickness of such deposits. Otherwise the CF:CS model could be applied if the event layer is identified (e.g., using XRF, ^{226}Ra or granulometry) and can be subtracted to produce a corrected depth-profile from which to determine derived CF:CS ages and mean mass accumulation rates.
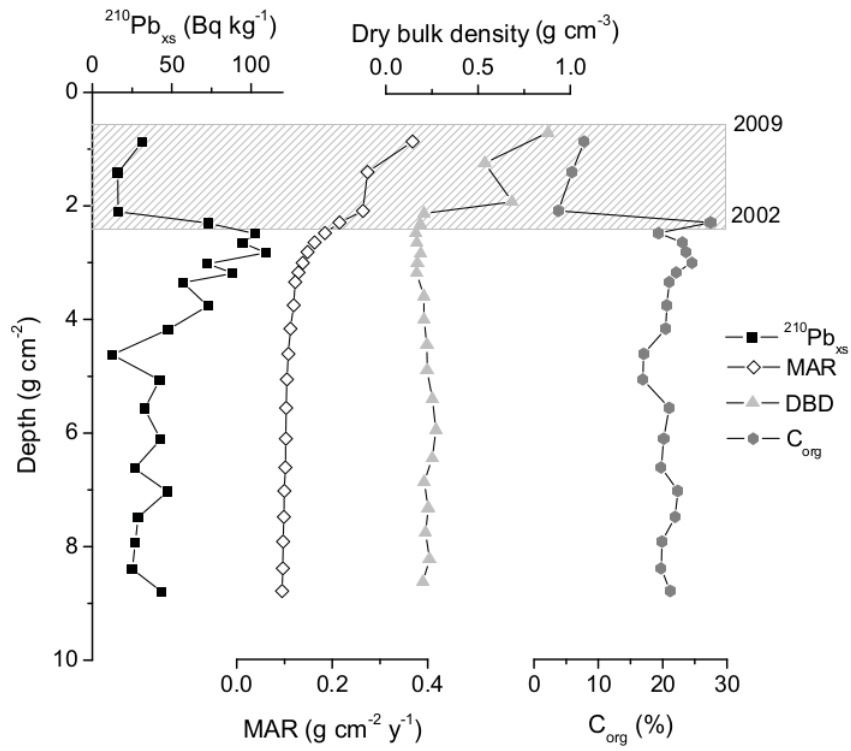
Figure B1: $^{210}Pb_{xs}$, mass sedimentation rates (MAR), dry bulk density and OC content in a mangrove sediment core at the Everglades, Florida. The gridded area represents the period 2002 - 2009, when Hurricane Wilma (2005) delivered a large pulse of sediment (Adapted from Smoak et al., 2013).

B2 Case study of sediment mixing

An example of bioturbation processes is documented by Smoak and Patchineelam (1999) where they showed a mixed $^{210}Pb_{xs}$ profile down to 11 cm depth in a mangrove ecosystem in Brazil evidenced from the ^{210}Pb, ^{234}Th and ^7Be specific activity profiles (Figure B2). The $^{210}Pb_{xs}$ activities decreased exponentially below the surface mixed layer, resulting in an estimated accumulation rate of 1.8 mm yr^{-1}. In the upper layers the $^{210}Pb_{xs}$ followed a complex pattern, with alternate relative maxima and minima, which could be representative of varying conditions of fluxes and sediment accumulation rates, presence of coarse sediments or physical or biological mixing. However, ^7Be penetrated down to 4 cm depth and excess ^{234}Th was detected only in the surface layer. Sediments that are buried for a period of more than 6 months will have undetectable ^7Be, hence its presence at 4 cm depth indicated that the activity of benthic communities had remobilised it downwards to a much greater degree than sedimentation.
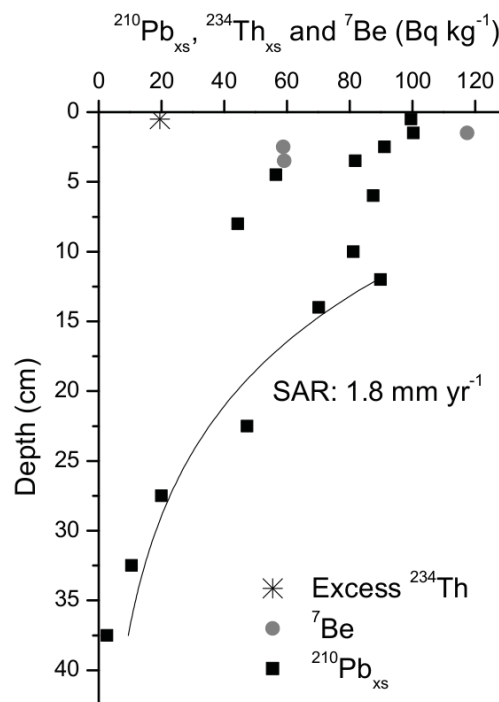
Figure B2: $^{210}Pb_{xs}$ specific activity profile affected by bioturbation. Short-lived ^7Be and excess ^{234}Th specific activity profiles are indicators of mixing in the zone of constant $^{210}Pb_{xs}$ (0 - 5 cm). (Adapted from Smoak and Patchineelam, (1999).

B3 Case study of rapid sedimentation rates

Alongi et al. (2005) studied the rates of sediment accumulation at three mangrove forests spanning the intertidal zone along the south coastline of the heavily urbanized Jiulongljiang Estuary (China). Mass accumulation rates (MAR) were rapid and one of the $^{210}Pb_{xs}$ specific activity profiles showed scattered concentrations with depth. This could be related to either a very high MAR during the last decades or an intense mixing down core. However, the excess ^{228}Th specific activity profile, determined from the difference between the total ^{228}Th and ^{228}Ra activities in the sediment, showed a clearly decaying trend down to 15 cm (Figure B3). The exponential decay curve fitted to the excess ^{228}Th profile yielded an accumulation rate of 10 cm yr^{-1}, which was consistent with the ^{210}Pb specific activity profile. Therefore, the evidence provided by excess ^{228}Th indicated that a very high MAR was the most plausible processes responsible for the sediment record.
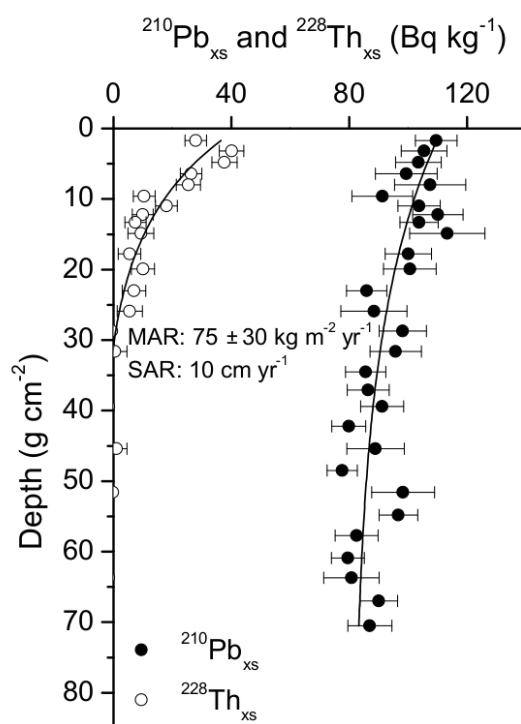
Figure B3: Vertical specific activity profiles of excess ^{210}Pb and ^{228}Th in core 3564 fom Alongi et al. (2005), produced by a rapid mass accumulation rate.

B4 Case study of erosion

Incomplete inventories of $^{210}Pb_{xs}$ indicative of erosion can be illustrated by the measured ^{210}Pb specific activity profiles in sediments from Oyster Harbor (Albany, Western Australia), some of which were devoid of seagrass vegetation since the 1980s due to eutrophication (Marbà et al., 2015). The measured $^{210}Pb_{xs}$ specific activities in unvegetated sediments were relatively low, and the horizon of $^{210}Pb_{xs}$ was detected at a shallower sediment depth than in neighbouring sediments, where seagrass meadows persisted (Figure B4). The inventory of $^{210}Pb_{xs}$ in the unvegetated sediment exhibited a deficit of 722 Bq m^{-2} compared to that in the vegetated site. This deficit could not solely result from the lack of accumulation of $^{210}Pb_{xs}$ while sediments were unvegetated (30 years; atmospheric flux of 25 Bq m^{-2} yr^{-1}), but also to the subsequent sediment erosion. These results, combined with OC analyses, showed that unvegetated sediments had an average deficit in accumulated OC stocks of 2.3 kg OC m^{-2} compared to vegetated sediments over the last ca. 100 years. This deficit was produced since seagrass loss in 1980 but was equivalent to a loss of approximately 90 years of OC accumulation.
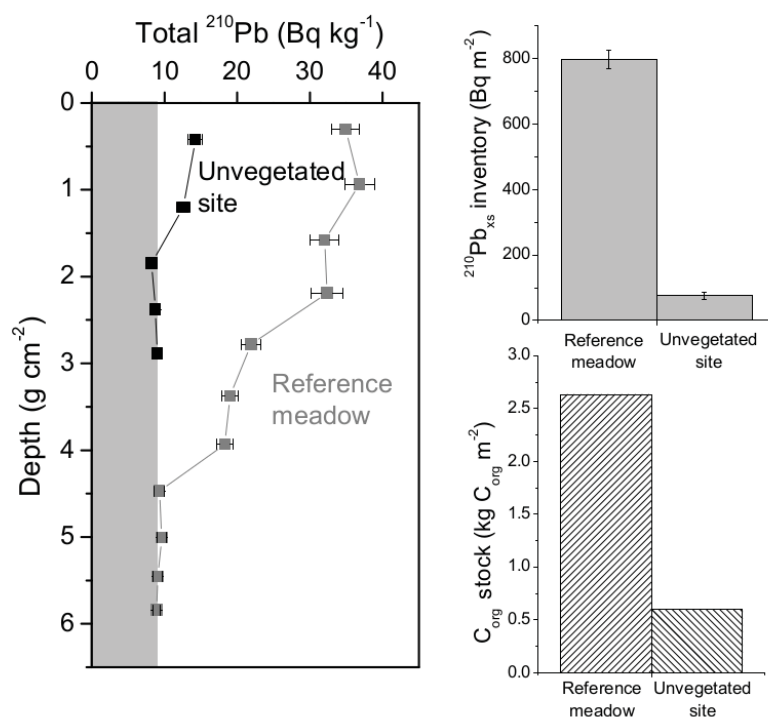
Figure B4: Comparison of ^{210}Pb specific activity profiles and inventories of $^{210}Pb_{xs}$ and organic carbon (C$_{org}$) between vegetated and unvegetated site. The grey area indicates supported ^{210}Pb specific activity (Adapted from Marbà et al., 2015).

Appendix C: Supplementary material for *Chapter 4*

Table C1: Published values for mean and global scale organic carbon sequestration rates of seagrass ecosystems.

Reference	N sites	mean C burial rate	Seagrass areal extent considered	Global C burial rate
		$g\ C\ m^{-2}\ yr^{-1}$	$x10^3\ km^2$	$Tg\ C\ yr^{-1}$
Duarte et al. (2005)	5	83[a]	300	27.4
Duarte et al. (2010)	123	119 ± 26[b]	300 - 600	21-51 ; 41-101
Kennedy et al. (2010)	403	160 - 186[c]	300 - 600	48 - 56 ; 96-112
McLeod et al. (2011)	123	138 ± 38[d]	300 - 600	48 - 112

[a] Estimated using: ^{14}C dating (Mateo et al., 1997;2005), from measurements of seagrass biomass accretion along a colonization process of 6 yr (Barron et al., 2004), at monthly intervals for one year using sediment traps (Gacia et al., 2002) and from C accumulation in the belowground parts of the plant including dead parts over a sediment record dating of 600 yr (Romero et al., 1994).

[b] Estimated from a mass balance approach and available estimates of production, respiration, net community production and production to respiration ratios.

[c] Estimated as the sum of their net community production estimated in Duarte et al.,2010 and the allochthonous C trapped in their sediments. For allochthonous C accumulation Kennedy et 2010 al uses a C burial rate in sediments of 83-133 $g\ C\ m^{-2}\ yr^{-1}$ (Duarte et al., 2005) multiplied by 0.5, the fraction of allochthonous C in seagrass sediments.

[d] Average estimated using the datasets from Duarte et al., 2005;2010 and Kennedy et al., 2010. Although McLeod et al., 2011 recalculated the average local C burial rate, they utilize the global C burial rate reported by Kennedy et al., 2010.

Table C2: Sediment dry bulk density, organic carbon content, mass accumulation rates and organic carbon burial rates of records from vegetated seagrass areas. EA stands for elemental analyzer and LOI+EA indicates that organic C content has been estimated with available site-specific equations. Nd is no data.

Site or core name, state/province, Country	Lat.	Lon.	WCD (m)	Species	DBD (g cm^{-3})	OC (%)	OC Method	Type ^{210}Pb profile	MAR (g cm^{-2} y^{-1})		OC burial rate (g C m^{-2} y^{-1})		Source
Kapisilit, GL	64.47	-50.23	3	*Z. marina*	1.44	0.42	LOI	⌣ideal	0.263	0.047	11.1	2.0	1
Ameralik, GL	64.19	-50.73	3	*Z. marina*	1.08	0.08	LOI	⌣ideal	0.045	0.028	0.4	0.2	1
Kobbe, GL	64.15	-51.61	3	*Z. marina*	1.61	0.54	LOI	⌣ideal	0.120	0.025	6.5	1.4	1
Gulf of Gdansk, PL	54.73	18.55	1.5	*Z. marina*	1.70	1.26	EA	⌣ideal	0.329	0.022	30.4	1.3	2
Portland, ME, USA	43.67	-70.24	nd	*Z. marina*	0.85	2.89	EA	surface mix	0.164	0.087	47.5	25.6	3
Great Bay, NH, USA	43.07	-70.88	3	*Z. marina*	0.92	1.92	EA	⌣ideal	1.19	0.15	229.1	28.8	3
Cohasset, MA, USA	42.25	-70.78	2	*Z. marina*	1.4	0.55	EA	intense mix					3
Niles Beach, MA, USA	42.60	-70.66	5	*Z. marina*	1.23	1.38	EA	surface mix	0.12	0.01	16.7	1.1	3
Pleasant Bay, MA, USA	41.75	-69.95	1	*Z. marina*	1.17	0.29	EA	⌣ideal	0.277	0.084	8.0	2.4	3
Pirate's Cove, MA, USA	42.42	-70.92	2	*Z. marina*	1.19	0.68	EA	surface mix	0.29	0.08	19.8	5.1	3
Boston Harbour, MA, USA	42.33	-70.96	nd	*Z. marina*	1.18	0.50	EA	*negligible* $^{210}Pb_{xs}$	0.00		0.0		3
Martha's Vineyard, MA, USA	41.46	-70.60	1	*Z. marina*	1.57	0.43	EA	intense mix					3
West Falmouth, MA, USA	41.61	-70.65	1	*Z. marina*	1.32	0.44	EA	*negligible* $^{210}Pb_{xs}$	0.00		0.0		3
Ninigret Pond, RI, USA	41.37	-71.64	2	*Z. marina*	0.63	3.44	EA	⌣ideal	0.26	0.03	89.4	9.9	3
Prudence Island, RI, USA	41.58	-71.32	nd	*Z. marina*	1.16	0.64	EA	surface mix	0.14	0.02	8.9	1.2	3
SB-10yr (VCR LTER), VA, USA	37.27	-75.81	1.25	*Z. marina*	1.2	0.62	EA	⌣ideal	0.19	0.03	11.5	2.1	4
HI - 4yr (VCR LTER), VA, USA	37.41	-75.73	1.25	*Z. marina*	1.4	0.45	EA	*negligible* $^{210}Pb_{xs}$	0.00		0.0		4
Delmarva (VCR LTER), VA, USA	37.27	-75.81	0.7	*Z. marina*	1.3	0.43	EA	surface mix	0.20	0.01	8.7	0.3	5
Ria Formosa ZN 1, PT	36.98	-7.89	-3.0 +0.1	*Z. noltii*	1.1	0.72	NDIR EA	⌣ideal	0.31	0.02	22.1	1.5	6

Table C2 continued	Lat.	Lon.	WCD (m)	Species	DBD (g cm^{-3})	OC (%)	OC Method	Type ^{210}Pb profile	MAR (g cm^{-2} y^{-1})		OC burial rate (g C m^{-2} y^{-1})		Source
Ria Formosa ZN 2, PT	36.99	-7.88	-3.0 +0.0	*Z. noltii*	1.3	0.53	EA	intense mix					6
Ria Formosa ZN 3, PT	37.00	-7.88	-3.0 +0.1	*Z. noltii*	0.7	2.11	EA	surface mix	0.77	0.04	162.5	7.7	6
Ria Formosa ZN 4, PT	37.00	-7.88	-3.0 +0.2	*Z. noltii*	0.82	1.74	EA	surface mix	0.209	0.018	36.4	3.1	6
Padilla Bay 1, WA, USA	48.54	-122.53	-3.0 +0.3	*Z. marina*	1.35	0.31	EA	⌣ideal	0.23	0.048	6.9	1.4	7
Padilla Bay 2, WA, USA	48.54	-122.53	-3.0 +0.4	*Z. marina*	1.18	0.60	EA	⌣ideal	0.21	0.043	11.7	2.4	7
Padilla Bay 3, WA, USA	48.54	-122.53	-3.0 +0.5	*Z. marina*	1.17	0.59	EA	⌣ideal	0.09	0.015	5.2	0.5	7
Padilla Bay 4, WA, USA	48.54	-122.53	-3.0 +0.6	*Z. marina*	1.32	0.38	EA	⌣ideal	0.28	0.044	10.6	1.6	7
Padilla Bay 5, WA, USA	48.54	-122.53	-3.0 +0.7	*Z. marina*	1.37	0.30	EA	⌣ideal	0.31	0.105	9.1	3.2	7
Padilla Bay 6, WA, USA	48.54	-122.53	-3.0 +0.8	*Z. marina*	1.49	0.30	EA	⌣ideal	0.60	0.100	17.8	3.0	7
North Caicos, TC	21.83	-72.07	1	*not specified*	0.93	1.43	LOI	⌣ideal	0.420	0.102	60.1	18.2	8
North Caicos, TC	21.83	-72.07	1.4	*not specified*	0.84	0.96	LOI	⌣ideal	0.377	0.029	36.2	5.6	8
Biscayne Bay, FL, USA	25.64	-80.17	0.5	*not specified*	1.58	2.42	LOI	⌣ideal	1.734	0.268	420.0	78.8	8
Biscayne Bay, FL, USA	25.64	-80.17	0.5	*not specified*	1.62	2.68	LOI	⌣ideal	0.792	0.145	212.2	44.0	8
Bob Allen Bank, FL USA	25.02	-80.66	nd	*T. testudinum*	0.71	2.13	LOI	surface mix	0.672	0.058	143.3	12.3	9
Rabbit Key, FL, USA	24.98	-80.84	nd	*not specified*	0.30	2.09	LOI	surface mix	0.106	0.015	22.0	3.1	10
Johnson Key, FL, USA	25.05	-80.91	nd	*not specified*	0.43	4.43	LOI	surface mix	0.160	0.017	70.9	7.7	10
Porjoe Key, FL, USA	25.13	-80.47	nd	*not specified*	0.61	3.00	LOI	surface mix	0.306	0.049	91.8	14.7	10
Crocodile Point, FL, USA	25.14	-80.73	nd	*not specified*	0.49	4.93	LOI	surface mix	0.161	0.029	79.3	14.4	10
Pass key FB-1, FL, USA	25.15	-80.57	0.3-1	*T. testudinum*	*0.91*	1.76	EA	nd	1.884		276.5		11
Russel Key FB-2, FL, USA	25.06	-80.63	0.3-2	*T. testudinum*	*0.80*	1.99	EA	nd	0.744		138.4		11
Bob Allen Key FB-3SG, FL, USA	25.02	-80.66	0.3-3	*T. testudinum*	*0.71*	2.23	EA	nd	0.548		123.1		11
Whiprey Basin (NE), FL, USA	25.07	-80.74	0.3-4	*T. testudinum*		4.43	EA	nd			85.7		11

Table C2 continued	Lat.	Lon.	WCD (m)	Species	DBD (g cm^{-3})	OC (%)	OC Method	Type ^{210}Pb profile	MAR (g cm^{-2} y^{-1})		OC burial rate (g C m^{-2} y^{-1})		Source
Bob Allen Key, FL, USA	25.02	-80.68	nd	*T. testudinum*	0.74	2.44	LOI + EA	⌣ideal	0.291	0.046	73.6	11.7	12
Bob Allen Key, FL, USA	25.02	-80.68	nd	*T. testudinum*	0.69	2.18	LOI + EA	intense mix					12
Russel Bank, FL, USA	25.03	-80.64	nd	*T. testudinum*	0.81	2.16	LOI + EA	⌣ideal	0.682	0.081	148.5	17.7	12
Russel Bank, FL, USA	25.03	-80.64	nd	*T. testudinum*	0.79	2.16	LOI + EA	⌣ideal	1.479	0.086	308.1	17.8	12
Ninemile Bank, FL, USA	24.94	-80.86	nd	*T. testudinum*	0.66	3.10	LOI + EA	⌣ideal	0.263	0.043	89.5	14.5	12
Ninemile Bank, FL, USA	24.94	-80.86	nd	*T. testudinum*	0.68	3.32	LOI + EA	⌣ideal	0.350	0.080	122.4	27.9	12
Trout Creek, FL, USA	25.21	-80.54	nd	*T. testudinum*	0.77	1.71	LOI + EA	surface mix	0.342	0.033	59.9	5.7	12
Trout Creek, FL, USA	25.21	-80.54	nd	*T. testudinum*	0.74	1.74	LOI + EA	⌣ideal	0.234	0.015	40.4	2.6	12
Celestun Lagoon, Yucatan, MX	20.93	-90.34	nd	*H. wrightii + R. maritima*	0.45	3.38	EA	⌣ideal	0.091	0.002	29.2	0.5	13
Chelem Lagoon, Yucatan, MX	21.27	-89.69	nd	*H. wrightii*	0.69	3.52	EA	*negligible $^{210}Pb_{xs}$*	0.000		0.0		13
Perezoso P.Th.1, CR	9.75	-82.82	nd	*T. testudinum*	0.53	2.77	LOI	intense mix					14
Perezoso P.Th.2, CR	9.75	-82.82	nd	*T. testudinum*	1.26	2.40	LOI	intense mix					14
Perezoso P.Th+Syr.1, CR	9.75	-82.82	nd	*Thalassia + Syringodium*	1.28	2.24	LOI	intense mix					14
Perezoso P.Syr.1, CR	9.75	-82.82	nd	*Syringodium*	1.38	2.19	LOI	intense mix					14
Puerto Vargas PV.Th.1, CR	9.74	-82.81	nd	*T. testudinum*	1.41	1.89	LOI	intense mix					14
Punta Cahuita PC.Th.1, CR	9.75	-82.82	nd	*T. testudinum*	1.72	1.91	LOI	intense mix					14
Punta Cahuita PC.Th.2, CR	9.75	-82.82	nd	*T. testudinum*	1.28	2.27	LOI	intense mix					14
Pollença, IB, SP	39.90	3.09	4	*P. oceanica*	0.47	5.99	LOI + EA	⌣ideal	0.065	0.003	38.8	1.6	15
Pollença, IB, SP	39.90	3.09	4	*P. oceanica*	0.52	4.78	LOI + EA	surface mix	0.058	0.002	27.9	1.1	15
Pollença, IB, SP	39.90	3.09	4	*P. oceanica*	0.49	5.82	LOI + EA	⌣ideal	0.096	0.004	55.7	2.1	15
Pollença, IB, SP	39.90	3.09	4	*P. oceanica*	0.48	5.45	LOI + EA	⌣ideal	0.066	0.003	36.0	1.9	15

Table C2 continued	Lat.	Lon.	WCD (m)	Species	DBD (g cm⁻³)	OC (%)	OC Method	Type ²¹⁰Pb profile	MAR (g cm⁻² y⁻¹)		OC burial rate (g C m⁻² y⁻¹)		Source
Pollença, IB, SP	39.90	3.09	4	*P. oceanica*	0.52	5.40	LOI + EA	⌣ideal	0.069	0.004	37.2	2.0	15
Pollença, IB, SP	39.90	3.09	5	*P. oceanica*	0.52	5.94	LOI + EA	⌣ideal	0.112	0.008	66.5	4.7	16
Porto Colom, IB, SP	39.42	3.27	9	*P. oceanica*	0.58	2.13	LOI + EA	⌣ideal	0.155	0.011	33.0	2.3	16
Sta Ponça, IB, SP	39.51	2.47	5	*P. oceanica*	0.87	1.48	LOI + EA	⌣ideal	0.154	0.047	22.8	7.0	16
Cala d'Or, IB, SP	39.37	3.23	7	*P. oceanica*	0.91	0.73	LOI + EA	⌣ideal	0.258	0.019	18.9	1.4	16
Magalluf, IB, SP	39.50	2.54	6	*P. oceanica*	0.90	0.93	LOI + EA	surface mix	0.169	0.056	15.8	5.2	16
Soller, IB, SP	39.79	2.69	11	*P. oceanica*	1.14	0.53	LOI + EA	*negligible ²¹⁰Pb$_{xs}$*	0.000		0.0		16
Es Port, IB, SP	39.15	2.95	17	*P. oceanica*	0.69	2.12	LOI + EA	⌣ideal	0.114	0.005	24.1	1.0	16
Es Castell, IB, SP	39.15	2.93	5	*P. oceanica*	0.97	0.44	LOI + EA	⌣ideal	0.239	0.018	10.5	0.8	16
Santa Maria, IB, SP	39.15	2.95	13	*P. oceanica*	1.13	0.90	LOI + EA	surface mix	0.207	0.061	18.7	5.5	16
Ses Illetes, IB, SP	38.76	1.43	5	*P. oceanica*	1.36	0.98	LOI + EA	intense mix					16
Es Pujols, IB, SP	38.73	1.45	4	*P. oceanica*	1.01	1.71	LOI + EA	intense mix					16
Ischia, IT	40.73	13.96	4	*P. oceanica*	0.97	1.75	LOI + EA	surface mix	0.236	0.049	38.4	8.0	17
Kalami, Crete, GR	35.47	24.14	7	*C. nodosa*	1.33	0.11	EA	surface mix	0.207	0.028	2.2	0.3	18
Kalami, Crete, GR	35.47	24.14	7	*C. nodosa*	1.32	0.14	LOI	surface mix	0.207	0.028	2.8	0.4	18
Maridati, Crete, GR	35.22	26.27	5.5	*C. nodosa*	1.31	0.05	EA	intense mix	0.219	0.065	1.2	0.4	18
Maridati, Crete, GR	35.22	26.27	5.5	*C. nodosa*	1.33	0.14	LOI	*negligible ²¹⁰Pb$_{xs}$*	0.000		0.0		18
Port, CY	34.64	33.01	6	*P. oceanica*	1.15	0.21	EA	surface mix	0.194	0.085	4.0	1.8	18
Limassol, CY	34.71	33.12	3.5	*C. nodosa*	1.23	0.17	LOI	*negligible ²¹⁰Pb$_{xs}$*	0.000		0.0		18
Limassol, CY	34.71	33.12	3.5	*C. nodosa*	1.24	0.08	EA	*negligible ²¹⁰Pb$_{xs}$*	0.000		0.0		18

Table C2 continued	Lat.	Lon.	WCD (m)	Species	DBD (g cm⁻³)	OC (%)	OC Method	Type ^{210}Pb profile	MAR (g cm⁻² y⁻¹)		OC burial rate (g C m⁻² y⁻¹)		Source
C1 Abu-Ali, SA	27.27	49.55	nd	*H. uninervis + H. stipulacea*	1.27	0.76	EA	intense mix	0.21	0.06	15.8	4.7	19
C2 Abu-Ali, SA	27.26	49.57	nd	*H. uninervis + H. stipulacea*	0.95	0.98	EA	intense mix	0.09	0.02	8.8	2.3	19
C2 Ecopark, SA	26.71	50.12	nd	*H. uninervis + H. stipulacea*	1.33	0.65	EA	intense mix	0.08	0.02	5.4	1.5	19
C3 Ecopark, SA	26.72	50.00	nd	*H. uninervis + H. stipulacea*	1.19	0.78	EA	surface mix	0.10	0.05	7.9	4.0	19
C1 Safaniya, SA	27.97	50.01	nd	*H. uninervis + H. stipulacea*	1.33	0.56	EA	surface mix	0.342	0.041	19.0	2.6	19
C3 Safaniya, SA	27.98	48.78	nd	*H. uninervis + H. stipulacea*	1.30	0.51	EA	surface mix	0.23	0.03	11.8	1.8	19
C2 Uqair, SA	25.73	50.23	nd	*H. uninervis + H. stipulacea*	1.23	0.57	EA	surface mix	0.16	0.06	8.9	3.4	19
C3 Uqair, SA	25.73	50.23	nd	*H. uninervis + H. stipulacea*	1.23	0.63	EA	intense mix	0.16	0.06	10.4	4.0	19
C3 Abu-Ali, SA	27.28	49.55	nd	*H. uninervis + H. stipulacea*	1.20	1.12	EA	intense mix					19
C1 Ecopark, SA	26.68	50.01	nd	*H. uninervis + H. stipulacea*	1.10	0.68	EA	intense mix					19
C2 Safaniya, SA	27.98	48.78	nd	*H. uninervis + H. stipulacea*	1.30	0.56	EA	intense mix					19
C1 Uqair, SA	25.72	50.23	nd	*H. uninervis + H. stipulacea*	1.10	0.49	EA	*negligible $^{210}Pb_{xs}$*	0		0.0		19
Thuwal Island TSA, SA	22.28	39.09	1	*H. stipulacea*	1.32	0.17	EA	*negligible $^{210}Pb_{xs}$*	0		0.0		20
Economic City RSJ, SA	22.38	39.13	<0.5	*T. ciliatum*	1.27	0.36	EA	*negligible $^{210}Pb_{xs}$*	0		0.0		20
Economic City RSB, SA	22.39	39.13	<0.5	*T. hemprichii*	0.92	0.75	EA	*negligible $^{210}Pb_{xs}$*	0		0.0		20
Economic City RSF, SA	22.40	39.13	3	*E. acoroides*	0.84	0.51	EA	*intense mix*					20
Economic City RSE, SA	22.38	39.13	1.5	*E. acoroides*	0.87	0.78	EA	*intense mix*					20
Khor Alkharar AHS1, SA	22.93	38.88	<0.5	*H. uninervis*	1.38	0.32	EA	*negligible $^{210}Pb_{xs}$*	0		0.0		20
Petro Rabigh PRSA, SA	22.75	39.01	<0.6	*T. ciliatum*	1.26	0.15	EA	*negligible $^{210}Pb_{xs}$*	0		0.0		20

Table C2 continued	Lat.	Lon.	WCD (m)	Species	DBD (g cm^{-3})	OC (%)	OC Method	Type ^{210}Pb profile	MAR (g cm^{-2} y^{-1})		OC burial rate (g C m^{-2} y^{-1})		Source
Khor Alkhara AHS9, SA	22.93	38.88	3	*H. stipulacea*	0.90	0.51	EA	*negligible* $^{210}Pb_{xs}$	0		0.0		20
Khor Alkhara AHS7, SA	22.93	38.89	7	*H. stipulacea*	0.87	0.45	EA	*intense mix*					20
02 Tsimipaika Bay, MD	-13.50	48.49	0.9	*E. acoroides*	1.16	0.50	EA	*negligible* $^{210}Pb_{xs}$	0		0.0		15
04 Tsimipaika Bay, MD	-13.51	48.49	2.4	*E. acoroides*	1.17	1.05	EA	*negligible* $^{210}Pb_{xs}$	0		0.0		15
08 Tsimipaika Bay, MD	-13.50	48.47	-3.0 - +0.3	*E. acoroides*	1.20	0.48	EA	*negligible* $^{210}Pb_{xs}$	0		0.0		15
10 Tsimipaika Bay, MD	-13.52	48.45	nd	*E. acoroides*	1.34	0.52	EA	*negligible* $^{210}Pb_{xs}$	0		0.0		15
11 Tsimipaika Bay, MD	-13.51	48.46	nd	*E. acoroides*	1.22	1.11	EA	*negligible* $^{210}Pb_{xs}$	0		0.0		15
16 Tsimipaika Bay, MD	-13.53	48.50	-3.0 - +0.3	*E. acoroides*	1.36	1.25	EA	*negligible* $^{210}Pb_{xs}$	0		0.0		15
22 Tsimipaika Bay, MD	-13.51	48.47	3	*E. acoroides*	1.39	0.71	EA	*negligible* $^{210}Pb_{xs}$	0		0.0		15
Shark Bay CCC19, WA, AU	-25.96	114.16	1.5	*A. antarctica*	0.68	3.81	EA	intense mix	0.169	0.064	63.1	23.9	21
Shark Bay CCC20, WA, AU	-25.97	114.12	2.5	*P. sinuosa*	0.72	1.51	EA	surface mix	0.144	0.019	14.1	1.8	21
Shark Bay CCC28, WA, AU	-25.89	113.84	3	*P. australis + A. antarctica*	0.85	1.61	EA	⌣ideal	0.139	0.010	20.8	1.5	21
Shark Bay CCC30, WA, AU	-25.89	113.84	4	*P. australis + A. antarctica*	0.70	5.37	EA	surface mix	0.193	0.016	92.8	7.5	21
Shark Bay CCC35, WA, AU	-25.79	113.85	2	*P. australis*	0.63	1.60	EA	⌣ideal	0.105	0.008	15.5	1.1	21
Shark Bay CCC37, WA, AU	-25.79	113.85	2	*P. australis*	0.63	2.44	EA	⌣ideal	0.145	0.016	27.6	3.0	21
Shark Bay CCC50, WA, AU	-25.78	113.45	1.5	*P. australis*	0.58	2.87	EA	⌣ideal	0.052	0.008	19.8	3.0	21
Shark Bay CCC48, WA, AU	-25.86	113.49	1.5	*P. sinuosa*	1.17	0.99	EA	intense mix	0.068	0.026	10.5	4.0	21
Shatk Bay CCC40, WA, AU	-26.00	113.55	3	*A. antarctica*	1.24	1.61	EA	*negligible* $^{210}Pb_{xs}$	0.000		0.0		21
Shatk Bay CCC45, WA, AU	-25.62	113.59	1.5	*A. antarctica*	1.04	1.80	EA	*negligible* $^{210}Pb_{xs}$	0.000		0.0		21
Shatk Bay CCC46, WA, AU	-25.69	113.60	2	*A. antarctica*	1.17	0.73	EA	*negligible* $^{210}Pb_{xs}$	0.000		0.0		21
Jurien Bay CCC54, WA, AU	-30.31	115.00	3.5	*P. sinuosa*	0.58	4.68	EA	surface mix	0.125	0.009	58.4	4.1	20

Table C2 continued	Lat.	Lon.	WCD (m)	Species	DBD (g cm⁻³)	OC (%)	OC Method	Type ²¹⁰Pb profile	MAR (g cm⁻² y⁻¹)		OC burial rate (g C m⁻² y⁻¹)		Source
Rottnest Island CCC16, WA, AU	-32.00	115.55	2	*P. sinuosa* + *A. antarctica*	0.84	1.71	EA	⌣ideal	0.163	0.009	27.9	1.6	22
Rottnest Island CCC72, WA, AU	-32.01	115.49	3	*P. sinuosa* + *A. antarctica*	1.19	0.89	EA	intense mix	0.226	0.065	20.8	6.0	22
Rottnest Island CCC2, WA, AU	-32.00	115.56	3	*P. sinuosa* + *A. antarctica*	1.11	0.69	EA	⌣ideal	0.107	0.027	6.6	1.7	20
Vasse-Wonnerup 2, WA, AU	-33.63	115.41	1.5	*R. megacarpa*	1.47	0.62	EA	surface mix	0.378	0.061	23.4	3.8	20
Vasse-Wonnerup 5, WA, AU	-33.61	115.44	1.5	*R. megacarpa*	0.81	1.37	EA	surface mix	0.298	0.034	40.7	4.6	20
CockburnSound#M, WA, AU	-32.16	115.67	2	*P. sinuosa*	0.88	1.76	EA	surface mix	0.191	0.072	43.6	4.6	23
CockburnSound#J, WA, AU	-32.16	115.67	4	*P. sinuosa*	0.89	1.88	EA	⌣ideal	0.150	0.053	28.4	10.0	23
CockburnSound#K, WA, AU	-32.16	115.67	6	*P. sinuosa*	0.85	0.88	EA	surface mix	0.103	0.045	11.2	4.9	23
CockburnSound#P, WA, AU	-32.16	115.67	8	*P. sinuosa*	1.11	0.83	EA	surface mix	0.102	0.014	9.7	0.7	23
CockburnSound#90, WA, AU	-32.27	115.70	2	*P. sinuosa*	0.95	2.81	EA	⌣ideal	0.216	0.026	15.5	3.2	24
CockburnSound#86, WA, AU	-32.19	115.75	6.5	*P. sinuosa*	1.16	1.04	EA	surface mix	0.318	0.095	26.6	8.0	24
Princess Royal Harbour, WA, AU	-35.07	117.89	1.5	*P. australis*	0.29	5.78	EA	⌣ideal	0.035	0.002	9.7	0.6	20
Oyster Harbour #F, WA, AU	-34.98	117.96	1.5	*P. australis*	0.54	2.12	EA	surface mix	0.062	0.003	13.5	0.6	25
Oyster Harbour #V, WA, AU	-34.98	117.97	1.5	*P. australis*	0.47	2.81	EA	⌣ideal	0.070	0.012	21.2	3.7	20
Oyster Harbour OM, WA, AU	-34.97	117.97	1.65	*P. australis*	0.56	6.83	LOI + EA	surface mix	0.040	0.002	25.4	1.2	26
Oyster Harbour R1994, WA, AU	-34.97	117.97	1.65	*P. australis*	0.58	4.34	LOI + EA	surface mix	0.038	0.003	15.4	1.4	26
Oyster Harbour R2004, WA, AU	-34.98	117.97	1.3	*P. australis*	0.61	5.20	LOI + EA	surface mix	0.043	0.004	22.1	2.1	26
Oyster Harbour DE1, WA, AU	-34.97	117.96	2	*P. australis*	0.48	5.97	EA	surface mix	0.019	0.002	11.1	1.3	24
Waychinicup #U, WA, AU	-34.89	118.33	1.5	*P. australis*	0.79	3.78	EA	surface mix	0.122	0.009	46.2	17.5	20
Waychincup, CS1, WA, AU	-34.89	118.33	2	*P. australis*	0.80	2.54	EA	surface mix	0.111	0.017	28.3	4.4	24
Waychincup, CS2, WA, AU	-34.89	118.33	2	*P. australis*	0.83	1.97	EA	intense mix	0.096	0.018	18.9	3.6	24
Port Pirie (Adelaide) DE2, SA, AU	-33.12	138.03	2	*P. australis*	0.98	4.51	EA	⌣ideal	0.045	0.011	20.4	5.0	24
Port Pirie (Adelaide) A15, SA, AU	-33.12	137.97	2.5	*P. australis*	0.81	1.73	EA	⌣ideal	0.069	0.012	11.9	2.0	27

Table C2 continued	Lat.	Lon.	WCD (m)	Species	DBD (g cm^{-3})	OC (%)	OC Method	Type ^{210}Pb profile	MAR (g cm^{-2} y^{-1})		OC burial rate (g C m^{-2} y^{-1})		Source
Port Pirie (Adelaide) A12, SA, AU	-33.12	137.97	2.5	*P. australis*	0.84	1.74	EA	surface mix	0.132	0.032	21.9	5.4	27
Port Pirie (Adelaide) A13, SA, AU	-33.12	137.97	2.5	*P. australis*	0.68	1.33	EA	intense mix	0.094	0.011	14.8	1.8	28
Port Pirie (Adelaide) PP1, SA, AU	-33.12	138.03	0.5	*P. australis*	0.42	5.85	EA	⌣ideal	0.056	0.004	32.9	5.2	28
Port Pirie (Adelaide) PP2, SA, AU	-33.11	137.99	0.5	*P. australis*	0.62	1.65	EA	⌣ideal	0.049	0.011	8.0	1.9	28
Port Pirie (Adelaide) PP3, SA, AU	-33.13	137.96	1	*P. australis*	0.53	2.80	EA	surface mix	0.081	0.040	22.6	11.6	28
Port Pirie (Adelaide) PP4, SA, AU	-33.14	137.95	1	*P. australis*	0.60	2.42	EA	surface mix	0.080	0.007	19.5	3.0	28
Port Pirie (Adelaide) PP5, SA, AU	-33.12	137.92	3	*P. australis*	0.88	1.19	EA	intense mix	0.086	0.011	10.2	1.4	28
Port Pirie (Adelaide) PP6, SA, AU	-33.14	137.92	2.5	*P. australis*	0.48	4.39	EA	intense mix	0.174	0.011	76.2	5.6	28
Port Pirie (Adelaide) PP7, SA, AU	-33.16	137.90	0.5	*P. australis*	0.60	2.93	EA	surface mix	0.154	0.012	45.3	4.2	28
Port Pirie (Adelaide) PP8, SA, AU	-33.14	137.89	2	*P. australis*	0.84	1.29	EA	intense mix	0.113	0.039	14.6	5.0	28
Port Pirie (Adelaide) PP9, SA, AU	-33.11	137.89	3	*P. australis*	0.81	1.40	EA	surface mix	0.168	0.021	23.4	5.2	28
Port Pirie (Adelaide) PP10, SA, AU	-33.14	137.86	5	*Z. marina*	1.01	0.60	EA	intense mix					28
Port Pirie (Adelaide) PP11, SA, AU	-33.17	137.86	1	*P. australis*	0.65	2.37	EA	surface mix	0.102	0.014	24.2	3.7	28
Port Pirie (Adelaide) PP12, SA, AU	-33.14	137.86	4	*P. australis*	1.00	1.05	EA	*negligible $^{210}Pb_{xs}$*	0		0.0		28
Whyalla A39, SA, AU	-32.98	137.67	nd	*P. australis + P. sinuosa*	0.97	1.49	EA	*intense mix*	0.143	0.078	22.1	12.0	28
Whyalla A32, SA, AU	-32.98	137.67	0-2	*P. australis + P. sinuosa*	1.09462	0.37	EA	*negligible $^{210}Pb_{xs}$*	0		0.0		28
Whyalla A34, SA, AU	-33.00	137.62	0-2	*P. australis*	0.86413	0.50	EA	*negligible $^{210}Pb_{xs}$*	0		0.0		28
Whyalla A37, SA, AU	-33.01	137.61	0-2	*P. australis*	0.982	0.47	EA	*negligible $^{210}Pb_{xs}$*	0.000		0.0		28
Barker Inlet A1, SA, AU	-34.72	138.46	8	*P. sinuosa*	0.931	0.32	EA	*negligible $^{210}Pb_{xs}$*	0.000		0.0		28

Table C2 continued	Lat.	Lon.	WCD (m)	Species	DBD (g cm^{-3})	OC (%)	OC Method	Type ^{210}Pb profile	MAR (g cm^{-2} y^{-1})		OC burial rate (g C m^{-2} y^{-1})		Source
Barker Inlet A2, SA, AU	-34.72	138.46	8	*P. sinuosa*	0.734	0.97	EA	*negligible* $^{210}Pb_{xs}$	0.000		0.0		28
Barker Inlet A3, SA, AU	-34.77	138.49	0.5	*Z. nigracaulis*	0.947	1.07	EA	*intense mix*					28
BK Sydney, NSW, AU	-34.01	151.19	2.5	*P. australis*	1.213	0.92	EA	surface mix	0.246	0.031	22.2	2.8	20

1 (Marbà et al., 2018); 2 (Jankowska et al., 2016); 3 Colarusso et al. unpublished; 4 (Greiner et al., 2013); 5 (Oreska et al., 2018); 6 de los Santos et al. unpublished; 7 (Poppe and Rybczyk, 2018); 8 (Tedesco and Aller, 1997); 9 (Wingard et al., 2007); 10 (Holmes et al., 2001); 11 (Orem et al., 1999); 12 Fourqurean, unpublished; 13 (Gonneea et al., 2004); 14 Samper-Villareal, unpublished; 15 Arias-Ortiz et al. unpublished; 16 (Mazarrasa et al., 2017); 17 Mazarrasa et al. unpublished; 18 Wesselmann et al. unpublished; 19 (Cusack et al., 2018); Serrano et al. unpublished; 21 (Arias-Ortiz et al., 2018b); 22 (Serrano et al., 2016b); 23 (Serrano et al., 2016d); 24 Salinas et al. unpublished; 25 (Serrano et al., 2016f); 26 (Marbà et al., 2015); 27 (Lafratta et al., 2019); 28 Lafratta et al. unpublished.

Table C3: Sediment dry bulk density, organic carbon content, mass accumulation rates and organic carbon burial rates of records from barren areas adjacent to seagrass meadows. EA stands for elemental analyzer and LOI+EA indicates that organic C content has been estimated with available site-specific equations. nd is no data.

Site or core name, state/province, Country	Lat.	Lon.	WCD (m)	Habitat	DBD (g cm⁻³)	OC (%)	OC Method	Type ^{210}Pb profile	MAR (g cm⁻² y⁻¹)		C burial rate (g C m⁻² y⁻¹)		Source
SB-0yr (VCR LTER), VA, USA	37.27	-75.81	1.25	*Bare*	1.66	0.25	EA	negligible ^{210}Pb$_{xs}$					1
HI - 0yr (VCR LTER), VA, USA	37.41	-75.73	1.25	*Bare*	1.35	0.61	EA	negligible ^{210}Pb$_{xs}$					1
Delmarva (VCR LTER), VA, USA	37.27	-75.83	0.7	*Bare*	1.19	0.26	EA	negligible ^{210}Pb$_{xs}$					2
Whipray Basin, FL, USA	25.07	-80.74	nd	*Bare*	0.56	4.31	LOI	⌣ideal	0.207	0.034	89.3	14.5	3
Bob Allen Bank, FL, USA	25.02	-80.66	nd	*Bare*	0.91	1.87	LOI	⌣ideal	0.987	0.091	184.9	17.1	3
Pass Key Bank, FL, USA	25.15	-80.57	nd	*Bare*	0.91	2.01	LOI	surface mix	1.868	0.143	374.8	28.6	3
South Russell Bank, FL, USA	25.06	-80.62	nd	*Bare*	0.94	1.77	LOI	⌣ideal	0.910	0.075	161.2	13.3	3
Bob Allen Key FB-3SG, FL, USA	25.02	-80.66	0.3-5	*Bare*	*0.91*	2.10	EA	nd	0.969		192.6		4
Punta Cahuita PC.BS.1, CR	9.75	-82.82	nd	*Bare*	1.59	2.17	LOI	intense mix					5
Pollença, IB, SP	39.90	3.09	4	*Bare*	0.55	5.27	LOI + EA	⌣ideal	0.076	0.005	40.1	2.7	6
MDG05 Tsimipaika Bay, MD	-13.50	48.49	2.2	*Bare*	1.55	0.18	EA	negligible ^{210}Pb$_{xs}$					6
MDG24 Tsimipaika Bay, MD	-13.51	48.46	2.8	*Bare*	1.21	0.32	EA	negligible ^{210}Pb$_{xs}$					6
CockburnSound#Q, WA, AU	-32.16	115.67	4	*Bare*	1.21	0.06	EA	negligible ^{210}Pb$_{xs}$					7
CockburnSound#89, WA, AU	-32.20	115.76	9	*Bare*	1.41	0.66	EA	intense mix	0.453	0.095	30.0	6.3	8
CockburnSound#CS1, WA, AU	-32.16	115.74	9	*Bare*	1.31	0.82	EA	intense mix	0.486	0.120	50.4	12.5	8
CockburnSound#84, WA, AU	-32.17	115.76	8	*Bare*	1.50	0.44	EA	surface mix	0.604	0.103	28.6	4.9	8
Oyster Harbour Bare, WA, AU	-34.97	117.97	1.65	*Bare*	0.78	3.86	LOI + EA	negligible ^{210}Pb$_{xs}$					9
Whyalla A30, SA, AU	-33.00	137.62	0-2	*Bare*	0.95	0.66	EA	negligible ^{210}Pb$_{xs}$					10
Barker Inlet A5, SA, AU	-34.72	138.45	9	*Bare*	0.96	1.25	EA	⌣ideal	0.174	0.038	19.0	4.0	10

1 (Greiner et al., 2013); 2 (Oreska et al., 2018); 3 (Holmes et al., 2001); 4 (Orem et al., 1999); 5 Samper-Villareal et al. unpublished; 6 Arias-Ortiz et al. unpublished; 7 (Serrano et al., 2016d); 8 Salinas et al. unpublished; 9 (Marbà et al., 2015); 10 Lafratta et al. unpublished.

Table C4: Percent contribution of each seagrass bioregion to the global seagrass area. Estimates of seagrass coverage for selected areas described in the World Atlas of Seagrass (Green and Short, 2003); *described in Telesca et al. (2015) **reported by Copertino, (2013). Note: Almost certainly an underestimate in most cases.

Bioregion	Location	Area (km²)	% Area contribution
Temperate North Atlantic	Scandinavia	1850	1.4
	Western Europe	338	
	Western North Atlantic coast USA	374	
North Pacific	Japan	495	0.9
	Republic of Korea	70	
	Pacific Coast of North America	1000	
Mediterranean	Western Mediterranean*	5107	8.1
	Eastern Mediterranean*	7139.9	
	Euro-Asian Seas	2600	
Tropical-Indo Pacific	Saudi Arabia	370	70.1
	Mozambique	439	
	India	39	
	Western Australia	25000	
	Eastern Australia	71371	
	Thailand	94	
	Peninsular Malaysia	3	
	Kosrae, Federated States of Micronesia	4	
	Indonesia	30000	
	Philippines	978	
	Vietnam	440	
Tropical Atlantic	Mid-Atlantic coast USA	292	14.2
	Gulf of Mexico	19349	
	East Coast of Florida	2800	
	Mexico	500	
	Belize	1500	
	Curaçao	8	
	Bonaire	2	
	Trinidad &Tobago**	5	

	Martinique	41	
	Guadeloupe	82	
	Grand Cayman	25	
	Colombia**	432	
	Venezuela**	800	
	Brazil	300	
Temperate Southern Oceans	Chile	2.5	5.4
	Brasil Sul, Uruguai, Argentina **	150	
	Magallanes/I. Malvinas**	50	
	South Australia	9620	
	New Zealand	44	
	Total	183671	100
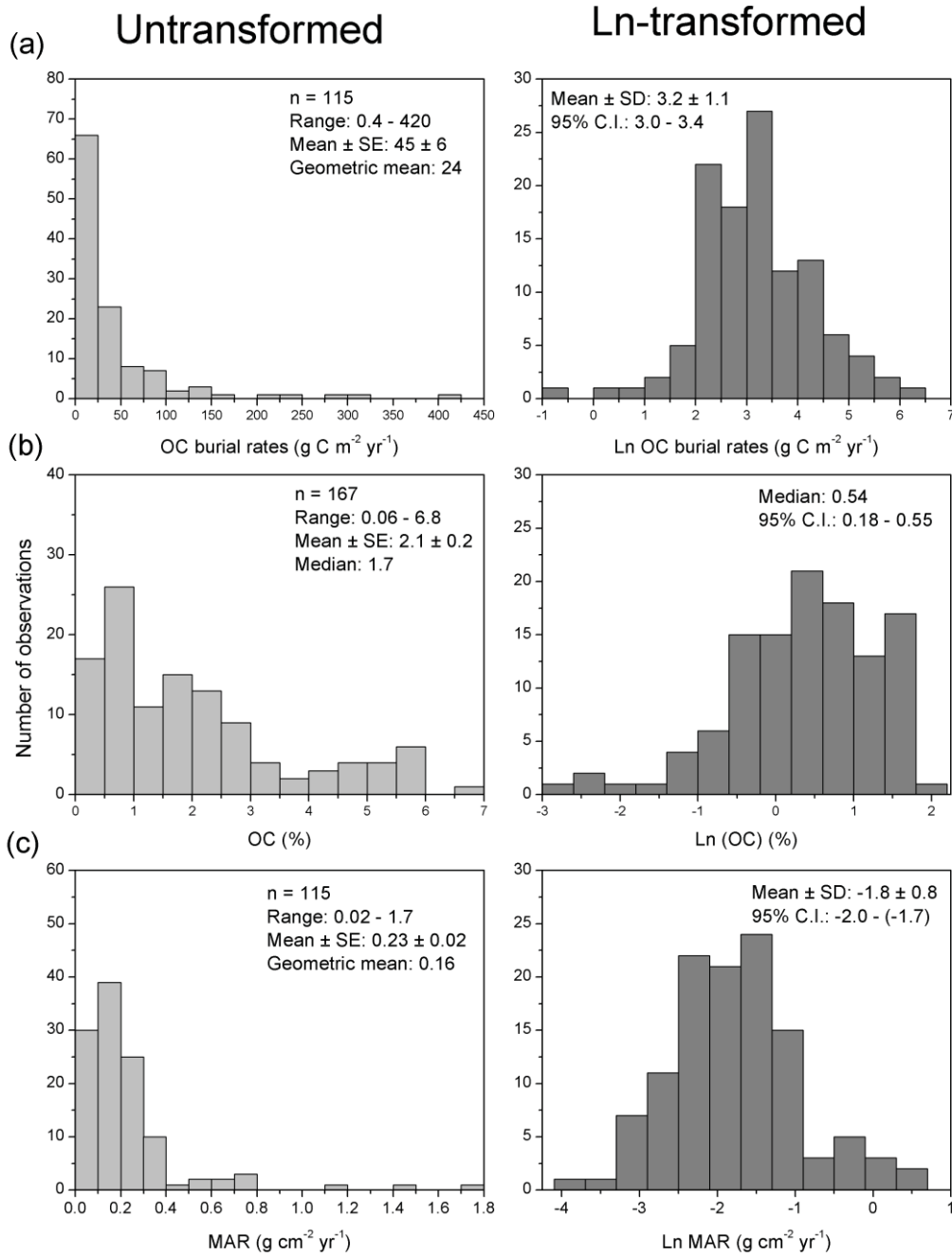
Figure C1: Frequency distribution of rates of organic carbon burial (a), organic carbon content (b) and mass accumulation (c) in modern seagrass sediments worldwide.
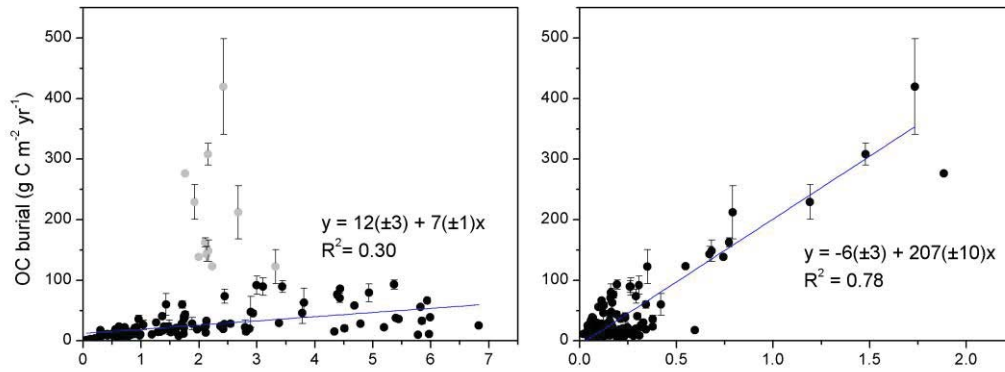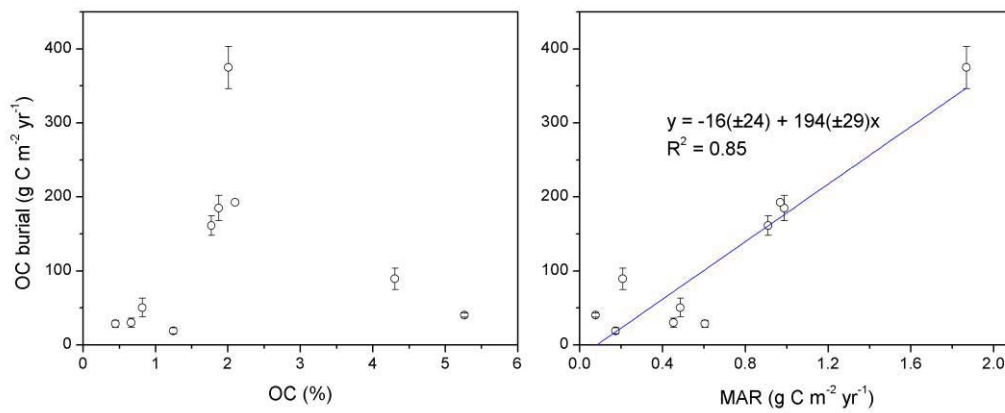
Figure C2: Relationship between organic carbon burial rates and measured sedimentary organic carbon content and mass accumulation rates in vegetated (a) and bare (c) sediments. Data points coloured in grey are masked data.
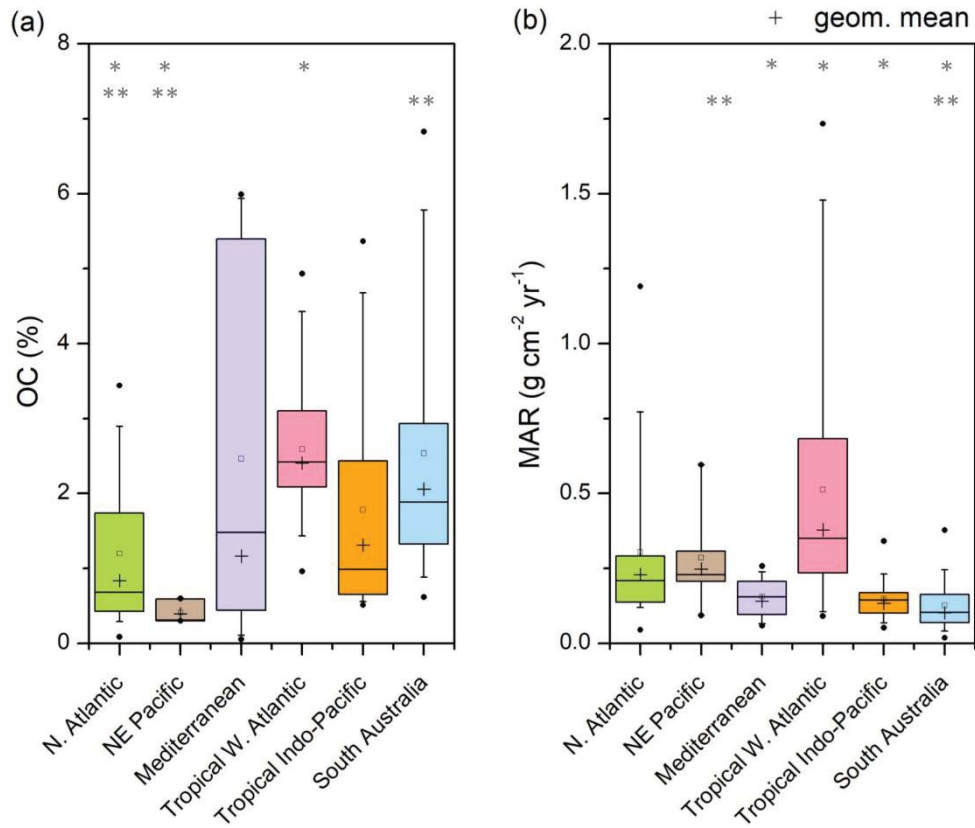
Figure C3: Boxplots showing organic carbon content (%) and mass accumulation rates (MAR) distribution in seagrass sediments across different bioregions. Boxes encompass the central 50% quantile; the line within the box represents the median, the square the average, and the cross the geometric mean. The whiskers extend to the 10 and 90% quantiles and the points represent the 1% and 99% quantiles of the distribution. Asterisks show significant differences in organic C content and MAR between bioregions.
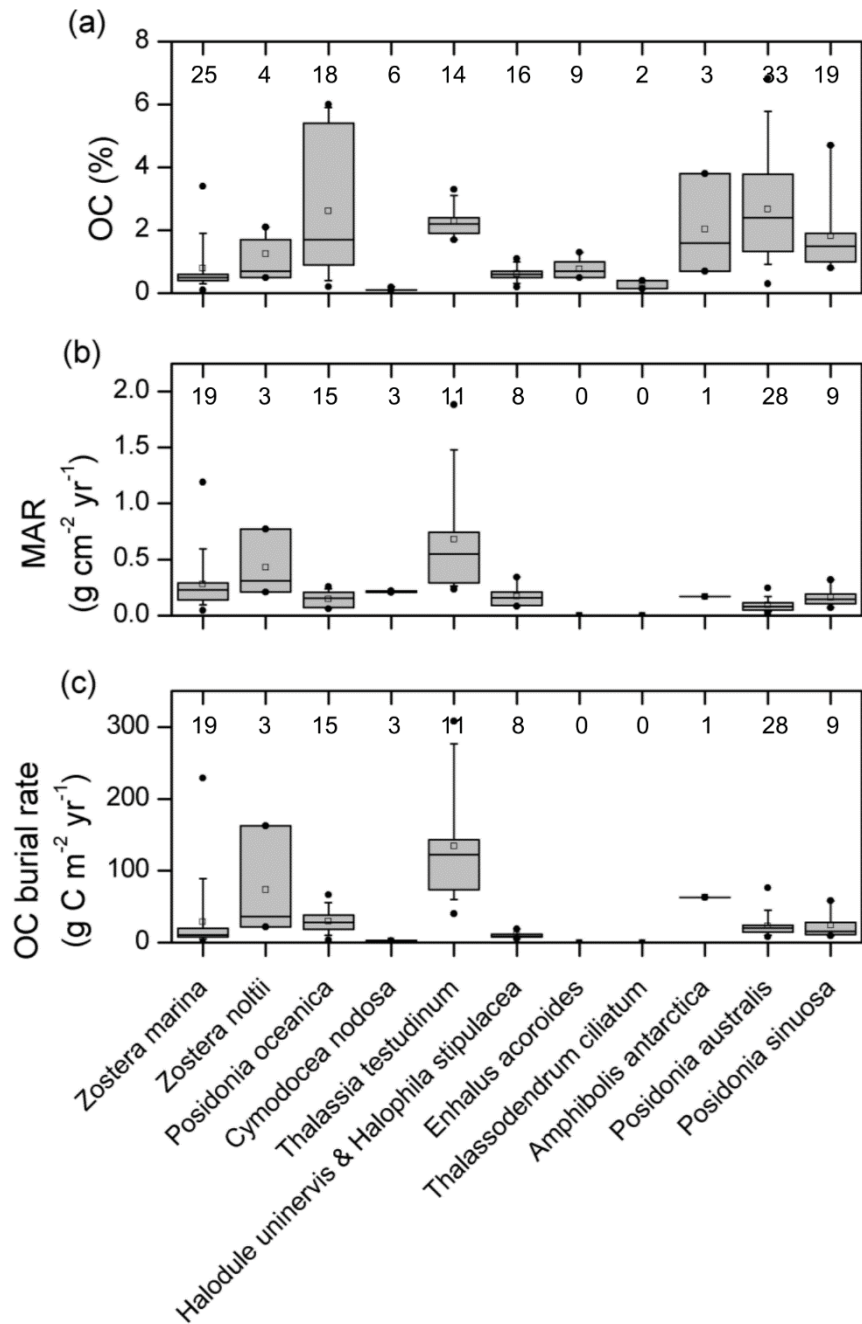
Figure C4: Boxplots showing organic carbon content (%), mass accumulation rates (MAR) and organic carbon burial rates in seagrass sediments across different species. Boxes encompass the central 50% quantile; the line within the box represents the median, the square the average. The whiskers extend to the 10 and 90% quantiles and the points represent the 1% and 99% quantiles of the distribution. Numbers along the upper axis show the number of records in each category.

Appendix D: Supplementary material for *Chapter 5*
Supplementary Discussion

Dry bulk density (DBD) of seagrass sediments sampled in Shark Bay had a wide range, from 0.06 to 1.86 g cm^{-3}, with median and mean values (0.96 g cm^{-3} and 0.94 ± 0.01 g cm^{-3}, respectively) similar to those found in carbonate systems and in seagrass sediments worldwide (1.03 ± 0.02 g cm^{-3}) (Fourqurean et al., 2012b). Spatially, DBD increased westwards towards Peron Peninsula (Fig. D1), opposite to C content, with which it was negatively correlated (ρ = -0.69; $P \leq$ 0.001) (Table D1). Grain size was dominated by medium sands (30% on average), followed by fine and coarse sands (21% and 20%, respectively on average). Mean particle diameter (d50) increased with depth (ρ = 0.25; $P \leq$ 0.001), though spatially it did not show a significant correlation with longitude, similarly than exposure (measured as sand:mud ratio) (ρ = -0.48; P =0.08 and ρ = -0.36; P =0.2, respectively). DBD was strongly negatively correlated with C, and positively correlated with sediment depth, particle size (d50) and sand:mud ratio. On the contrary, the correlation between particle size and C was weak (ρ = -0.13; $P \leq$ 0.05) and between exposure and C was not significant (P > 0.05) (Table D1), suggesting that the seagrass-derived C plays a large role in sediment C storage than does the accumulation of fine, organic-rich allochthonous particles (Serrano et al., 2016a).

C burial rates are driven by sedimentation and by the C content available for storage. The high sediment C stocks in the Wooramel Bank and Faure Sill (average top meter: 245 ± 33 Mg C ha^{-1}; average last 4,000 cal yr BP: 514 ± 45 Mg C ha^{-1}) were supported by a 1.6-fold and 2-fold faster accretion of sediments (2.8 - 1.1 mm yr^{-1} compared to the 1.7 - 0.5 mm yr^{-1} measured in meadows at Peron Peninsula), in the short- and long-terms, respectively, and by a 2.7-fold higher concentration of C relative to the other sites surveyed (Table 5.1) (Arias-Ortiz et al., 2017). The rapid sediment accumulation rates would have contributed to higher accumulation and preservation of C after burial (Serrano et al., 2016d) due to the prevention of oxygen exchange and limitation of redox potentials, which reduce remineralization(Keil and Hedges, 1993). This, together with the recalcitrant nature of seagrass-derived C (Trevathan-Tackett et al., 2015) available for storage led to the formation of these organic-rich sediment deposits within South Wooramel and Faure Sill seagrass banks.
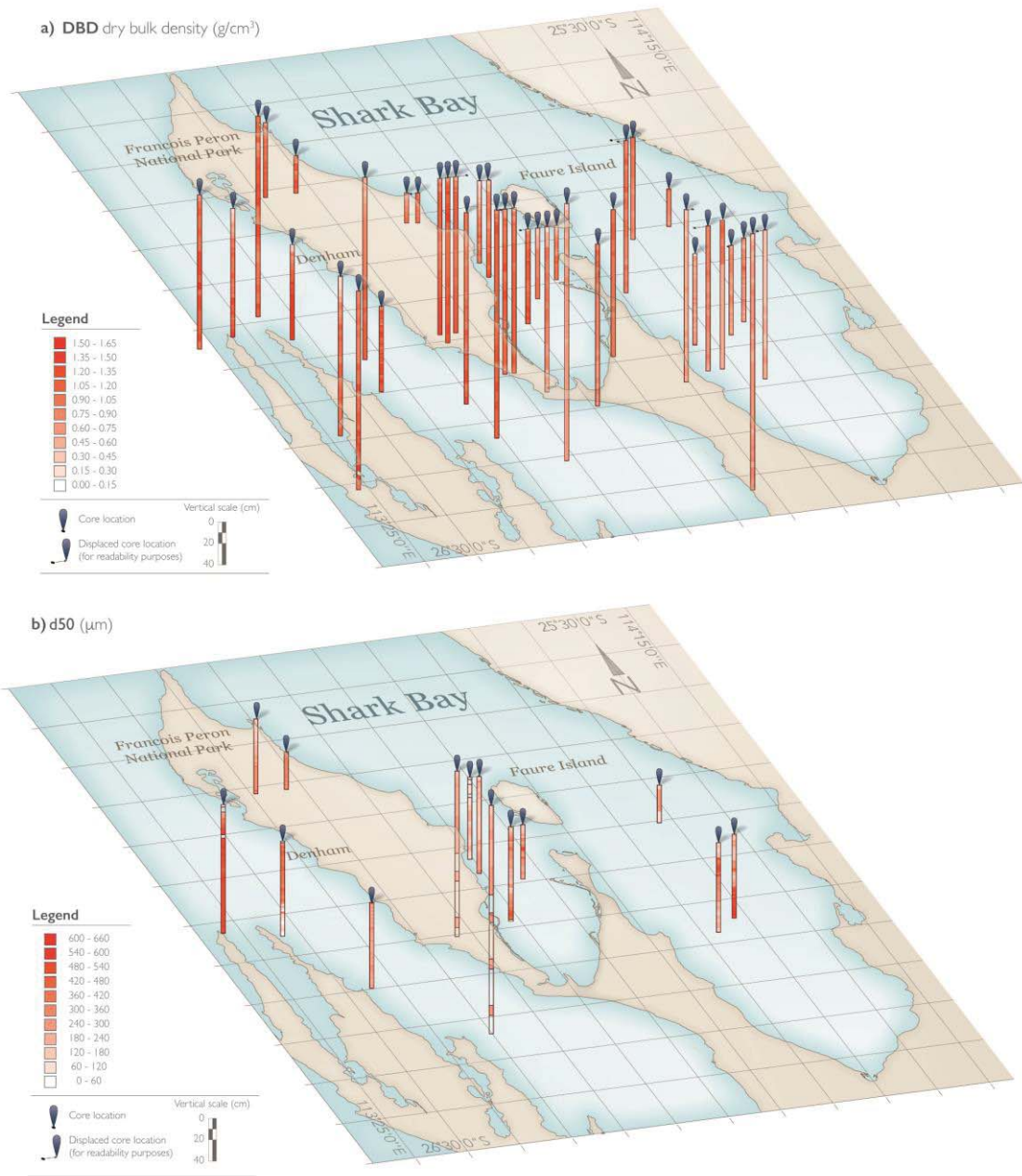
Figure D5: Spatial distribution of sediment properties. (a) Dry bulk density (DBD) and (b) d50 (median diameter of particles) measured in seagrass sediments of Shark Bay
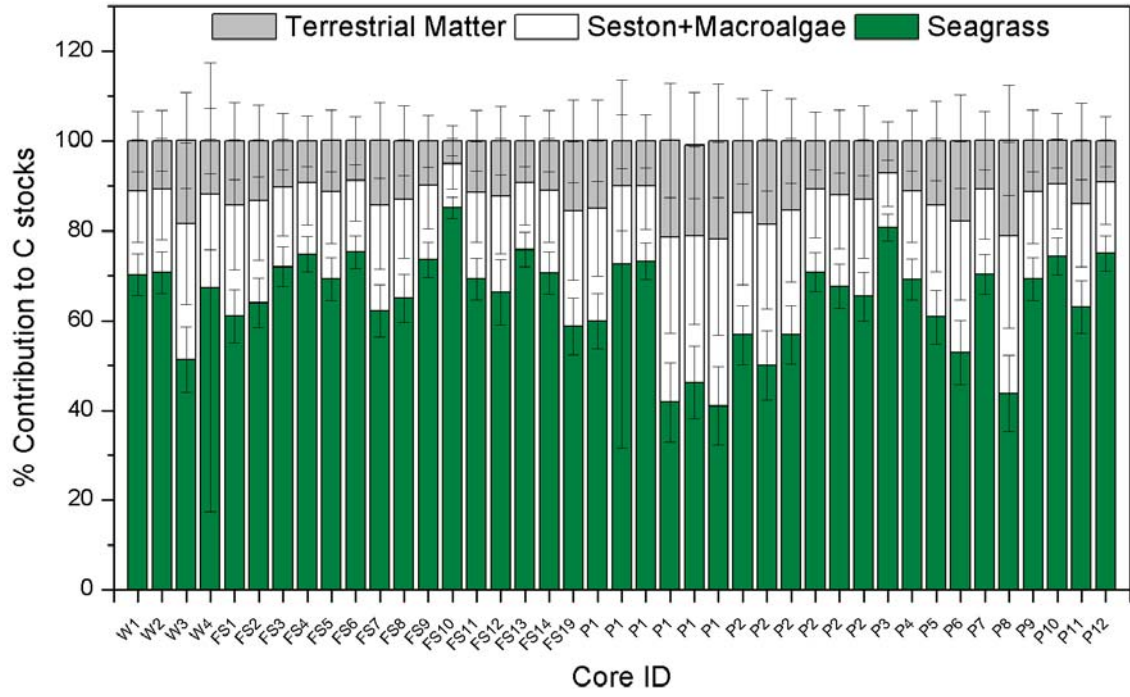
Figure D6: Percentage contribution of seagrass, seston and macroalgae and terrestrial matter to the sediment organic carbon (C) pools in Shark Bay.
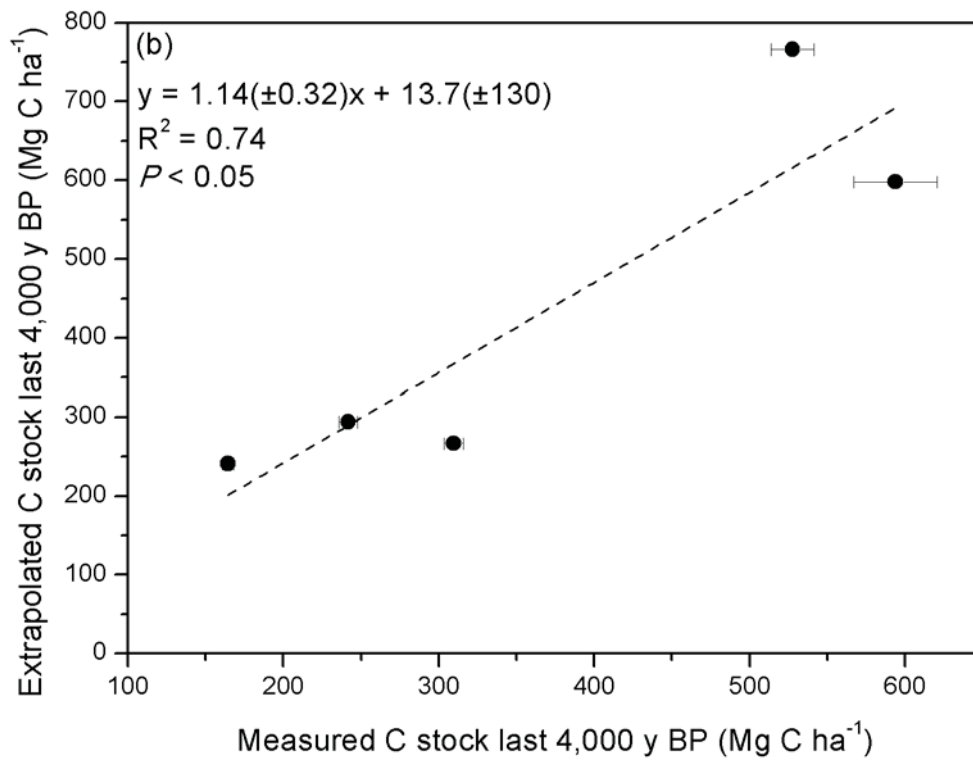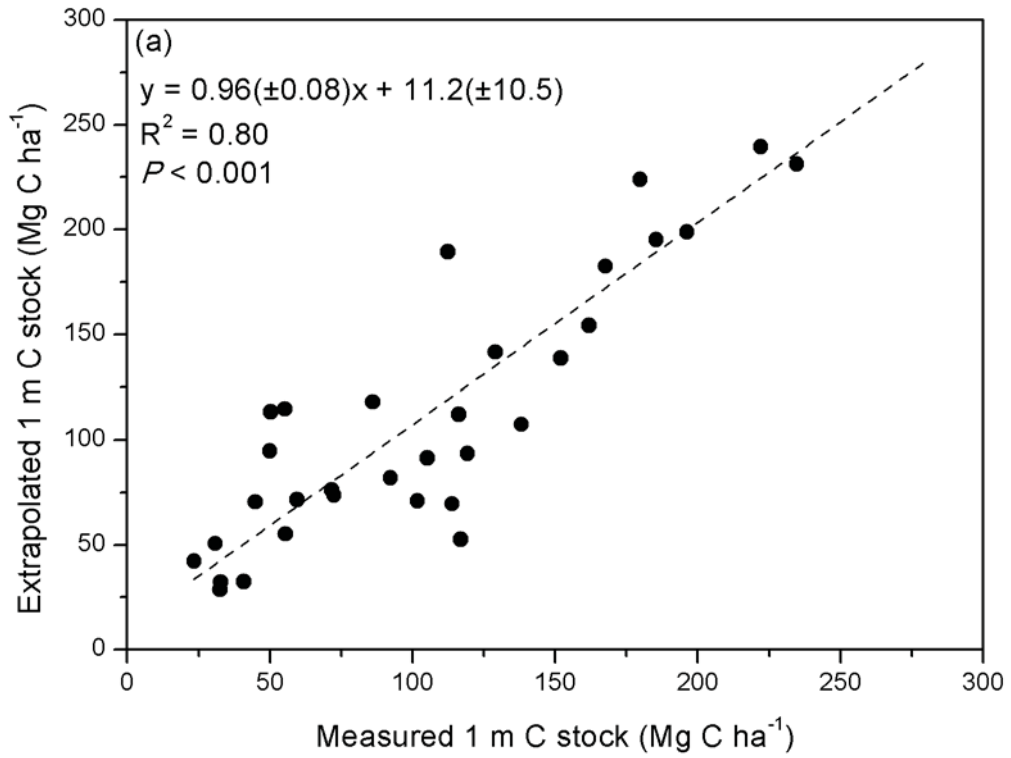
Figure D7: Relationship between extrapolated and measured organic carbon (C) stocks. (a) From 25 cm to 100 cm in sediment cores ≥ 1 m depth; (b) Accumulated over the last 2,000 to 4,000 yr in cores dating ≥ 4,000 cal yr BP.
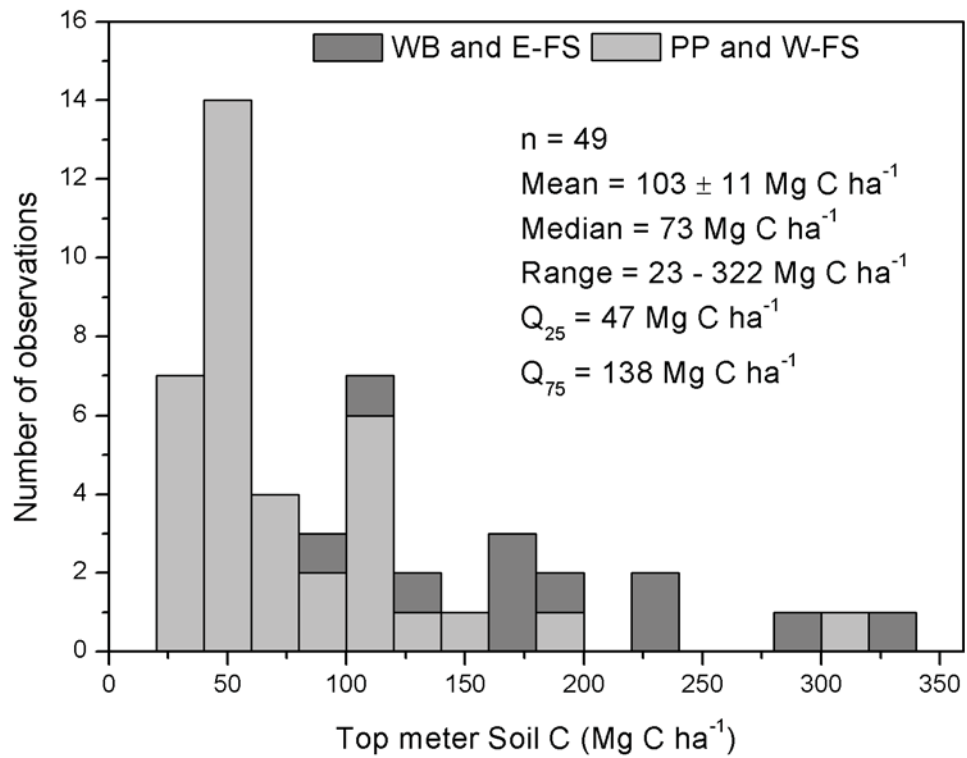
Figure D8: Frequency distribution of published and calculated observations of top meter sediment organic carbon (C) stocks in seagrass sediments in Shark Bay. Different shading is given to highlight spatial patterns. Light grey indicates observations from Peron Peninsula and West Faure Sill. Dark grey, Wooramel Bank and East Faure Sill.

Table D3: Spearman correlation coefficients between sediment organic carbon (C) concentration (%) and physicochemical and biological variables determined in seagrass cores of Shark Bay. ***$P \leq 0.001$, **$P \leq 0.01$, *$P \leq 0.05$, NS, $P \geq 0.05$; significant correlations ($P \leq 0.05$) in bold (ρ value).

	n	Depth	DBD	%C	$\delta^{13}C$	d50	% Mud	%Sand	Sand:Mud
Depth	1102		***	***	***	***	NS	NS	NS
DBD	1102	**0.32**		***	***	***	***	***	***
%C	1102	**-0.24**	**-0.69**		***	*	NS	NS	NS
$\delta^{13}C$	854	**-0.26**	**-0.25**	**0.34**		***	***	***	***
d50	369	**0.25**	**0.29**	**-0.13**	**-0.20**		***	***	***
% Mud	369	-0.06	**-0.31**	0.03	**0.31**	**-0.72**			***
%Sand	369	0.06	**0.31**	-0.04	**-0.31**	**0.72**			***
Sand:Mud	369	0.06	**0.29**	-0.02	**-0.31**	**0.71**	**-0.98**	**0.98**	

Table D4: Sediment $\delta^{13}C$ descriptive statistics estimated for the entire length (no older than 4,000 cal yr BP) of the seagrass sediment cores and putative sources of organic carbon (C) in Shark Bay. Same labels are used for cores with same coordinates sampled ~10 m apart from one another.

| Core ID	Sections			$\delta^{13}C$(‰)		
	n	Mean	SD	Minimum	Median	Maximum
W1	21	-12.9	0.4	-13.8	-12.9	-12.2
W2	23	-12.8	0.6	-13.6	-12.9	-11.3
W3	38	-15.1	2.0	-19.9	-14.8	-11.5
W4	7	-13.2	0.3	-13.8	-13.1	-12.9
FS1	31	-13.9	1.3	-15.7	-14.5	-11.6
FS2	25	-13.6	1.5	-15.6	-13.7	-10.3
FS3	25	-12.7	1.1	-15.5	-12.6	-9.6
FS4	24	-12.3	1.4	-13.9	-13.0	-9.9
FS5	25	-13.0	1.0	-14.5	-13.2	-10.9
FS6	24	-12.3	1.1	-14.3	-12.3	-10.3
FS7	34	-13.8	1.0	-15.2	-14.0	-10.9
FS8	37	-13.5	0.8	-16.3	-13.3	-12.4
FS9	41	-12.4	1.4	-18.9	-12.3	-9.9
FS10	10	-11.1	0.9	-12.5	-11.3	-9.0
FS11	21	-12.9	2.1	-21.1	-12.8	-9.3
FS12	24	-13.3	1.0	-14.5	-13.5	-9.6
FS13	37	-12.2	0.8	-13.6	-12.4	-8.9
FS14	32	-12.8	1.0	-15.6	-12.8	-11.2
FS19	29	-14.2	1.0	-15.8	-14.3	-12.1
P1	5	-14.1	0.2	-14.4	-14.1	-13.9
P1	4	-12.6	0.9	-13.3	-12.9	-11.3
P1	5	-12.5	0.8	-13.6	-12.2	-11.8
P1	5	-16.2	1.2	-18.0	-16.3	-15.1
P1	5	-15.7	1.6	-17.8	-16.0	-13.7
P1	5	-16.3	1.2	-17.5	-16.3	-14.3
P2	5	-14.4	0.8	-15.7	-14.0	-13.9
P2	5	-15.2	1.7	-18.0	-14.8	-13.5

Table D2 continued

P2	5	-14.4	0.8	-15.1	-14.5	-13.0
P2	5	-12.8	1.2	-14.1	-12.5	-11.7
P2	5	-13.2	0.5	-13.8	-13.0	-12.7
P2	5	-13.4	1.0	-14.5	-14.0	-12.2
P3	24	-11.7	0.7	-12.7	-11.9	-10.0
P4	27	-13.0	1.1	-14.3	-13.4	-9.7
P5	34	-14.0	1.3	-15.8	-14.4	-9.9
P6	30	-14.9	2.2	-18.5	-15.3	-9.3
P7	31	-12.9	1.7	-15.8	-13.1	-10.0
P8	17	-16.0	2.5	-21.3	-16.0	-12.4
P9	28	-13.0	1.1	-14.4	-13.5	-10.8
P10	22	-12.4	3.6	-21.1	-11.1	-8.9
P11	23	-13.7	1.1	-16.1	-13.8	-12.0
P12	50	-12.3	1.8	-16.6	-12.0	-8.9
Seagrass mean*		-9.41	±	1.32	Burkholder et al. 2011	
Macroalgae mean		-18.12	±	3.93	Burkholder et al. 2011	
Seston		-19.3	±	2.05	Cawley et al. 2012	
Wooramel river DOM		-25.08			Cawley et al. 2012	

* Mean of all seagrass organs from tropical and temperate species in the Bay.

Table D5: Top meter sediment organic carbon (C) stocks, location and main features of sampled seagrass meadows. Number of deep-cores, water column depth and sediment depth after compression corrections. Same labels are used for cores with same coordinates sampled ~10 m apart from one another.

Core ID	Latitude	Longitude	Site	Water depth (m)	Seagrass Species	Core length (cm)	Top meter C stock (Mg C ha⁻¹)
W1	-25.9526	114.1838	Wooramel Bank	3.0	*Amphibolis* spp	232	111
W2	-25.9230	114.1458	Wooramel Bank	1.5	*Amphibolis* spp	205	124
W3	-25.9626	114.1561	Wooramel Bank	1.5	*Amphibolis* spp	199	220
W4	-25.8500	114.1020	Wooramel Bank	3.2	*Amphibolis* spp	206	322
W5	-25.7413	114.0746	Wooramel Bank	1.0	*Halodule uninervis, Amphibolis antarctica*	103	169
W6	-25.7448	114.0797	Wooramel Bank	0.9	*Halodule uninervis, Amphibolis antarctica*	55	185
W7	-25.9565	114.1741	Wooramel Bank	4.3	*Halodule uninervis, Amphibolis antarctica*	138	162
W8	-25.8940	114.1140	Wooramel Bank	3.0	*Halodule uninervis*	100	235
FS1	-25.8476	113.8352	Faure Sill	1.5	*Posidonia australis*	323	50
FS2	-25.8474	113.8356	Faure Sill	1.5	*Posidonia australis*	311	49
FS3	-25.8426	113.8359	Faure Sill	1.5	*Posidonia australis*	275	32
FS4	-25.7719	113.8227	Faure Sill	0.5	*Posidonia australis*	249	72
FS5	-25.7723	113.8236	Faure Sill	0.5	*Posidonia australis*	269	54
FS6	-25.7726	113.8250	Faure Sill	0.5	*Posidonia australis*	256	113
FS7	-25.9747	114.1240	Faure Sill	2.5	*Posidonia sinuosa*	202	91
FS8	-25.9789	114.0684	Faure Sill	2.5	*Amphibolis* spp	207	111
FS9	-25.8894	113.8410	Faure Sill	3.0	*Posidonia australis, Amphibolis antarctica*	263	101
FS10	-25.8893	113.8412	Faure Sill	3.0	*Posidonia australis, Amphibolis antarctica*	75	81
FS11	-25.8894	113.8409	Faure Sill	4.0	*Posidonia australis, Amphibolis antarctica*	83	313
FS12	-25.8900	113.8407	Faure Sill	4.0	*Amphibolis antarctica*	230	39
FS13	-25.7870	113.8516	Faure Sill	2.0	*Posidonia australis*	261	104
FS14	-25.7870	113.8518	Faure Sill	2.0	*Posidonia australis*	146	118
FS15	-25.9306	114.0961	Faure Sill	1.7	*Amphibolis antarctica*	99	180

Table D3 continued

FS16	-25.8746	113.9992	Faure Sill	0.7	*Amphibolis antarctica*	99	86
FS17	-25.9378	113.9364	Faure Sill	2.0	*Amphibolis antarctica*	109	281
FS18	-25.8513	113.9380	Faure Sill	2.0	*Halodule uninervis, Amphibolis antarctica*	139	168
FS19	-25.8449	113.7821	Faure Sill	2.0	*Amphibolis antarctica*	274	31
P1	-25.7942	113.7224	Peron Peninsula	0.5	*Posidonia australis*	27	45
P1	-25.7942	113.7224	Peron Peninsula	0.5	*Posidonia australis*	27	62
P1	-25.7942	113.7224	Peron Peninsula	0.5	*Amphibolis antarctica*	27	30
P1	-25.7942	113.7224	Peron Peninsula	0.5	*Amphibolis antarctica*	27	26
P1	-25.7942	113.7224	Peron Peninsula	0.5	*Posidonia australis*	27	51
P1	-25.7942	113.7224	Peron Peninsula	0.5	*Amphibolis antarctica*	27	29
P2	-25.7927	113.7189	Peron Peninsula	1.0	*Amphibolis antarctica*	27	42
P2	-25.7927	113.7189	Peron Peninsula	1.0	*Amphibolis antarctica*	27	47
P2	-25.7927	113.7189	Peron Peninsula	1.0	*Amphibolis antarctica*	27	42
P2	-25.7927	113.7189	Peron Peninsula	1.0	*Posidonia australis*	27	57
P2	-25.7927	113.7189	Peron Peninsula	1.0	*Posidonia australis*	27	63
P2	-25.7927	113.7189	Peron Peninsula	1.0	*Posidonia australis*	27	58
P3	-25.9358	113.5277	Peron Peninsula	1.5	*Posidonia australis*	246	70
P4	-25.9668	113.5387	Peron Peninsula	2.0	*Amphibolis antarctica*	251	54
P5	-26.0021	113.5546	Peron Peninsula	3.0	*Amphibolis antarctica*	248	150
P6	-25.6071	113.5883	Peron Peninsula	1.5	*Amphibolis antarctica, Posidonia* spp	289	30
P7	-25.6209	113.5897	Peron Peninsula	1.5	*Amphibolis antarctica, Posidonia* spp	273	137
P8	-25.6914	113.5986	Peron Peninsula	2.5	*Amphibolis antarctica*	99	59
P9	-25.7524	113.6733	Peron Peninsula	2.0	*Amphibolis antarctica, Posidonia* spp	259	44
P10	-25.8635	113.4928	Peron Peninsula	1.5	*Posidonia sinuosa*	275	110
P11	-25.7419	113.4157	Peron Peninsula	2.0	*Amphibolis antarctica*	214	23
P12	-25.7779	113.4483	Peron Peninsula	1.5	*Posidonia australis*	280	194

Table D06: Estimates of seagrass sediment thicknesses accumulated over the last 4,000 cal yr BP based on radiocarbon results. The total thickness of sediments surveyed, and the age of the bottom sections are indicated, together with the % of sampled sediment thickness encompassing the last 4,000 yr.

Core ID	Total thickness surveyed (cm)	Age of bottom section (cal yr BP)			Estimated sediment thickness (4,000 cal yr BP)			% of sampled sediment thickness encompassing 4,000 cal yr BP
W3	199	3404	±	444	234	±	18	85
W4	206	1911	±	587	431	±	84	48
FS7	202	1367	±	54	591	±	11	34
FS9	263	3563	±	123	295	±	9	89
FS13	261	3757	±	96	278	±	5	94
FS14	146	1117	±	61	523	±	16	28
P5	248	5816	±	159	171	±	1	145
P7	273	4125	±	86	265	±	1	103
P8	99	2538	±	68	156	±	1	63
P10	275	6989	±	227	157	±	5	175
P12	280	3777	±	170	296	±	10	94

Appendix E: Supplementary material for *Chapter 6*
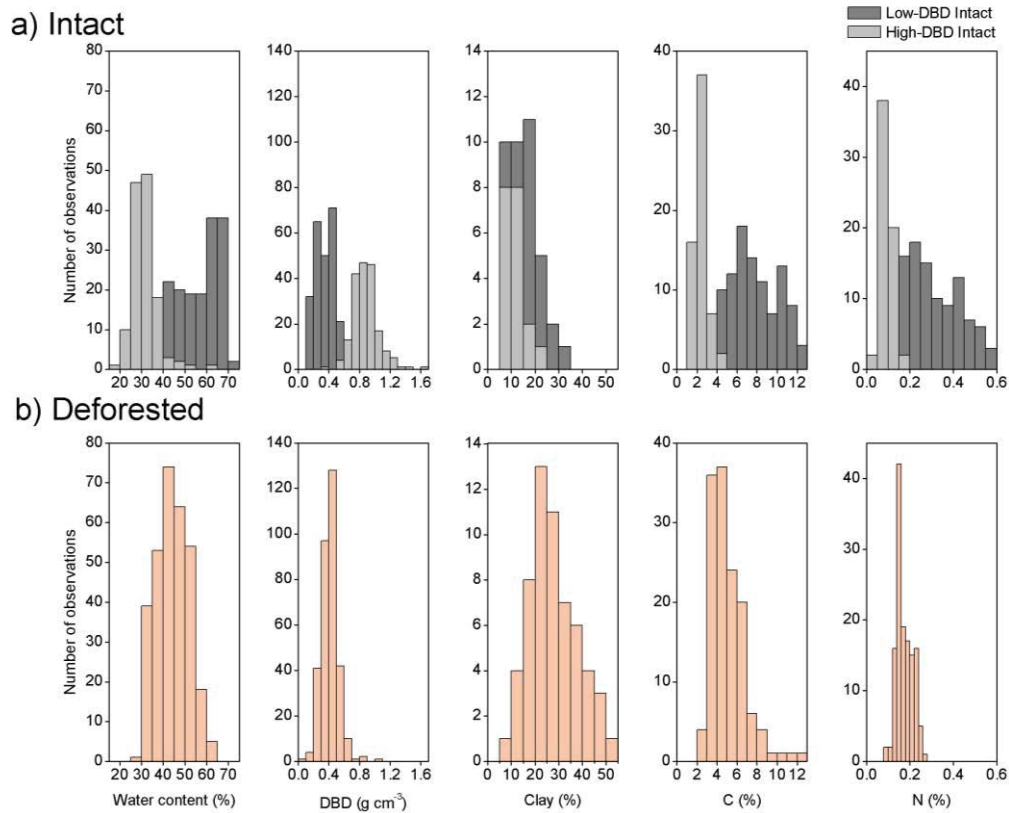
Figure E9: Frequency distribution of soil properties (water content, DBD, clay and C and N contents) of intact (a) and deforested (b) mangrove soils. All observations were normalized to the upper 45 g cm^{-2} of accumulated soil (or ~ 1 m). Mean and median values for each soil class are reported in Table 6.2.

Figure E10: Soil C:N molar ratio with cumulative mass in intact and deforested mangrove soils.

Figure E11: Sediment grain size at intact and deforested mangrove soils. Average grain size distribution in the upper meter of soils.

Figure E12: Soil elevation loss observed from tree stumps that remain in deforested plots.

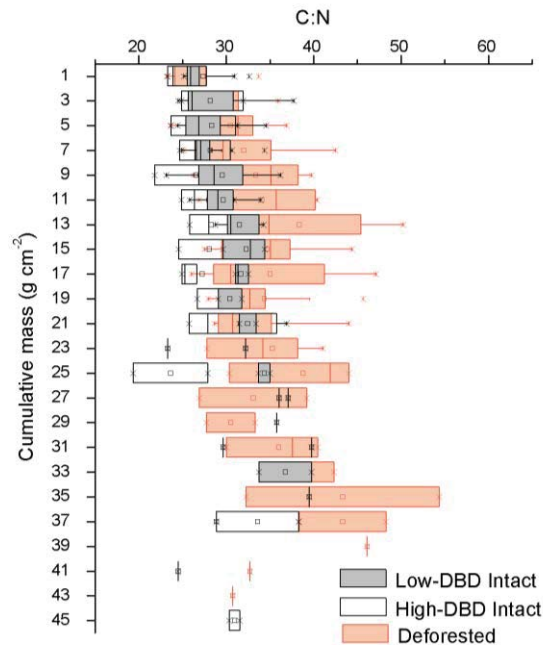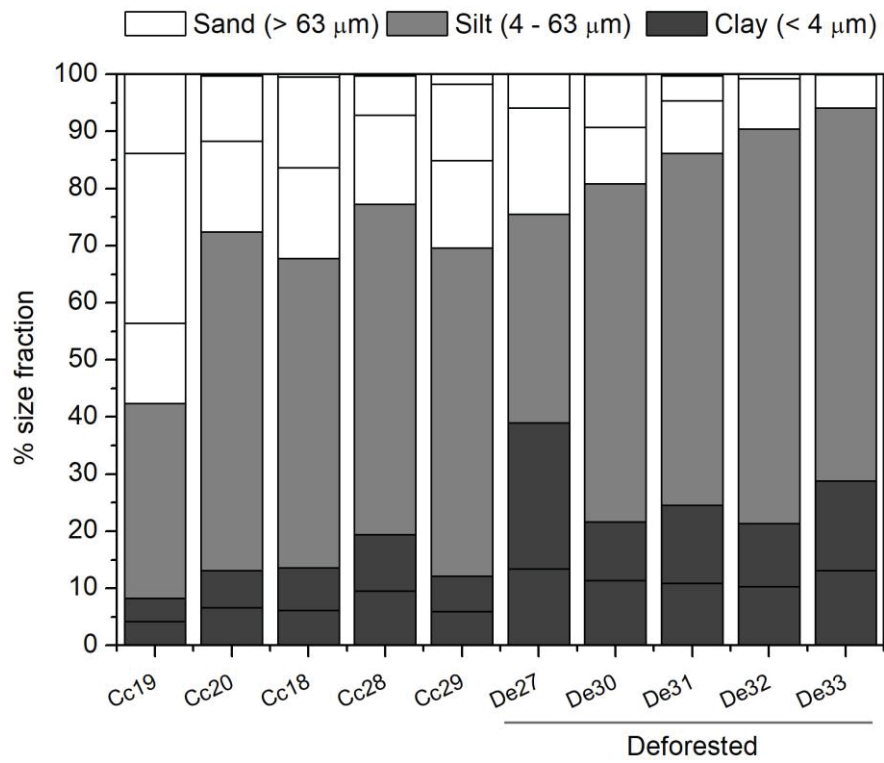**Table E7:** Biomass of mangroves by component of the sampled plots in Tsimipaika Bay, Madagascar. Aboveground (AGB) and belowground (BGB) tree biomass were measured following methods laid out by (Kauffman and Donato, 2012). Species specific allometric equations were derived using the parameters, along with wood density values, previously reported by Jones et al. (2016b) in the same area. Belowground biomass was estimated using the standard equation by (Komiyama et al., 2005). Biomass estimates for standing dead wood were made according to the decay classes determined by Kauffman and Donato (2012). A density of 0.69 g cm^{-3} was used to calculate dead tree biomass from its estimated volume.

Core ID	Class	Species dominance	Live AGB (Mg ha^{-1})	Dead AGB (Mg ha^{-1})	Live BGB (Mg ha^{-1})	Dead BGB (Mg ha^{-1})	Live AGC (Mg C ha^{-1})	Dead AGC (Mg C ha^{-1})	Live BGC (Mg C ha^{-1})	Dead BGC (Mg C ha^{-1})
Cc18	Closed canopy	*S. alba*	244	0	99	0	122	0	39	0
Cc19	Closed canopy	*B. gymnorhiza*	389	3	149	0	194	1.6	58	0
Cc20	Closed canopy	*R. mucronata*	329	25	147	9	165	12	57	4
Cc28	Closed canopy	*R. mucronata*	186	4	84	0	93	1.8	33	0
Cc29	Closed canopy	*R. mucronata*	132	37	61	11	66	19	24	4
De27	Deforested	*B. gymnorhiza*	4	0.4	2.1	0	2	0.2	0.8	0
De30	Deforested	*B. gymnorhiza*	0	3.6	0	0	0	1.8	0	0
De31	Deforested	*R. mucronata*	0	0.11	0	0	0	0.06	0	0
De32	Deforested	*C. tagal*	0	2.7	0	0	0	1.4	0	0
De33	Deforested	*C. tagal*	0	19	0	0	0	10	0	0

Table E8: Equivalent depths in cm (decompressed) for the soil mass layers used as a reference for comparisons between intact and deforested soil cores.

Core ID	Type	Equivalent depth			
		14 g cm^{-2}	45 g cm^{-2}	Mixing depth	^{210}Pb$_{xs}$ horizon
				cm	
Cc19	High-DBD intact	17	53	2	8
Cc20	High-DBD intact	15	48	3	11
Cc18	Low-DBD Intact	59	115	4	50
Cc28	Low-DBD Intact	33	101	4	31
Cc29	Low-DBD Intact	54	170	6	65
Mean (SE) High-DBD Intact		**16**	**51**	**2**	**10**
Mean (SE) Low-DBD Intact		**49**	**129**	**5**	**49**
De27	Deforested	30	104	10	30
De30	Deforested	29	98	10	17
De31	Deforested	32	106	55	55
De32	Deforested	46	158	25	28
De33	Deforested	55	119	70	70
Mean (SE) deforested		**38**	**117**	34	40

Table E9: Mann-Witney and Two-sample t- test results for the comparison of soil properties between intact and deforested mangrove soils. ***Significance at 0.001 level, ** at 0.01 and * at 0.05. NS is no significant.

Soil Class	Cores	Statistic	Water content (%)	DBD (g cm^{-3})	C (%)	N (%)	C:N	Clay (%)
High-DBD Intact	Upper 14 g cm^{-2}	Mean ± SE	31.2 ± 1.2	0.87 ± 0.03	2.45 ± 0.10	0.105 ± 0.005	27.6 ± 0.6	11.9 ± 1.8
		Median	29.0	0.891	2.3	0.095	27.7	10.6
	14 - 45 g cm^{-2}	Mean ± SE	29.2 ± 0.5	0.93 ± 0.03	2.06 ± 0.09	0.083 ± 0.004	29.6 ± 1.0	10.7 ± 0.9
		Median	29.2	0.89	2.0	0.08	29.6	10.2
Low-DBD Intact	Upper 14 g cm^{-2}	Mean ± SE	59.1 ± 0.7	0.290 ± 0.009	8.4 ± 0.2	0.350 ± 0.012	28.7 ± 0.4	14.3 ± 1.5
		Median	62.2	0.254	8.1	0.33	27.8	13.1
	14 - 45 g cm^{-2}	Mean ± SE	49.5 ± 0.9	0.432 ± 0.008	5.2 ± 0.3	0.187 ± 0.011	33.2 ± 0.8	16.4 ± 1.3
		Median	50.3	0.442	5.6	0.199	32.7	16.8
Deforested	Upper 14 g cm^{-2}	Mean ± SE	42.0 ± 0.5	0.436 ± 0.011	4.7 ± 0.2	0.169 ± 0.005	32.4 ± 0.8	27 ± 3
		Median	41.8	0.441	4.6	0.158	30.8	25
	14 - 45 g cm^{-2}	Mean ± SE	47.0 ± 0.6	0.393 ± 0.006	5.4 ± 0.2	0.180 ± 0.004	36.4 ± 1.1	28.3 ± 1.6
		Median	47.7	0.397	5.3	0.181	35.0	26.3
Treatment					**Prob>|U|**			**Prob>|t|**
High-DBD Intact vs. Deforested (upper 14 g cm^{-2})			2.8·10^{-15}***	1.9·10^{-21}***	2.8·10^{-10}***	1.4·10^{-09}***	0.002**	
High-DBD Intact vs. Deforested (bottom 14 - 45 g cm^{-2})			1.6·10^{-27}***	1.4·10^{-32}***	1.6·10^{-12}***	2.3·10^{-12}***	2.0·10^{-04}***	
Low-DBD Intact vs. Deforested (upper 14 g cm^{-2})			0***	0***	3.8·10^{-19}***	5.5·10^{-21}***	5.8·10^{-04}***	
Low-DBD Intact vs. Deforested (bottom 14 - 45 g cm^{-2})			0.06 NS	2.3·10^{-04}***	0.72 NS	0.32 NS	0.30 NS	
High-DBD Intact upper vs. Bottom layers							0.13 NS	0.5 NS
Low-DBD Intact upper vs. Bottom layers							1.8·10^{-05}***	0.3 NS
Deforested upper vs. bottom							0.002**	0.7 NS